UNIVERSITÀ DEGLI STUDI
DI MILANO

DOTTORATO DI RICERCA IN INFORMATICA
DELLA
SCUOLA DI DOTTORATO IN INFORMATICA
XXIII Ciclo
Settore Scientifico Disciplinare INF/01

Tesi di Dottorato di Ricerca

Recognition of Primary Colors in Electroencephalographic Signals using Support Vector Machines

Saim Rasheed

Relatore: Prof. Daniele Marini

Correlatore: Prof. Alessandro Rizzi

Il Direttore della Scuola di Dottorato in Informatica:
Prof. Ernesto Damiani

Anno Accademico 2009/2010

In The Name

of

ALLAH

The Most Beneficent

and

The Most Merciful

To

Parents, Huba and Zainab…

Acknowledgements

All praises, thanks and acknowledgments goes to Almighty ALLAH, Who created us, flourished us with insight and cognition to distinguish the right from the wrong and provoked us to delve into the mysteries of life and of the Universe. ALLAH sent His thousands of messengers starting from Adam (AS) to Muhammad (PBUH), as the benefactors and advisors for the mankind, who have revealed for us the multi-dimensional golden principles to understand the purpose of life and also help us perceiving the alliance between man and God. The masterpiece gift from God is the "mind" which leads us to learn, how to serve the humanity and to explore the world and the Universe.

It is also a pleasure for me to acknowledge the efforts of those people whose valuable suggestions and criticism always helped me to improve the quality of this work. First of all, I would like to express my deepest gratitude for Prof. Daniele Marini who guided me and enlightened my work with his valuable suggestions and lifelong experiences at every step. He has not only guided me technically, with his vision and knowledge, but has also been very helpful and benign as a person by helping me managing "Italian" bureaucratic stuffs at several times. I still remember the first email when I contacted him and the subsequent conversations between us in which he had always been answering my queries that started motivating me to depart for Italy for PhD. He also ensured all the needed resources during this time span. Above all, he is a very kind and cooperative gentleman; here goes a *Salute* to him. I also express my feelings of thankfulness for Prof. Alessandro Rizzi who floated the idea of working with colors during a meeting in the laboratory. He made always very useful and innovative comments and kept the work moving. Subsequently, my thanks to Prof. Raffaella Folgieri who on her visit to our lab reviewed my work. She not only encouraged and motivated me but also provided very constructive thoughts with appreciation and cleared some doubts to improve the quality of my work. How can I forget Prof. Davide Gadia, one of key members of our lab who also contributed with his comments and suggestions to improve the work and remained very active in the lab at all the times.I would also like to extend my acknowledgements for Prof. Ernesto Damiani, the Director of our PhD School, whose tireless efforts are also involved in successful completion of our PhD program. He also helped me in managing my bureaucratic stuff.

I am feeling pleasure to express my gratitude for the referees, Profssa. Christine FERNANDEZ-MALOIGNE, Prof. Claudio De'Sperati and Prof. Shiliang Sun. They not only

constructively criticized the work but also gave very useful suggestions and directions which ultimately helped me improving the contents and quality of the work.

I would also love to acknowledge the help and support of my colleagues in lab who remained with me during these three years, Cristian, Alberto, Dario and Francesco and others who came in the lab after me and left before me. I am also very glad for the reason that Cristian and Alberto are also completing their PhD degrees this year. Indeed, they are all my teachers as they kept teaching me Italian, especially Cristian who has always been motivating me not only in learning Italian but also helped me in conducting experiments in Virtual Theater, "*Grazie mille per tutti, spero che un giorno inizierò a parlare italiano con fluentemente* ☺" and obviously I cannot forget thanking "Google" who made my life so easier in translating and understanding so many emails and other documents from our secretary ☺. I think, it would not be justified, if I don't mention her name, Lorena Sala who always kept informing us about any updates and especially if there is any new course announcements. Thank you Lorena for all your efforts ☺.

I would also like to thank Adnan Abid from Pakistan, a PhD student at Politecnico di Milano and one of my best friends. He is really one, about whom I could definitely say, "*A friend in need is a friend indeed*". He remained always ready helping me out while solving many technical issues. Adding a bit more about him, he is really a generous man. I also wish him good luck for the next year when he would be writing his thesis. Moreover, I am thankful to all the subjects who voluntarily participated in the experiments and became one of the important means for completing this study. Adding my thanks to the source from whom I was getting my scholarship that made me enable to pursue higher studies in Italy i.e. Italian Government.

I present very special thanks to Dr. Tajammal and his family along with Irfan. All of them have been very close to me as they are living in Milan. When I started my PhD, I remember I always requested Tajammal to accompany me to help dealing with the Italian bureaucracy as he speaks good Italian and know the tricks as well☺. Sanober and Irfan always cooked very delicious Italian and Pakistani food for me and I really enjoyed their company especially with Namwar and Kayenat ☺.

I am really glad to extend my acknowledgement, heartiest gratitude, respect and affection for all my family, especially my parents, wife 'Huba' and daughter 'Zainab'. I have managed to accomplish this milestone with their unprecedented love, moral support and prayers, which have been a great source of strength for me in every field of life. "*One of the beautiful things in this*

world is to see them happy and smiling and the next beautiful thing is to know that you are the Reason of their happiness and smile" and I would love to become a part of that reason because they deserve ALL the fruits I will be getting after successful completion of my PhD. They never left me alone whenever they felt I am in depression or worried about my work especially Huba who always proved herself practically to be one half of my life. She had always lets me talk to Zainab whose innocent voice brought me back to track to restart my work. I always miss them a lot especially Zainab and Farooq, my nephew. Thanks to 'Skype' that always kept us connected and watching each other ☺.

Finally, I wish to thank all those who helped me out directly or indirectly in completion of this thesis. Throughout this study I have relied on many technical advices from several additional sources that have provided me helpful feedback and contributed a lot to improve the quality of the final text of this thesis.

Saim Rasheed
Jan 2011, Milan

Abstract

In this study we have worked on the classification of EEG signals produced by the exposure of primary colours (RGB). The main goal of this study was to perform an offline analysis and classification of color information obtained from EEG signals recorded in response to individual RGB colours presentation in order to verify our hypothesis, if the observation of different colors can be detected or not by selecting different frequency bands. We have also performed an offline analysis of EEG signals produced by the colour imagination to observe similarities in EEG signals between actual color exposure and their corresponding imagination in order to find a Way-In to further establish our argument for developing future BCI applications that utilizes colour information from EEG signals unlike the Wadsworth and Graz noninvasive BCI applications that utilizes sensory motor rhythm. It was seen that it is possible to detect the information, not only of actual colour exposure but also the information of colours imagination, from EEG signals. It was also seen that the colour information obtained through the imagination of colours was similar to the actual colour exposure in some subjects. The experiment was designed in a way to expose the colours to the subjects in random order of presentation and also their corresponding imaginations. Different features are extracted and analyzed. The EEG signals have to be classified into Red, Green and Blue classes.

We have used Support Vector Machines with event-related spectral perturbation as features for the classification task using three different kernels, linear, polynomial and RBF which came out with the average classification accuracy of 84% with linear, 89% with polynomial and 97% with RBF kernel for real exposure of colors whereas for imagination of colors accuracy was 64%, 70% and 76% respectively. As an alternative, we have also performed extreme energy ratio (EER) and extreme energy difference (EED) criterions to extract energy features using only linear kernel with SVM. The classification was performed on three different groups of colors i.e. (Blue, Green), (Red, Green) and (Red, Blue). The accuracies found with both of EER and EED are (79%, 78% and 80%) and (82%, 83% and 84%) respectively for real exposure of colors and for imagination of colors are (72%, 70% and 73%) and (73%, 75% and 72%) respectively. EED performed better than EER.

Another experiment was performed with different shapes of colors and the EEG data was categorized as four different groups for classification. In group1, the classification accuracies for circle, square and triangle are found to be (88%, 52%, 94%), (84%, 47%, 89%) and (84%, 49%, 94%) respectively as triplet (linear, polynomial, RBF). In group 2, 3 and 4 classification accuracies achieved are (71%, 50%, 94%), (60%, 48%, 92%) and (57%, 29%, 94%) respectively as triplet of (linear, polynomial, RBF) kernels.

After the successful classification of colour information from EEG signals we are planning to work for online classification in order to implement with any possible future Brain-Computer Interface applications. We believe that this study could further be extended to find out the possibilities for e.g. simulating a scenario of traffic light signals in virtual environment or to identify and explore any possibility of analyzing the EEG signals and developing BCI applications for color blind and/or blind people. Since such applications are quite novel in their fields of BCI therefore requires extensive collaborative research work in different domains.

Contents

Chapter 0: Introduction to Context and Aims of Work ----------1

Chapter 1: Human Brain and Functional Properties of Neuron ---------- 5

1.1 Introduction ---------- 5

1.1.1 Frontal lobe ---------- 5

1.1.2 Parietal lobe ---------- 6

1.1.3 Occipital lobe ---------- 6

1.1.4 Temporal lobe ---------- 6

1.1.5 Neurons and Glia ---------- 6

1.2 The Neuronal Membrane at Rest ---------- 8

1.2.1 Distribution of Ions across the Membrane ---------- 9

1.2.2 Relative Ion Permeability of the Membrane at Rest ---------- 10

1.3 Action Potential ---------- 10

1.4 Synaptic Transmission ---------- 11

1.4.1 Types of Synapses ---------- 12

1.4.2 Principles of Chemical Synaptic Transmission and Integration ---------- 15

Bibliography of Chapter 1 ---------- 19

Chapter 2: The Visual System and Color Perception ---------- 21

2.1 The Visual System ---------- 21

2.1.1 The Eyeball and the Retina ---------- 21

2.1.2 Visual Pathways ---------- 25

2.1.3 The Visual Cortex and Processing of Visual Information ---------- 27

2.2 Color Perception ---------- 28

Bibliography of Chapter 2 ---------- 30

Chapter 3: Interpretation and Basic Principles of Event-Related Potentials ---------- 32

3.1 What is EEG and ERP? ---------- 32

3.1.1 Reliability of ERP Waveforms ---------- 34

3.1.2 Visual Sensory Responses ---------- 36

3.2 Designing ERP Experiments ---------- 37

3.2.1 Avoiding Ambiguities in Interpreting ERP components ---------- 38
3.3 ERP Recording ---------- 39
3.3.1 Active and Reference Electrodes ---------- 39
3.3.2 Electrical Noise and Electrode Impedance ---------- 40
3.4 Artifact Rejection and Correction ---------- 43
3.4.1 Independent Component Analysis ---------- 45
3.5 Plotting, Measurement and Analysis ---------- 46
3.5.1 Measuring ERP Amplitudes and Latencies ---------- 47
3.5.2 Statistical Analysis ---------- 50
Bibliography of Chapter 3 ---------- 52
Chapter 4: Support Vector Machines for Pattern Classification ---------- 54
4.1 Introduction to Support Vector Machines ---------- 54
4.1.1 Two-Class SVM with hard and soft margins ---------- 54
4.1.2 Multiclass SVM ---------- 59
4.2 Training Methods ---------- 64
4.3 Generalized Error Estimate and Model Selection for Support Vector Classifiers 65
4.3.1 Training Set ---------- 66
4.3.2 Test Set ---------- 66
4.3.3 K-fold Cross Validation ---------- 66
4.3.4 Bootstrap ---------- 67
4.4 Support Vector Machines for EEG Signals ---------- 67
Bibliography of Chapter 4 ---------- 70
Chapter 5: Noninvasive EEG-based Brain-Computer Interfaces ---------- 72
5.1 Introduction ---------- 72
5.2 Main Components of BCIs ---------- 73
5.3 Types of EEG signals used for Noninvasive BCI Systems ---------- 75
5.3.1 BCI based on P300 Potentials ---------- 75
5.3.2 BCI based on Motor Potentials ---------- 77
5.3.3 Slow Cortical Potentials ---------- 78

5.4 Well Known Brain-Computer Interfaces ---------- 79
5.4.1 Noninvasive BCI at Wadsworth Center ---------- 79
5.4.2 Noninvasive Graz BCI ---------- 82
5.5 Applications ---------- 84
5.5.1 Spelling Devices ---------- 84
5.5.2 Environment Control ---------- 84
5.5.3 Wheelchair Control ---------- 85
5.5.4 Neuromotor Prostheses ---------- 85
5.5.5 Gaming and Virtual Reality ---------- 85
Bibliography of Chapter 5 ---------- 86
Chapter 6: Experimental Design with Single Shape ---------- 90
6.1 Introduction ---------- 90
6.2 Experimental Design and Methods ---------- 92
6.3. Results and Discussion ---------- 95
6.3.1 ERP Waveforms ---------- 95
6.3.2 Spectral Plots ---------- 96
6.3.3 Event-related Spectral Perturbation ---------- 98
6.3.4 Inter-Trial Coherence ---------- 107
6.3.5 ERP Image Plots ---------- 116
6.4 Classification using SVM with ERSP Features for real exposure of colors ------- 120
6.5 Classification using SVM with ERSP as Features for Imagination of Colors ----- 125
6.6 Classification using SVM with Extreme Energy Ratio and Difference Criterions 128
6.6.1 Extreme Energy Ratio Criterion ---------- 128
6.6.2 Extreme Energy Difference Criterion ---------- 136
Bibliography of Chapter 6 ---------- 143
Chapter 7: Experimental Design with Multiple Shapes ---------- 145
7.1 Introduction ---------- 145
7.2 Experimental Protocol ---------- 146
7.3 Analysis of ERP and ERSP results ---------- 147

7.3.1 ERP Waveforms ---------- 147
7.3.2 Event-Related Spectral Perturbation ---------- 151
7.4 Classification results using SVM with ERSP features ---------- 159
7.4.1 Classification of RGB colors within shapes: Group 1 ---------- 159
7.4.2 Classification of RGB colors across shapes: Group 2 ---------- 166
7.4.3 Classification of shapes: Group 3 ---------- 169
7.4.4 Classification of all conditions simultaneously: Group 4 ---------- 172
Chapter 8: Summary and Conclusion ---------- 176

List of Figures

Figure 1 The lobes of the cerebrum from lateral view ---------- ----------5
Figure 2 Brodmann's divisions of cerebral cortex ---------- 6
Figure 3 Neuron Structure ---------- 7
Figure 4 Glial cells: Astrocytes ---------- 8
Figure 5 The sodium-potassium pump ---------- 10
Figure 6 An action potential and its parts ---------- 11
Figure 7 (a) and (b) Gap junction channels and Electrical synapse ---------- 13
Figure 8 Chemical synapse and its components ---------- 14
Figure 9 Process of exocytosis ---------- 16
Figure 10 Transmitter-gated ion channels, EPSP and IPSP ---------- 17
Figure 11 Integration of EPSP ---------- 18
Figure 2.1 Half part of the left eye and horizontal cross section viewed from above ---------- 22
Figure 2.2 The visual field for both eyes ---------- 23
Figure 2.3 Layered structure of retina ---------- 24
Figure 2.4 Optic radiation ---------- 25
Figure 2.5 Visual pathways with a visual field for each eye ---------- 26
Figure 2.6 Three different kinds of visual pigments ---------- 28
Figure 3.1 Presentation of Stimulus: Odd-ball paradigm ---------- 33
Figure 3.2 Average of frequent stimuli X's and infrequent stimuli O's ---------- 33
Figure 3.3 Variability in ERP waveforms ---------- 35
Figure 3.4 Faraday cage ---------- 41
Figure 3.5 Absolute rejection of eye blinks using threshold value ---------- 43
Figure 3.6 Several artifacts include Saccades, EMG, EKG, Blocking and Skin Potentials ---------- 44
Figure 3.7 The general process of ICA ---------- 46
Figure 3.8 A) Bad way B) Good way ---------- 47
Figure 3.9 ERP waveforms ---------- 48
Figure 4.1 A separating hyperplane in two class problem for hard margin case ---------- 55

Figure 4.2 A separating hyperplane in two class problem for soft margin case ---------- 57
Figure 4.3 Unclassifiable shaded regions by the One-against-all approach ---------- 60
Figure 4.4 Unclassifiable regions are resolved by membership functions ---------- 62
Figure 4.5 Decision-tree based formulation to resolve the unclassifiable regions ---------- 63
Figure 4.6 Unclassifiable shaded region with pairwise formulation ---------- 64
Figure 4.7 Flow chart of the FSVM application on EEG signals ---------- 69
Figure 5.1 10-20 International electrode placement system ---------- 74
Figure 5.2 Generic model architecture for a brain-computer interface ---------- 75
Figure 5.3 The hardware for P300-based BCI for home ---------- 76
Figure 5.4 P300 evoked potential. Positive is plotted downward ---------- 77
Figure 5.5 Sensorimotor Rhythms ---------- 78
Figure 5.6 Slow cortical potential ---------- 79
Figure 5.7 SMR task for one and two dimensional targets ---------- 80
Figure 5.8 Scalp topographies ---------- 81
Figure 5.9 6 × 6 matrix display and average waveform of each cell ---------- 82
Figure 5.10 Experimental tasks and timing ---------- 83
Figure 5.11 Topographical maps of grand average classification accuracies ---------- 83
Figure 6.1 Experimental environment: ---------- 92
Figure 6.2 International 10-20 electrode placement layout and subject with mounted cap ---- 93
Figure 6.3 Experiment protocol ---------- 94
Figure 6.4 (a) Raw EEG signals (in black) and Artifact free EEG signals ---------- 94
Figure 6.4 Averaged ERP waveforms for each color exposure ---------- 95
Figure 6.5 Power spectrum of each real color exposure ---------- 97
Figure 6.6 Averaged ERSP plots of each real color exposure and imagination ---------- 99
Figure 6.7 Subject '01': ERSP plots of each real color exposure and imagination ---------- 100
Figure 6.8 Subject '02': ERSP plots of each real color exposure and imagination ---------- 101
Figure 6.9 Subject '03': ERSP plots of each real color exposure and imagination ---------- 102
Figure 6.10 Subject '04': ERSP plots of each real color exposure and imagination ---------- 103
Figure 6.11 Subject '05': ERSP plots of each real color exposure and imagination ----------104

Figure 6.12 Subject '06': ERSP plots of each real color exposure and imagination ---------- 105
Figure 6.13 Subject '07': ERSP plots of each real color exposure and imagination ---------- 106
Figure 6.14 Averaged ITC plots of each real color exposure and imagination ---------- 108
Figure 6.15 Subject '01' ITC plots of each real color exposure and imagination ---------- 109
Figure 6.16 Subject '02' ITC plots of each real color exposure and imagination ---------- 110
Figure 6.17 Subject '03' ITC plots of each real color exposure and imagination ---------- 111
Figure 6.18 Subject '04' ITC plots of each real color exposure and imagination ---------- 112
Figure 6.19 Subject '05' ITC plots of each real color exposure and imagination ---------- 113
Figure 6.20 Subject '06' ITC plots of each real color exposure and imagination ---------- 114
Figure 6.21 Subject '07' ITC plots of each real color exposure and imagination ---------- 115
Figure 7.1 Experiment protocol for multiple shapes ---------- 146
Figure 7.2 ERP waveforms for Circle ---------- 148
Figure 7.3 ERP waveforms for Square ---------- 149
Figure 7.4 ERP waveforms for Triangle ---------- 150
Figure 7.5 ERSP: Red, Green and Blue Circles for channel TP7 ---------- 153
Figure 7.6 ERSP: Red, Green and Blue Squares for channel TP7 ---------- 154
Figure 7.7 ERSP: Red, Green and Blue Triangles for channel TP7 ---------- 155
Figure 7.8 ERSP: Red, Green and Blue Circles for channel O2 ---------- 156
Figure 7.9 ERSP: Red, Green and Blue Squares for channel O2 ---------- 157
Figure 7.10 ERSP: Red, Green and Blue Triangles for channel O2 ---------- 158
Figure 7.11 Summarized classification accuracies for Circle: Group1 ---------- 162
Figure 7.12 Summarized classification accuracies for Square: Group1 ---------- 163
Figure 7.13 Summarized classification accuracies for Triangle: Group1 ---------- 166
Figure 7.14 Summarized classification accuracies: Group2 ---------- 169
Figure 7.15 Summarized classification accuracies: Group3 ---------- 172
Figure 7.16 Summarized classification accuracies: Group4 ---------- 175

List of Tables

Table 1 Classification with linear kernel using ERSP for real exposure of colors ---------- 122

Table 2 Classification with polynomial kernel using ERSP for real exposure of colors---------- 122

Table 3 Classification with RBF kernel using ERSP for real exposure of colors ---------- 123

Table 4 Classification with linear kernel using ERSP for imagination of colors ---------- 126

Table 5 Classification with polynomial kernel using ERSP for imagination of colors ---------- 126

Table 6 Classification with linear kernel using ERSP for imagination of colors ---------- 127

Table 7 Classification of (Blue, Green) using EER for real exposure of colors ---------- 132

Table 8 Classification of (Red, Green) using EER for real exposure of colors ---------- 132

Table 9 Classification of (Red, Blue) using EER for real exposure of colors ---------- 133

Table 10 Classification of (Blue, Green) using EER for imagination of colors ---------- 134

Table 11 Classification of (Red, Green) using EER for imagination of colors ---------- 134

Table 12 Classification of (Red, Blue) using EER for imagination of colors ---------- 135

Table 13 Classification of (Blue, Green) using EED for real exposure of colors ---------- 138

Table 14 Classification of (Red, Green) using EED for real exposure of colors ---------- 138

Table 15 Classification of (Red, Blue) using EED for real exposure of colors ---------- 139

Table 16 Classification of (Blue, Green) using EED for imagination of colors ---------- 140

Table 17 Classification of (Red, Green) using EED for imagination of colors ---------- 140

Table 18 Classification of (Red, Blue) using EED for imagination of colors ---------- 141

Table 19 Summary of Classification using ERSP ---------- 142

Table 20 Summary of Classification using EER ---------- 142

Table 21 Summary of Classification using EED ---------- 142

Table 7.1 Classification with linear kernel using ERSP for Circle, Group1 ---------- 160

Table 7.2 Classification with polynomial kernel using ERSP for Circle, Group1 ---------- 161

Table 7.3 Classification with RBF kernel using ERSP for Circle, Group1 ---------- 161

Table 7.4 Classification with linear kernel using ERSP for Square, Group1 ---------- 162

Table 7.5 Classification with polynomial kernel using ERSP for Square, Group1 ----------163

Table 7.6 Classification with RBF kernel using ERSP for Square, Group1 ---------- 163

Table 7.7 Classification with linear kernel using ERSP for Triangle, Group1 ---------- 164
Table 7.8 Classification with polynomial kernel using ERSP for Triangle, Group1 ---------- 165
Table 7.9 Classification with RBF kernel using ERSP for Triangle, Group1 ----------165
Table 7.10 Classification with linear kernel using ERSP for Group2 ----------167
Table 7.11 Classification with polynomial kernel using ERSP for Group2 ---------- 168
Table 7.12 Classification with RBF kernel using ERSP for Group2 ----------168
Table 7.13 Classification with linear kernel using ERSP for Group3 ----------170
Table 7.14 Classification with polynomial kernel using ERSP for Group3 ---------- 171
Table 7.15 Classification with RBF kernel using ERSP for Group3 ----------171
Table 7.16 Classification with linear kernel using ERSP for Group4 ----------173
Table 7.17 Classification with polynomial kernel using ERSP for Group4 ---------- 174
Table 7.18 Classification with RBF kernel using ERSP for Group4 ----------174
Table 7.19 Summary of Classification of all Groups ----------175

0. Introduction to Context and Aims of Work

Visual information is distributed to several brain structures in the form of action potentials by the axons of retinal neurons which are bundled into optic nerves. Different brain structures perform different functions. As an example, visual information is processed in occipital and parietal lobe of the brain. In the visual cortex, it appears that parallel paths may process different visual attributes. For example, the distinction in the retina between neurons that do and do not convey certain stimuli can be found mapped in the visual cortex. In general, each one of the more than two dozen visual cortical areas may be specialized for the analysis of different types of retinal output. Visual *phototransduction* is a process by which light is converted into action potential in the rod cells, cone cells and photosensitive ganglion cells of the retina of the eye. This continuous process of signal generation result in a change in the action potential firing frequency of the ganglion cells whose receptive field centers receive input from long, middle and short wave sensitive cones (briefly: red, green and blue). In general, color sensation derives from the spectrum of light interacting with the spectral sensitivities of the light receptors. These signals are carried to the human brain, that forms color sensation by the comparison of the readout of three cone types, e.g. upon equal activation of all types of cones (red, green and blue), white color sensation derives.

One of the senses in humans is vision. Vision actually involves numerous different properties of objects i.e. color, form, movement and different cells of visual system are responsible for concurrent processing of these properties. There are approximately 1 million axons in the optic nerve, constituting almost 40% of the total number of axons in the cranial nerves. The visual system begins with the eye and *retina* lies at the back of the eye. The retina contains photoreceptors which are specialized to transform the light energy into neural activity. The receptors for sight, photoreceptors, are the rods and cones of the retina. Their adequate stimulus is electromagnetic waves with a wavelength between 400 and 700 nm. The photoreceptors do not react to light with shorter (ultraviolet light) or longer (infrared light) wavelengths. The rods are responsible for vision in dim light, whereas the cones are responsible for vision in daylight and for color vision. Visual information is distributed in the form of action potentials, to other parts of the brain through axons of retinal neurons which are bundled into optic nerves. Optic nerves are involved in regulating biological rhythms and controlling eye position and optics. However, the first synaptic relay in the pathway that serves visual perception occurs in a cell group of the dorsal thalamus called the lateral geniculate nucleus or LGN. From the LGN, visual information ascends to the cerebral cortex where it is interpreted and remembered. Conscious use of visual information and many reflex effects elicited by visual

stimuli are necessary and sufficient conditions to completely understand the visual system. The visual information that arrives in different parts of the brain in the form potential can be recorded fortunately from the scalp by placing electrodes. This potential is known as electroencephalography or EEG.

In this thesis we shall discuss about the analysis and classification of EEG signals recorded from the scalp by exposing visual RGB colors. We also know that several applications of Brain-Computer Interaction (BCI) like P300 Speller application or mu rhythm cursor movement have been developed but regarding colors different types of other studies are done, for example, a similar work was done by a Japanese researcher A. Yoto (2007) in which he has used only RGB colored sheets of paper to examine the arousal-calming effects, using each EEG band power and the total band power (beta+alpha+theta) and the alpha attenuation test as standard indices of arousal and to analyze the human brain activities in perception and attention referred to EEG alpha band response but not particularly related to BCI application's point of view. As we know that normally people use speech, gestures or writing to communicate with other people. Imagine if somebody is not able to communicate with other people through these channels but he/she is aware of the environment. Such a condition is called locked-in syndrome. Indeed the patients are truly locked in their bodies and remain unable to express themselves. There are some neurological diseases that may cause the body towards paralyses of the motor system restricting both verbal and nonverbal communication. Locked-in means that the people are conscious and alert but not able to utilize their muscles that cause them to restrict the communication of their needs, wishes and emotions therefore, our main aim is to extend our future work for BCI applications in order to facilitate such patients.

Although we are not going to develop a BCI application here but for the sake of comprehensive understanding we shall prepare ourselves for necessary background required to understand the basic principles and underlying theory involved in developing brain-computer interfaces. It is necessary for the onwards implementation of our results based on our hypothesis. The ultimate task of any BCI system is the classification of EEG signals which reflects the growing interest of researchers in EEG-based BCI. For any successful BCI application, it is necessary to implement online classification in order to see real time execution which is a challenging task for signal processing and machine learning experts. However, an earlier offline analysis of EEG signals helps us in improving our classification accuracies. Once the brain signal is classified, it is fed to the outer world application to perform the desired operation.

In this study, we have presented and discussed the results for offline spectral analysis and classification (using three different kernels, linear, polynomial and RBF) of EEG signals recorded from the scalp, produced by primary colours stimuli, red, green and blue presented at random. To the best of our knowledge, we did not find any brain-computer interface system that relies

only on color information because all the BCI systems we have studied during this course are based on EEG signals produced either by motor execution or its imagination, visual or auditory stimulation in terms of instructions given to the subjects in order to perform the required tasks. Our main focus and goal in the experiment is on the offline analysis and classification of color information into red, green and blue classes using Support Vector Machine (SVM), obtained from EEG signals produced by the uniform primary colors stimulation in order to be utilized for future BCI applications. In this context we have used only three colors, Red, Green and Blue for our experiments in order to avoid expected complications and to achieve more precise results. We believe that the results we obtained and presented in the next chapters, would serve as necessary means to develop future BCI applications. To explore the dynamics of brain in response to presentation of primary colors, i.e. red, green and blue, we performed an experiment in which subjects were exposed to random occurring of RGB colors and instructed to imagine the same color that was exposed most recently while keeping the eyes closed, in a Virtual Reality set to provide an immersive experience on a large screen keeping the luminance of colors constant. Frequency bands that would be investigated are delta (0.1 – 4 Hz), theta (4 – 8 Hz), alpha (8 – 12 Hz) and beta (12 – 30 Hz).

The purpose of the experiment is to verify, if either the observation of different real colours or their corresponding imagination of colours can be detected in the selected EEG frequency combination, and to select best frequency combination to maximize differences through colour signals in order to find a Way-In to further establish our argument and to provide a baseline to be compared with more complex visual stimuli to evaluate the effects of colours to navigate in an immersive VR environment. For example, we can develop a virtual reality (VR) application in which first and preliminary version will exhibit the traffic light signals. A moving vehicle is expected to stop when turning ON the Red light, upon recognition of red colour through EEG signals. Similarly, upon recognition of the green light, a stopped vehicle is expected to start moving. We suggest that this method would be faster and provide more effective communication channel than those BCI applications that based on motor imagery because colors deliver fastest information and help greatly in making decision immediately. As a simple example, in real life traffic signal light colors let us decide in a fraction of second either to keep going or slowdown or stop even while driving at the farther distance. Moreover, on several other public places different colors are used for recognition of terminals for services quickly and easy to understand, react immediately and greatly affects human emotional status.

This way we may use colours as controllable parameter in VR environments. Another application of such colour recognition system could be for colour blind and/or blind people. These applications are quite novel in their fields and needs extensive collaborative research work in different domains. We shall extend this study to further investigate the dynamics of brain activities to provide feedback for BCI systems to navigate into virtual environments to

control motion, referring to consider the effects of color stimuli in VR environment. The results obtained and presented in the next chapters are not used yet for online BCI system but we believe that this would be a useful first step towards contribution to provide a base for BCI applications based on uniform color stimuli.

In chapter 1 we shall discuss about the human brain and functional properties of neuron and the concepts regarding visual system and color perception will be presented in Chapter 2. In chapter 3 we shall discuss about the Interpretation and Basic Principles of EEG and Event-Related Potentials (ERPs) whereas detailed description of classifier (SVM) used in this study is given in chapter 4. Chapter 5 explains how to develop Noninvasive EEG-based Brain-Computer Interfaces. This chapter makes an overview of BCI that could give back the basic communication abilities and some degree of autonomy to the individuals in locked-in condition, and that could augment the human capabilities and enables them to interact with computers or other technological devices. A partial state of the art of well-known Brain-Computer Interfaces is provided and different applications are quickly listed. In chapters 6 and 7 we have described our experiment in detail and presented and analyzed their results and all the work is summarized and concluded in chapter 8.

1. Human Brain and Functional Properties of Neuron

1.1 Introduction

The center of the human nervous system is the brain that is considered to be very complex organ. There are two main divisions of the nervous system i.e. central nervous system (CNS) and the peripheral nervous system (PNS). The CNS consists of the brain and the spinal cord. The major parts of the brain are the cerebrum, the cerebellum and the brain stem. However, PNS consists of the nerves and nerve cells that lie outside the brain and spinal cord. The nerves are used by the brain for communication with the body. Different functions in the human body are performed by the different identifiable parts of the brain. These parts of the brain or cortical divisions that constitute the cerebrum are shown in figure 1.

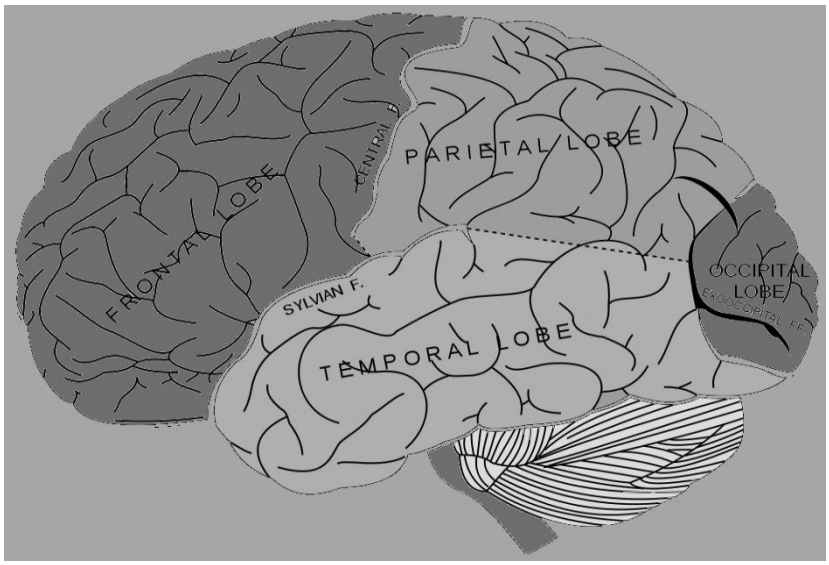

Figure 1 The lobes of the cerebrum from lateral view

The deeper part that separates the frontal lobe from the temporal lobe is called sylvian fissure and the central sulcus divides the frontal and parietal lobes of the cerebrum whereas occipital lobe lies at the back of the brain. All the actions and corresponding reactions are monitored as well as regulated by the brain upon receiving the sensory information and rapid analyzes of the data. Breathing, heart rate, and other autonomic processes that are independent of conscious brain functions are controlled by the brainstem. The cerebellum is responsible for the body's balance, posture, and the coordination of movement.

1.1.1 Frontal lobe

This part of the brain is located at front of cerebral hemisphere and posed anterior to parietal lobe and above the temporal lobe as shown in figure 1. Frontal lobe is considered

responsible for planning and recognizing future outcomes, differentiating between good and bad and identifying similarities and differences between things.

1.1.2 Parietal lobe

This part of the brain is positioned posterior to the frontal lobe and superior to occipital lobe and above the temporal lobe as shown in figure 1. The sensory information that is sensed by the different parts of the body is integrated by the parietal lobe and is also responsible for manipulating the objects.

1.1.3 Occipital lobe

This is the smallest part in the cerebral cortex and located in the rearmost side of the skull and posterior to all parts of the brain as shown in figure 1. This part contains the primary visual cortex and is responsible for processing of visual information. According to Brodmann's area 17 as shown in figure 2, also called V1, primary visual cortex is located on medial side of the occipital lobe.

1.1.4 Temporal lobe

This part of the brain is positioned below the sylvian fissure on both sides of the hemispheres of the brain as shown in figure 1. The main responsibility of this lobe is to process the auditory information and to understand the semantics of speech. It contains the hippocampus and plays important role in the formulation of long-term memory.

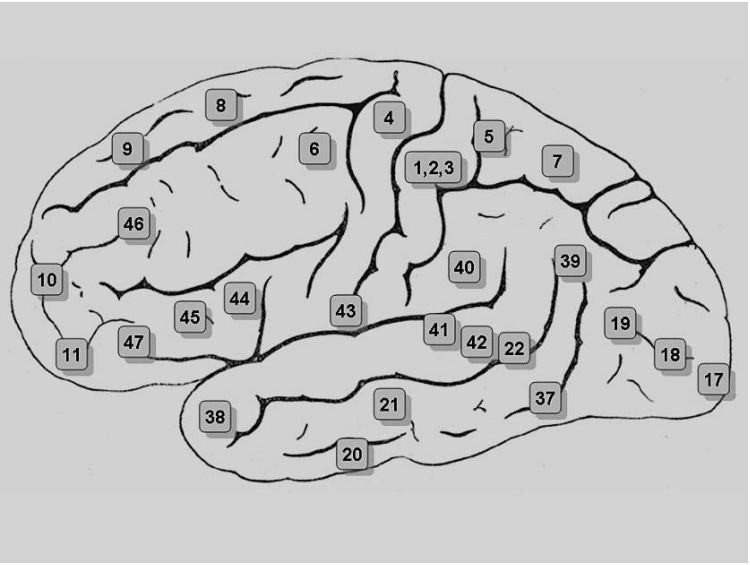

Figure 2 Brodmann's divisions of cerebral cortex

1.1.5 Neurons and Glia

All the tissues and organs in the body consist of cells. The functions of these organs are determined by the specialized functions of cells and their interaction. There are different types of cells in the nervous system i.e. *neurons* and *glia*. It is important to know the

distinction between neurons and glia. There exist 100 billion neurons in the human brain but the glia outnumbers the neurons by tenfold. However, neurons are the most important cells and considered to be the basic unit of brain because neurons sense changes in the environment and communicate these changes to other neurons and command the body's responses to these sensations. A neuron has different parts, cell body, dendrites and an axon. Multiple dendrites grow up from the cell body of a neuron but only one axon at a site called the axon hillock. Dendrites or nerve endings, branch-like projections of the cell make connections called synapses, to other cells as well as to other dendrite and axons. Axon is a cable-like projection of the cell that carries the electrochemical message (nerve impulse or action potential) along the length of the cell. Signals travel from an axon of one neuron to a dendrite of another. Cell body has the nucleus, endoplasmic reticulum, ribosomes (for building proteins) and mitochondria (for making energy). If the cell body dies, the neuron dies. A typical neuron structure is shown in figure 3.

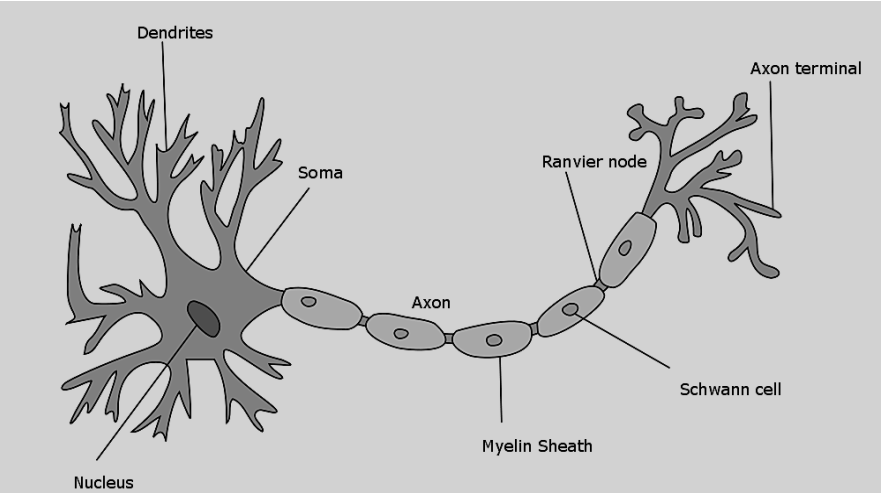

Figure 3 Neuron Structure

A neuron processes and transmits information by electrical and chemical signals. Chemical signals are produced at synapses and specialized connections with other cells. Networks are formed by connecting different neurons and considered to be the core components of the nervous system, which includes the brain, spinal cord, and peripheral ganglia. There exist different types of neurons, sensory neurons, motor neurons and interneurons. Sensory neurons respond to outer world affecting cells of the sensory organs which send signals to the central nervous system. Motor neurons carry signals from the central nervous system and cause muscle movements and affect glands. Interneurons act as bridge to connect neurons to other neurons within the same region of the brain.

On the other side, glial cells are thought to contribute to brain function mainly by insulating, supporting and nourishing neighboring neurons. Astrocytes are the most numerous glia in the brain and fill the spaces between the neurons to provide support and protection to neurons. It probably influences the space, about 20 nm that remains between neurons and astrocytes, causes a neurite can grow or retract. Synaptic junctions are enveloped by the

astrocytes, therefore the neurotransmitter molecules which are released during transmission of neuronal signals, are restricted from spreading, thereby regulating the chemical content of extracellular space. Astrocytes also regulate the concentration of potassium ions in the extracellular fluid.

Myelinating glia is another type of glial cells that provide layer of membrane to insulate axons, called myelin, spirals around axons in the brain. Axon fits inside the spiral wrapping named as *myelin sheath* and axonal membrane is exposed periodically after a short length where the sheath is interrupted. This point is called *node of Ranvier* as shown in figure 3. Myelin serves to speed the propagation of nerve impulses down the axon. There are also other non-neuronal cells, *ependymal cells* that provide the lining of fluid filled ventricles within the brain. Another type of non-neuronal cells called *microglia* function as phagocytes to remove debris left by dead or degenerating neurons and glia.

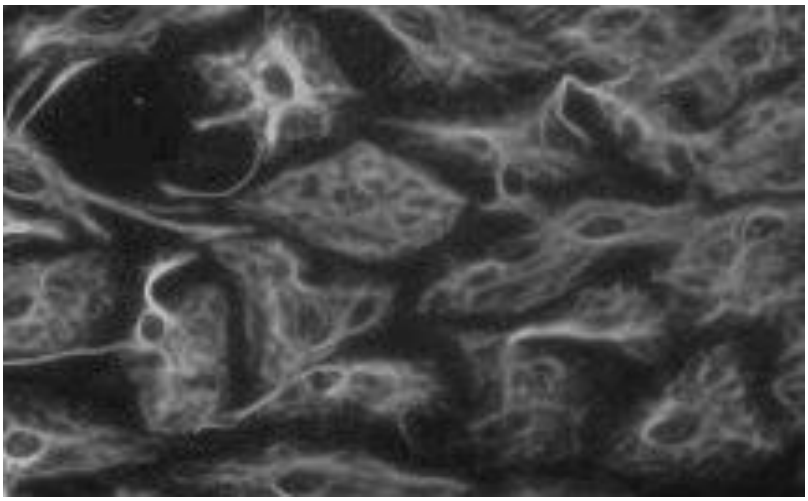

Figure 4 Glial cells: Astrocytes

1.2 The Neuronal Membrane at Rest

You might have heard about reflex action phenomena. Striking lightly the right spot on the knee with a rubber hammer, sensory neurons are activated and generates signal and send it to spinal cord. Interneurons carry that signal in the spinal cord. These neurons connect with other parts of your brain that interpret the signals as being painful. This information is handed over to the motor neurons which controls the movement of your leg. This reflex action requires the nervous system to collect, distribute and integrate information. Conduction of information over a distance is done by neuron using electrical signals that sweep along the axon. Within the cytosol, electrical charge is transferred by electrically charged atoms (ions) instead of free electrons, making cytosol far less conductive. Thus the electrical current passively conducting down the axon would not go very far before it would leak out.

There are some properties that enable the axonal membrane to conduct a special type of signal i.e. the nerve impulse or *action potential.* Individual neurons have encoded information not only in the frequency of their action potentials but also in the distribution and number of neurons firing action potentials in a given nerve. Those cells which are capable of generating and conducting action potentials are said to have *excitable membrane*. Sometimes cells having excitable membrane do not generate impulses then the cells are said to be at rest. During this resting state, the cytosol is charged with negative electrical charge within the surface of the membrane compared to outside. The difference in electrical charge across the membrane is known as the *resting membrane potential*.

1.2.1 Distribution of Ions across the Membrane

Neuronal membrane potential depends on the ionic concentrations on either side of the membrane. These concentrations are estimated in table 1. Importantly, it should be noted that K^+ is more concentrated on the inside whereas on the outside, Na^+ and Ca^{2+} are more concentrated.

Table 1 Ionic concentration on both sides of the neuronal membrane

Ion	Concentration outside (mM)	Concentration Inside (mM)	Ratio Out : In	E_{ion} (at 37^oC) (membrane potential)
K^+	5	100	1 : 20	-80 mV
Na^+	150	15	10 : 1	62 mV
Ca^{2+}	2	0.0002	10,000 : 1	123 mV
Cl^-	150	13	11.5 : 1	-65 mV

These ionic concentration gradients are based on the actions of the ion pumps in the neuronal membrane. The sodium-potassium pump and the calcium pump are very important in the distribution of ions. The *sodium-potassium* pump is an enzyme that breaks down ATP in the presence of internal Na^+. This reaction releases the chemical energy and drives the pump to exchange internal Na^+ for external K^+. The actions of this pump ensure that K^+ is concentrated inside the neuron and that Na^+ is concentrated outside. These ions are pushed by the pumps, which are membrane-associated protein, against their concentration gradients across the membrane at the expense of metabolic energy. The *calcium pump* is also an enzyme that actively carries Ca^{2+} out of the cytosol across the cell membrane. The main objective of these ion pumps is to ensure that the ionic concentration gradients are established and maintained. The sodium-potassium pump is illustrated in figure 5.

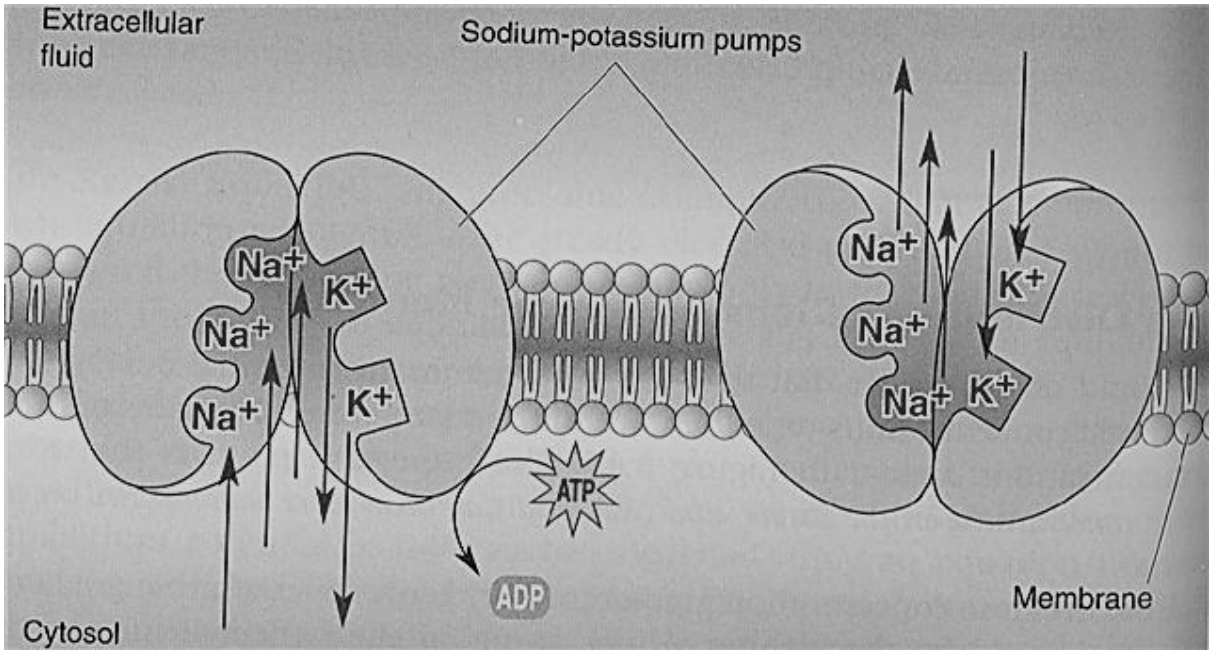

Figure 5 The sodium-potassium pump: Source (2)

1.2.2 Relative Ion Permeability of the Membrane at Rest

Equilibrium potential for an ion is the membrane potential that results if a membrane is selectively permeable to that ion alone. However, in reality neurons are permeable to more than one type of ion. Taking into account, Na^+ and K^+, if only K^+ is allowed to be permeable through membrane of neuron then according to table 1, membrane potential E_k is -80 mV and in case if only Na^+ is allowed then its membrane potential E_{Na} would be 62 mV. However, if both are allowed to be permeable equally then resulting membrane potential would probably be some average of E_k and E_{Na}. Moreover, if the membrane were 40 times more permeable to K^+ than it is to Na^+ then the membrane potential would again be between Na^+ and K^+ but much closer to E_k than to E_{Na}. To calculate resting membrane potential *Goldman equation,* given in (1), is used which is a mathematical formula that considers the relative permeability of the membrane to different ions.

$$V_m = 61.54 \log \frac{P_k [K^+]_o + P_{Na} [Na^+]_o}{P_k [K^+]_i + P_{Na} [Na^+]_i} \quad (1)$$

1.3 Action Potential

An action potential is generated when a stimulus is received by the dendrites of nerve cell of another neuron. It opens the Na^+ channels and if there is sufficient potential is produced to drive from -70 mV up to -55 mV then the process for generation of action potential continues. If the potential reaches the threshold of -55 mV then more Na^+ channels are open. These channels are also known as voltage-gated channels. The influx of Na^+ drives the potential up to about +30 mV. This phase of the action potential is known as rising phase and called *depolarization* phase. In other words, depolarization of the membrane beyond

threshold produces an action potential. How the action potential looks like is shown in figure 6.

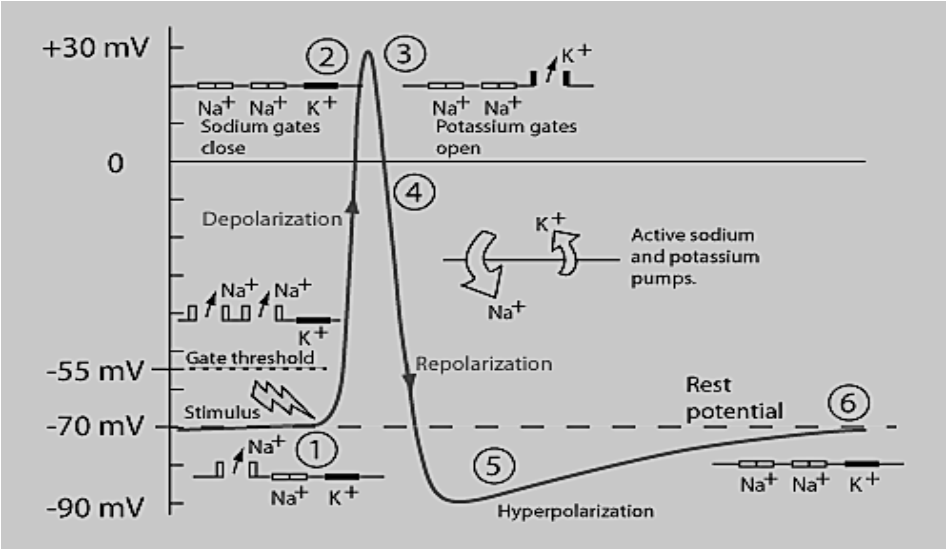

Figure 6 An action potential and its parts

The part of the action potential where the inside of the neuron is positively charged with respect to the outside is called *overshoot*. After reaching the peak point the action potential starts falling down which closes the Na^+ channels and opens K^+ channels. However, K^+ channels are slower to open so a point comes when both Na^+ and K^+ channels are open that causes the system to be neutral and prevent the creation of the action potential. After Na^+ channels are closed and K^+ channels are opened, the membrane begins to repolarize back towards its resting state. This phase of the action potential is known as falling phase and called *repolarization* phase. During the falling phase potential typically undershoots to about -90 mV before coming back to resting potential of -70 mV. This is called *hyperpolarization* phase. This phase either prevents receiving another stimulus during or at least raises the critical threshold for any new stimulus. Finally, after hyperpolarization the Na+ and K+ channels are closed and bring the membrane back to its resting state of -70 mV. From beginning to end, an action potential lasts about 2 milliseconds.

Action potential must be conducted down the axon in order to transfer information from one point to another in the nervous system. Once an action potential is generated at one end of an axon, it propagates only in one direction and does not turn back in the opposite direction. This is because the Na^+ channels are closed therefore the membrane behind it becomes refractory. However, an action potential is generated at either end of an axon by depolarization, hence can propagate in either direction.

1.4 Synaptic Transmission

A *synapse* is a specialized junction where a part of neuron contacts and transfers information to another neuron or cell type. Information flows in one direction from a

neuron to its target cell. First neuron is said to be *presynaptic* and the target cell is said to be *postsynaptic*. Synaptic transmission is the process of information transfer from one neuron to another at the synapse.

1.4.1 Types of Synapses

There are two different types of synapses. Electrical synapses and chemical synapses.

Electrical Synapses

These synapses consist of relatively simple structure and function and allow the ionic current to be transferred directly from one cell to the next. These particular types of synapses occur at specialized sites called *gap junctions*. There is a distance of about only 3 nm between the membranes of two cells to separate them from each other at the junction gaps. Such narrow gaps are spanned by the clusters of special proteins called *connexins*. A channel called *connexon* is formed by the combination of six connexins and two connexons, one from each cell membrane combine together to form a gap junction. These channels are used to pass the ions directly from the cytoplasm of one cell to the cytoplasm of other cell. Almost all the gap junctions have relatively large pore of about 1-2 nm in diameter that is big enough for all the major cellular ions and several small organic molecules to pass through. Gap junction channels and electrical synapses are shown in figure 7.

Electrical synapses are bidirectional because the ionic current pass uniformly well in both directions through these gap junctions and the cells connected by gap junctions are said to be electronically coupled. A *post synaptic potential (PSP)* is produced in the postsynaptic (second) neuron due to action potential in presynaptic (first) neuron that causes flow of small amount of ionic current across the gap junction channels. Similarly, a PSP is produced in the first neuron due to flow of ionic current from second neuron.

Chemical Synapses

The main components of chemical synapses are shown in figure 8. There are synaptic clefts between the membranes of presynaptic and post synaptic neurons to keep them separated that are 20 – 50 nm wide. Matrix of fibrous extracellular protein fills up these clefts. One of the objectives of this matrix is to adhere, the pre and post synaptic membranes with each other. It is the axon terminal also known as presynaptic element as shown in figure 8. This terminal contains *synaptic vesicles* each having a diameter of about 50 nm. These synaptic vesicles are dozens in number and enclosed in small membrane spheres. These vesicles store a chemical used to communicate with postsynaptic neuron. Such chemicals are known as *neurotransmitters*. *Secretory granules* are the larger vesicles having diameter of about 100 nm found on many axon terminals. These granules are sometimes called dense-core vesicles due to dark appearance of soluble proteins in secretory granules.

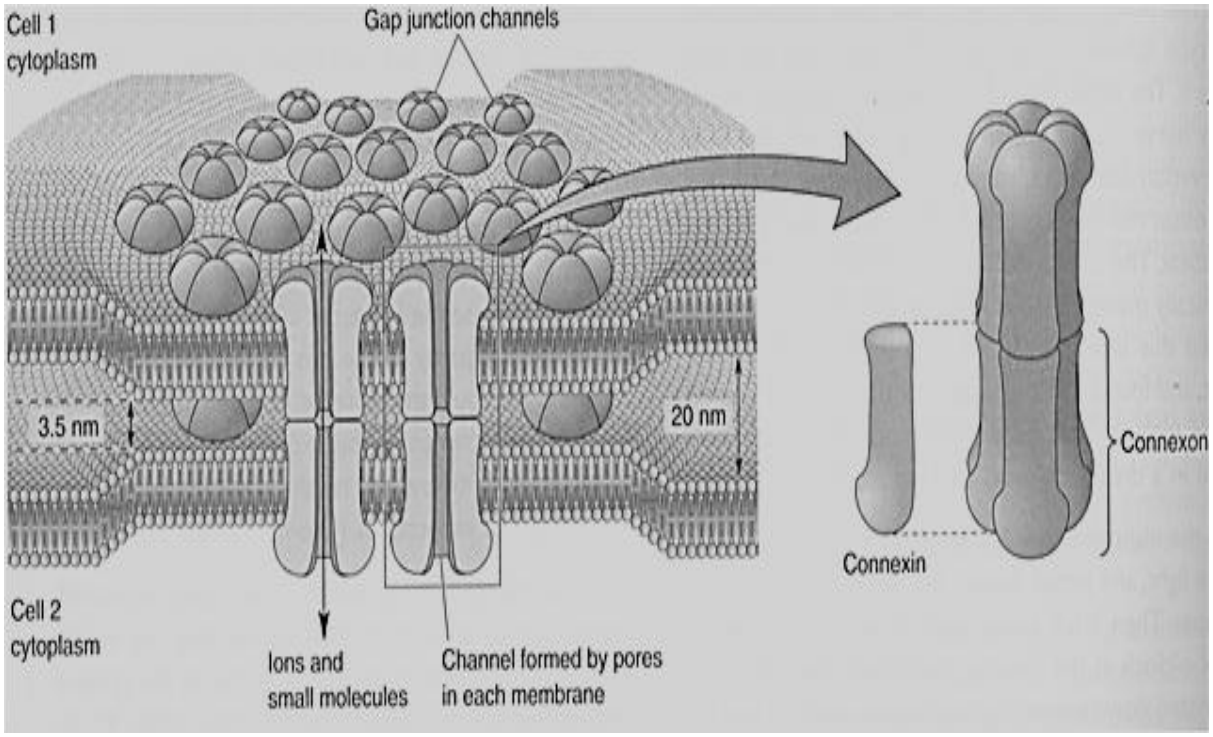

(a)

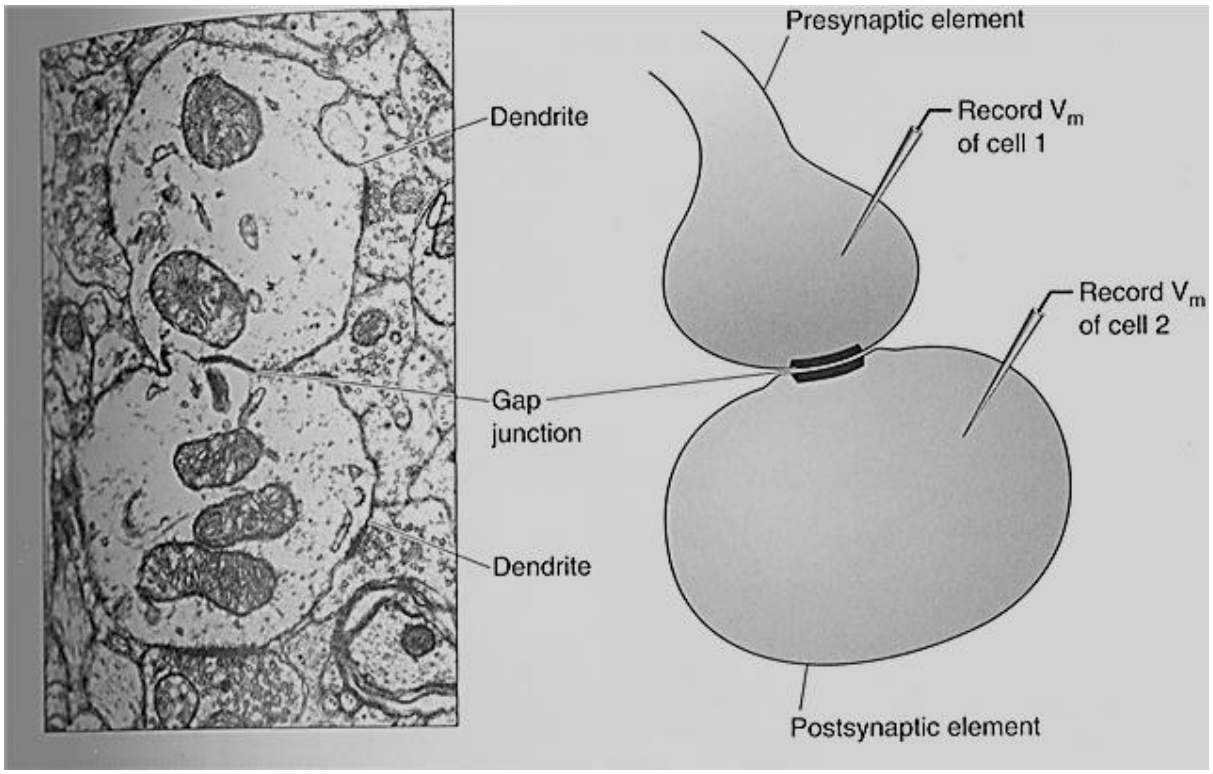

(b)

Figure 7 (a) Gap junction channels (b) electrical synapse: Source (2)

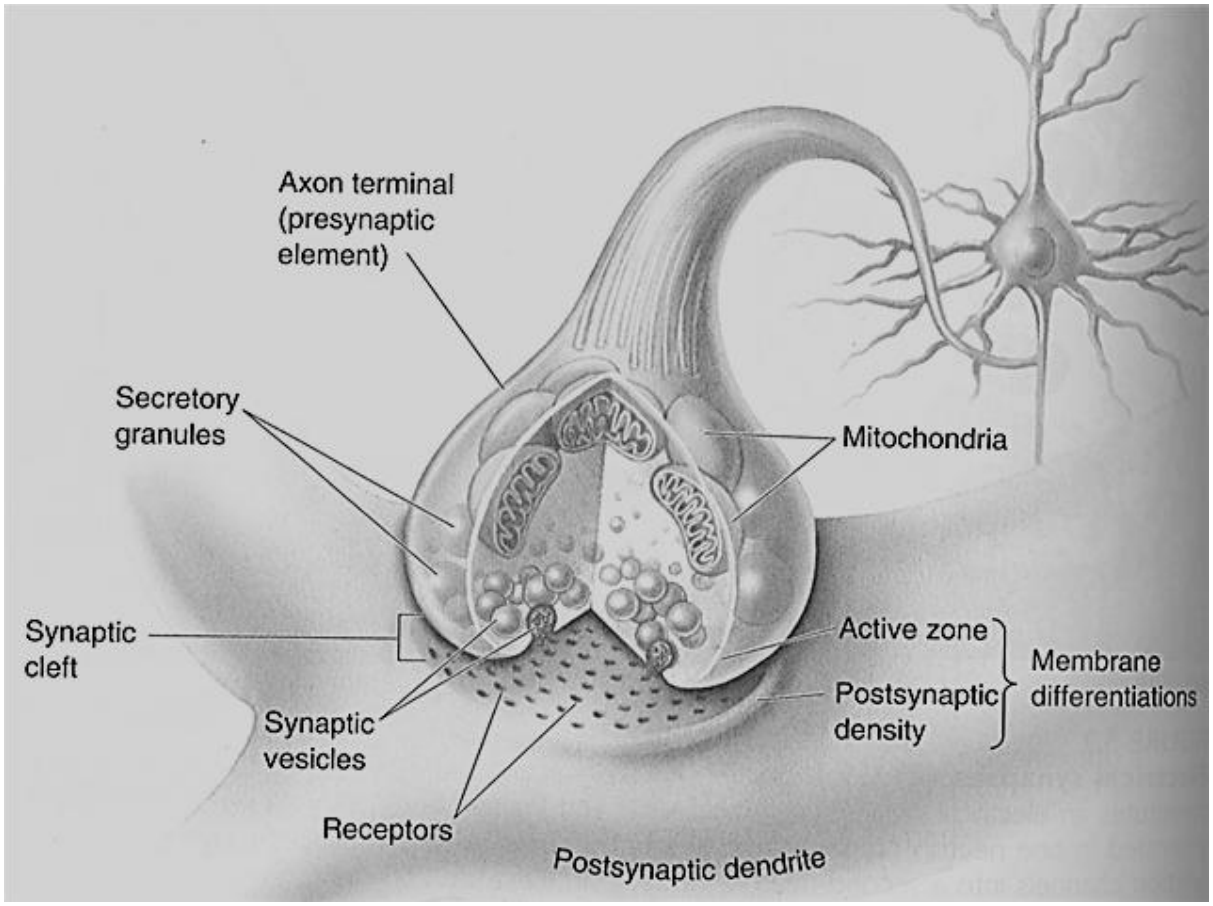

Figure 8 Chemical synapse and its components Source (2)

Active proteins on the presynaptic side transferring into the cytoplasm of the terminal along the intracellular face of the membrane sometimes look like a face of tiny pyramids. The pyramids and the membranes associated with them are the actual sites of neurotransmitter release, called *active zones*. Synaptic vesicles are clustered in the cytoplasm adjacent to the active zones. The protein thickly accumulated in and just under the postsynaptic membrane is called the postsynaptic density. The postsynaptic density contains the neurotransmitter receptor, which convert the intercellular chemical signal into an intracellular signal in the postsynaptic cell.

Moreover, CNS synapses may be distinguished depending on their synaptic arrangements in the CNS i.e. which part of the neuron is post synaptic to the axon terminal. The synapse is said to be *axodendritic*, if the postsynaptic membrane is on a dendrite. The synapse is said to be *axosomatic*, if the post synaptic membrane is on a cell body. The synapse is said to be *axoaxonic*, if the postsynaptic membrane is on another axon. CNS synapses may generally be classified into *Gray's type I synapses* and *Gray's type II synapses*. In Gray's type I synapse, postsynaptic membrane is thicker than that on the presynaptic membrane. Such synapses are also known as *asymmetrical synapses*. Where as in Gray's type II synapse membrane differentiation are of similar thickness, also known as *symmetrical synapses*.

1.4.2 Principles of Chemical Synaptic Transmission and Integration

To understand the principles of chemical synaptic transmission and its integration we must understand the mechanisms, how the neurotransmitters are synthesized and how it is packed into synaptic vesicles, how the vesicles pour out their contents into the synaptic cleft, how the electrical or biochemical response to neurotransmitter is produced in the postsynaptic neuron and how the neurotransmitters are removed from the synaptic cleft.

Neurotransmitters

Transmission of signals from a neuron to a target cell across a synapse is done by neurotransmitters which are packed into synaptic vesicles clustered on presynaptic membrane and released into the synaptic cleft where they are received by receptors on the postsynaptic membrane. Arrival of action potential at the synapse releases neurotransmitters. Neurotransmitters have three main chemical categories, amino acids, amines and peptides. Amino acids and amines are all small organic molecules and are stored in and released from synaptic vesicles. Whereas peptides are large molecules stored in and released from secretory granules. Glutamate, acetylcholine and cholecystokinin are the examples for each neurotransmitter group amino acids, amines and peptides respectively.

Synthesis and Storage of Neurotransmitter

For chemical synaptic transmission it is necessary for the neurotransmitter to be synthesized and ready for release. To synthesize different neurotransmitters there exist different ways. For instance, glutamate and glycine are the building blocks of protein therefore they are present in great quantity in all cells of the body including neurons. However, GABA and the amines are made only by the neurons that release them. A specific enzyme is contained in these neurons that synthesize neurotransmitters from various metabolic precursors. Peptides are synthesized with entirely a different mechanism. Synthesizing is done in the rough ER for a precursor peptide and an active neurotransmitter is yielded by splitting into the Golgi apparatus. Secretory vesicles containing the peptide bud off from the Golgi apparatus and the secretory granules are transported down the axon to the terminal where the peptide is stored.

Neurotransmitter Release

Arrival of an action potential in the axon terminal triggers the release of neurotransmitters. Voltage-gated calcium channels in the active zones are opened due to the depolarization of the terminal membrane. Due to very low concentration of calcium ion about 0.0002 mM, Ca^{2+} will flood the cytoplasm of the axon terminal as long as the calcium channels are open. Exocytosis is a process by which vesicles release their contents. Synaptic vesicles spill out their contents into the synaptic cleft by fusing their membrane to the presynaptic membrane at the active zone. The point at which the synaptic vesicles get ready and wait to release their contents, Ca^{2+} enters exactly at the same point making the exocytosis process

very quick. Endocytosis is a process that recovers the vesicle membrane and refills the recycled vesicle by neurotransmitter. Figure 9 illustrates how the neurotransmitters are released by the process exocytosis.

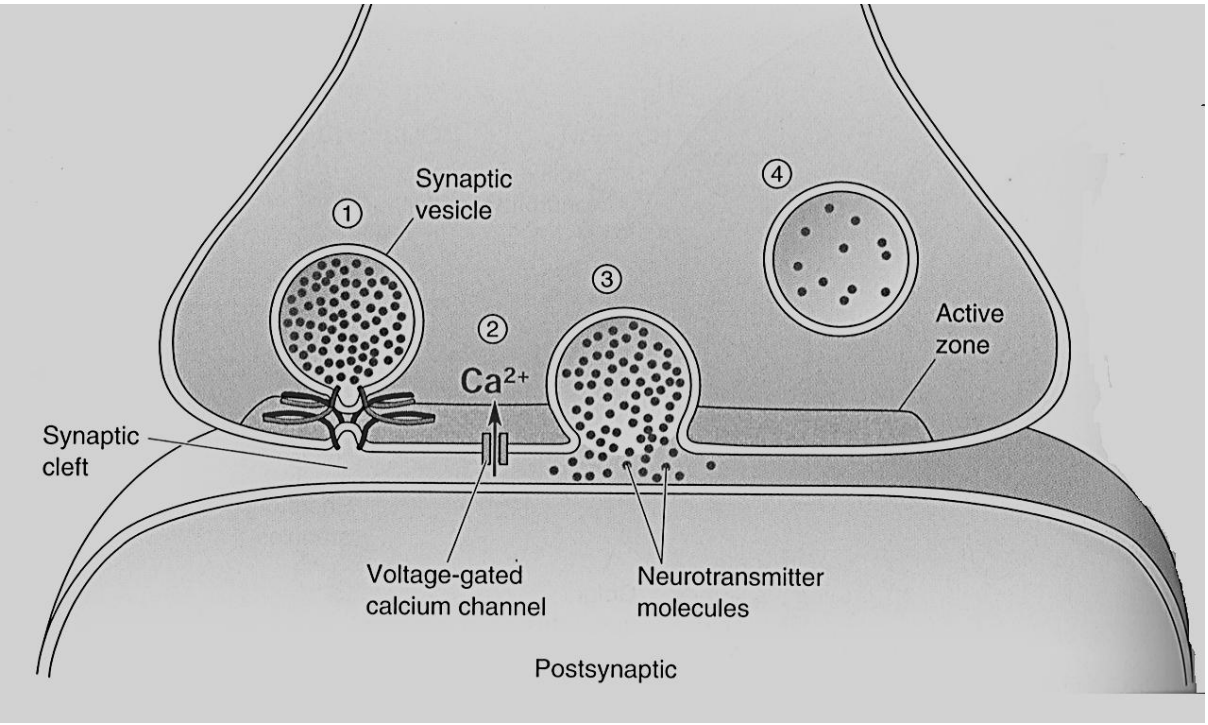

Figure 9 Process of exocytosis: Source (2)

Neurotransmitter Receptors

Although there are 100 different receptors but can broadly be classified into two types, transmitter-gated ion channels and G-protein-coupled receptors. The release of neurotransmitter binds to specific receptor proteins and affects the postsynaptic membrane. Four or five subunits of membrane spanning proteins combines together to form a structure of transmitter-gated ion channels and keeps a pore between them. The pore remains closed in the absence of neurotransmitter. Neurotransmitter induces a conformational change upon binding to particular sites on the extracellular region of the channel. Like the voltage-gated channels, in general, transmitter-gated channels do not show the same degree of ion selectivity. The net effect will be to depolarize the postsynaptic cell from the resting membrane potential, if the open channels are permeable to Na^+. This effect is known as excitatory as it brings the membrane potential toward threshold for generation of action potentials. A transient postsynaptic membrane depolarization caused by the presynaptic release of neurotransmitter is called an *excitatory postsynaptic potential (EPSP)*. However, a transient hyperpolarization of the postsynaptic membrane potential caused by the presynaptic release of neurotransmitter is called an *inhibitory postsynaptic potential (IPSP)*. Transmitter-gated ion channels along with EPSP and IPSP are shown in figure 10.

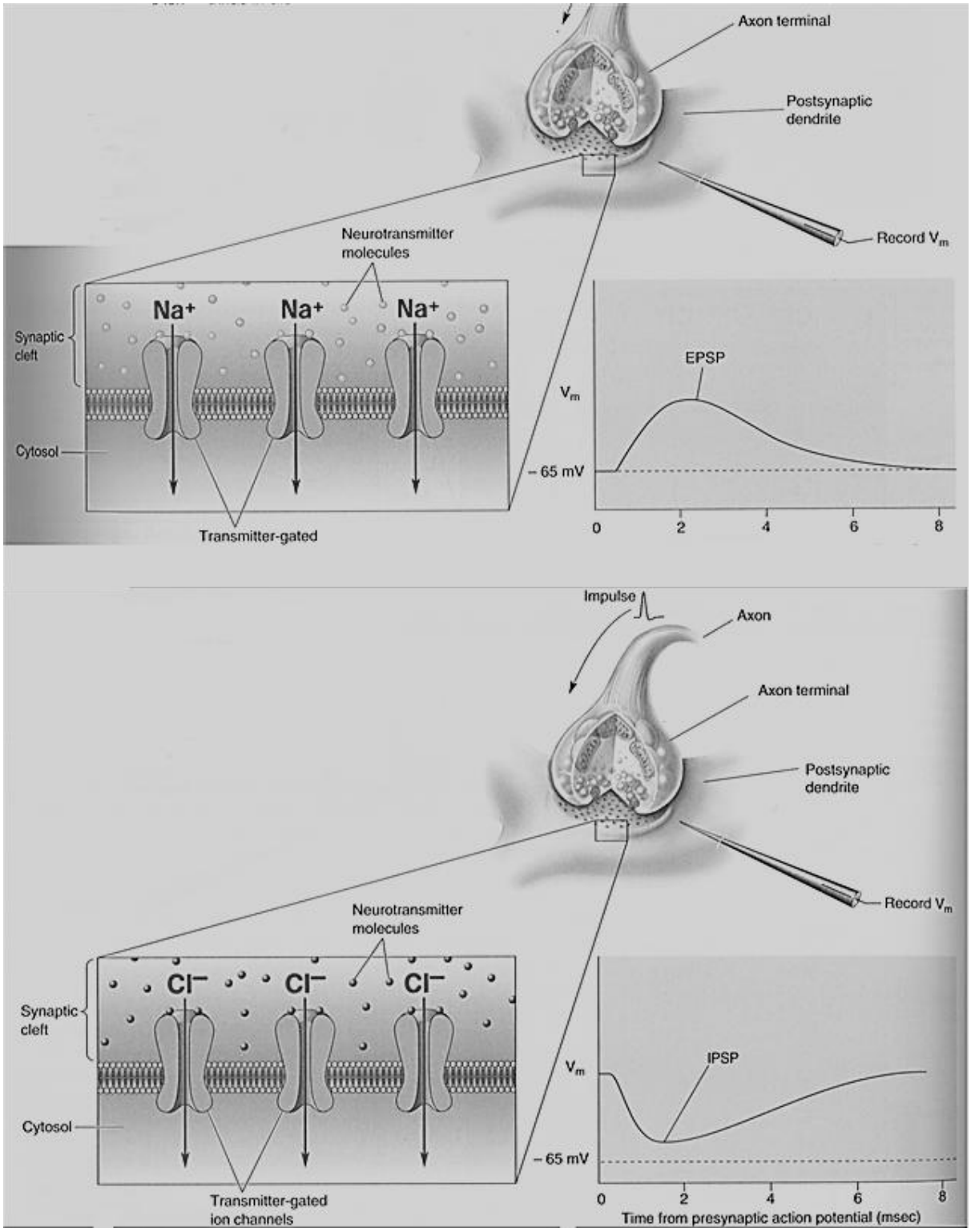

Figure 10 Transmitter-gated ion channels, EPSP and IPSP: Source (2)

Synaptic Integration

The process that combines multiple synaptic potentials into one postsynaptic neuron is known as synaptic integration. To determine, how many vesicles release neurotransmitter into the synaptic cleft during normal transmission, a method can be used that can compare

the amplitudes of miniature and evoked postsynaptic potentials. Such a method is known as *quantal analysis*. This analysis reveals that during transmission of neurotransmitter, about 200 synaptic vesicles are triggered through exocytosis upon arrival of a single action potential at the presynaptic terminal, resulting in an EPSP of 40 mV or plus. In contrast, by the release of single vesicle causes an EPSP of only a few tenths of a millivolt. The difference between excitatory transmission at neuromuscular junctions and CNS synapses is not surprising. A significant postsynaptic depolarization is produced by the addition of many EPSPs i.e. integration of EPSPs. EPSP summation represents the simplest form of synaptic integration in the CNS. There are two types of summation: spatial and temporal. In spatial sum, EPSPs are added together, generated at many different synapses on a single dendrite whereas in temporal summation EPSPs are added together generated at the same synapse occurred in succession of about 1-15 msec. The stronger the sum of excitatory effects, the shorter the time necessary to depolarize the cell to the threshold for eliciting another action potential. This means that the frequency of action potentials, or firing frequency, is an expression of the total synaptic input to a neuron. Figure 11 shows, how the integration of EPSPs take place.

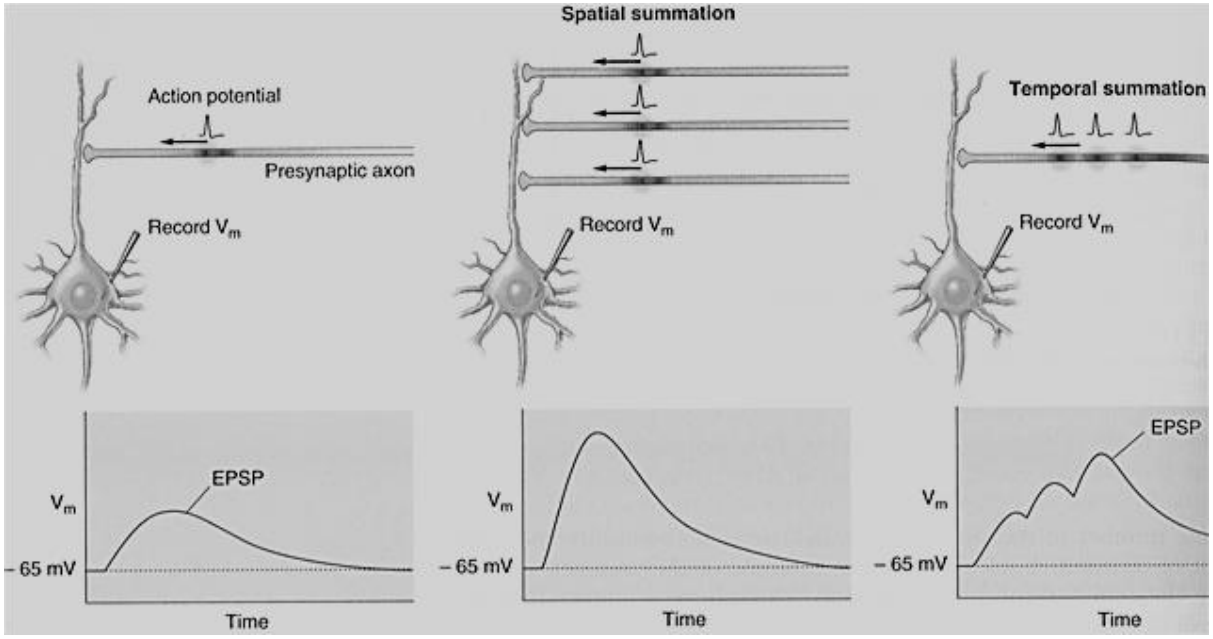

Figure 11 Integration of EPSP: Source (2)

In this chapter we have given an introduction to human and functional properties of neurons, i.e. how the processes take place from one neuron to another. In the next chapter we will discuss about the human visual system and color perception as these are important factors of our study and involves extensive understanding of the concepts in our study.

Bibliography

1. **Clarke E, O'Malley C.** 1968. *The Human Brain and the Spinal cord*, 2nd ed Los Angeles: University of California.

2. **Bear, M., F., Connors, B., W., Paradiso, M., A.** 2007 *Neuroscience: Exploring the Brain.* 3rd ed Lippincott Williams & Wilkins.

3. **Finger S.** 1994. *Origins of Neuroscience*. New York: Oxford University Press.

4. **Grafstein B., Forman DS.** 1980. Intracellular transport in neurons. *Physiological Reviews* 60: 1167-1283.

5. **Levitan I., Kaczmarek L.,** 1997. *The Neuron: Cell and Molecular Biology*, 2nd ed New York: Oxford University Press.

6. S**teward O., Schuman EM.,** 2001. Protein synthesis at synaptic sites on dendrites. *Annual Review of Neuroscience* 24: 299-325.

7. **Doyle DA., Cabral JM., Pfuetzner RA., Kuo A., Gulbis JM., Cohen SL., Chait BT., Mackinnon R.,** 1998. The structure of the potassium channel: molecular basis of K^+ conduction and selectivity. *Science* 280: 69-77.

8. **Hille B.** 2001. *Ionic channels of Excitable membranes*, 3rd ed Sunderland, MA: Sinauer.

9. **Li M, Unwin N., Staufer KA., Jan YN., Jan L.,** 1994. Images of purified shaker potassium channels. *Current Biology* 4: 110-115.

10. **Mackinnon R.** 2003. Potassium channels. *Federation of European Biochemical Societies Letters* 555: 62-65.

11. **Nicholls J., Wallace B., Fuchs P., Martin A.,** 2001. *From Neuron to Brain*, 4th Sunderland, MA: Sinauer.

12. **Armstrong CM., Hille B.** 1998. Voltage-gated ion channels and electrical excitability. *Neuron* 20: 371-380.

13. **Connors B., Gutnick M.** 1990. Intrinsic firing patterns of diverse neocortical neurons. *Trends in Neurosciences* 13:99-104.

14. **Huguenard J., McCormick D.,** 1994. *Electrophysiology of the Neuron.* New York: Oxford University Press.

15. **Neher E.** 1992. Nobel Lecture: ion channels or communication between and within cells. *Neuron* 8: 605-612.

16. **Unwin N.,** 1989. The structure of ion channels in membrane of excitable cells. *Neuron* 3: 665-676.

17. **Connors BW., Long MA.,** 2004. Electrical synapses in the mammalian brain. *Annual Review of Neuroscience*. 27.393-418.

18. **Heuser J., Reese T.,** 1977. Structure of the synapse. In *Handbook of Physiology - Section 1. The Nervous System, Vol I. Cellular Biology of Neurons* eds. Brookhart JM., Mountcastle VB. Bethesda, MD: Americal Physiological Society.

19. **Matthews G.,** 1996. Neurotransmitter Release. *Annual Review of Neuroscience* 19: 219-233.

20. **Stevens CF.** 2004. Presynaptic function. *Current opinion in Neurobiology* 14:341-345.

2. The Visual System and Color Perception

2.1 The Visual System

One of the senses in humans is vision. There are approximately 1 million axons in the optic nerve, constituting almost 40% of the total number of axons in the cranial nerves. The visual system begins with the eye and *retina* lies at the back of the eye. The retina contains photoreceptors which are specialized to transform the light energy into neural activity. The receptors for sight, photoreceptors, are the rods and cones of the retina. Their adequate stimulus is electromagnetic waves with a wavelength between 400 and 700 nm. The photoreceptors do not react to light with shorter (ultraviolet light) or longer (infrared light) wavelengths. The rods are responsible for vision in dim light, whereas the cones are responsible for vision in daylight and for color vision. Visual information is distributed in the form of action potentials, to other parts of the brain through axons of retinal neurons which are bundled into optic nerves. Optic nerves are involved in regulating biological rhythms and controlling eye position and optics. However, the first synaptic relay in the pathway that serves visual perception occurs in a cell group of the dorsal thalamus called the lateral geniculate nucleus or LGN. From the LGN, visual information ascends to the cerebral cortex where it is interpreted and remembered. Conscious use of visual information and many reflex effects elicited by visual stimuli are necessary and sufficient conditions to completely understand the visual system.

2.1.1 The Eyeball and the Retina

The Eyeball

The eyeball is contained in an orbit of dense connective tissues which are covered by the light sensitive retina from the inside. Six small striated muscles or extraocular muscles move the eyeball inside the orbit. The muscles originate in the wall of the orbit, and their tendons insert in the sclera. The choroid is highly pigmented vascular layer that exists between connective tissues and retina. This layer allows the light to enter only through the pupil and also prevents the reflection of light. The amount of light is controlled by the diameter of the pupil that acts as shutter in camera. Cornea and lens are used for refraction of the light. In order to focus the image sharply, ciliary muscles are used that can vary the curvature of the lens. To control and coordinate the position of eyeballs extraocular muscles are attached to the eyeballs externally so that the visual images are formed at corresponding points of the two retinas. Figure 2.1 shows the left eye that is divided in two and horizontal cross section of eye. The space inside the eye in front of the lens and the iris is called the anterior chamber. Small processes of ciliary body produce a clear watery fluid that fills up anterior

chamber. The space behind the lens is filled with a clear jellylike substance called the vitreous body.

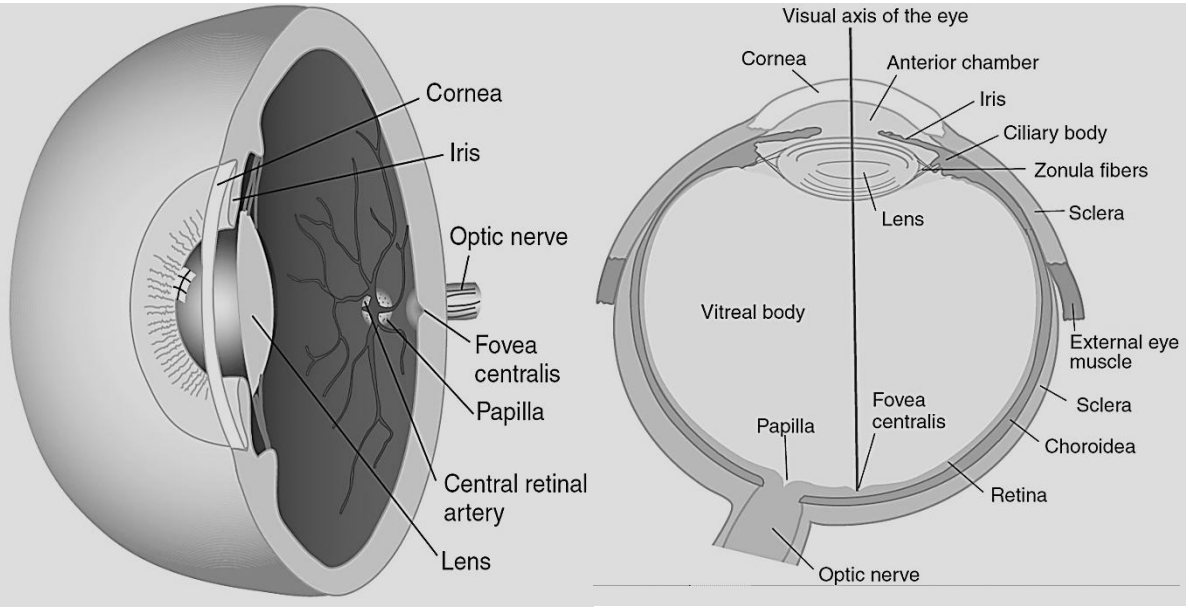

Figure 2.1 left) half part of the left eye divided along the visual axis. Right) Horizontal cross section viewed from above: Source (1)

The light, an eye perceives from our surroundings without moving the eyes and head spans the visual field around us. Obviously the two eyes cover a larger area than a single eye. The visual field of the human eye is shown in figure 2.2. When the light passes through the cornea and lens from a particular point in the visual field, it is refracted to form the inverted image on the retina at a particular point. The visual area covered by single eye is called monocular zone and the visual area covered by both eyes is called binocular zone.

The Retina

The innermost layer of the eye is retina. It forms a very complex structure of layers which are interconnected with several other layers of neurons by synapses. Those neurons sensitive to light are said to be photoreceptor cells. The volume of the retina is spanned by approximately 72% of a sphere about 22 mm in diameter among adult humans. A layered structure of retinal cell types is shown in figure 2.3. Pigmented epithelium that adjoins the choroid is the outer part of the retina. It consists of one layer of cuboid cells with huge amount of granules in their cytoplasm. A layer with photoreceptors and two layers of neurons come after the pigmented epithelium on the internal side of the retina. Next come, the bipolar cells from which retinal ganglion cells receive the transmitted signals. When the light on small circular spots on the retina shines, it excites the retinal ganglion cells most effectively and it is common among all the retinal ganglion cells. These small circular spots are known as receptive fields of the ganglion cells. The axons of the ganglion cells further transmit the signals out of the eye towards the optic nerve that ends up in the diencephalon and mesencephalon. Retina contains photoreceptors, bipolar and ganglion cells only in

those parts which are positioned at the back of the ciliary body. The photoreceptors belong to the central nervous system, unlike other receptors.

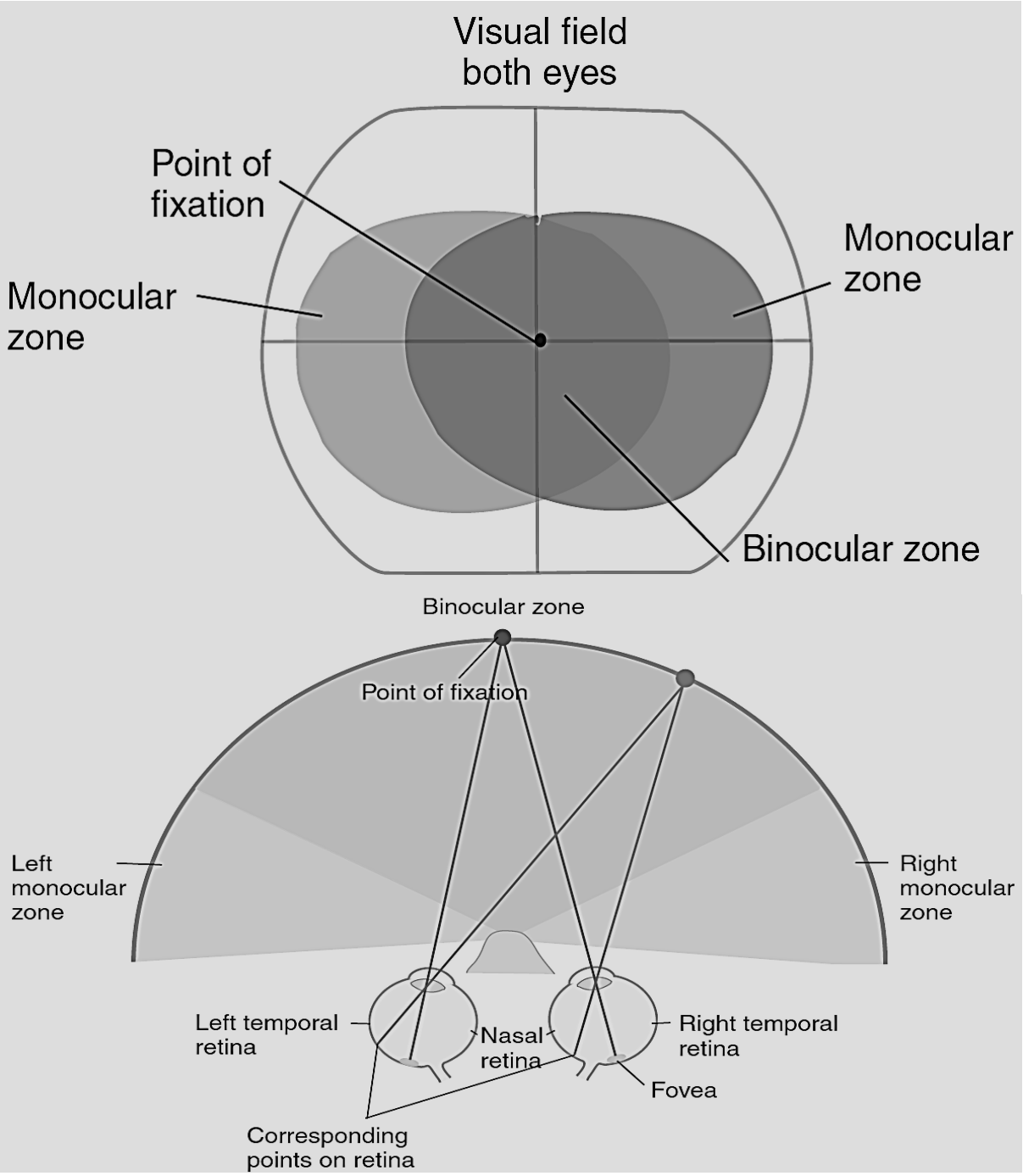

Figure 2.2 The visual field for both eyes. Source (1)

There are two different types of photoreceptors, the rods and the cones which are distinguishable from each other because the outer segments of the cones are tapering and usually somewhat shorter than those of the rods with fewer membranous disks. Rods enable us to see in low light (scotopic vision) whereas cones make our vision possible in daylight (photopic vision). Functional differences between rods and cones are correlated

with structural differences. For instance, as the rods have more number of disks and higher concentration of photopigment which makes them more sensitive to light than cones over one thousand times.

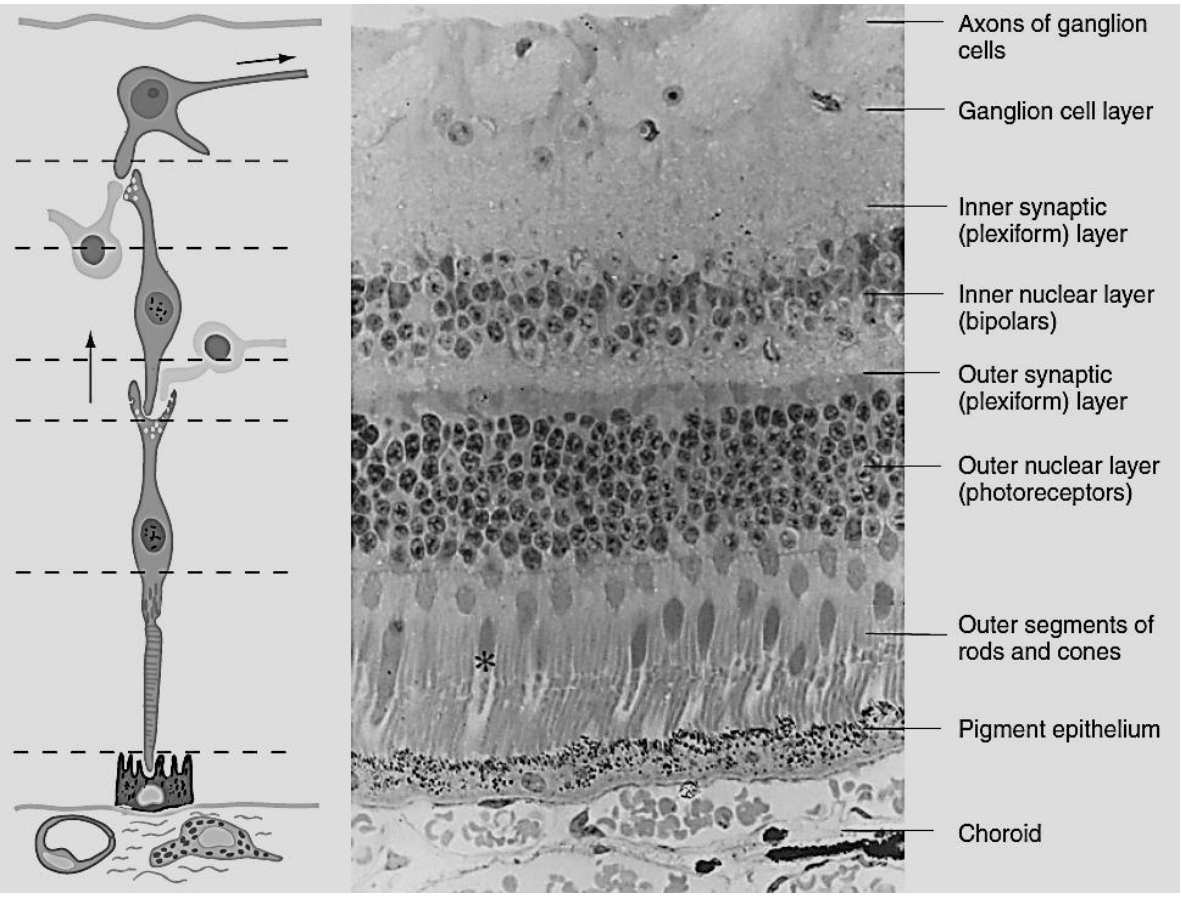

Figure 2.3 Layered structure of retina. Source (1)

All the rods have same distribution of light sensitivity which makes the rods having no discrimination among the light of different wavelengths which is a requirement for **color vision**. The light sensitivity to different wavelengths is maximum in cones. There are three different types of cones out of which one is more reactive to the light having wavelengths in blue part of the spectrum. Second is more reactive to red part and third type is more reactive to green part of the spectrum. Only one type of cone is not sufficient to convey the color information which is possible when all the three types of cones become reactive to color information. The cones are not very sensitive to light, so a strong light is required to perceive the color of objects whereas in the times of dim light objects appeared to be grayish.

Rods and cones also differentiate each other with respect to their connections with other neurons in the retina. There are many connections of rods with each bipolar cell that tends to high degree of convergence. In contrast, there are few connections of cones with one bipolar cell that makes the cones to be much less convergent. Such a difference in convergence shows that the information provided by the cones has higher spatial resolution

than the rods i.e. two points must be farther apart sufficient enough that these are perceived as two but not one, when rods transmit information than when the cones. Therefore, these are the cones that are not only responsible for color vision but also for the perception of patterns and form.

2.1.2 Visual Pathways

The first connection in the visual pathways is established by the axons of the retinal ganglion cells. The ganglion cells move to the back of the eye where they constitute the optic nerve and pass through the orbit to enter the cranial cavity. Here the optic chiasm is formed by combining two optic nerves. Figure 2.5 shows the visual pathways for both the eyes. Some of the axons meet and pass in the optic chiasm and continue to arrive in lateral geniculate body of the thalamus. Here the synaptic contacts are formed between the axon terminals of the retinal ganglion cells and with those neurons which further transmit the signals posterior to the occipital lobe of the brain to establish the optic radiations by the nerve fibers that carry signals from the lateral geniculate body. Figure 2.4 illustrates the optic radiation which show that how the fibers turn around the lateral ventricle and spread partly into the temporal lobe and also show the flow of fibers from the lateral geniculate body to the striate area.

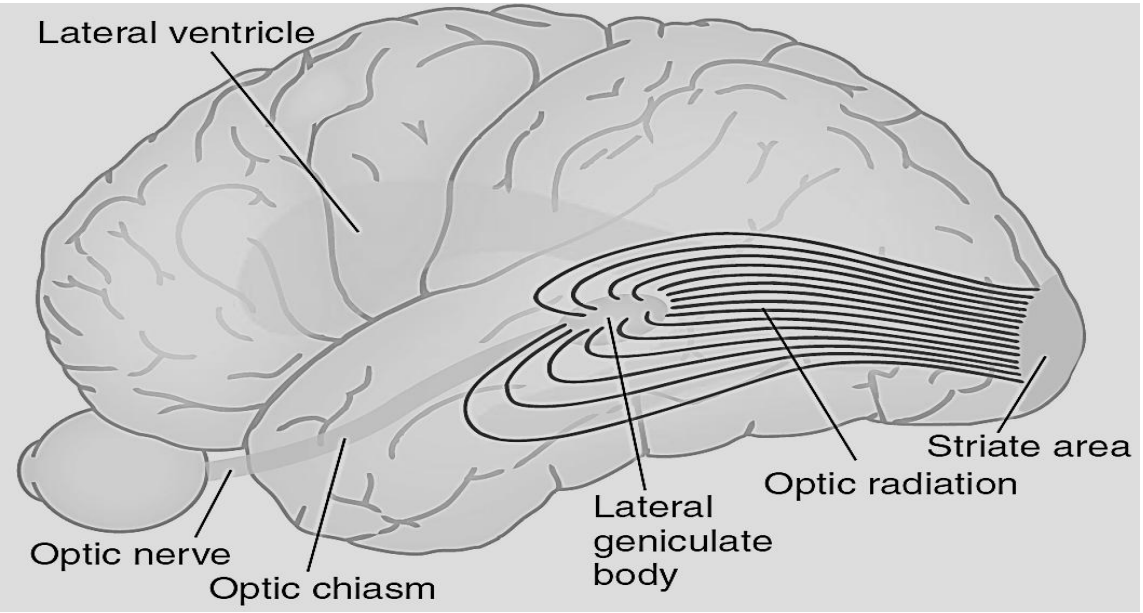

Figure 2.4 Optic radiation. Source (1)

The radiation move towards front from its origin and then laterally towards the back side of the lateral ventricle where it ends up in primary visual cortical area that is present near the calcarine sulcus. Primary visual cortex is also known as striate area or area 17 according to Brodmann's divisions of the brain. Figure 2.5 shows the arrangement of fibers in the optic chiasm. The fibers generated from nasal halves enter into the contralateral sides of the brain and the fibers coming from temporal halves remain on the ipsilateral sides, therefore

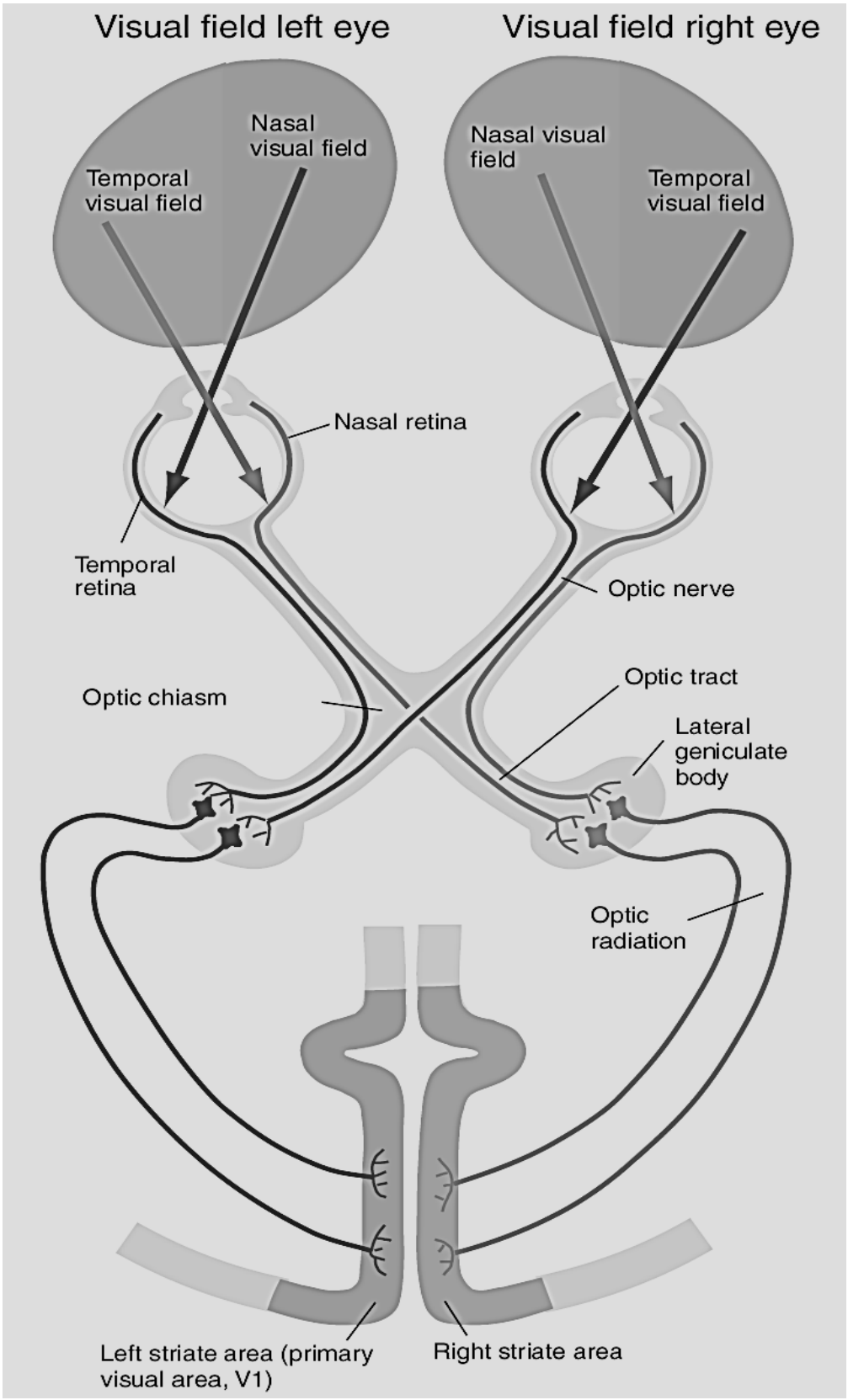

Figure 2.5 Visual pathways with a visual field for each eye. Source (1)

the fibers from nasal half of the right eye joins the left lateral geniculate body and nasal half of the left eye joins the right lateral geniculate body. However, temporal halves of both

sides join the lateral geniculate body on the same side. As we already know that lateral geniculate body has six layers so half of them are devoted to the fibers from opposite side and half of the layers are devoted to the fibers from the same side which means the fibers generated from the optic nerve are kept separate in order to connect with different layers of lateral geniculate body. Usually, two images are formed on the retina and perceived as one through the phenomenon known as fusion, for which the visual axes must be aligned properly. Lower part of the striate area below the calcarine sulcus receive the information coming from upper half of the visual field whereas the area above the calcarine sulcus receive the information coming from the lower half of the visual field. In retinotopic localization, posterior parts of the striate area are associated with central parts of the visual field and anterior parts of the striate area represent the peripheral parts of the visual field.

2.1.3 The Visual Cortex and Processing of Visual Information

In 1962, two Nobel laureate, Hubel and Wiesel discovered that elongated fields of light with contrast between darkness and light affect many cells in the striate area. Moreover, it was shown that a property known as orientation selectivity, requires the light stimulus to be oriented in a specific direction by turning a bar of light to some degrees reduces the response in a clear noticeable manner. Some of other properties were also discovered about the cells in the striate area. The response to moving stimulus is better than the response to stationary stimulus because a moving line or moving contour in a particular direction receives preferable response by many cells. In this way, orientation of the contour is detected along with the direction in which it is moving by the direction-selective cells.

The regions surrounding the striate area are called extrastriate visual areas which are mainly consist of areas 18 and 19 according to Brodmann's subdivisions, where the further processing of visual information take place. Therefore, the visual cortex is not only constituted by the primary visual cortex (V1) but also by the regions surrounding it and parts of extrastriate areas are known as V2 to V5. Normally, the signal arrive the striate area first and later sent to other cortical areas. Different subdivisions of extrastriate area are responsible for different visual processing, like analysis of color, form and movement. This may produce blindness in a part of the visual field if striate area is damaged. The neurons in the striate area provide the basis for cortical analysis of form, movement, depth and color which means that initial analysis and sorting of raw data is done in the striate area and then processed further somewhere else to provide the basis for conscious visual experiences. There are numerous but reciprocal interconnections between the striate and extrastriate areas. However, these interconnections are extremely complex in order to identify and determine the role of each individual area for processing of visual information.

It is clear that visual information in the striate and extrastriate areas is segregated to some extent. Striate area give rise to the bands of projections onto other visual areas and the termination of patches defines the anatomical segregation. It was revealed that there also exist pathways between the cells in the striate area that are influenced by the magnocellular

layers of lateral geniculate. These pathways control the signals for movement and depth cues. Second type of pathways from the striate cells which are influenced by the parvocellular layers of the lateral geniculate have small receptive fields and are orientation-selective and signaling information about forms and patterns. Third type of pathways signals information about color and are originated from striate neurons which are wavelength specific to a large extent. These pathways are considered to be kept partly separate. From striate area (V1) there is an adjacent area V2 through which the information about movement is sent to area V5 whereas the information about color is sent to area V4. From V5 the outflow goes to posterior parietal cortex and from V2 signals about forms and patterns are channeled into inferotemporal visual areas which are present inferiorly in the temporal lobe.

2.2 Color Perception

Strictly speaking, color is not considered to be the characteristic of an object but an experience of the subject while seeing it, which is based on how the information of light reflected from object, having different composition of wavelengths, is processed by the brain. An obvious question about colors is that where and how these are represented in our memory. Although there are some fragmentary answers to such questions, however it is seen that the relationships are reasonably constant between the patterns of stimuli and outside events which strongly motivate us to firmly rely on our brain's interpretation, carried out after processing of stimuli in a certain part of our brain i.e. traffic light colors, forms and movement of objects etc. Color vision is possible with three different kinds of cones which are sensitive to light having different wavelengths as shown in figure 2.6.

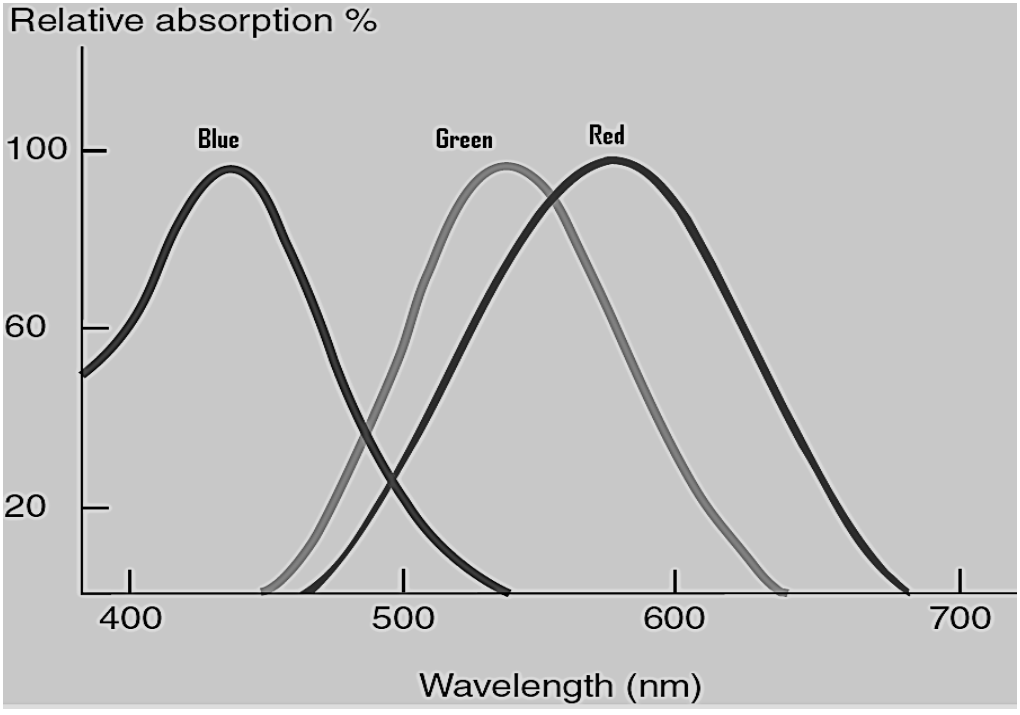

Figure 2.6 Three different kinds of visual pigments. Source (1)

It shows the spectrum of cones sensitive to red, green and blue colors. It is necessary for the brain to measure the degree of stimulation of three kinds of cones in order to assess the composition of wavelengths of light to recognize the color of an object. Figure 2.6 shows the large overlap between the curves, especially between red and green which raises an obvious question of discrimination of each color being critical. To better discriminate colors, these cones are linked to the next pathway to cortex where exist narrower sensitivity curves than cones in retinal ganglion cells and neurons in the lateral geniculate body. Color opponency is a phenomenon in which many ganglion and lateral geniculate cells react with opposite signs to light having different wavelengths where one wavelength excites the cell and other inhibits the cell. For example, red light in the central zone of the receptive field turns ON the response i.e. excites the cell and green light in the peripheral zone turns OFF the response i.e. inhibits the cell. However sometimes blue and yellow light which is a combination of red and green, exhibit the color opponency in some neurons as well as white light that is possible only when all three kinds of cones are stimulated, and darkness. Color constancy is a property of visual system in which, for instance, a banana is identified consistently as yellow, an apple as red and grass as green and so forth even when the differences are perceived. Therefore the composition of wavelength depends on the physical properties of the surface and the light shining on the object. Humans are normally referred to as *trichromats* because they use three-color system. However, colors perceived by all the trichromats are not necessarily the same. Those who lack either the red or the green pigment caused them to be red-green color blind because only two-color system left with them and it is known as *dichromats*.

To visualize the spectral information, trichromatic and color-opponent theories are used and differences in spectral properties are used in discriminating two lights. To fit wavelength discrimination data, Helmholtz used a model that measures difference in stimulation of three types of photoreceptors to quantify the two lights. The aim of color opponent theory is again to find discrimination in data by determining color appearance that also determines discriminability. To isolate color detection mechanism, a habituation technique was used by the Krauskopf and colleagues. They exposed their observers to high contrast modulations of chromaticity during their experiments for a lengthy time and identified that it desensitizes observers in a color-selective way. It was revealed in the results that both red-green and yellow-blue opponent mechanisms were possessed by the observers and can be desensitized independently of one another. However the results also suggested that there exist hue sensitivities along with color opponent mechanisms in observers.

Bibliography

1. **Brodal P.** 2010. *The Central Nervous System: Structure and Function*, 4th ed Oxford University Press.

2. **Arshavsky VY, Lamb TD and Pugh EN.** 2002. G proteins and phototransduction. *Annual Review of Physiology* 64:153-187.

3. **Baylor DA.** 1987. Photoreceptor signals and vision. *Investigative Ophthalmology and Visual Science* 28: 34-49.

4. **Dacey DM, Packer OS.** 2003. Colour coding in the primate retina: diverse cell types and cone-specific circuitry. *Current Opinion in Neurobiology* 13:421-427.

5. **Dowling JE.** 1987. *The Retina: An approachable part of the Brain*. Cambridge, MA: Harvard University Press.

6. **Schnapf JL, Baylor DA.** 1987. How photoreceptor cells respond to light. *Scientific American* 256:40-47.

7. **Gegenfurtner KR.** 2003. Cortical Mechanisms of colour vision. *Nature Reviews Neuroscience* 4:563-572.

8. **Demb, J.B.** 2008. Functional circuitry of visual adaptation in the retina. *Journal of Physiology* 586:4377–4384.

9. **Aine, C.J., et al.** 1996. Retinotopic organization of human visual cortex: departures from the classical model. *Cereb. Cortex* 6:354–361.

10. **Das, A.** 1996. Orientation in visual cortex: a simple mechanism emerges. *Neuron* 16:477−480.

11. **Downing, P.E., et al.** 2001. A cortical area selective for visual processing of the human body. *Science* 293:2470−2473.

12. **Goodale, M.A., Milner, A.D.** 1992. Separate visual pathways for perception and action. *Trends Neurosci*. 15:20−25.

13. **Gulyas, B., Roland, P.E.** 1994. Processing and analysis of form, colour and binocular disparity in the human brain: functional anatomy by positron emission tomography. *Eur. J. Neurosci*. 6:1811−1828.

14. **Livingston, M.S., Hubel, D.H.** 1987. Psychophysical evidence for separate channels for the perception of form, color, movement, and depth. *J. Neurosci*. 7:3416−3468.

15. **Parker, A.J.** 2007. Binocular depth perception and the cerebral cortex. *Nat*. *Rev*. N*eurosci*. 8:379−391.

16. **Self, M.W., Zeki, S.** 2005. The integration of colour and motion by the human visual brain. *Cereb*. *Cortex* 15:1270−1279.

17. **Zeki, S.** 1993. *A vision of the brain*. Oxford: Blackwell Scientific.

18. **Barbur, J.L., et al.** 1994. Insights into the different exploits of colour in the visual cortex. *Proc*. *Roy*. *Soc*. *Lond*. *B* 258:327−334.

19. **Conway, B.R.** 2009. Color vision, cones, and color-coding in the cortex. *Neuroscientist* 15:274−290.

20. **Gegenfurter, K.R.** 2003. Cortical mechanisms of colour vision. *Nat*. *Rev*. *Neurosci*. 4:563−572.

21. **Komatsu, H.** 1998. Mechanisms of central color vision. *Curr*. *Opin*. *Neurobiol*. 8:503−408.

22. **Solomon, S.G., Lennie P.** 2007. The machinery of colour vision. *Nat*. *Rev*. *Neurosci*. 8:276−286.

3. Interpretation and Basic Principles of EEG and Event-Related Potentials

3.1 What is EEG and ERP?

In 1929, Hans Berger discovered that it is possible to measure the electrical activity from the human brain by connecting electrodes to the scalp. The activity recorded has very low voltage, therefore amplified its signal to plot the changes in voltage over time (1). Such an electrical activity is known as electroencephalogram or EEG. After its discovery, its usage started increasing in both scientific and clinical applications. Due to the coarse measurement of the brain activity, it is difficult to assess neuronal processes that focus the cognitive neuroscience. One of the draw backs of EEG is that it is mixed up from hundreds of different sources of neuronal activity, due to which it makes it difficult to isolate individual neurocognitive processes. However, there are other responses associated with sensory, motor and cognitive events, embedded within the EEG and it is possible to extract these responses out of EEG by using many available sophisticated mathematical techniques. These extracted responses or electrical potentials associated with specific event are called event-related potentials or ERP.

In 1964, Walter and his colleagues reported an ERP component known as contingent negative variation or CNV (2). In the trial study, a warning signal was exposed after 500 or 1000 ms of the target stimulus. When the subjects were supposed to press a button upon the target exposure, a large negative voltage was found in the frontal region of the brain. Researchers observed that this negative peak reflects the subject preparation for the upcoming target that separated the response of a warning signal and target stimuli. This discovery motivated many researchers to explore further cognitive ERP components which led to the discovery of P3 component by Sutton et al. (3) that peaked around 300 ms of post-stimulus. An example experiment is shown in figure 3.1 in two different stimuli were presented to the subject i.e. frequent stimuli X's and infrequent stimuli O's, on the screen and the EEG was recorded form Pz electrode site, filtered and amplified. The rectangles in the figure 3.1 show an 800 ms epoch after the onset of stimuli. Although there is much larger variability in each trial, however averaged ERPs for the X's and O's are shown in figure 3.2 and a large peak i.e. P3 is visible around 300 to 400 ms after the stimulus was presented, during the infrequent O's. Note that positive side is shown downward. There is a sequence of positive and negative peaks or waves or components. These peaks are labeled as P1, N1, P2, N2 and P3 in which P and N represent positive and negative deflections and the number represent peak's position with respect to time. Furthermore, these peaks represent flow of information through the brain. Regardless of what task the subject is doing, P1 is elicited as an obligatory sensory response and P1 amplitude may be influenced with task

variations, whereas the stimulus parameters such as luminance may strongly influence the P1 wave.

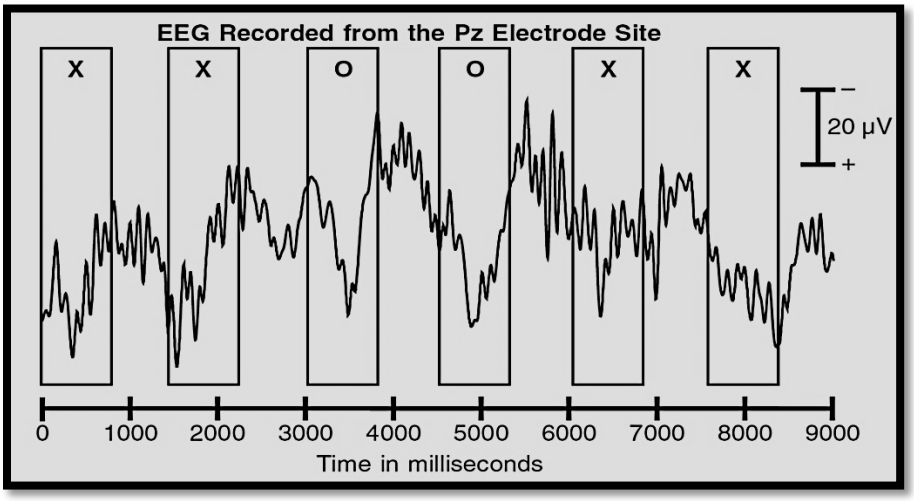

Figure 3.1 Presentation of Stimulus: Odd-ball paradigm

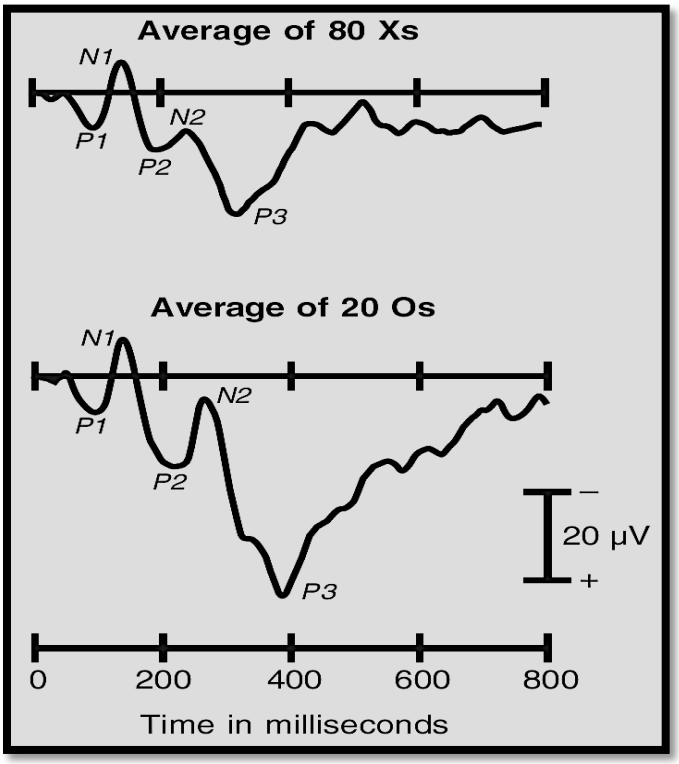

Figure 3.2 Average of frequent stimuli X's and infrequent stimuli O's. Source (11)

P3 wave do not depend on the physical properties of the presented stimulus but may vary depending on the task performed by the subject. Although there are distinctive scalp

distributions of each ERP component that shows the location of patch of cortex where it was actually produced even then the neural source generator of ERP is not easy to determine simply by analyzing the distribution of voltage over the scalp. Here the following steps to conduct such type of experiment and to analyze the results. After designing a suitable protocol for the experiment that devise the order and sequence of different stimuli to be elicited, an EEG is recorded by placing electrodes on the subject's scalp. Since the EEG recorded on the scalp has very low voltage, therefore it is amplified and digitized in order to see the visual output on the monitor screen. Various artifacts like EMG/EOG are embedded in the EEG. To remove these artifacts, some trials are dropped from the EEG manually and some are subtracted using mathematical algorithms like independent component analysis and various other signal processing techniques. Once the artifacts are eliminated and the noise is removed, an averaging is performed to extract the epochs. The size of ERP and the exact time at which the event is occurred are measured to perform statistical analyses. After all the necessary preprocessing, different features are extracted to visualize and analyze the ERP components for further interaction with other modalities. There exist very huge versatility and different techniques in this regard and require practical experience to understand the EEG/ERP study.

3.1.1 Reliability of ERP Waveforms

In most of the published work grand average ERP waveforms are presented which are produced by averaging all the waveforms of the individual subjects. Grand averaged ERPS could both be good and bad, good in a sense that it hides the large variability in waveforms which makes things difficult to find similarities and bad in a sense that it loses the accurate information for individual subjects. Figure 3.3 shows different waveforms in different subjects chosen randomly from an experiment, e.g. left column shows three waveforms from three individual subjects and right column shows three waveforms from the same subjects recorded in different sessions. We can observe a large variation in ERP waveforms among different subjects and very small variation within the same subject in different sessions. Note that every waveform has P1 and N1 peaks having different amplitudes from subject to subject. The lower part in figure 3.3 shows a time line and average of all subjects.

An obvious question arises, what are the possible causes for such variability. As the variability within a subject is very small from session to session, this may be influenced by the number of hours of sleep taken in the last night, time since the last meal, body temperature (4). On the other hand, the variability is very large from subject to subject and this may be influenced by location and orientation of the cortical generator source of an ERP component due to unique cortical pattern for each individual subjects. Moreover, shape of the ERP waveforms be certainly affected by the number of other factors, like drugs, age, psychopathology and even personality. We can notice one attribute in grand average ERP that its peaks are neither high as

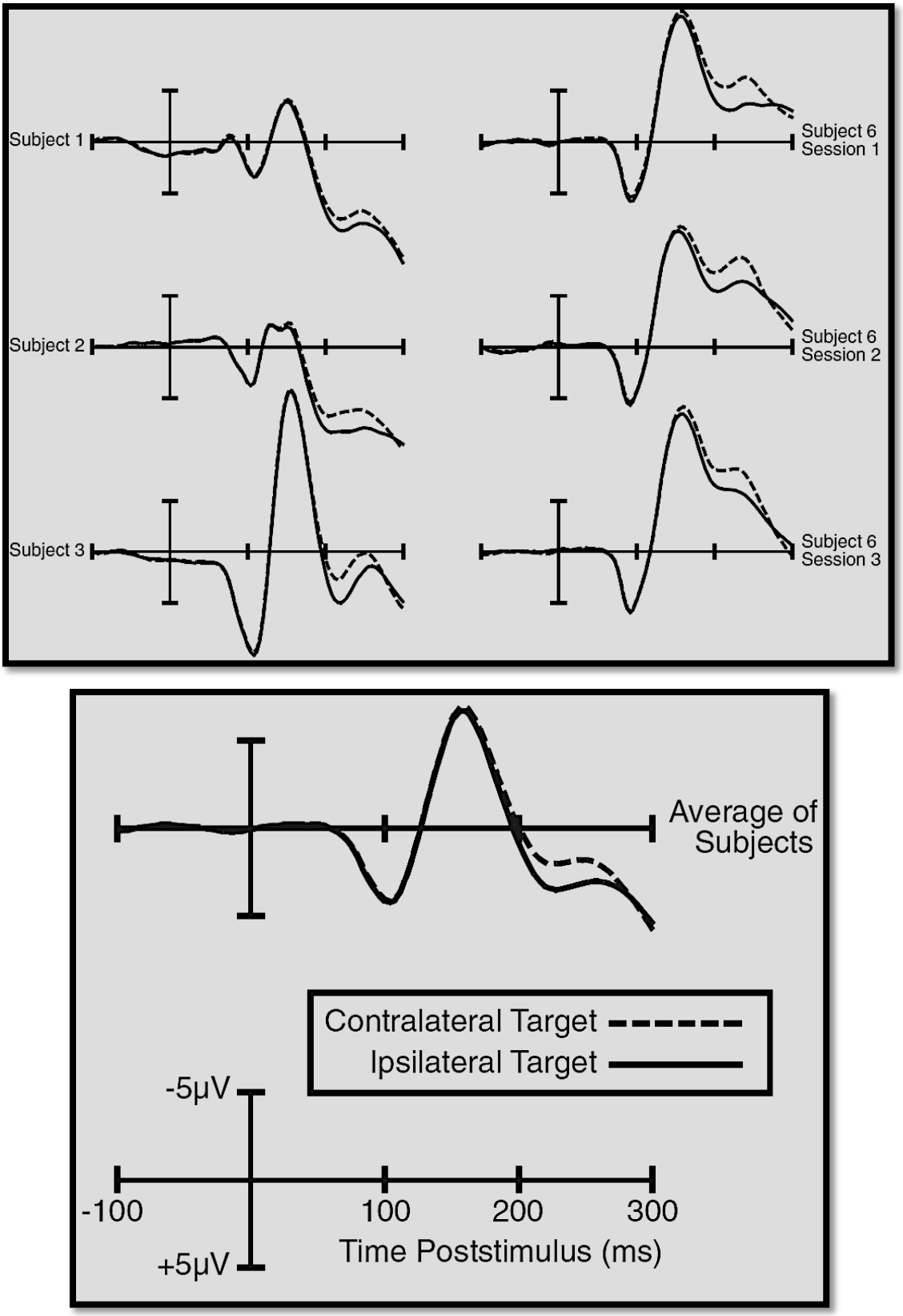

Figure 3.3 Variability in ERP waveforms Source (11)

in the individual waveforms from subject to subject nor lower as in individual waveforms from subject to subject. Furthermore, the time points at which peak value for one subject are not the same as for another subject and if the voltage is positive at some time points in one subject, it may be negative in another subject at the same time points. Grand average looks quite attractive than any other average of different subjects, however the waveforms looks different and odd if the stimulus and corresponding task are different between the experiments.

3.1.2 Visual Sensory Responses

C1 Wave

C1 wave is the first major visual ERP component that is largest at midline electrode sites in posterior region. Due to its polarity variation, it is not labeled as P or N and it is generated in area V1 i.e. primary visual cortex. The information coming from the lower visual field is decoded above the calcarine fissure and the information coming from the upper visual field is decoded below the calcarine fissure, therefore the scalp above the calcarine fissure generates a positive voltage for stimuli in the lower visual field and the scalp below the calcarine fissure generates a negative voltage for stimuli in the upper visual field (5) (6). C1 wave is very sensitive to stimulus parameters e.g. contrast and spatial frequency and typically onsets 40-60 ms post-stimulus and peaks at 80-100 ms post-stimulus.

P1 Wave

P1 wave starts after the C1 wave and it is largest at lateral occipital electrode sites. P1 wave's onset time is around 60-90 ms post-stimulus and peaks between 100-130 ms, however it is difficult to accurately assess the onset time for this wave due to overlap with the C1 wave. P1 latency also varies because of stimulus contrast. Studies suggest that beginning of P1 wave is localized in dorsal extrastriate cortex and later segment of P1 wave is localized ventrally in the fusiform gyrus (7). This wave is also sensitive to stimulus parameters and to the direction of spatial attention (8).

N1 Wave

N1 wave starts after the P1 wave and it has several visual subcomponents. First peak of N1 comes at 100-150 ms post-stimulus at anterior electrode sites and two other posterior N1 components peaks around 150-200 ms post-stimulus, one of them arising from parietal cortex and the other from lateral occipital cortex. When subjects perform discriminative task, lateral occipital N1 subcomponent appears to be larger than when subjects perform detection tasks (9).

P2 Wave

N1 wave is followed by distinct P2 wave at anterior and central scalp sites. N1 wave depends on stimuli that contains target features and is enhanced whenever there are infrequent target stimuli (10) which makes P2 wave similar to P3 wave. If the target is defined by simple stimulus features then P2 effects occur, however P3 effects occur for complex target stimuli. Posterior P2 wave is not much known to the researcher's community because it is difficult to distinguish from the overlapping N1, N2 and P3 waves.

3.2 Designing ERP Experiments

Experimental design is one of the important elements of an ERP experiment for further analysis and processing which if in the beginning is over looked, it may cause to produce unreliable results. Literature suggests some rules and strategies to be carefully observed while performing experiments and later offline analysis and processing. As we know there exist series of peaks and valleys in an ERP waveform that show voltage deflections acquired by the sum of several relatively independent and latent components. One of tedious problems in designing and interpreting ERP experiments is to isolate such latent components in order to measure them independently. One of very important aspects is to distinguish between the observable peaks and the latent components. However some rules and strategies (11) are described below.

Rule 1. Peaks and components should not be considered same because the point at which the voltage arrives a local maximum, do not contain anything special.

Rule 2. Just a single ERP waveform cannot be effective and supposed to be impossible in estimating the peak latency and time course.

Rule 3. It is not considered to be appropriate to compare raw ERP waveforms with an experimental effect.

Rule 4. Differences in peak amplitude and latency do not necessarily correspond with differences in size and timing of latent components, respectively.

Rule 5. Averaged ERP waveforms do not represent accurately the individual waveforms; however the earlier onsets and latest offsets from individual trial are reflected in onset and offset of averaged waveform.

Rule 6. Try to avoid same physical stimuli across different psychological conditions.

Rule 7. If it is not possible to avoid the physical stimulus confounds, a controlled experiment is conducted to evaluate their validity because an ERP may be affected by a small physical stimulus difference.

Rule 8. While comparing averaged ERPs which are based on different number of trials, be careful and informed e.g. if averaged ERP1 is obtained using 20 trials and an averaged ERP2 is obtained using 40 trials then both ERPs are expected to have differences that cannot be ignored.

Rule 9. Be cautious when the presence or timing of motor responses differs between conditions.

Rule 10. Whenever possible, experimental conditions should be varied within trial blocks rather than between trial blocks.

Rule 11. Never assume that the amplitude and latency of an ERP component are linearly or even monotonically related to the quality and timing of a cognitive process. This can be tested, but it should not be assumed.

The Hillyard Principle.

Always compare ERPs elicited by the same physical stimuli, varying only the psychological conditions.

3.2.1 Avoiding Ambiguities in Interpreting ERP components

Apparently it seems that there exists no general approach to determine the latent components from observed ERP waveforms, however researchers are encouraged to follow some strategically approach that should minimize the factors leading to ambiguous relationship between the latent components and the observed ERP waveforms. For example, if two different ERP waveforms are obtained from two sets of words then it is important to know which set of words has elicited larger effect in N400 or P3. Here we present some strategies that should be carefully observed.

Strategy 1. *Focus on a specific component*. It is better to focus on one or two components to keep the things simpler to have more reliable and precise results because the more the components the larger mess will be created during analysis.

Strategy 2. *Use well-studied experimental manipulations*. It is sometimes good to analyze the well-characterized component under nearly the same conditions which were used to study the same component.

Strategy 3. *Focus on large components*. It is better to focus on larger components like P3 and N400 because such components dominate the observed ERP waveform and become relatively insensitive to interference from other components.

Strategy 4. *Isolate components with difference waves*. The difference waves are used sometimes to isolate the components. For instance, if you are interested in some particular component like P3 or N400 for two different conditions 1 and 2 then each trial should contain a sequence of two conditions in order to see any differences observed between condition 1 and condition 2.

Strategy 5. *Focus on components that are easily isolated*. The strategy of isolating components may be refined by focusing on those ERP components which are relatively easy to isolate. For example, movement preparation which is reflected by lateralized readiness potential and is distinguished by its contralateral scalp distribution.

Strategy 6. *Use component-independent experimental designs*. One of the good approaches is to design a component independent experiment which means that the changes observed in ERP waveforms do not consider which latent ERP component is responsible for that change.

3.3 ERP Recording

In this section we will discuss the basic principles of ERP recording to make sure the importance of clean data. Having low level of noise increases the likelihood of obtaining statistically significant results. It is difficult to view the ERPs individual trial in EEG and using signal averaging it is possible to isolate ERPs from the EEG noise. The more the number of trials, the smaller the amount of residual EEG noise therefore it is very crucial to decide the number of trials sufficient for ERP averages to minimize the noise. However, 30 percent noise may be decreased by doubling the number of trials and 50 percent reduction in noise requires four times the number of trials (11).

3.3.1 Active and Reference Electrodes

A certain number of voltages are recorded using two terminals, positive and negative and current flows from positive to negative terminals. EEG is also recorded as potential between two electrodes mounted on the scalp. If we measured the electrical potential between an electrode on a subject's scalp and a stake driven into the ground, the voltage would reflect any surplus of electrical charges that had built up in the subject (assuming the subject was not touching a conductor that was connected to earth), and this static electricity would obscure any neural signals. We could put an electrode somewhere on the subject's body that was connected to earth, and this would cause any static electricity in the subject to discharge into the earth, eliminating static differences and making it easier to measure changes in neural signals over time. However, it is dangerous to directly connect a subject to earth, because the subject might receive a dangerous shock if touched by an improperly grounded electrical device (such as a button box used for recording responses). It is possible to create a virtual ground in the amplifier's circuitry that is isolated from earth and connect this ground to a ground electrode

somewhere on the subject. You could then record the voltage between a scalp electrode and this ground electrode. However, voltages recorded in this way would still reflect electrical activity at both the scalp electrode and the ground electrode, so it would not provide some sort of absolute measure of electrical activity at the scalp electrode. Moreover, any environmental electrical noise that the amplifier's ground circuit picks up would influence the measured voltage, leading to a great deal of noise in the recording.

The ground circuit that picks up the noise creates problem and this problem is solved using differential amplifiers in EEG amplification system. For this purpose, three electrodes are used to record EEG activity i.e. active electrode (A), reference electrode (R) and ground electrode (G). Active electrode is place on the scalp at desired site; whereas reference electrode is placed elsewhere on the body e.g. ear lobe and ground electrode is located at some convenient location on subject's head or body. The difference between AG and RG is amplified and since ground activity is same for AG and RG therefore it is eliminated by the subtraction.

An ERP waveform reflects the difference of electrical properties at the active and reference electrodes sites. If a potential could be measured for charges to move from one point to the average of the rest of the surface of the body then we can reasonably say that the voltage is recorded at a single site. Naturally, the active electrodes are placed near the active tissues and the reference electrode is kept at a distance assuming the site to be neutral. As the activity near the active electrode changed, researchers assumed that this would influence the voltage at the active site but not at the reference site. When obtaining recordings from several active sites, the same reference electrode is typically used for all of them.

3.3.2 Electrical Noise and Electrode Impedance

Scalp EEG has tiny voltage fluctuations which are typically less than 1/100,000th of a volt and must be amplified by 10,000 – 50,000 times to measure accurately. A typical laboratory contains many other sources of electrical activity which are quite larger in voltage than EEG that could cause to produce small voltage fluctuations in the subject, in the electrodes and in the wires connected to subject and amplifier. These induced voltages may be eliminated using filters and by other post-processing techniques, however it is always good to eliminate the noise at the source. As we already know that voltage oscillations in a conductor induce small voltage oscillations in the nearby conductors so it also shows up in the EEG. We may consider two sources of noise in an ERP lab i.e. AC line current and video monitors. AC line current has sinusoidal oscillations and operates at 50 or 60 Hz and it may induce a line noise in EEG recording whereas video monitors operate at a refresh rate between 50 – 120 Hz and induces spiky noise rather being sinusoidal and remains unable to reduce by the averaging process because such noise is time-locked.

These sources of noise may be controlled using several approaches. Using amplifier's filter to attenuate the noise is considered to be the most common approach. Usually in cognitive experiments, the meaningful information is contained in 0.1 – 30 Hz band so the noise can easily be filtered out by eliminating everything above 30 Hz that includes line noise and video noise with attenuating the actual ERPs. Moreover, line filter is embedded in many amplifiers to specifically eliminate 50 or 60 Hz noise. Another approach is adopted by placing the subject in an electrically shielded chamber to minimize the noise. If still there are noise sources inside the chamber then this approach could not be effective. However, two common approaches are used to solve this problem. First, the video monitor can be placed just outside the window in the chamber provided the window is made up of treated shielded glass. Secondly, the monitor can be placed inside the Faraday cage as shown in figure 3.4, that is cheaper to build for just a 200 – 400 €.

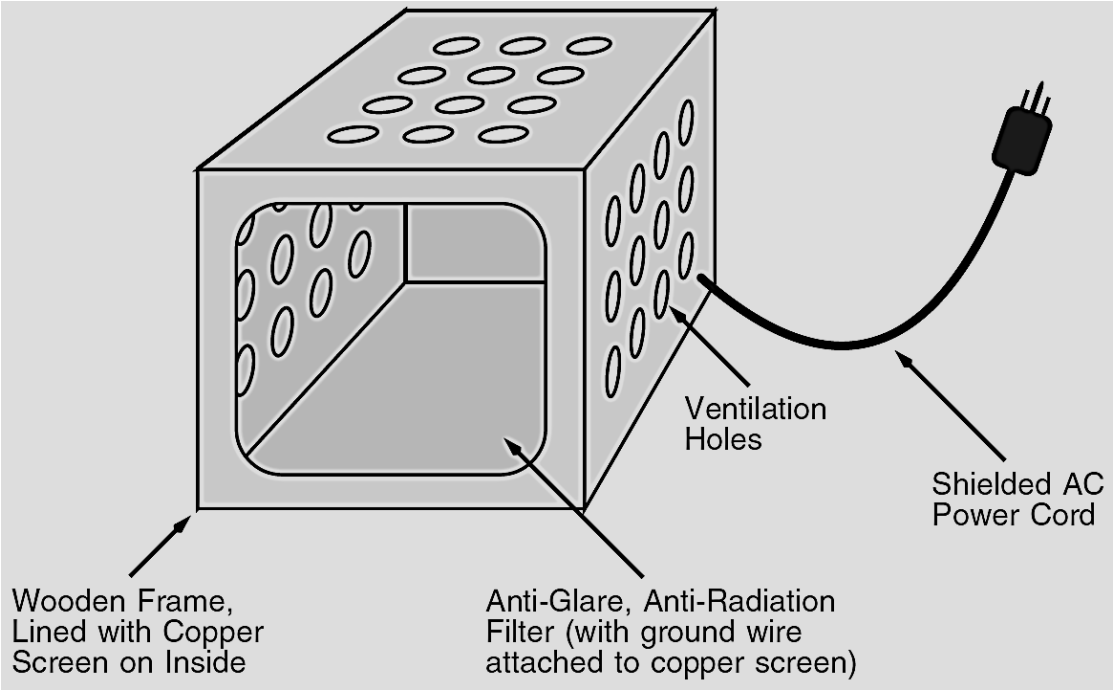

Figure 3.4 Faraday cage

Faraday cage has copper screen shielding which is surrounded by wooden exterior having ventilation holes. To make the monitor visible to the subject, a shielded piece of glass having ground wire along with a shielded AC power cord is placed at the front. Electrical noise in the EEG may dramatically be reduced using a well shielded Faraday cage. Ideally, it is important to make sure that there is nothing that could create electrical noise inside the chamber. It is also noticed that the cables leading from amplifier inside the chamber create significant electrical noise. Such noise may be eliminated by encasing these wires. Furthermore an online frequency spectrum module can be developed to see what frequency bands are involved in the recorded

EEG data and this will help in getting immediate noise effects that can be further removed by modifying and/or controlling the physical parameters which are responsible for inducing electrical noise.

Having discussed the nature of voltages recorded at the scalp leads us to further discussion about electrodes. An electrode is just a conductive material (some metal) placed on the scalp through the wire. Since some metals corrode quickly and loose the conductance so it is important to take care of the metal choice. The electrodes covered with thin coating of silver-chloride (Ag/AgCl) have nice properties but difficult to maintain had been used by most researchers until 1980s. Theoretically, tin electrodes were supposed to attenuate low frequencies more than Ag/AgCl electrodes (12) but Polich et al. found no differences in using both electrode types (13) and both of them should be adequate for most purposes unless you are interested in DC potentials. The term resistance is used when the voltage does not change over the time and should be low between the scalp and the electrode whereas the term *impedance* is used when the voltage varies over the time i.e. alternating current or AC. Since the voltage fluctuates in the context of ERP recordings therefore it is more appropriate to use the term impedance rather than resistance. Impedance is denoted by the letter Z and measured in units of Ohms (Ω) or thousands of Ohms (kΩ). It is important to keep the impedances below 5kΩ for each electrode before EEG recording in order the EEG signals to be more meaningful. To keep the impedance of electrode lower, researchers follow usually two different methods depending on the type of electrode being used. If you are using electrodes without an electrode cap to place the electrode on the scalp using some adhesive, the skin is cleaned first at each with alcohol and then rubbed with an abrasive gel. On the other hand, if you are using an electrode cap to place the electrode on the scalp then use the abrasive gel to rub the underlying skin through the holes in cap after putting the cap ON. For rubbing purpose, any cotton-tipped needle made of plastic or wood may be used.

If the amplifier is capable of subtracting away environmental noise accurately then it is known as common-mode rejection and mostly measured in decibels (dB). This is one of the main problems that can generate high impedances and considered to be less effective if the impedance is higher. The higher the impedance, the worst the common-mode rejection, therefore low electrode impedance causes to avoid picking up environmental noise. The surface of the skin and deep layers of the skin contains a tonic potential in between them and whenever skin's impedance changes, this potential voltage also changes. These changes in voltage are called skin potentials and this potential could be a major source of low frequency noise in ERP recording due to its large variation. Picton et al. had shown that if the impedance of the skin is decreased, it reduces dramatically the skin potentials and it becomes the sufficient reason to decrease the impedance before recording ERPs (14).

3.4 Artifact Rejection and Correction

EEG is contaminated with different types of artifacts like eye blinks, eye movements, muscle activity and skin potentials which create problems in ERP studies leading to misinterpretation of EEG signals. During EEG recording the subjects are instructed however, to minimize these artifacts but it is not possible to completely avoid them, therefore we use some techniques to remove them to make EEG artifact free. There are two ways that these artifacts could be problematic. Firstly, S/N ratio may greatly decrease for averaged waveform because these artifacts are very large compared to ERP signal. Secondly, these artifacts are time-locked due to which averaging process does not remove them. However, there are two main techniques which help us in eliminating these artifacts. First, we can possibly identify the contaminated trials with in a single-trial EEG epochs and simply remove them from the averages ERP waveforms which is known as *artifact rejection* whereas in the second technique, we can possibly estimate the influence of artifacts by means of some mathematical algorithms and then subtract away these estimated artifacts from the contaminated EEG, which is known as artifact correction. Eye blink produces a large deflection in voltage as compare to normal EEG so the presence of eye blink in a given EEG segment is detected by measuring the largest voltage deflection i.e. If the deflection crosses a certain threshold in a given EEG segment or trial then we can simply discard that trial assuming the presence of eye blink otherwise that trial is included in the averaged ERP waveform. Setting low threshold will cause to reject also those trials which do not have eye blinks and it will decrease the signal-to noise ratio whereas setting high threshold will overlook those trials which may contain eye blinks so only changing threshold will not work properly and we will need other procedures for measuring artifacts. Figure 3.5 shows an absolute voltage threshold for artifact rejection.

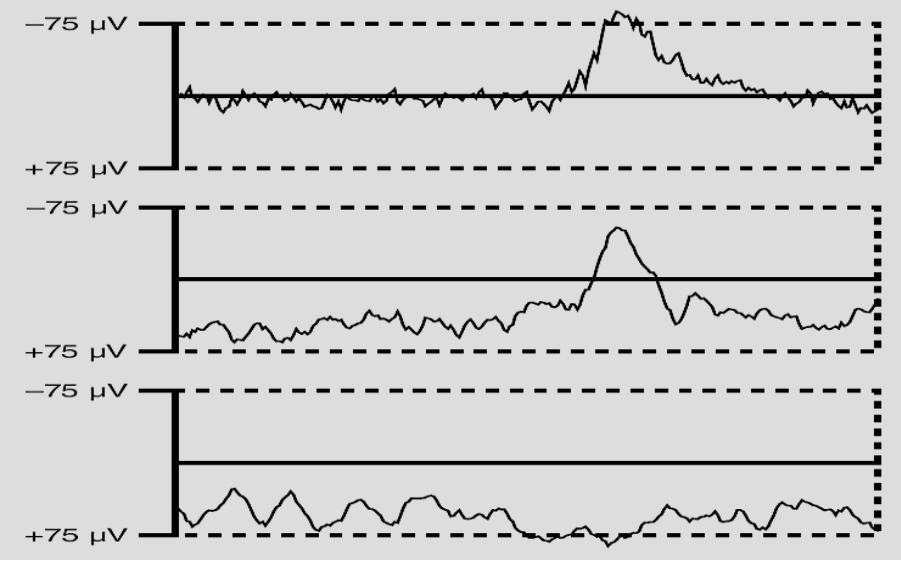

Figure 3.5 Absolute rejection of eye blinks using threshold value.

We can see in figure 3.5 that wherever voltage deflection crosses a certain threshold of ±75µV, the trial is discarded by the visual inspection or by automated routine.

Similarly, eye movements also produce voltage deflection in the EEG recording, assuming the dipole with its positive end pointing toward the front of the eye. A constant DC voltage gradient is produced when the eyes are in stationary position whereas the voltage gradient changes across the scalp when the eyes move. It is noticed that if the eyes move toward left side then the left side of the scalp appeared to have positive voltage deflection and negative on the opposite side of the scalp. With bipolar recordings, it becomes easier to monitor these deflections having one active electrode lateral on one side of eye and a reference electrode lateral to the other side of eye. Eye movement may be detected as small as 1 to 2 degrees on individual trials using step function but signal-to-noise ratio of the EOG signal makes it impossible to detect smaller eye movements without an unacceptably large number of false alarms. However, averaged EOG waveforms may be used to show that the ERP waveform is not contaminated by small eye movements. Different types of artifacts including eye movements are shown in figure 3.6, positive are plotted downwards.

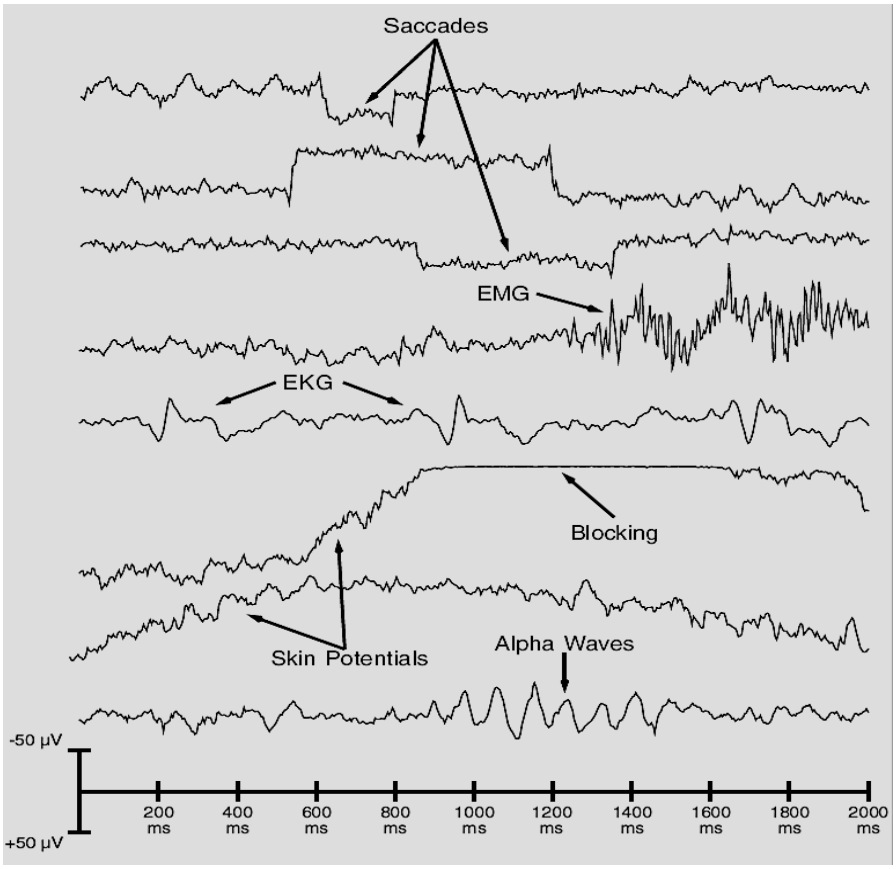

Figure 3.6 Several artifacts include Saccades, EMG, EKG, Blocking and Skin Potentials. Source (11)

The majority of eye movements are mostly saccades when the subject is being exposed some moving objects or having gradual head movements. We can see the top three recordings in figure 3.6 to be saccades having sudden transition from the zero voltage level to a non-zero voltage level followed by a gradual return toward zero caused by the amplifier's high pass filter. It makes the saccades boxcar-shaped like function. Small eye movement can be distinguished from the normal EEG deflections using boxcar characteristic by the visual inspection of individual trials which may be discarded if a certain threshold is exceeded.

EMG signals or electromyogram as shown in figure 3.6 are produced when the muscles are contracted. These signals have high frequency and are eliminated using low pass filter. To reduce the efforts of filtering the subjects may be instructed to try to minimize the eye blinks, eye movement and also the muscle movements. EMG signals are sometimes not required to eliminate unless you have taken all appropriate precautions to minimize EMG. However, if in some cases it is required to eliminate then the best way is to perform a Fourier transform on each trial and calculate the amount of high frequency power whereas alternatively every consecutive pairs of points are used to compute difference and if it exceeds a particular threshold then it is rejected. Moreover the heat beat (EKG) signal, again shown in figure 3.6 is sometimes recorded along with EEG. It is picked up from mastoid or ear lobe used as a reference which may be reduced by shifting lightly position of reference electrode. It is recorded almost every one second during entire recording session so it may lead to unacceptable number of rejection of trials.

As we have discussed that artifact rejection eliminates a subset of trials from the ERP waveforms and is a process that leads to some problems (15). 1) After rejection of trials contaminated with eye blinks and eye movements may leave behind unrepresentative sample of trials. 2) It is not possible for every subject to control eye blinks and eye movements causing very less number of artifact free trials. 3) Sometimes eye blinks and eye movements are the integral to experimental paradigm so rejection of trials would be counterproductive. Having these problems in mind researchers better preferred to correct the ocular artifacts rather being rejected simply by subtracting away the voltages due to eye blinks and eye movements and therefore developed artifact correction procedures (16), (17), (18), (19), (20) and (21) in order to keep the maximum number of trials which contains meaningful information. Since there are different methods available to correct EOG artifacts but one of the most popular method is to separate the blind sources (BSS) using independent component analysis (ICA).

3.4.1 Independent Component Analysis

ICA is a method that provides us the capability to solve the problem of Blind Source Separation. It can identify N independent source signals, $S = s_1(t), s_2(t), \ldots s_N(t)$ (e.g. different voices,

music or other sound sources) from N linear mixtures matrix $M = [m_1(x), m_2(x), \cdots m_N(x)]$, that can be modeled by multiplying the source matrix S by an unknown square matrix T such that $M = TS$. In order to discriminate the source signals from mixtures, it is assumed that sources s_i are independent and their mixtures are not. Having no prior knowledge of source signals or about the process, how the signals were mixed, the objective is to approximate another matrix $U = [u_1(x), u_2(x), \cdots u_N(x)]$, identical to source signals by specifying the filter to linearly invert the mixing process such that $U = VM$ where V is a square matrix.

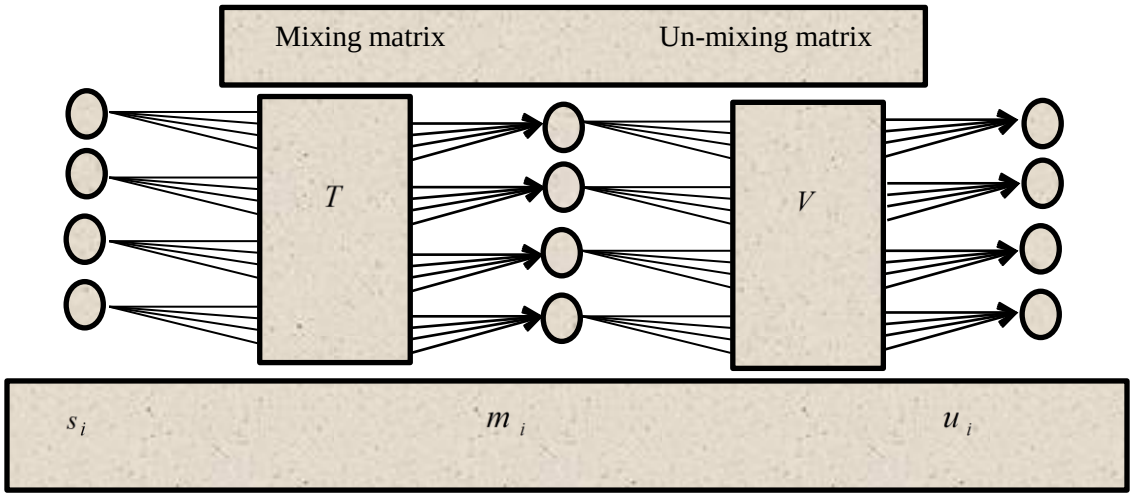

Figure 3.7 The general process of ICA.

The general overview of process of ICA is shown in figure 3. Electrode measurements m_i are assumed to be composed of a linear mixture of independent sources s_i. Un-mixing matrix V is produced using ICA, which decompose m_i to estimate the independent sources u_i. After identification of components, the one that contains EOG/EMG artifacts is subtracted and artifact free EEG is obtained for further feature extraction and classification. Software routines are available to the researcher's community for detection of artifacts based on ICA, however marking and rejection of artifacts is done manually as we have discussed earlier.

3.5 Plotting, Measurement and Analysis

It is very important to visualize actual shape of ERPs before validating any results. The Society for Psychophysiological Research (SPR) has presented some guidelines to represent the ERPs data. 1) The data should be presented from maximum number of electrodes placed on the scalp however it is not that much important because the different components involved in EEG can be isolated using different methods like ICA. 2) ERP waveforms should be plotted on time versus voltage scale in order to see the latencies and amplitudes involved and electrode sites should be labeled in the figure as shown in figure 3.8 illustrating the good way and bad way to

plot ERPs data. It is not possible from figure 3.8(A) to determine the exact pattern of effects i.e. when the polarities are switched between rare and frequent, because there is no overlapped shown, however in figure 3.8 (B) it is easily possible to distinguish the rare and frequent waveforms without any confusion in mind. Another important thing to be considered while the presentation of ERP data is to reflect the pre-stimulus time period of about 200 ms which will help us in our analysis and to decide how much the ERP is affected after the stimulus onset. Also keep in mind the factor of overlapping the waveforms as in figure 3.8 (B) i.e. not more than three otherwise it will become very difficult to assess and distinguish the individual ERPs.

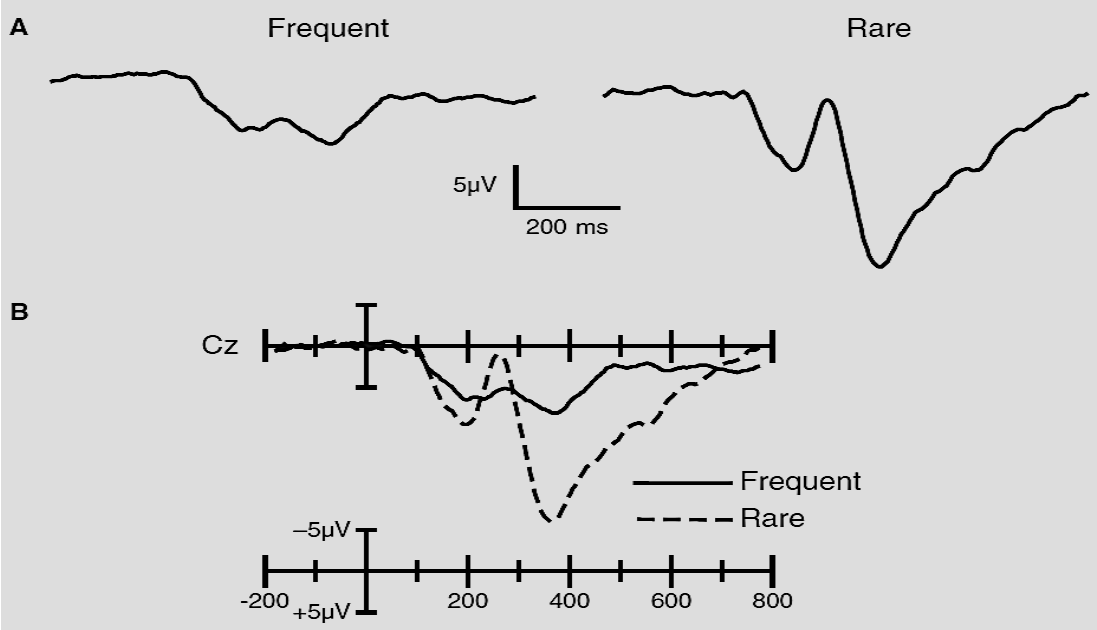

Figure 3.8 A) Bad way B) Good way. Positive is shown downward.

Regarding the question of how many electrode sites should be presented. It depends on the how many electrode sites you are using because it is better to show some representative sites rather presenting all of them.

3.5.1 Measuring ERP Amplitudes and Latencies

Let us first discuss ERP amplitudes. Most of the ERP studies rely on amplitudes and there exist two common methods to measure amplitudes. 1) Define a time window and find the maximum voltage in that time window. This is known as *peak amplitude* measure. 2) Define a time window and calculate average amplitude at all-time points within that time window. This is known as *mean amplitude* measure. Another approach is to calculate the sum of all voltages within the time window, multiplied by the number of points in that time window. This is known as *area amplitude* measure. We can use the peak amplitude measure for some reasons but

there are several other reasons that convince us not to use peak amplitude, at least without having basic procedure to be modified.

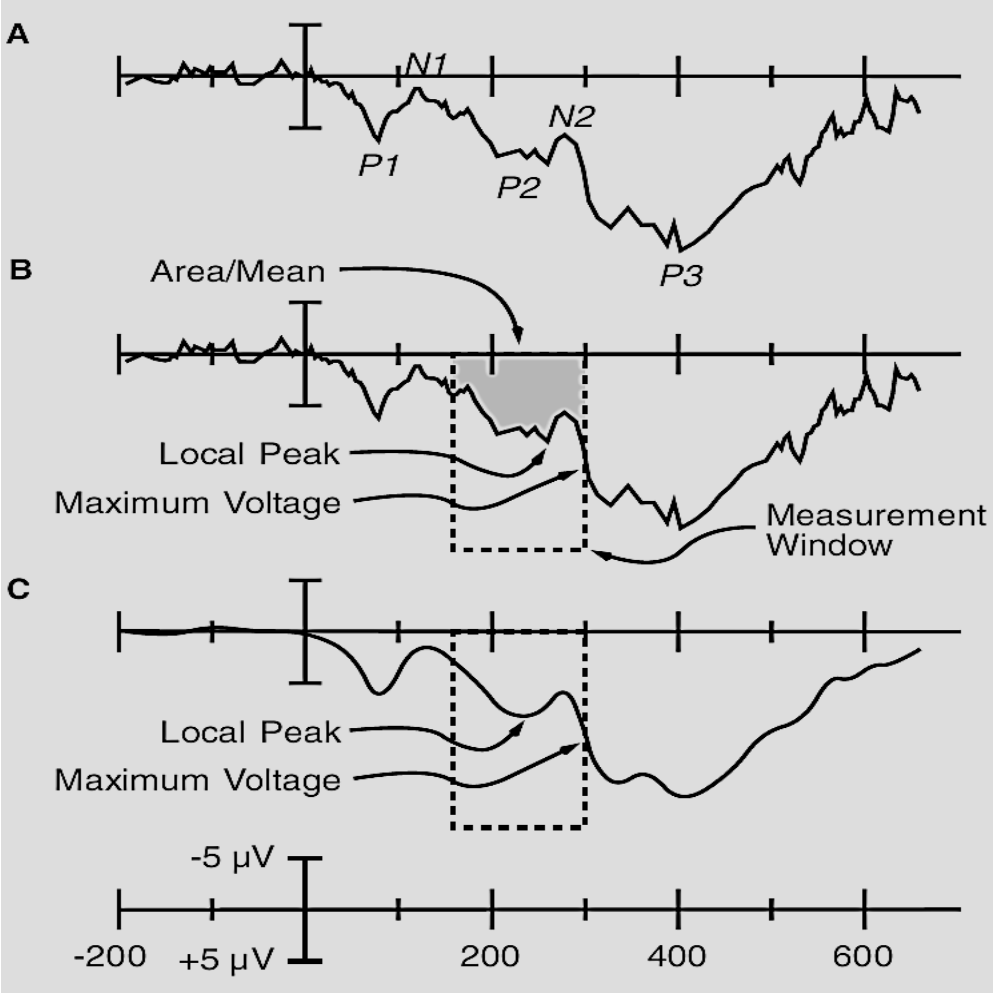

Figure 3.9 ERP waveforms A) with several peaks B) with time window and several measures C) Filtered ERP. Positive is plotted downward. Source (11)

In figure 3.9 (A), suppose you want to measure the P2 wave then you would be required to define a time window for measuring voltage at all points e.g. a window of 150 – 300 ms as shown in figure 3.9 (B), gives the peak voltage at the end of this time window due to onset of P3 wave but this point is far from actual P2 wave which is not a good estimate however this problem can be resolved by narrow downing the time window even then peak latencies needs to be taken care while defining the time window. Another good way to measure P2 wave is to find a point which has smaller points on each side, it is known as local peak amplitude. Figure 3.9 (B) shows that peak amplitude of P2 wave is not in the center of the time window but shifted towards right due to noise deflection. It should be kept in mind that the peak amplitude at a single time point would be used to identify a component that lasts for around 150 – 300

milliseconds which may increase the likelihood of occurrence of large noise deflection that causes the peak amplitude measurement to be larger for noisy data and wider measurements window. Filter the waveform could be one solution to high frequency noise as shown in figure 3.9 (C) which is obtained after low-pass filtering. In this waveform local peak amplitude provides a good measure of P2 wave but the simple peak amplitude still gives the distorted measure. Having the filtered waveform means that voltage at each point reflects the weighted contribution of the voltages from the nearby time points which solves the problem of using the voltage at single time point to represent a component that lasts around hundreds of milliseconds.

Now we discuss the mean amplitude which has some advantages over peak amplitude. 1) A narrower measurement time window can be used because it is ignorable even if the maximum amplitude lies outside the window for some electrode sites or subjects. Indeed, the narrower the window, the lesser the influence of overlapping component will be contributed to the measurement. Looking at figure 3.9 (C), it is understandable that a window of 200 – 250 ms would be suitable to use rather using a window of 150 – 300 ms. 2) While measuring the mean amplitude, there is no need to use the narrower measurement window because mean amplitude is less sensitive to high frequency noise than peak amplitude and the mean amplitude uses the range of time points as compare to peak amplitude that uses only a single time point. Also note that filtering is not required when you intend to calculate the mean amplitude because by definition mean amplitude include the voltages from multiple nearby points which is same thing as done in filtering so no filtering is needed before measuring the mean amplitude. 3) In any case, either using a longer measurement time window or when the noise level increases, mean amplitude do not become biased which means that variance may change but these factors of time window or noise level do not depend on the expected value. Thus, it is appropriate to compare the mean amplitude from waveforms based on different numbers of trials and peak amplitude does not comply with this condition. 4) Mean amplitude is a linear measure i.e. the mean of the mean amplitude of a component from each subject is equal to the mean of the same component from the grand average waveform which makes it possible to compare directly your grand average waveforms with the means from your statistical analyses. It is also applicable to averaging of single-trial EEG data.

Mean amplitude may lead to spurious results being sensitive to the overlapping problem if the latency of a component varies across conditions. Moreover, there is no particular reason for selecting a particular measurement time window and it is encouraged by fishing by trying different windows.

To measure the ERP latencies, peak latency measures are usually used in order to find the maximum amplitude within a time window and latency of this peak is used as a measure of the

latency of the underlying component. Where we discussed earlier the peak amplitude measures, there also comes few shortcomings on peak latency measures. 1) The problem of maximum voltage within a time window is solved using a local peak latency measure in which peak exists only if there are some smaller point values on each side of it. 2) Peak latency measures are also sensitive to high frequency noise like peak amplitude measures and as we know that high frequency may cause the peak to be far from the middle of the time window which is even more significant problem for peak latency than for peak amplitude. 3) Due to increase in noise the average peak latency appears to be closer to the middle of time window e.g. consider measuring the peak latency between 200 – 400 ms of an ERP waveform full of random noise, the peak latency is expected to be at any value within this range. The average will tend to be somewhere between the actual peak and the center of the range, if there is a signal as well as noise. 4) Peak latency is non-linear i.e. peak latency measured from the single subject waveforms would not be the same as peak latency measured from the grand average.

One must be careful when measuring the peak latencies. To filter out high frequency noise, to use local peak measure, to make sure the waveforms being compared have similar noise levels and be well aware that peak latency is a coarse and non-linear measure of a component's timing.

3.5.2 Statistical Analysis

After recording the ERP waveforms from multiple subjects and finding amplitude and latency measures we need to analyze the significance of effects by performing some statistical analyses. Analyses of variance (ANOVA) (22) (23) is one of the most commonly used and dominant approach than several other approaches. In many of the cognitive ERP experiments, main effects or an interaction in a completely crossed factorial design is followed for which ANOVA is most suitably suggested. For this purpose, we need a criterion either to accept or reject while examining the experimental effects. An alpha value of .05 has come up to be very tricky. It is better advised to design the experiment first in order to have experimental effects quite large relative to the noise level and p-values to be very low i.e. .01 or better. To focus our attention, we will have to decide which of component of the waveform should be considered for analyses, e.g. P3 wave. ANOVA is performed for a number of factors, for example, stimulus probability to be either frequent or rare, stimulus brightness to be either bright or dim, anterior-posterior electrode position either to be frontal, central or parietal and left-right electrode position either to be left hemisphere, midline or right hemisphere. It should be noticed that the more the number of factors, the more the number of p-values will be calculated. However, a separate ANOVA may be performed for each electrode site instead of performing a single ANOVA assuming electrode as a factor. This approach may increase probability of type I error (false rejecting) and type II error (false accepting). Performing ANOVA

for each electrode site would require more p-values to be computed causing the type I error to increase leading to a greater probability that a spurious effect will reach .05 level. Moreover, type II error will be increased because a small effect may fail to reach significance at any individual site.

Bibliography

1. **Berger, H.** 1929 *Ueber das Elektrenkephalogramm des Menschen.* Vol. 87. pp. 527-570.

2. **Walter W G, Cooper R, Aldridge V J, McCallum W C and Winter A L.** 1964 *Contingent Negative Variation: An electric sign of sensorimotor association and expectancy in the human brain.*, Nature, Vol. 203, pp. 380-384.

3. **Sutton S, Braren M, Zubin J and John E R.** 1965 *Evoked Potential Correlates of stimulus uncertainty.*, Science, Vol. 150, pp. 1187-1188.

4. **A, Polich J and Kok.** 1995, *Cognitive and biological determinants of P300: An integrative review.* Biological Psychology, Vol. 41, pp. 103-146.

5. **Clark V P, Fan S and Hillyard S A.** 1995 *Identification of early visually evoked potential generators by retinotopic and topographic analyses.*, Human Brain Mapping, Vol. 2, pp. 170-187.

6. **J, Jeffreys D and Axford.** 1972 *Source locations of patterns specific compnents of human visual evoked potentials. I: Components of striate cortical origin*, Experimental Brain Research, Vol. 16, pp. 1-21.

7. **Di Russo F, Martinez A, Sereno M I, Pitzalis S and Hillyard S A.** 2002 *Cortical sources of the early components of the visual evoked potential.*, Human Brain Mapping, Vol. 15, pp. 95-111.

8. **Hillyard S A, Vogel E K and Luck S J** *1998 Sensory gain control (amplification) as a mechanism of selective attention: Electrophysiological and Neuroimaing evidence.* Philosophical Transactions of the Royal Society, Biological Sciences, Vol. 353, pp. 1257-1270.

9. **Hopf J M, Vogel E K, Woodman G F, Heinze H J and Luck S J.** 2002 *Localizing visual discriminative processes in time and space*, Journal of Neurophisiology, Vol. 88, pp. 2088-2095.

10. **A, Luck S J and Hillyard S.** 1994 *Electrophysiological correlates of feature analysis during visual search.*, Psychophysiology, Vol. 31, pp. 291-308.

11. **Luck, Steven J.** 2005 *An Introduction to the Event-Related Potential Technique.* MIT Press.

12. **Picton T W, Lins O G and Scherg M.** 1995 *The recording and analysis of event-related potentials,* New York: Elsevier, Vol. 10. pp. 3-73.

13. **D, Polich J and Lawson.** 1985 *Event-related potentials paradigms using tin electrodes*, American Jouranl of EEG Technology, Vol. 25, pp. 187-192.

14. **A, Picton T W and Hillyard S.** 1972 *Cephalic skin potentials in electroencephelography.*, Electroencephalography and Clinical Neurophysiology, Vol. 33, pp. 419-424.

15. **Gratton, G., Coles, M. G. H., & Donchin, E.** 1983 *A new method for off-line removal of ocular artifacts.*, Electroencephalography and Clinical Neurophysiology, Vol. 55, pp. 468-484.

16. **Berg, P., & Scherg, M.** 1991 *Dipole modelling of eye activity and its application to the removal of eye artifacts from EEG and MEG.*, Clinical Physics & Physiological Measurement, pp. 49-54.

17. **Berg, P. & Scherg, M.** 1994 *A multiple source approach to the correction of eye artifacts.*, Electroencephalography & Clinical Neurophysiology, Vol 90. pp. 229-241.

18. **Jung, T., et al.** 2000 *Independent component analysis of biomedical signals.* Helsinki, Proc. 2nd Int. Workshop on Independent Component Analysis and Blind Signal Separation. pp. 633-644.

19. **Jung, T., Makeig, S., Westerfield, M., Townsend, J., Courchesne, E., and Sejnowski, T. J.** 2000 *Removal of eye activity artifacts from visual event-related potentials in normal and clinical subjects.*, Clinical Neurophysiology, Vol. III, pp. 1745-58.

20. **James, C. J. and and Hesse, C. W.** 2005 *Independent component analysis for biomedical signals*, Physiological Measurement, Vol. 26, pp. R15-R39.

21. **Stone, J. V.** 2004 *Independent Component Analysis: A Tutorial Introduction.* London : MIT Press.

22. **Dunki, R., M. and Dressel, M** *2006 Statistics of biophysical signal characteristics and state specificity of the human EEG.* ELSEVIER, PHYSICA A, Vol. 370, pp. 632-650.

23. **Nemoto, I. and Abe, M. and Kotani, M.** 2008 *Multiplicative correction of Subject Effect as Preprocessing for Analysis of Variance*, IEEE Trans. on Biomedical Engineering, Vol. 55.

4. Support Vector Machines for Pattern Classification

4.1 Introduction to Support Vector Machines

Support Vector Machines (SVMs) were developed in the reverse order to the development of Neural Networks (NNs) which followed more heuristic path. SVM has proved to be very successful in classification tasks as many examples are available in the literature (1) (2) (3) (4) (5). SVM constructs a hyperplane in the simplest case that is used for classification to separate the data points belonging to two different classes. This hyperplane is chosen in such a way to maximize the distance margin δ , as shown in figure 4.1 and 4.2, to the closest training data points of any class. In general, the larger the margin is, the higher is the classification accuracy. SVM may broadly be categorized as hard margin and soft margin in (6). However, the SVM theory was developed by Vapnik in (7) and a good review on classification algorithms for BCI research is presented in (8).

4.1.1 Two-Class SVM with hard and soft margins

To classify M, $m-$ dimensional training data points x_i ($i = 1,\cdots,M$) which either belong to class 1 or class 2 and the associated labels be $y_i = 1$ for class 1 or $y_i = -1$ for class 2. A decision function is defined as $F(x) = w^T x + b$, where w is an $m-$ dimensional vector and b is the bias term. If the data is linearly separable then no data points will satisfy

$$w^T x + b = 0 \tag{1}$$

So, for $i = 1,\cdots,M$

$$w^T x_i + b \begin{cases} \geq 1 \\ \leq -1 \end{cases} \text{ for } \begin{matrix} y_i = 1 \\ y_i = -1 \end{matrix} \tag{2}$$

Equation (2) may be written as

$$y_i(w^T x_i + b) \geq 1 \text{ for } i = 1,\cdots,M \ . \tag{3}$$

The function,

$$F(x) = w^T x + b = c \text{ for } -1 < c < 1 \tag{4}$$

defines the hyperplane that separates the data points x_i ($i = 1, \cdots, M$). For $c = 0$, the separating hyperplane lies in the middle of two hyperplanes with $c = 1$ and -1. Pictorial representation of SVM in case of two class problem for hard margin is shown in figure 4.1. The optimal separating hyperplane can be obtained by solving the optimization problem,

Minimize,

$$Z(w) = \frac{1}{2}\|w\|^2 \tag{5}$$

subject to the constraints,

$$y_i(w^T x_i + b) \geq 1 \text{ for } i = 1, \cdots, M \tag{6}$$

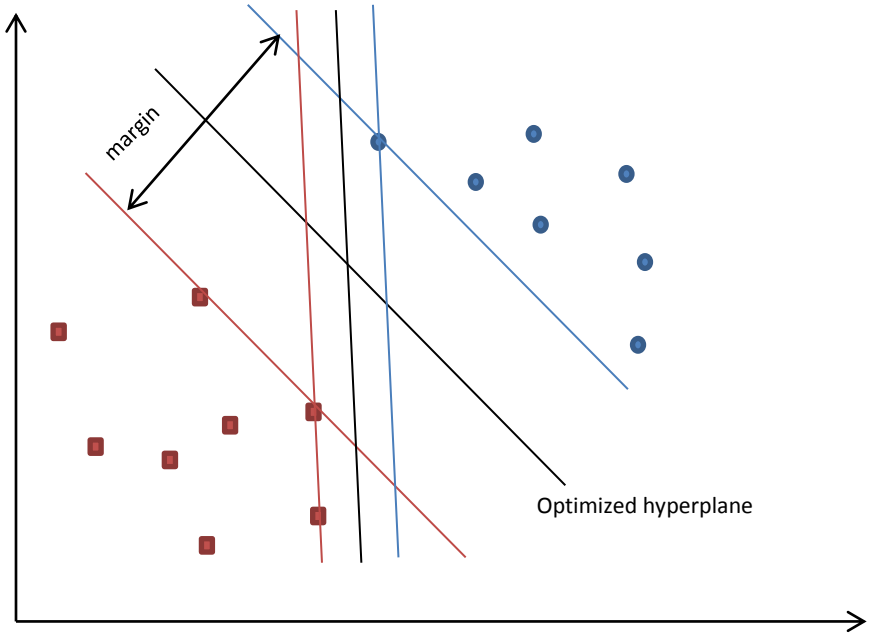

Figure 4.1 A separating hyperplane in two class problem for hard margin case. Source (6)

Equation (5) forms a quadratic optimization problem with inequality constraints expressed by equation (6). This constrained optimization problem can be solved by solving its equivalent unconstrained problem using the saddle points of the Lagrangian functional,

$$Z(w, b, \alpha) = \frac{1}{2} w^T w - \sum_{i=1}^{M} \alpha_i \left[y_i (w^T x_i + b) - 1 \right] \tag{7}$$

Where $\alpha = (\alpha_1, \cdots, \alpha_M)^T$ and α_i are the non-negative Lagrange multipliers. Lagrangian must be minimized with respect to w and b, and needs to be maximized w.r.t $\alpha_i \geq 0$. This problem can be solved into its primal space of parameters w and b and also in dual space of Lagrange multipliers α_i. The approach of dual space gives us insightful results as it has the number of variable as the number of training data. Equation (7) is manipulated with Karush-Kuhn-Tucker (KKT) conditions in (6) to get the dual problem,

Maximize,

$$Z(\alpha) = \sum_{i=1}^{M} \alpha_i - \frac{1}{2} \sum_{i,j=1}^{M} \alpha_i \alpha_j y_i y_j x_i^T x_j \tag{8}$$

with respect to α_i subject to the constraints

$$\sum_{i=1}^{M} y_i \alpha_i = 0 \text{ and } \alpha_i \geq o \qquad \text{for } i = 1, \cdots, M \tag{9}$$

which is a hard margin SVM. Using Lagrangian functional in equation (7) with KKT conditions we obtain

$$w = \sum_{i=1}^{M} \alpha_i y_i x_i \tag{10}$$

And

$$\sum_{i=1}^{M} \alpha_i y_i = 0 \tag{11}$$

to finally get the decision function as

$$F(x) = \sum_{i \in S} \alpha_i y_i x_i^T x + b \tag{12}$$

where S is the set of support vector indices along with

$$b = \frac{1}{|S|} \sum_{i \in S} \left(y_i - w^T x_i \right) \tag{13}$$

Hence the unknown datum x belongs to either class 1 if $F(x) > 0$, or class 2 if $F(x) < 0$ and remains unclassifiable if $F(x) = 0$.

Now SVM introduces slack variables $\xi_i \geq 0$ in case of soft margins and the optimization problem turned into,

Minimizing $Z(w,b,\xi) = \frac{1}{2}\|w\|^2 + C\sum_{i=1}^{M} \xi_i^l$ (14)

subject to the constraints

$y_i(w^T x_i + b) \geq 1 - \xi_i$ for $i = 1,\cdots,M$. (15)

Where $\xi = (\xi_1,\cdots,\xi_M)^T$ and C is the margin parameter that determines the trade-off between the maximization of the margin and minimization of the classification error. The values for l are either 1 or 2 calling SVM either L1 soft margin SVM (L1SVM) or L2 soft margin SVM (L2SVM) respectively. Pictorial representation of SVM in case of two class problem for soft margin is shown in figure 4.2. Considering L1SVM, Lagrangian multipliers α_i and β_i are introduced likewise linearly separable case and we get,

$$Z(w,b,\xi,\alpha,\beta) = \frac{1}{2}\|w\|^2 + C\sum_{i=1}^{M} \xi_i - \sum_{i=1}^{M} \alpha_i(y_i(w^T x_i + b) - 1 + \xi_i) - \sum_{i=1}^{M} \beta_i \xi_i \quad (16)$$

where $\alpha = (\alpha_1,\cdots,\alpha_M)^T$ and $\beta = (\beta_1,\cdots,\beta_M)^T$ with $\alpha_i + \beta_i = C$.

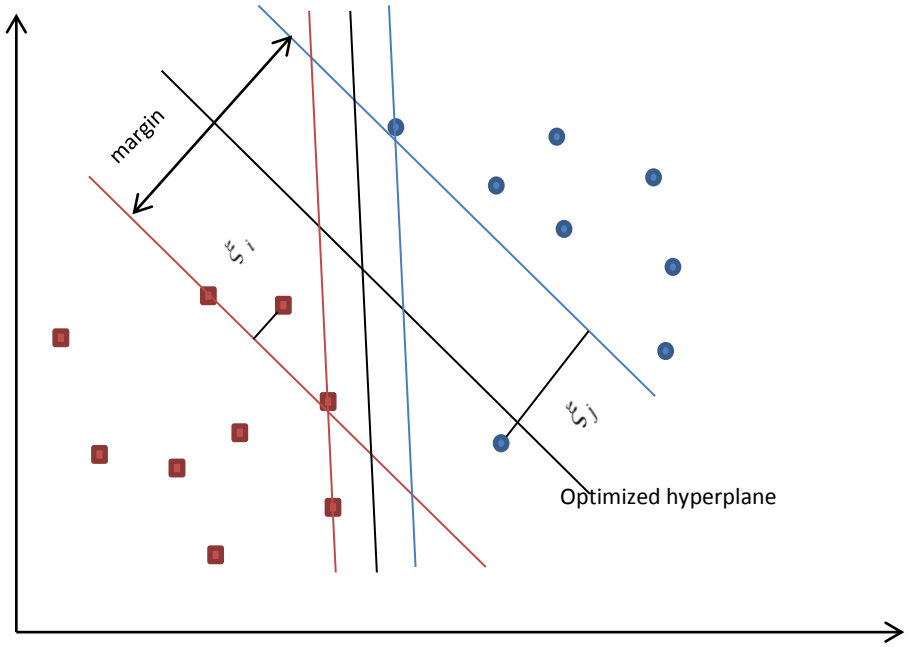

Figure 4.2 A separating hyperplane in two class problem for soft margin case.

The Dual problem for L1SVM is the same as dual problem for hard margin SVM described in equations (8) and (9). The only difference is that α_i cannot exceed C i.e. causing an extension in one of the constraints in equation (9) is $C \geq \alpha_i \geq 0$ for $i = 1, \cdots, M$.

If the data is not linearly separable then we can define a function that map the original input lower dimensional data into higher dimensional feature space also called dot-product space in order to enhance the linear separability. Such functions that perform mapping from lower to higher dimensional feature space are called Kernels which give us the advantage of not treating the higher dimensional feature space explicitly. This approach is also known as *kernel trick*. Given that the non-linear vector function

$$q(x) = (q_1(x), \cdots, q_n(x))^T \tag{17}$$

maps the $m-$ dimensional input vector x into the $n-$ dimensional feature space and the linear decision function in the feature space is defined as

$$F(x) = w^T q(x) + b \tag{18}$$

where w is an $n-$ dimensional vector and b is a bias term. Hilbert-Schmidt theory says that if a function $K(x, x')$ is symmetric and satisfies

$$\sum_{i,j=1}^{M} k_i k_j K(x_i, x_j) \geq 0 \tag{19}$$

then there exists a function $q(x)$ that maps x into the dot product feature space and satisfies

$$K(x, x') = q^T(x) q(x') \tag{20}$$

This $K(x, x')$ is used in training and classification instead of $q(x)$. The dual problem in the feature space using kernel is as follows

Maximize,

$$Z(\alpha) = \sum_{i=1}^{M} \alpha_i - \frac{1}{2} \sum_{i,j=1}^{M} \alpha_i \alpha_j y_i y_j K(x_i, x_j) \tag{21}$$

subject to the constraints

$$\sum_{i=1}^{M} y_i \alpha_i = 0 \text{ and } \quad C \geq \alpha_i \geq 0 \quad \text{for } i = 1, \cdots, M \tag{22}$$

The decision function that contain kernel expression becomes

$$F(x) = \sum_{i \in S} \alpha_i y_i K(x_i, x) + b \tag{23}$$

where b is given by

$$b = \frac{1}{U} \sum_{j \in U} (y_j - \sum_{i \in S} \alpha_i y_i K(x_i, x_j)) \tag{24}$$

Here U is the set of unbounded support vector indices.

Generally used kernels in SVM are linear kernel, polynomial kernel and Radial Basis Function (RBF) kernel. However, three-Layer Neural Network Kernels and some other kernels are briefly discussed in (6) and (9). Most commonly used kernel in BCI community is RBF or Gaussian kernel. The mathematical expression for linear, polynomial of degree d and RBF kernels are given in equations (25), (26) and (27) respectively.

$$K(x, x') = x^T x' \tag{25}$$

$$K(x, x') = (x^T x' + 1)^d \tag{26}$$

$$K(x, x') = \exp(-\gamma \left\| x - x' \right\|^2) \tag{27}$$

Here γ is a parameter for controlling the radius.

SVM that uses RBF kernel is known as Gaussian SVM or RBF-SVM. RBF converts the data space to higher dimensional feature space making separation much more likely for nonlinear cases. An SVM with linear kernel, called linear SVM is also used widely.

4.1.2 Multiclass SVM

There exist almost several different types of SVMs which are capable of dealing with multiclass problems e.g. One-against-all SVM, pairwise SVM, error-correcting output code and all-at-Once SVM. In this section, we will discuss only first two approaches. Let's first discuss *One-against-all SVM with discrete decision function*. In this type of SVM, n direct decision functions are determined to separate one class from the remaining assuming n - class problem. Let the class i be separated from the remaining classes by the ith decision function having maximum margin, given as follows,

$$D_i(x) = w_i^T g(x) + b_i \tag{28}$$

where w_i is the $l-$ dimensional vector, $g(x)$ is the mapping function that maps x into the $l-$ dimensional feature space and b_i is the bias term. The optimal separating hyperplane is defined by $D_i(x) = 0$, separates the class i which satisfy $D_i(x) \geq 1$ from the remaining classes, all of which satisfy $D_i(x) \leq -1$ and the support vectors satisfy $y_i D_i(x) = 1$. In classification, if for the input vector x,

$$D_i(x) > 0 \qquad (29)$$

is satisfied for one i, x is classified into class i because only the sign of the decision function is used, the decision is discrete. If equation (29) is satisfied for plural i or if there is no i that satisfies equation (29) then x is unclassifiable. Now for example, considering three class problem as shown in figure 4.3, we can see that the data points 1 and 2 belong to the unclassifiable shaded regions because for data point 1 the decision functions are $D_1(x_1) > 0$, $D_2(x_2) > 0$ and $D_3(x_3) < 0$ which means that data point 1 belongs to both classes 1 and 2 and remains unclassifiable. Similarly data point 2 belongs to no class and also remains unclassifiable due to $D_i(x_i) < 0$ for $i = 1,2,3$.

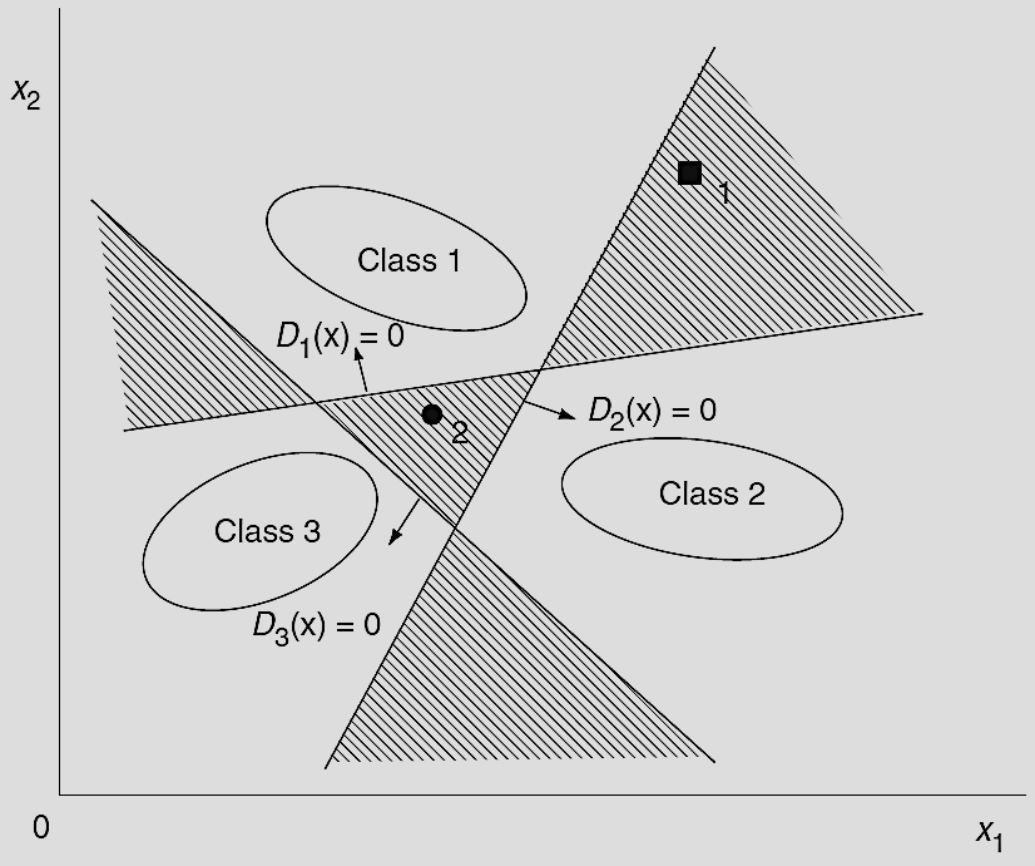

Figure 4.3 Unclassifiable shaded regions by the One-against-all approach. Source (6)

In (6), Abe has discussed three solutions to avoid this problem of unclassifiable regions i.e. One-against-all with continuous decision functions, fuzzy SVM and decision-tree-based SVM. In the first case a continuous decision function is proposed instead of discrete decision function for classification as follows:

$$\arg \max_{i=1,\cdots n} D_i(x) \tag{30}$$

So the data point 1 in figure 4.3 is classified into class 1 because $D_1(x_1)$ is the maximum among the three. Similarly, data point 2 is also classified into class 1. In second case of fuzzy SVM, one dimensional membership function $m_{ij}(x)$ in the directions orthogonal to the optimal separating hyperplanes $D_j(x) = 0$, is introduced for class i to resolve the problem of unclassified regions, defined as follows:

For $i = j$, $$m_{ii}(x) = \begin{cases} 1 \; for D_i(x) \geq 1 \\ D_i(x) otherwise \end{cases} \tag{31}$$

For $i \neq j$, $$m_{ij}(x) = \begin{cases} 1 \; for D_j(x) \leq -1 \\ -D_j(x) otherwise \end{cases} \tag{32}$$

To define the membership function of classes, two operators, minimum and average are defined for the class i membership function of x for $m_{ij}(x)$ $(j = 1,\cdots n)$ as follows, respectively:

$$m_i(x) = \min_{j=1,\cdots,n} m_{ij}(x) \tag{33}$$

$$m_i(x) = \frac{1}{n} \sum_{j=1,\cdots,n} m_{ij}(x) \tag{34}$$

The data point x is classified into the class,

$$\arg \max_{i=1,\cdots n} m_i(x) \tag{35}$$

According to this formulation based on the membership functions, the unclassifiable regions in figure 4.3 are resolved as shown in figure 4.4 which has the similar class boundaries produced in (10). In the third approach, a decision-tree-based SVM (11) is used to resolve the unclassified regions shown in figure 4.3. In this type of SVM, $n-1$ support vector machines are trained. To separate the class i data from data belonging to one of classes $i+1, i+2, \cdots, n$, the ith SVM is trained and then classification is performed from first to the $(n-1)st$ support vector machines.

Classification is terminated upon the classification of data point into class i, otherwise it is repeated until the data point goes into the definite class.

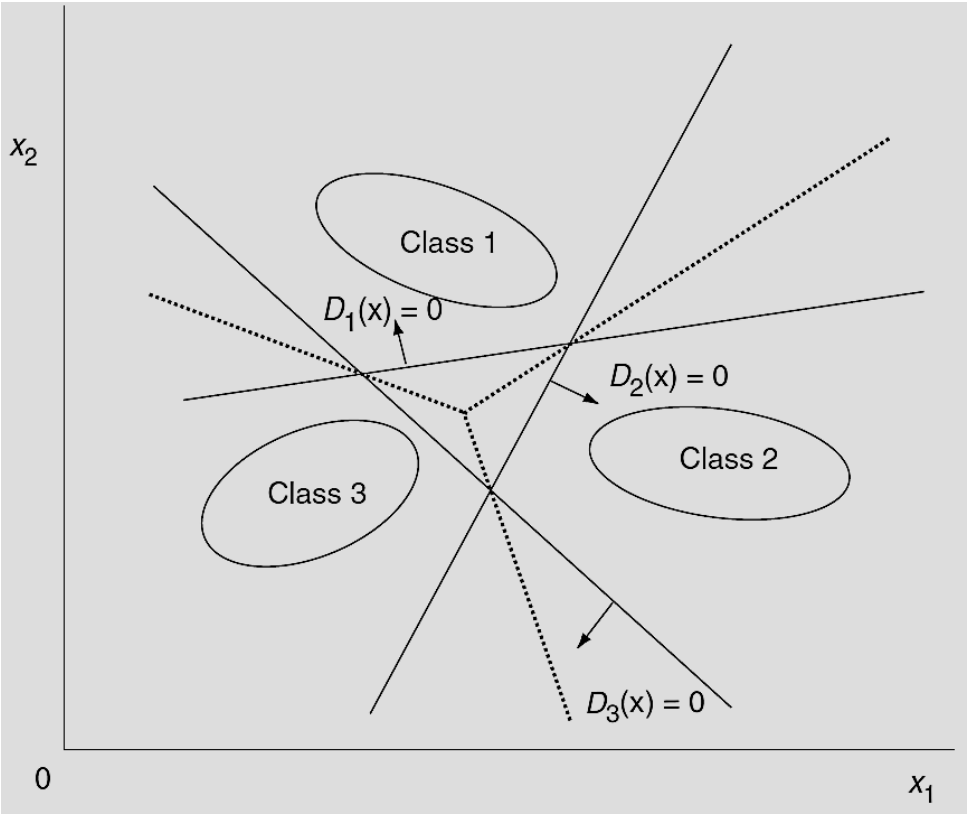

Figure 4.4 Unclassifiable regions are resolved by membership functions.

Class boundaries for four classes are shown in figure 4.5 based on decision-tree classification using linear kernels. In this case, it should be noticed that the processing order affects the generalization ability because the classes with smaller class numbers have larger class regions.

Now we will discuss the second type of support vector machines that can handle the multiclass problem i.e. *Pairwise SVM*. Using pairwise SVM, unclassifiable region reduces but is not reduced completely so to resolve unclassifiable regions fuzzy SVM and decision-tree-based SVM approaches are used. In this type of SVM, all combinations of class pairs are made to determine the decision functions for a class pair and the data corresponding to those two classes is used which reduces the training data considerably in comparison with One-against-all which uses all the training data. For pairwise approach, the number of decision functions is $n(n-1)/2$ as compared to n decision functions for one-against-all SVM, where n is the number of classes. To define decision function of class i against class j with the maximum margin, $D_{ij}(x)$ is written as

$$D_{ij}(x) = w_{ij}^T g(x) + b_{ij} \tag{36}$$

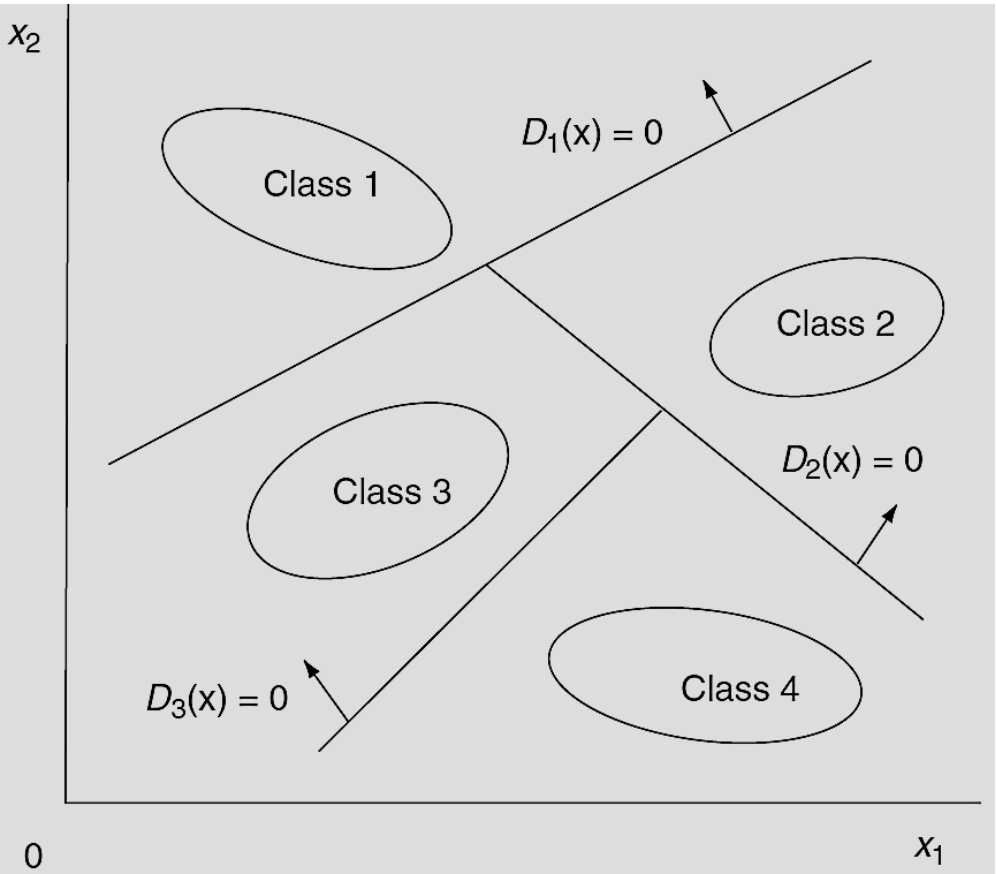

Figure 4.5 Decision-tree based formulation to resolve the unclassifiable regions. Source (6)

Where w_{ij} is the $l-$dimensional vector, $g(x)$ is a mapping function that maps x into the $l-$dimensional feature space, b_{ij} is the bias term and $D_{ij}(x) = -D_{ji}(x)$. The regions R_i do not overlap, which contain those data points x for which $D_{ij}(x) > 0,\ j = 1,\cdots,n,\ j \neq i$ and it means that x is classified into class i. If any x is not contained in R_i then x is classified by voting. To classify the input vector x, $D_i(x)$ is calculated as follows,

$$D_i(x) = \sum_{j \neq i,\ j=1}^{n} sign\ (D_{ij}(x)) \tag{37}$$

where $sign\ (x) = 1$ for $x \geq 0$ and $sign\ (x) = -1$ for $x < 0$. So x is classified into the class

$$\arg \max_{i=1,\cdots,n} D_i(x) \tag{38}$$

Figure 4.6 illustrates the pairwise SVM approach in which the shaded region is unclassifiable but much less than shown in figure 4.3 for One-against-all SVM approach.

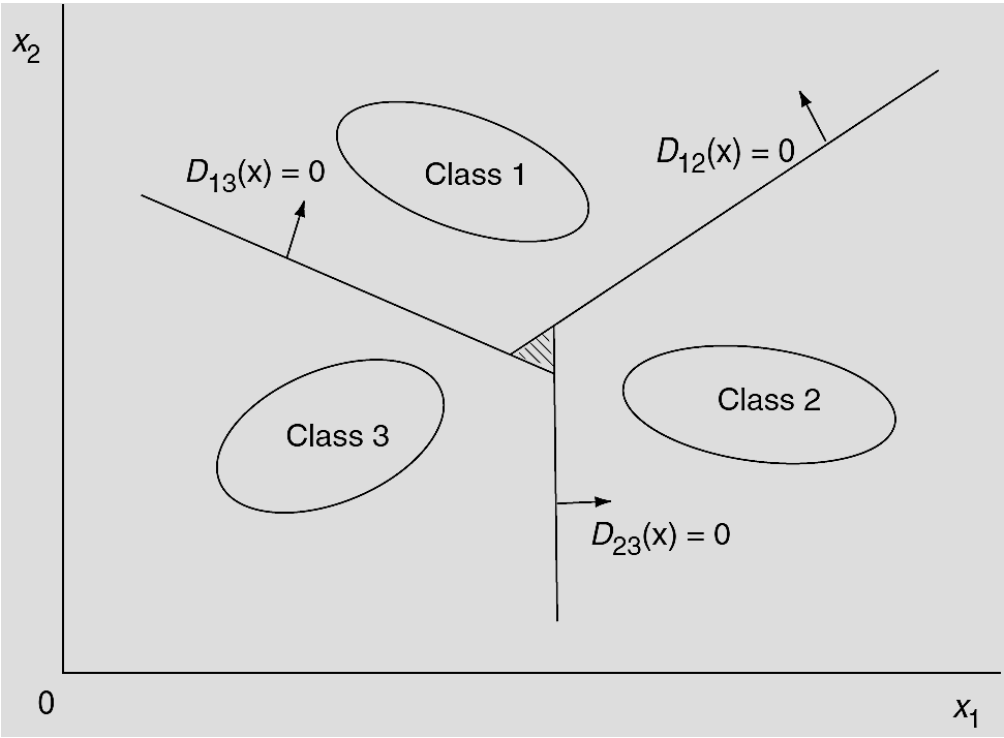

Figure 4.6 Unclassifiable shaded region with pairwise formulation.

Once again to resolve the shaded unclassifiable region, a similar approach that was followed in one-against-all is adopted by introducing the membership functions while realizing the same classification results. For other types of support vector machines and further details that deals with multiclass problems and to resolve the corresponding unclassifiable regions, please refer to (6).

4.2 Training Methods

A quadratic programming problem needs to be solved while training L1 or L2 support vector machines having the number of variables equal to the number of training data. Thus training takes time when the number of variables is large or the training data is large. Osuna et al. proposed in (12) , decomposing the problem into two to reduce the number of variables in training. Suppose the index set $\{1,\cdots,M\}$ is divided into two sets W and N such that $W \cup N = \{1,\cdots,M\}$ and $W \cap N = \phi$. Then decomposing $\{\alpha_i \mid i = 1,\cdots,M\}$ into $\alpha_W = \{\alpha_i \mid i \in W\}$ and $\alpha_N = \{\alpha_i \mid i \in N\}$. Fixing α_N , maximize

$$Q(\alpha_W) = \sum_{i \in W} \alpha_i - \frac{1}{2} \sum_{i,j \in W} \alpha_i \alpha_j y_i y_j H(x_i, x_j) - \sum_{i \in W, j \in N} \alpha_i \alpha_j y_i y_j H(x_i, x_j) - \frac{1}{2} \sum_{i,j \in N} \alpha_i \alpha_j y_i y_j H(x_i, x_j) + \sum_{i \in N} \alpha_i$$

(39)

subject to the constraints,

$$\sum_{i \in W} y_i \alpha_i = -\sum_{i \in N} y_i \alpha_i , \qquad 0 \le \alpha_i \le C \quad \text{for} \quad i \in W \tag{40}$$

Since the constraint in equation (40) is satisfied for $|W| \ge 2$, so the minimum number of $|W|$ is two. Such decomposition technique is usually known as *chunking*. A fixed size chunking and variable size chunking is given in (13) and (12).

4.3 Generalized Error Estimate and Model Selection for Support Vector Classifiers

This is one of the important issues to discuss the estimation of generalized error or in other words, how to estimate the probability of misclassification of new patterns by the learned machine assuming that the new data derives from the same (unknown) distribution underlying the original training set. Unknown generalization error is represented by π and its estimate by $\hat{\pi}$. Here it is desired for the worst case probability to find an upper bound of the true generalization error for which few methods are discussed below (14) i.e.

$$\pi \le \hat{\pi} \tag{41}$$

which holds with probability $1 - \delta$, where δ is a user defined value usually equals 0.05 or less. The empirical error is defined by,

$$v = \frac{1}{l} \sum_{i=1}^{l} I(y_i, \hat{y}_i) \tag{42}$$

Where $I(y_i, \hat{y}_i) = 1$ if $y_i \ne \hat{y}_i$ and zero otherwise.

Generalization estimate and model selection are closely related because it allows to choose the optimal hyperparameters of the SVM i.e. C, γ or P. The value $\hat{\pi}$ is computed for several hyperparameter values and the optimal SVM is selected as the one for which the minimum is attained and this minimum can be used for model selection, if not for estimating the true generalization error as described in (15), (16) and (17).

4.3.1 Training Set

In this case the generalization error is estimated by the following formula but it not recommended in general because there is a strong dependency between errors as all the data is used for training SVM.

$$\hat{\pi}_{train} = v + \frac{\hat{\sigma}}{\sqrt{l}} F^{-1}(1-\delta) \tag{43}$$

choosing SVM with Gaussian kernel having large γ results in $v = 0$ even though $\pi >> 0$.

4.3.2 Test Set

In this case generalization error is estimated with the following formula that also contains the term v_{test} used for error performed on the test set.

$$\hat{\pi}_{test} = v_{test} + \sqrt{\frac{-\ln \delta}{2m}} \tag{44}$$

Due to partitioning of the data in two parts, some information goes useless because the test data does not contribute to the learning process that could be managed by retraining the new SVM on the entire data set without changing the hyperparameters with the training-test data partition.

4.3.3 K-fold Cross Validation

This technique is similar to the technique described in 4.3.2 with minor difference. Here the training data is partitioned into k subsets consisting of k/l patterns each out of which $k-1$ are used for training and the one is used for testing, so the generalization estimate is given by the following formula:

$$\hat{\pi}_{kcv} = v_{test}^{(k)} + \sqrt{\frac{-k \ln \delta}{2l}} \tag{45}$$

Unlike Test Set technique, the procedure is repeated for k times using each one of the k subsets as test set exactly once. In this approach all the data is used for training and also for model selection. The most commonly used value for k are 5 or 10. Moreover, $k-fold$ procedure could be iterated $\binom{l}{k}$ many times without repeating the same training-test set partitioning but this approach is infeasible (9). One problem with this technique is that it finds k different SVMs, each one is trained on a set of $(k-1)l/k$ samples.

4.3.4 Bootstrap

This technique (18) is similar to k -fold cross validation with different approach for splitting training-testing data. For training, l patterns are extracted with replacement from the original training set in which some patterns are included multiple times into new set and some others are left out. On average, one-third of the patterns are left for the test set. If the training set is created with this procedure that is known as bootstrap replicate and the maximum number of replicate that can be generate are $N_B = \begin{pmatrix} 2l-1 \\ l \end{pmatrix}$. To perform a good error estimate 1000 replicates are usually sufficient.

The following average test error performed on each bootstrap replicate determines the estimate of generalized error:

$$v_{boot} = \frac{1}{N_B} \sum_{i=1}^{N_B} v_{test}^{(i)} \tag{46}$$

And the bound is given by

$$\hat{\pi}_{boot} = v_{boot} + \frac{\hat{\sigma}_{boot}}{\sqrt{N_B}} F^{-1}(1-\delta) \tag{47}$$

Where $\hat{\sigma}_{boot}$ is the standard error, assuming the distribution is Gaussian and can be found with the following formula:

$$\hat{\sigma}_{boot} = \sqrt{\frac{1}{N_B - 1} \sum_{i=1}^{N_B} (v_{test}^{(i)} - v_{test}^{boot})^2} \tag{48}$$

Avoiding Gaussian assumption and computing $\delta - th$ percentile point of the test error results in more accurate estimate and also by making use of nested bootstrap replicates (19).

There are also other methods that can be used for generalized error estimate, e.g. Leave-one-out (20), VC-Bound (21), Margin Bound, Maximal Discrepancy and Compression Bound. For details to see these methods, see (9).

4.4 Support Vector Machines for EEG Signals

In this section an application of fuzzy support vector machine (FSVM) is discussed for the classification of EEG signals based on wavelet features (22). Radial basis function kernel was used for the classification of motor imagery tasks and to choose the kernel parameter along

with the trade-off parameter, a low fraction of support vectors was used as a criterion, together with the membership parameter based solely on training data and it was proven that FSVM classifier performed better than the normal SVM approach. The optimal hyperplane could be sensitive to noise and outliers in the training set due to its dependency on the small part of data points. This problem was solved by introducing the fuzzy memberships of data points by the FSVM. The FSVM classifier was also intended to maximize the margin similar to normal SVM classifier. To find the optimal hyperplane, problem for FSVM classifier was defined as follows:

Minimize $$\frac{1}{2} w.w + C\sum_{i=1}^{l} s_i \xi_i \tag{49}$$

Subject to the constraint,

$$y_i(w.x_i + b) \geq 1 - \xi_i \text{ , for } \quad i = 1,\cdots,l \text{ and } \xi_i \geq 0 \tag{50}$$

Where C is a constant, $s_i \in [\sigma,1]$ is fuzzy membership with sufficiently small $\sigma > 0$. The term $s_i\xi_i$ is considered to be the measure of error with different weighting.

While designing the FSVM classifier, selection of appropriate fuzzy memberships is very important and relative importance of data points to their own classes could serve as a rule during the assignment of membership values to data points. For efficient training of data set S, it is divided into two sets S^+ with $y_i = 1$ and S^- with $y_i = -1$. The density function $\rho(x_i)$ for the point x_i being the number of data points in its neighborhood is divided into two groups, positive and negative, given by,

$$\rho^+(x_i) = \begin{cases} N(\{x \mid \|x - x_i\| \leq r.d, x \in S^+\}) \forall x_i \in S^+ \\ N(\{x \mid \|x - x_i\| \leq r.d, x \in S^-\}) \forall x_i \in S^- \end{cases} \tag{51}$$

$$\rho^-(x_i) = \begin{cases} N(\{x \mid \|x - x_i\| \leq r.d, x \in S^-\}) \forall x_i \in S^+ \\ N(\{x \mid \|x - x_i\| \leq r.d, x \in S^+\}) \forall x_i \in S^- \end{cases} \tag{52}$$

Where $\|.\|$ denotes the Euclidean distance and $N(.)$ denotes the cardinality of the set containing the data points. The distance between the two classes S^+ and S^- is denoted by d and r is a fractional multiplier. Using equations (51) and (52), membership function is formulated as follows:

$$s_i = \frac{\rho^+(x_i)}{\rho^+(x_i) + \rho^-(x_i)} . \frac{\rho^+(x_i)}{\rho^+_{\max}} \tag{53}$$

where $\rho^{+}_{\max}$ is the maximum of $\rho^{+}(x_i)$ for all training data points.

Parameter selection for FSVM classifier with RBF kernel was predetermined by the kernel parameter σ and the trade-off parameter C (23). However, the optimal values for these parameters were found first firstly for normal SVM algorithm using two dimensional grid by $C = (1,2,10,50,100,1000)$ and σ with 100 equidistant values between 1 and 5. The general flow chart for the classification of EEG signals is shown in the figure 4.7

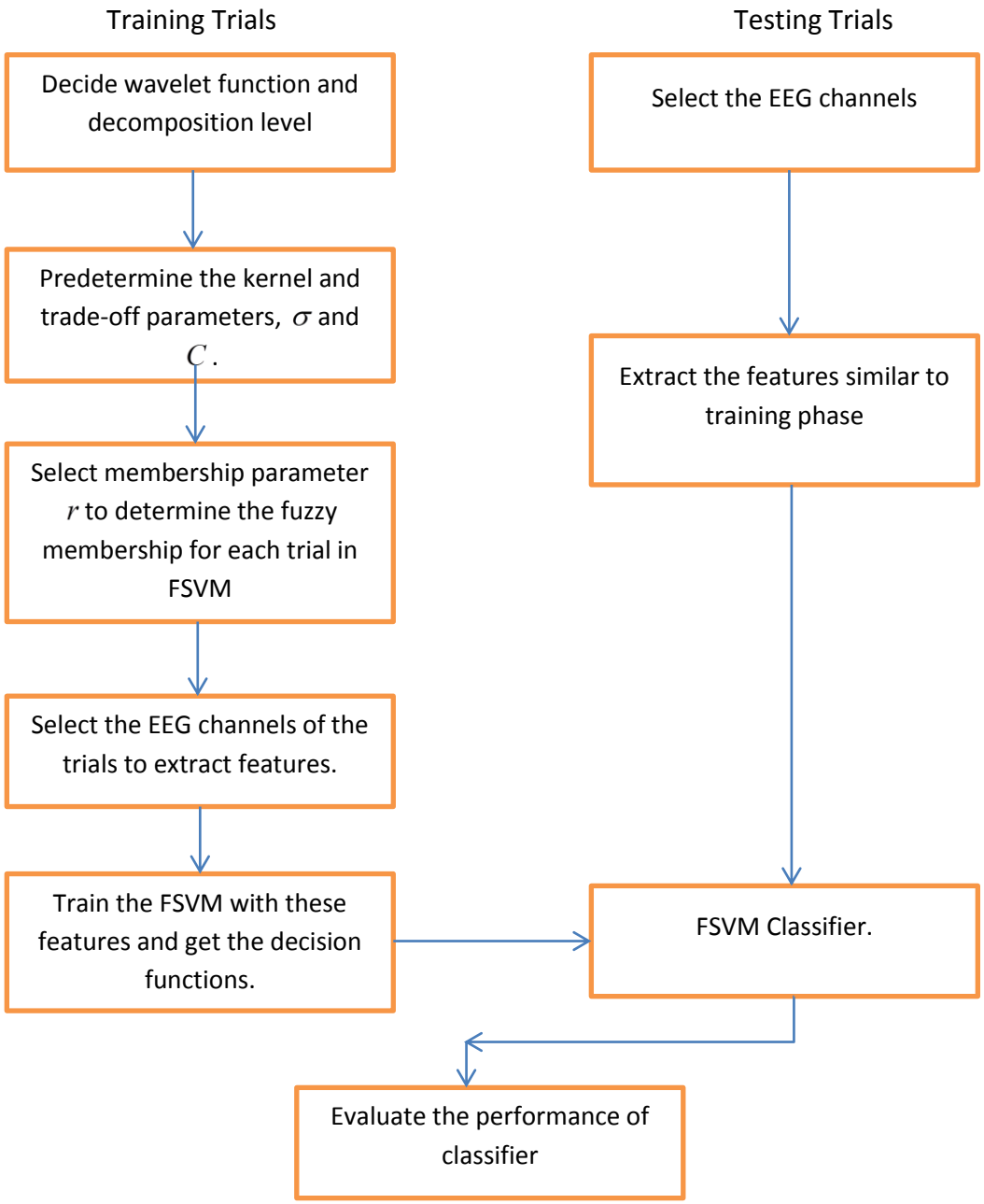

Figure 4.7 Flow chart of the FSVM application on EEG signals.

Bibliography

1. **Kaper, M., et al.** 2004 *BCI compition 2003 - data set IIb: Support vector machines for P300 speller paradigm*, IEEE Transactions on Biomedical Engineering, Vol. 51, pp. 1073-76.

2. **Rakotomamonjy, A., Guigue, V. and Mallet, G. and Alvarado, V.** 2005 *Ensemble of SVM for improving brain computer interface P300 speller performances.* Berlin : Springer, Artificial Neural Networks: Biological Inspirations - ICANN, pp. 45-50.

3. **Peterson, D. A., et al.** 2005 *Feature selection and blind source separation in an EEG-based brain computer interface*, Journal on Applied signal processing, Vol. 19, pp. 3128-40.

4. **Kousarrizi, M. R. N., et al.** 2009 *Feature Extraction and Classification of EEG Signals Using Wavelet Transform, SVM and Artificial Neural Networks for Brain Computer Interfaces.* International Joint Conference on Bioinformatics, Systems Biology and Intelligent Computing, IJCBS. pp. 352-355.

5. **Guo, L., et al.** 2010 *Classification of Mental Task from EEG Signals Using Immune Feature Weighted Support Vector Machines*, IEEE Transactions on Magnetics.

6. **Abe, S.** 2005 *Support Vector Machines for Pattern Classification.* [ed.] S. Singh. London : Springer.

7. **Vapnik, V. N.** 2000 *The Nature of Statistical Learning Theory.* [ed.] M. et al. Jordan. New York : Springer.

8. **Lotte, F., et al.** 2007 *A review of classification algorithms for EEG-based brain-computer interfaces.*, Journal of Neural Engineering, Vol. 4, pp. R1-R13.

9. **Wang, L.** 2005 *Support Vector Machines: Theory and Applications.* [ed.] J. Kacprzyk. Netherlands : Springer pp. 10-29.

10. **Bennett, K. P.** 1999 *Combining support vector and mathematical programming methods for classification.* [ed.] B. Scholkopf and C. J. C. and Smola, A. J. Burges. Cambridge : MIT Press pp. 307-326.

11. **Takahashi, F. and Abe, S.** 2002 *Decision-tree--based multiclass support vector machines.* Singapore, Proceedings of Ninth International Conference on Neural Information Processing (ICONIP 02). Vol. 3, pp. 1412-22.

12. **Osuna, E. and Freund, R. and Girosi, F.** 1997 *An improved training algorithm for support vector machines.*. Neural Networks for Signal Processing VII—Proceedings of the 1997 IEEE Signal Processing Society Workshop. pp. 276-285.

13. **Saunders, C., et al.** 1998 *Support vector machine reference manual.* Royal Holloway, University of London. 1998. Technical Report CSD-TR-98-03.

14. **Wang, L.** 2005 *Support Vector Machines: Theory and Applications.* [ed.] J. Kacprzyk, Springer.

15. **Anguita, D., Boni, A. & Ridella, S.** 2000 *Evaluating the generalization ability of Support Vector Machines through the Bootstrap.*, Neural Processing Letters, Vol. 11, pp. 51-58.

16. **Anguita, D., Ridella, S., Rivieccio, F. & Zunino, R.** 2003 *Hyperparameter design criteria for support vector classifiers.*, Neurocomputing, Vol. 6, pp. 109-134.

17. **Duan, K., Keerthi, S. & Poo, A.** 2001 *Evaluation of simple performance measures for tuning SVM parameters.* University of Singapore. Technical Report CD-01-11.

18. **Efron, B., Tibshirani, R.** 1993 *An introduction to the bootstrap.* Chapmann and Hall.

19. **Politis, D.N.** 1998 *Compute intensive methods in statistical analysis.*, IEEE Signal Processing Magazine, Vol. 15, pp. 39-55.

20. **Devroye, L., Wagner, T.** 1979 *Distribution-free inequalities for the deleted and hold-out error estimates.*, IEEE Trans. on Information Theory, pp. 202-207.

21. **Vapnik, V.** 1998 *Statistical learning theory.* s.l. : Wiley.

22. **Xu, Q., Zhou, H., Wang, Y., & Huang, J.** 2009 *Fuzzy support vector machine for classification of EEG signals using wavelet based features.*, Medical Engineering & Physics, Vol. 31, pp. 858-865.

23. **Belousov, AI., Verzakov, SA., & von Frese, J.** 2002 *A flexible classification approach with optimal generalization performance: support vector machines*, Chemometrics and Intelligent Laboratory Systems, Vol. 64, pp. 15-25.

5. Noninvasive EEG-Based Brain-Computer Interfaces

5.1 Introduction

In this chapter we shall discuss the brief overview of brain-computer interfaces (BCI) in order to understand its objectives, background and the phases involved in this BCI projects. Normally people use speech, gestures or writing to communicate with other people. Imagine if somebody is not able to communicate with other people through these channels but he/she is aware of the environment. Such a condition is called locked-in syndrome. Indeed the patients are truly locked in their bodies and remain unable to express themselves. There are some neurological diseases that may cause the body towards paralyses of the motor system restricting both verbal and nonverbal communication. Locked-in means that the people are conscious and alert but not able to utilize their muscles causing them to restrict the communication of their needs, wishes and emotions: keeping the healthy brain locked into a paralyzed body. Amyotrophic lateral sclerosis (ALS) (1) is such a disease that causes the patients to go into locked-in syndrome. It is a progressive, neurodegenerative disease and is characterized by the death of motor neurons which in turn leads to the loss of control over voluntary muscles. This situation motivates us to restore their communication of those individuals who have lost the ability to communicate by speech or other muscular activities.

Brain-computer interfaces (BCI) are a new means of channels that could give back the basic communication abilities and some degree of autonomy to the individuals in locked-in condition. BCI technology augments the human capabilities and enables them to interact with computers and other physical devices through brainwaves after a short training period. So the underlying idea to develop BCI technology is to record the electric or magnetic signals from the human brain through invasive or non-invasive approaches. A BCI establishes a communication channel between the human brain and the computer. It translates the human brain activity into messages or commands after necessary signal processing, feature extraction and classification which means that the idea is to detect the patterns of brain activities and then these patterns are translated into commands to interact with computer or other physical devices e.g. wheelchairs. There are several ways to record human brain signals e.g. EEG, fMRI etc. but here we will discuss brain-computer interfaces based on EEG signals and non-invasive approach. Applications for BCI may be developed either in physical or virtual world (2) (3) so an individual can control the devices such as movement of cursor on monitor screen, typing using virtual keyboard and controlling wheelchair using EEG-based non-invasive BCI. The electrical activity produced by the brain is recorded using electrodes placed over the scalp. The experiments are usually designed to record EEG signals such as P300, or mu rhythm. Event-related potentials (ERPs) that can more precisely

describe the dynamics of brain related activities are extracted from the recorded EEG signals. For instance, BCI users concentrate on imagination of hand or foot movement (4) or fixate their gaze on monitor screen to interact with speller applications (5). These mental activities are selected in such a way to activate the related brain area and may vary widely across different experiments, subjects and the related application. Such BCI systems performances may be improved with the help of feedback.

Wolpaw in (6) has presented an overall generic review of brain-computer interface systems that provide comprehensive detail on fundamental studies. He categorizes the BCI into dependent and independent classes. In dependent BCI brain's normal output pathways are not used to carry the message but activity in these pathways is required to generate the brain activity that does carry it. For instance, a matrix of letters is presented to the user with flashing one letter at a time or a complete row/column of letters in an odd-ball paradigm manner and users intension is to select the letter by fixing its gaze on it in order to generate visual evoked potential (VEP) recorded from the scalp preferably over the visual cortex (7). Here the brain's output channel is EEG whose generation depends on gaze direction which turns on the extraocular muscles and the cranial nerves that activate them. Whereas an independent BCI does not depend in any way on brain's normal output pathways. The message is not carried by the peripheral nerves and muscles and the activity in these pathways is not required to generate the brain activity that does carry the message. In this case, the brain's output channel is EEG, and the generation of the EEG signal depends mainly on the user's intent, not on the precise orientation of the eyes (8) (9) (10).

In BCI applications, the movements and their associated the nerves and muscles are replaced with electrophysiological signals and the hardware and software which translate these signals into commands to initiate actions. It should be kept in mind that user's specific skills are required to perform successful BCI operation because the users require a skill not only to control the muscles but also require how to produce and control specific electrophysiological signals in order to accomplish the user's intent so BCI use is a skill. Such skills are also required even when the initial training is not needed e.g. BCI based on P300 potential that is generated in response to the desired letter without training and successfully implemented in speller application. Basic research on BCI systems commenced in the early 1970's and has seen renewed interest in recent years. While increases in computing power and advances in measurement technology have led to a large variety of proof-of-concept systems, none of the systems described in the scientific literature is suited for daily use by disabled persons. This is due to the fact that the technology underlying BCIs is not yet mature enough for usage out of the laboratory.

5.2 Main Components of BCIs

In general, any BCI system consists of these components. 1) Signal acquisition, preprocessing, feature extraction, classification and application interface. General model architecture of a BCI system is shown in figure 5.1 with respect to offline and online or real

time methods. The electrophysiological signals are recorded and stored with signal acquisition component and the electrodes are placed over the scalp according to 10-20 electrode placement system as shown in figure 5.1.

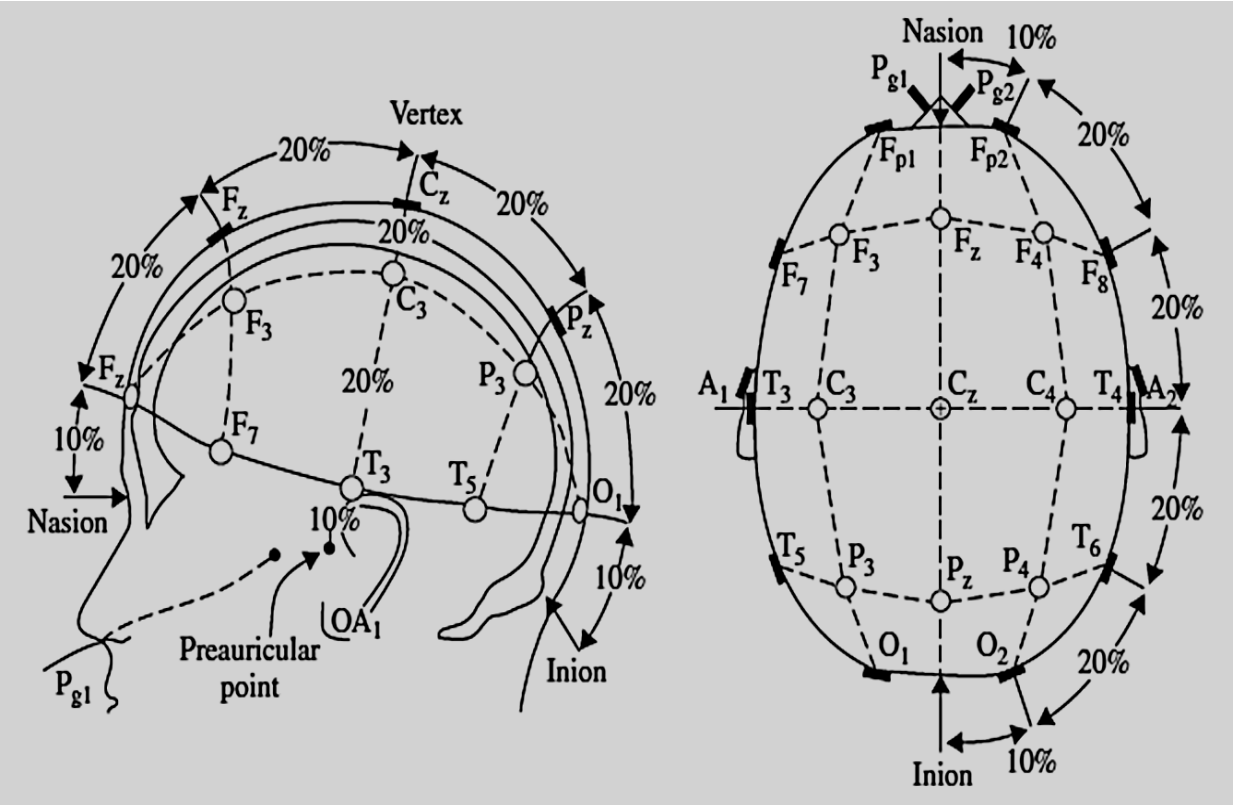

Figure 5.1 10-20 International electrode placement system. Source (Wikipedia)

Once the signals are acquired, preprocessing component performs artifact reduction in terms of removal of electrooculogram (EOG) and electromyogram (EMG) signals. This component is also responsible for the application of low pass and/or high pass filters in order to remove the influence of noise e.g. line frequency, and to perform spatial filtering in case of multichannel data. After the signals are preprocessed, it is assumed to have EEG signals in hand which are subjected to further signal processing algorithms for feature extraction. It is assumed that the extracted feature must be suitable for subsequent classification of specific brain patterns. A variety of feature extraction methods exists that can be used with BCI systems e.g. amplitude and latency measures (already discussed in chapter 3), band power, Hjorth parameters, autoregressive parameters and wavelets. Features may be extracted both in time and frequency domain depending on the application. To assign the recorded samples of the signal to a particular category or class, classification component is activated that receive the input from feature extractor. There is variety of linear and non-linear classification methods available e.g. linear discriminant analysis, neural networks and support vector machines. After the signal is classified into a particular class, the output of the classifier that could simply be an on/off signal is transformed into a control signal in order to interact with application interface to control

the physical device or to navigate in the virtual environment as shown in figure 5.2. Once the device attached to the BCI system is started controlling, the feedback of the application's output could be used to improve the performance of a BCI system. For further literature on BCI systems readers may find useful (11) (12) (13).

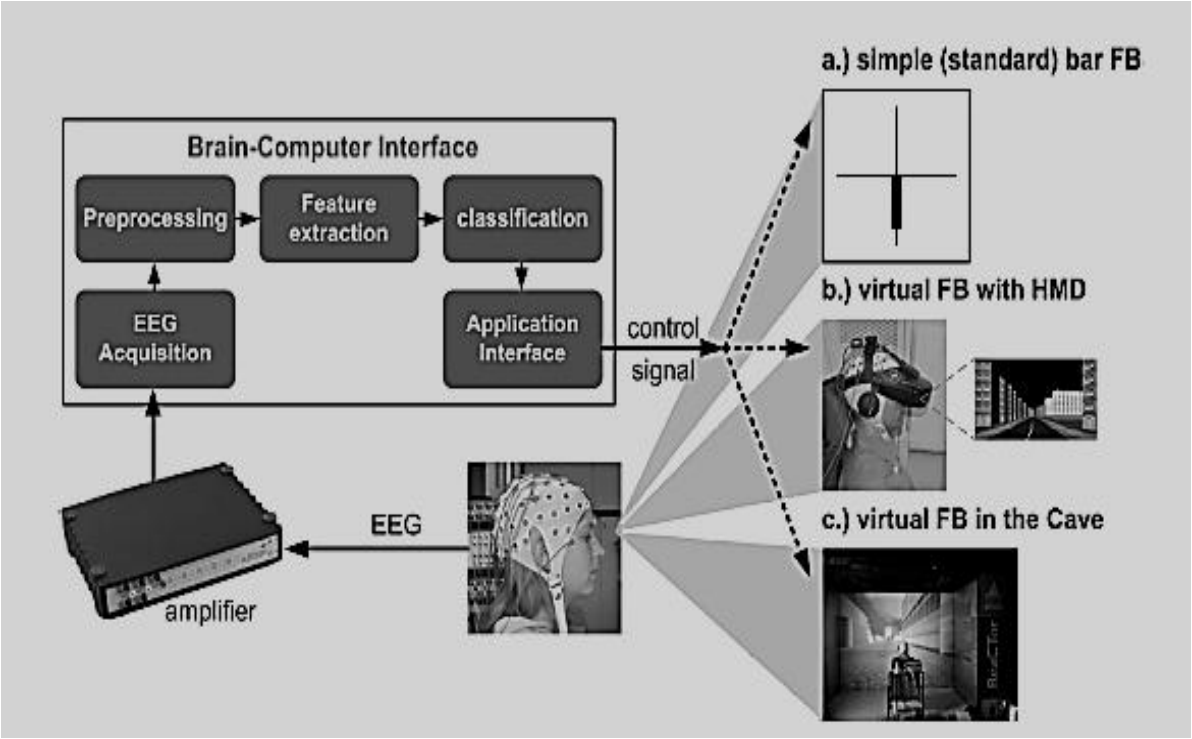

Figure 5.2 Generic model architecture for a brain-computer interface. Source (2)

5.3 Types of EEG signals used for Noninvasive BCI Systems

BCI communication systems are based on a variety of EEG signals being currently used for the demonstration of proof of concept. These are P300 potentials (5), steady-state evoked potentials (14), motor potentials (15), event-related synchronizations/desynchronizations (16) and slow cortical potentials (17) (18). These are the potentials generally recorded over the surface of the brain and provide safer way to invasive approaches and provide useful BCI communication devices for individuals with disabilities. Here we shall discuss BCI based on P300 potentials and motor potentials due to limited scope of the chapter.

5.3.1 BCI based on P300 Potentials

P300 has been extensively studied within the context of oddball paradigm. It is a large positive potential over the midline areas and appears around 300 ms after the onset of stimulus and in response to target stimuli that occur infrequently to which the subject is supposed to respond to in some manner. Farwell and Donchin et al. (5) (19) were the first who reported the use of P300 potential for BCI communication system. The paradigm they used consists of a 6 × 6 matrix of grey symbols on a dark background. The rows and columns were randomly intensified and the subjects were supposed to respond in terms of counting

(by heart) the letter being attended. The P300 was elicited when the attended row or column flashed. The symbol was selected by averaging the certain number of trials. Hardware and software setup for P300-based BCI is shown in figure 5.3.

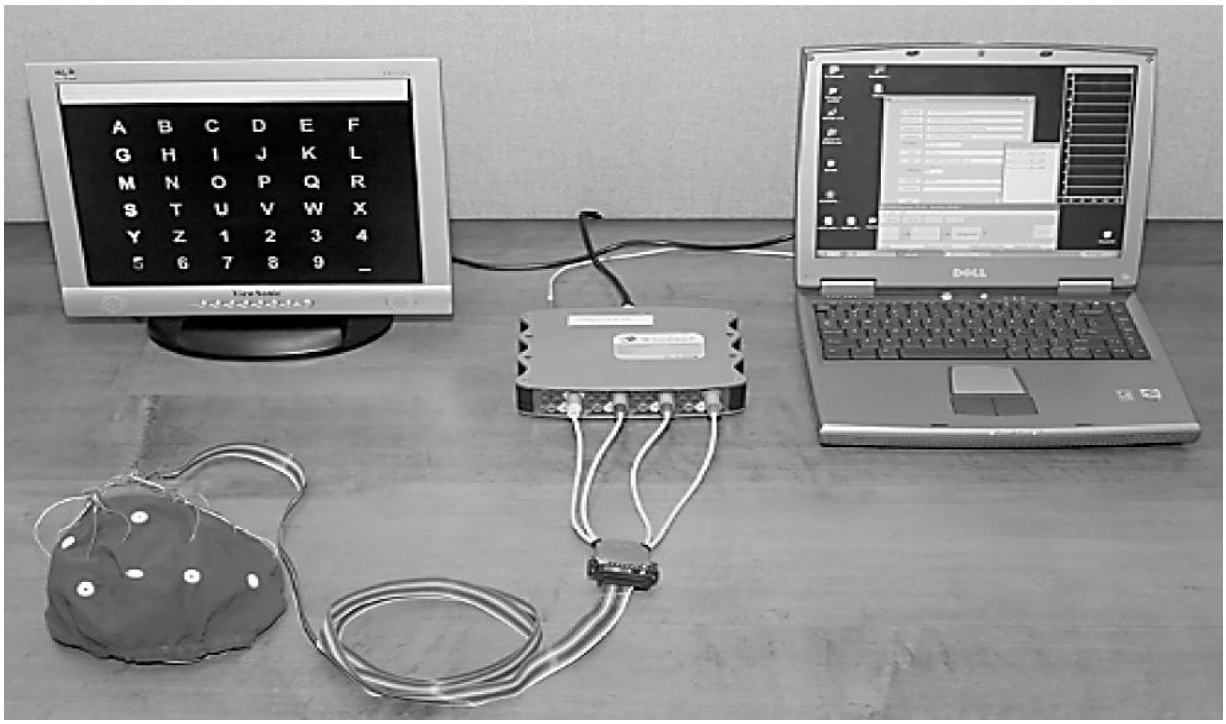

Figure 5.3 The hardware for P300-based BCI for home.

The users with and without disabilities showed accurate performance however the users performance varies depending on the size of matrix and inter-stimulus interval (20). In (21), Krusienski et al. have shown that the online performance of a P300 based BCI is significantly improved when the midline electrodes are supplemented with posterior locations. Serby et al. (22) have shown that the offline performance is improved by using 6 × 6 matrix with independent component analysis and a matched filter. A P300-based BCI system is being used in-home by a patient with ALS (23). This system has reduced set of electrodes, portable amplifier and a laptop computer with a specific instance of BCI2000 (24). Literature suggests that if the subjects are visually impaired then auditory stimuli (25) may be used to elicit P300 potential and is quite successful for BCI use (26). An apparent advantage of P300-based BCI is that it does not require initial training. Bayliss (27) recorded P300s in a virtual environment and suggested during the offline analyses that single-trial P300 amplitudes might be used for environmental control. A typical P300 potential is shown in figure 5.4

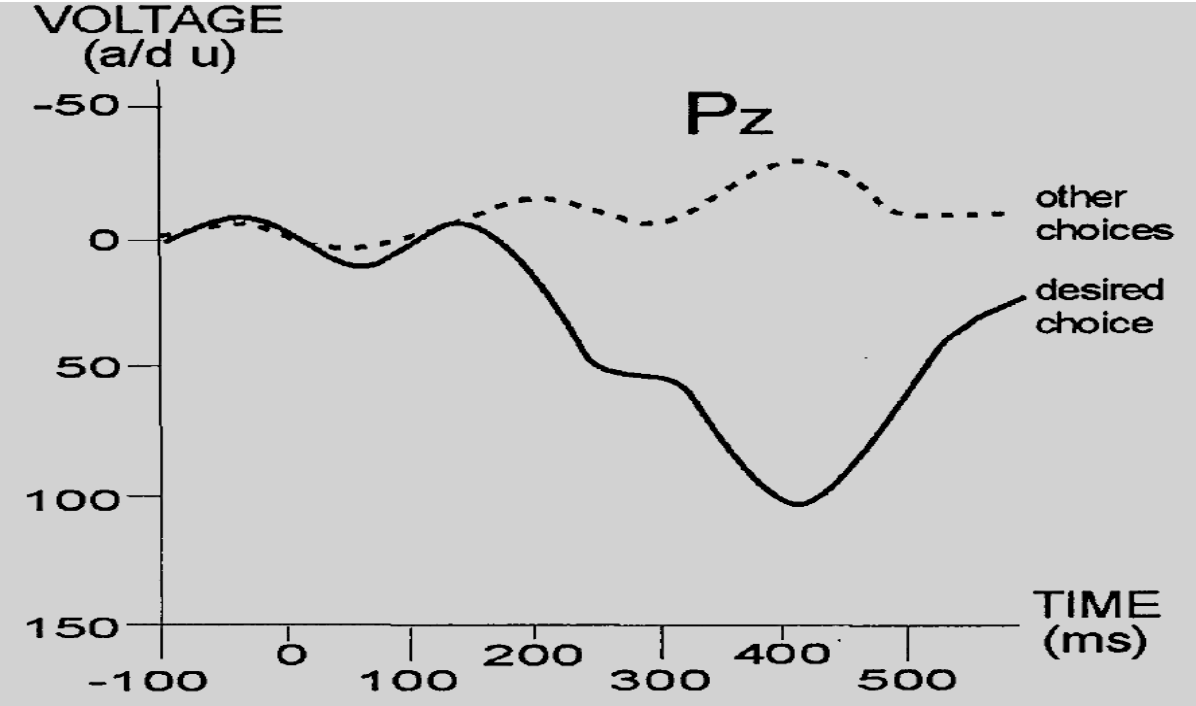

Figure 5.4 P300 evoked potential. Positive is plotted downward. Source (6)

5.3.2 BCI based on Motor Potentials

When primary sensory or motor cortical areas are not engaged in processing sensory input or producing motor output, EEG activity is produced among 8 – 12 Hz band (28). This idling EEG activity is known as my rhythm when it is recorded over the somatosensory or motor cortex and alpha rhythm when recorded over the visual cortex (29). Until 1976, mu rhythm was mostly seen in minority, however Pfurtscheller reveal that my rhythm is found mostly in adults (30). Some mu rhythms lies between 18 – 26 Hz beta rhythms and some beta rhythms happens to be the harmonics of mu rhythms. Since the mu and beta rhythms are generated from those cortical areas of the brain which are connected to brain's normal motor output channels, therefore, these signals could be good features for EEG based BCI communication. Mu and beta rhythms usually decrease when the subject is moving or preparing for movement. Such decrease is known as *even-related desynchronization*. Whereas when the subject comes to rest after movement, rhythm starts increasing and is known as *even-related synchronization* (31). Moreover, to produce these EEG activities, actual movements are not required because only imagination of movements (32) is sufficient to produce these activities which might be the cause for a BCI system to be independent BCI. One example of application of such imaginations of movements is successfully implemented in (2). Figure 5.5 illustrates how sensory motor rhythms produced by recording over the sensorimotor cortex during the control of a cursor movement towards the target at the top of the screen and towards the bottom of the screen. Frequency spectrum clearly shows that the EEG activity lies between 8 – 12 Hz mu rhythm and slight activity is also found in beta rhythm 18 – 28 Hz.

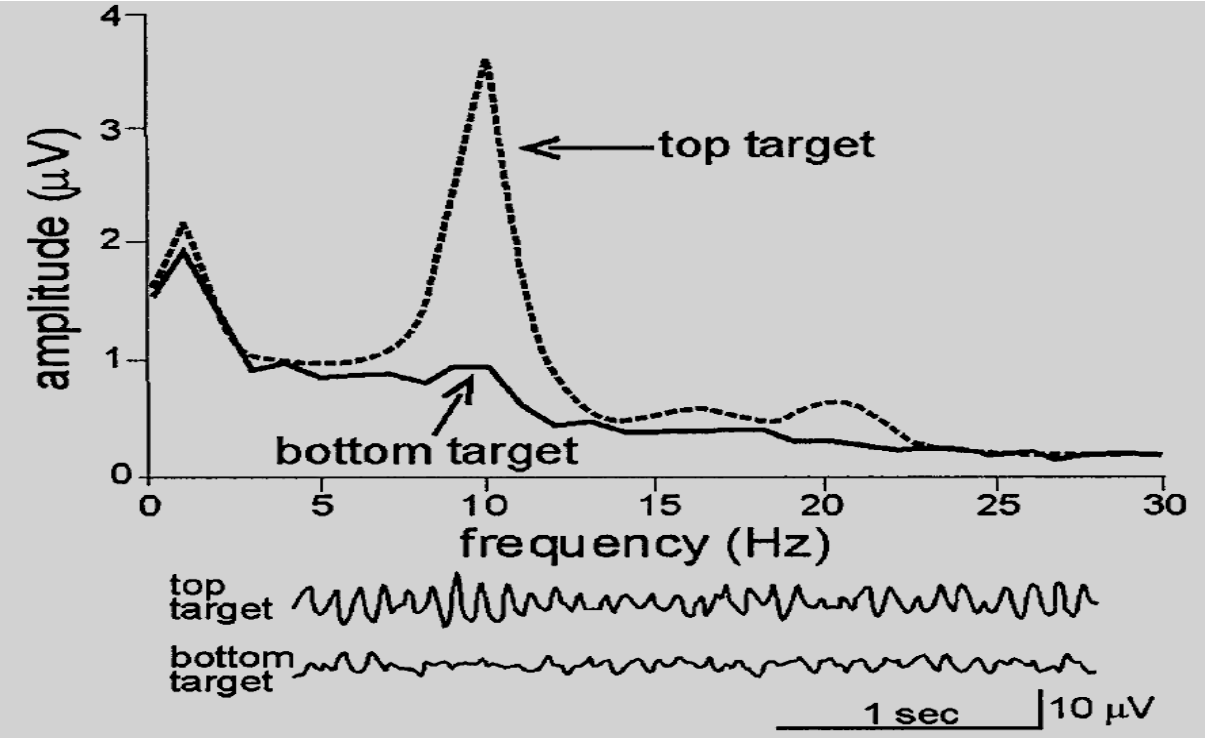

Figure 5.5 Sensorimotor Rhythms. Source (6)

These motor-related potentials are also used in (33) in context with BCI communication system but the authors emphasized on self-paced or user initiated BCI paradigms unlike Graz-BCI (2) which depends on auditory external cue. For self-paced BCI either the actual movements are necessary or some other means to verify the user's intension therefore training of classifier for such BCI system is a challenging task because the observable movements are not feasible with severely motor impaired users whereas Mason et al (15) have used sip-and-puff switch to verify the intent in paralyzed users. Among other applications of motor-related potentials Blankerts et al. (34) have used left and right key strokes and in (35) they have demonstrated the existence of detectable motor potentials from limb commands recorded from patients with amputations.

5.3.3 Slow Cortical Potentials

Slow Cortical Potentials (SCPs) are the scalp recorded EEG features that occur within 0.5 – 10 s having the lowest frequency and slow voltage changes generated in cortex. Increased cortical activation is associated with scalp negativity and decreased activation is associated with positivity (17). It is possible to learn how to control SCPs and therefore an object may be controlled on a computer screen using SCPs in (36) which is known as thought translation device (TTD). The patients with late stage ALS are also able to produce SCP and have the capability of using such communication capability (37). Figure 5.6 illustrates the variation is SCPs, for which EEG was recorded at the vertex linked to mastoids. The subject was supposed to select the target at the top and bottom of the screen. It took 4 s to select the object. The main disadvantage of such BCI systems is that it took long training time.

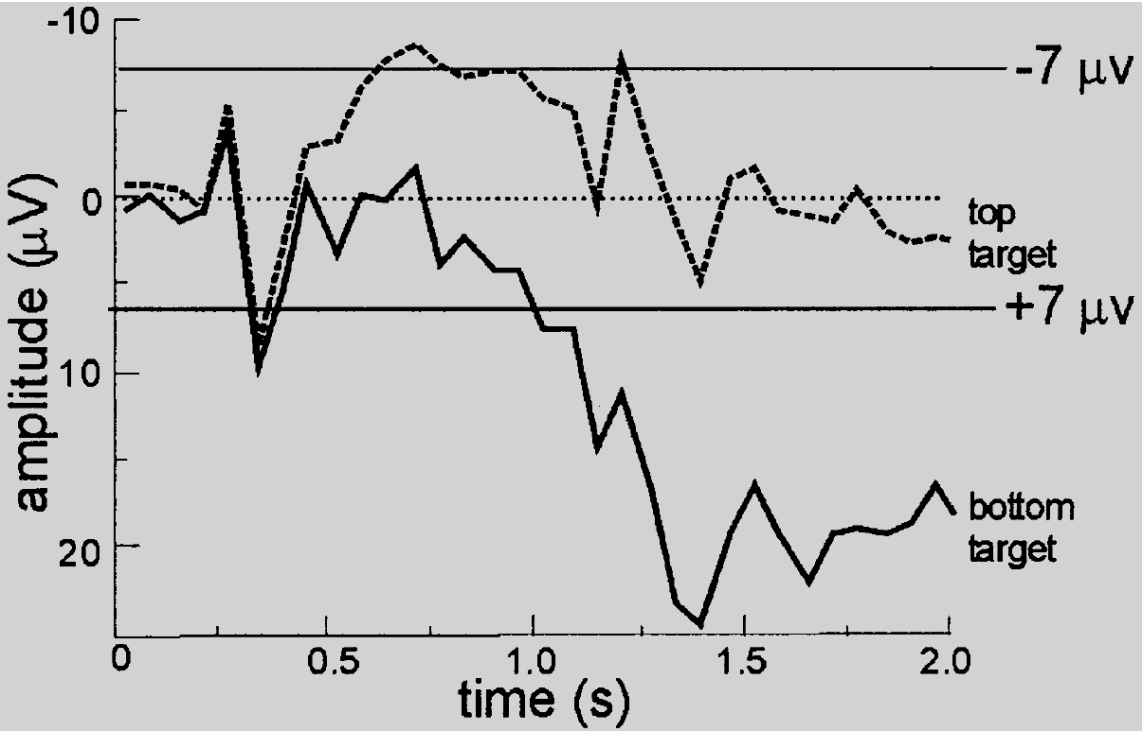

Figure 5.6 Slow cortical potential. Positive is plotted downward.

It requires 1 – 2 h per week over weeks or even months to train the users. After the users achieve 75% of consistent accuracies, they are switched to language support program (LSP) that enables the user to choose a letter or combination of letters (38).

5.4 Well Known Brain-Computer Interfaces

There are several BCIs which provide state of the art. For example, Wadsworth's BCI, Graz's BCI and Berlin's BCI and there might be other systems but we shall describe here only couple of BCI systems.

5.4.1 Noninvasive BCI at Wadsworth Center

At Wadsworth center the objective was to develop a BCI that could be used in a daily life by severely disabled people at their homes. Firstly, researchers developed a BCI that controls a cursor in one or two dimension using mu and/or beta rhythms recorded over the sensorimotor cortex. They further extended their BCI to include the use of P300 response and additionally developed general purpose software (BCI2000) for BCI research (24).

Wadsworth's Mu Rhythm Based Communication

In order to utilize sensorimotor rhythm (SMR) amplitudes in mu (8 – 12 Hz) and/or beta (18 – 26 Hz) bands, users require a series of training sessions to learn to move a cursor on a video screen in one or two dimensions. The more the practice the user does, the more the improvement of user performance comes out. They demonstrated that they used two channels of EEG to control cursor movement independently in two dimensions so users

could hit targets located at one of the four corners of the monitor (39). They also demonstrated using one-dimensional cursor control with two to five targets arranged along the right edge of the monitor (40). Figure 5.7 illustrates the visual application design of the experiment in five steps for one dimension and two dimension cursor movement. 1) Trial begins and it lasts 1 s for the target and cursor to be present on the screen. 2a) The cursor moves steadily across the screen for 2 s with its vertical movement controlled by the user. 2b) The cursor moves in two dimensions with direction and velocity controlled by the user until the user hits the target or 10 s have elapsed. 3) The target flashes for 1.5 s when it is hit by the cursor. If the cursor misses the target, the screen is blank for 1.5 s. 4) The screen is blank for a 1-s interval. 5) The next trial begins.

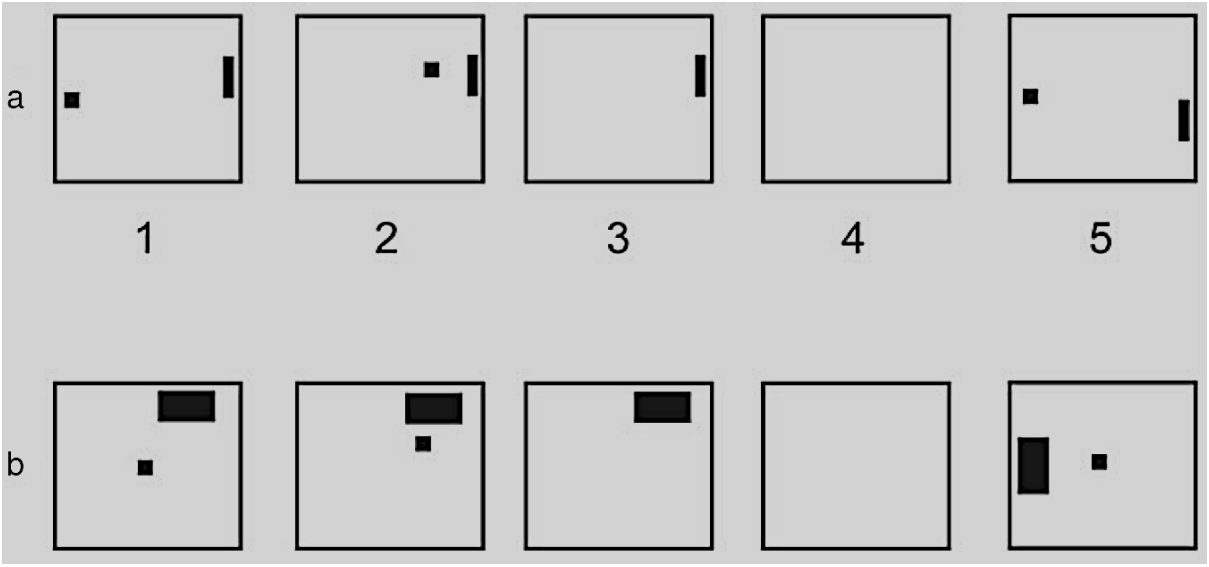

Figure 5.7 a) SMR task for one dimensional four target b) SMR task for two dimensional eight targets. Source (11)

To control each dimension, weighted sum of one or two spectral features was used. For example, an increase in the amplitude of 10Hz mu rhythm was used to move the target up and a decrease for moving the target down. Users initially learned cursor control in one dimension (i.e., horizontal) based on a regression function. Next they were trained on a second dimension (i.e., vertical) using a different regression function. Finally the two functions were used simultaneously for full two-dimensional control. Various regression models were evaluated for controlling cursor movement acquired from a four-choice, one-dimensional cursor movement task and it was also shown that using more than one EEG feature improved performance was found. Moreover, they evaluated nonlinear models with linear regression by including cross-product (i.e., interaction) terms in the regression function. Topographies of Pearson's r correlation values for one user are shown in figure 5.8, where it can be seen that two distinct patterns of activity controlled cursor movement. Horizontal movement was controlled by a weighted difference of 12-Hz mu rhythm activity between the left and right sensorimotor cortex (see figure 5.8, left topography). Vertical movement was controlled by a weighted sum of activity located over left and right

sensorimotor cortex in the 24-Hz beta rhythm (see figure 5.8, right topography). This study illustrated the generalizability of regression functions to varying target configurations. In addition, they conducted a study according to which users are also able to control a robotic arm in two dimensions by applying the same techniques which were already used for cursor control. They have also shown that users are able to select or reject the target by performing or withholding hand-grasp imagery (41).

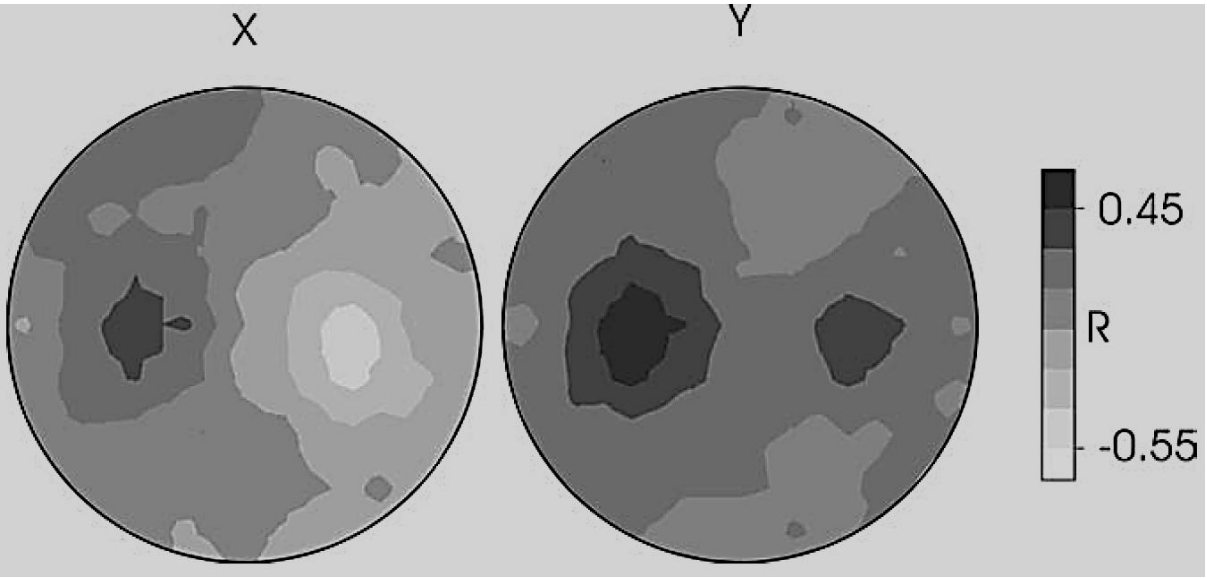

Figure 5.8 Scalp topographies (nose at top) of Pearson's r values for horizontal (x) and vertical (y) target positions. Source (11)

Wadsworth's P300 Based Communication

They also developed a BCI based on P300 feature of the EEG signal whose objective was to type letters without using hands with brainwaves, commonly known as Speller application. The subjects were presented a matrix paradigm described by (5) i.e. 6 × 6 matrix containing 36 symbols. The user focuses attention on the desired symbol in the matrix while the rows and columns of the matrix are highlighted in a random sequence of flashes. A P300 response occurs when the desired symbol is highlighted. To identify the desired symbol, the classifier determines the row and the column that the user is attending to (i.e., the symbol that elicited a P300) by weighting specific spatiotemporal features that are time-locked to the stimulus. The intersection of this row and column defines the selected symbol. Figure 5.9 shows a typical P300 matrix display and the averaged event-related potential responses to the intensification of each cell. The cell containing the letter "O" was the target cell and elicited the largest P300 response when highlighted. To a lesser extent the other characters in the row or the column containing the O also elicited a P300 because these cells are simultaneously highlighted with the target cell.

They evaluated the classification accuracy based on several variables e.g. channel set, channel reference, decimation factor and the number of model features using the stepwise

discriminant analysis (SWDA) method. They used different channel sets in order to have statistically significant effects on classification accuracy. Set 1 comprised of Fz, Cz and Pz. Set 2 contains PO7, PO8 and Oz. Set 3 contains both set 1 and set 2. Set 4 contains set 1, 2 and 3 with 19 electrodes in total. They showed that set 1 and set 2 were equal in performance but worse than set 3 whereas set 4 was no better than set 3.

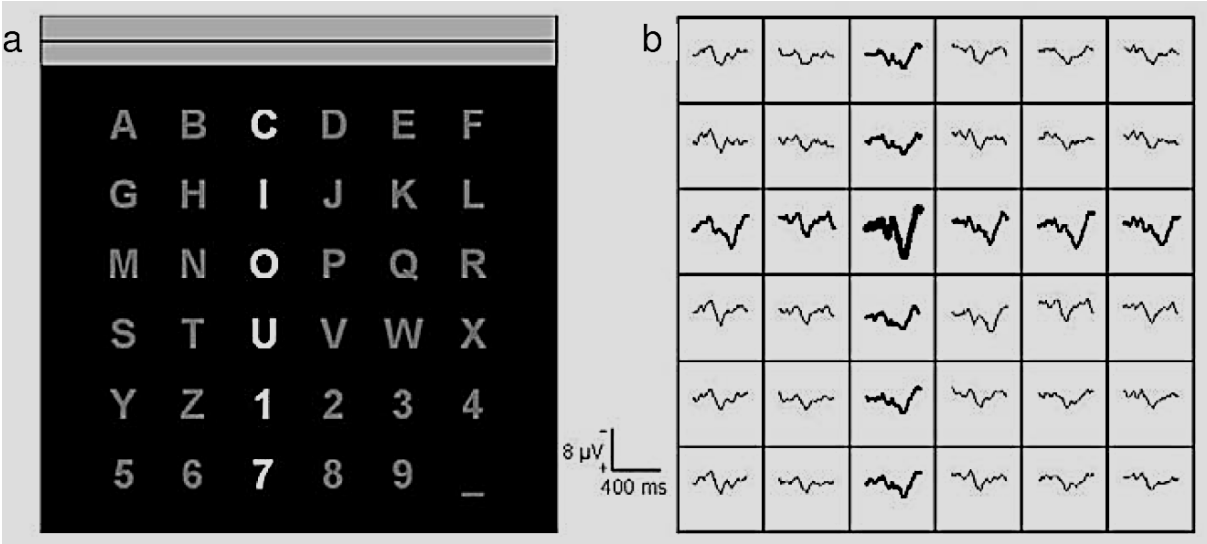

Figure 5.9 a) 6 × 6 matrix display b) average waveform of each cell.

From these results, one thing was clear that set 3 which contained 6 electrodes was suitable for this application rather using set 4 that contained 19 electrodes with excess of information to be processed.

5.4.2 Noninvasive Graz BCI

Graz BCI is based mainly on synchronous mode (which means that the time windows are limited for mental activities and therefore the signal has to be analyzed in epochs), two types of event-related potentials, the visual and somatosensory steady-state potentials (SSVEP, SSSEP) were used as input signal for the Graz-BCI and uses motor imagery and associated oscillatory EEG signals from the sensorimotor cortex for device control. Mu (8–12 Hz), sensorimotor rhythm (12–15 Hz) and beta (15 – 30 Hz) frequency bands were considered. To control an external device based on brain signals, it is essential that imagery related brain activity can be detected in real time from the ongoing EEG. They studied the effects of kinesthetic and visual representation of actions so the two actions, kinesthetic motor imagery (first person, MIK, in which the subjects were supposed to imagine self-performed action) and visual motor imagery (third person, MIV, in which the subjects were supposed to imagine a previously viewed 'actor') were instructed to the subjects to perform. Moreover, two other actions were also given to the subjects i.e. real movements (motor execution, ME) and visual observation of physical hand movement (OOM). Figure 5.10 show the experimental task and timing. Separate runs were executed consisting of each forty trials for the four tasks (OOM, MIV, ME and MIK). Each started with the

presentation of a fixation cross at the center of the monitor (0 s). A beep tone (2 s) indicated the beginning of the respective task: Subjects should either watch the movements of the animated hand, or perform movements themselves, or imagine hand movements until a double beep tone marked the end of the trial (7 s). A blank screen was shown during the inter-trial period varying randomly between 0.5 and 2.5 s.

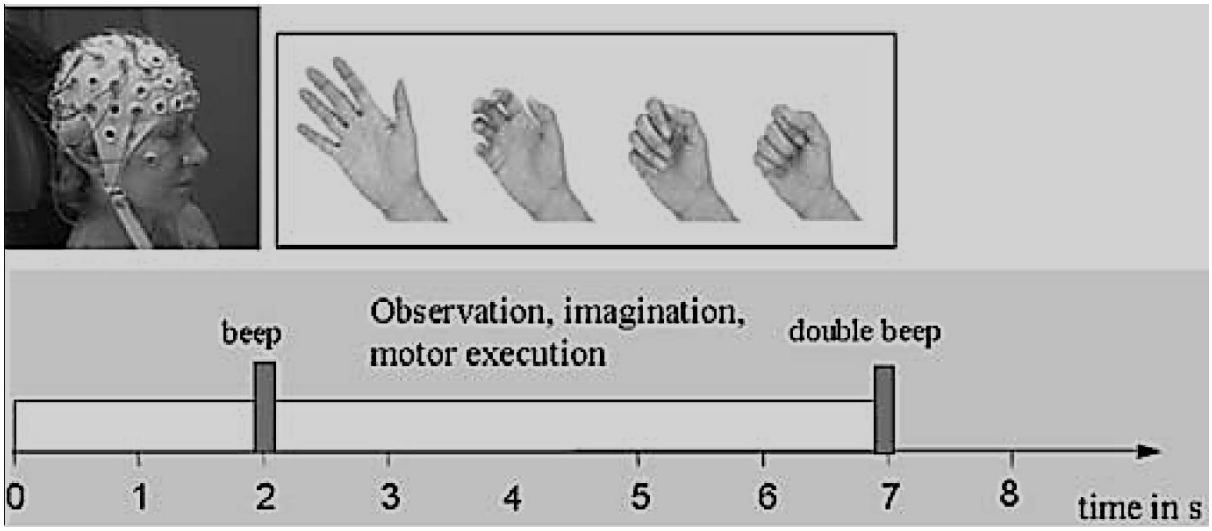

Figure 5.10 Experimental tasks and timing.

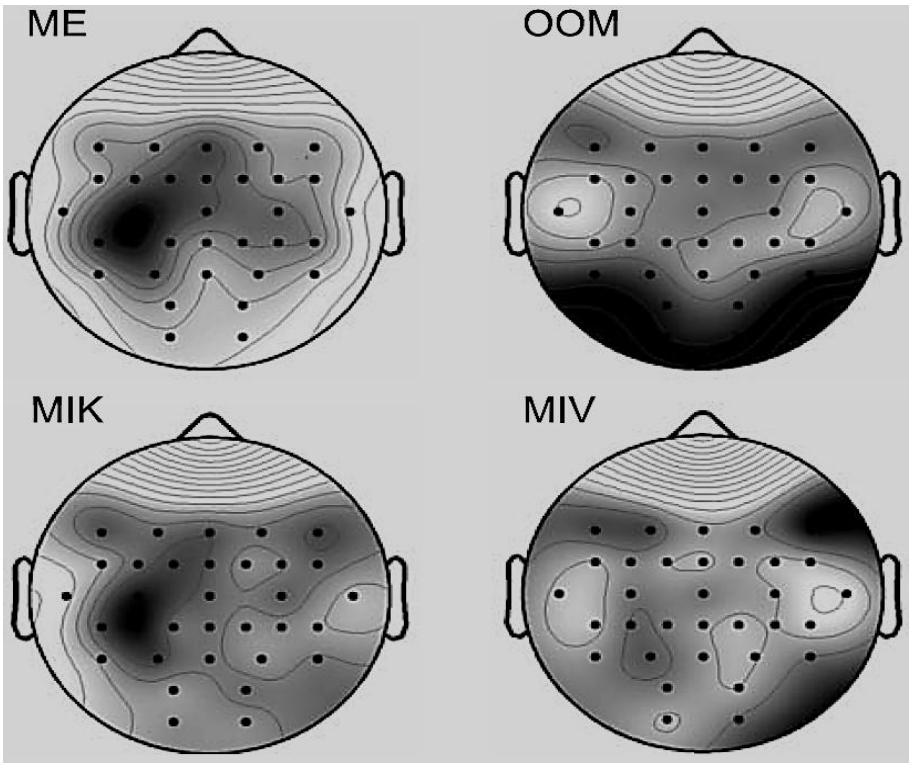

Figure 5.11 Topographical maps of grand average classification accuracies. Source (11)

The distinction-sensitive learning vector quantization (DSLVQ) (42) method was used as learning classifier to feed the results of fourteen right-handed participants based on

multichannel EEG recordings. Electrode locations and reactive frequency components were used as features for the classifier to recognize the respective mental states. Real conditions (ME and OOM) showed the highest classification accuracy of about 80% on average which is also visible in figure 5.11 that the corresponding representation areas for both conditions were mostly active i.e. occi-parietal cortical area for visual observation and motor area for ME near electrode C3. It is also clear from the figure that classification for MIK is also localized on left side of the brain similar to ME for right hand movement whereas MIV was not able to localize clearly thereby resulted in unsatisfactory single-trial EEG classification.

5.5 Applications

In theory any device that can be connected to a computer or to a microcontroller could be controlled with a BCI. In practice however, the set of devices and applications that can be controlled with a BCI is limited. To understand this, one has to consider that the amount of information which can be transmitted with present day BCI systems is limited. The typical information transfer rate achievable with an EEG based BCI is about 20 to 40 bits/min. As an additional obstacle most present day BCI systems function only in synchronous mode. In synchronous mode, communication is possible only during predefined time intervals. This means the system tells the user when it is ready to receive the next command and limits severely the possible type of applications. In asynchronous mode users can send commands whenever they want. Some of the applications possible with current BCIs are described below.

5.5.1 Spelling Devices

Spelling devices allow severely disabled users to communicate with their environment by sequentially selecting symbols from the alphabet. One of the first spelling devices mentioned in the BCI literature is the P300 speller (5). A system based on SCPs was described by (43). In their system the alphabet is split into two halves and subjects can select one halve by producing positive or negative SCPs. The selected halve is then again split into two halves and this process is repeated recursively until only one symbol remains. An advanced version of this system in which the relative frequency of letters in natural language is taken into account is presented by (38). System based on sensorimotor rhythms is described by (44).

5.5.2 Environment Control

Environment control systems allow controlling electrical appliances with a BCI. Gao in (45) has described a proof-of-concept environment control system based on SSVEPs and Bayliss in (46) described the control of a virtual apartment based on the P300.

5.5.3 Wheelchair Control

Disabled subjects are almost always bound to wheelchairs. If control over some muscles remains, these can be used to steer a wheelchair. For example systems exist that allow to steer a wheelchair with only a joystick or with head movements. If no control over muscles remains, a BCI can potentially be used to steer a wheelchair. Because steering a wheelchair is a complex task and because wheelchair control has to be extremely reliable, the possible movements of the wheelchair are strongly constrained in current prototype systems. In the system presented by (47) the wheelchair is constrained to move along paths predefined in software joining registered locations and a P300-based interface is used to select the desired location. Millan et al. has described in (48) that a miniature robot can be guided through a labyrinth, based on oscillatory brain activity recorded with the EEG. Control of the robot is simplified by implementing a wall following behavior on the robot and allowing for turns only if there is an open doorway.

5.5.4 Neuromotor Prostheses

The idea underlying research on neuromotor prostheses is to use a BCI for controlling movement of limbs and to restore motor function in tetraplegics or amputees. Different types of neuromotor prostheses can be envisioned depending on the information transfer rate a BCI provides. If neuronal ensemble activity is used as control signal, high information transfer rates are achieved and 3D robotic arms can be controlled (49). If an EEG based BCI is used, only simple control tasks can be accomplished. For example in the system described by Pfurtscheller (50) sensorimotor rhythms were used to control functional electric stimulation of hand muscles and so to restore grasp function in a tetraplegic patients.

5.5.5 Gaming and Virtual Reality

Besides the applications targeted towards disabled subjects, prototypes of gaming and virtual reality applications have been described in the literature. Examples for such applications are the control of a spaceship with oscillatory brain activity (51), the control of an animated character in an immersive 3D gaming environment with SSVEPs (52) and the control of walking in a virtual reality environment with sensorimotor rhythms (2).

Bibliography

1. **Bear, M., F., Connors, B., W., Paradiso, M., A.** 2007 *Neuroscience: Exploring the Brain.* 3rd ed. Lippincott Williams & Wilkins.

2. **Leeb, R., Keinrath, C., Friedman, D., Guger, C., Scherer, R., Neuper, C., Garau, M., Antley, A., Steed, A., Slater, M.** 2006 *Walking by thinking: The brainwaves are crucial, not the muscles!*, Presence, Vol. 15, pp. 500-514.

3. **Pires, G., Castelo-Branco, M., & Nunes, U.** 2008 *Visual P300-based BCI to steer a wheelchair: a bayesian approach.* Vancouver , 30th Annual Int. IEEE EMBS Conf. pp. 658-661.

4. **Pfurtscheller, G., & Neuper, C.** 2001 *Motor imagery and direct brain – computer communication.*. Proc. of the IEEE. Vol. 89, pp. 1123-1134.

5. **Farwell, L. A., & Donchin, E.** 1988 *Talking off the top of your head: toward a mental prosthesis utilizing event-related brain potential.*, Electroencephalography and Clinical Neurophysiology, Vol. 70, pp. 510-523.

6. **Wolpaw, J. R., Birbaumer, N., Mcfarland, D. J., Pfurtscheller, G. & Vaughan, T. M.** 2002 *Brain-computer interfaces for communication and control*, Clinical Neurophysiology, Vol. 113, pp. 767-791.

7. **Sutter, EE.** 1992 *The brain response interface: communication through visually-induced electrical brain responses*, J Microcomput Appl, Vol. 15, pp. 31-45.

8. **Sutton, S., Braren, M., Zubin, J., John, ER.** 1965 *Evoked correlates of stimulus uncertainty*, Science, Vol. 150, pp. 1187-1188.

9. **Donchin, E.** 1981 *Presidential address, 1980. Surprise!…Surprise?*, Psychophysiology, Vol. 18, pp. 493-513.

10. **Polich, J.** 1999 *P300 in clinical applications.* [ed.] E., Lopes da Silva, FH. Niedermeyer. 4th ed. Williams and Wilkins pp. 1073-1091.

11. **Dornhege, G., Millan, J. R., Hinterberger, T., McFarland, D. J., Muller, K. R., [ed.]** 2007 *Toward Brain-Computer Interfacing,* MIT Press.

12. **Tan, D. S., & Nijholt, A., [ed.].** 2010 *Brain-Computer Interfaces: Applying our Minds to Human-Computer Interaction.* s.l. : Springer.

13. **Berger, T. W., Chapin, J. K., Gerhardt, G. A., McFarland, D. J., Principe, J. C., Soussou, W. V., Taylor, D. M., & Tresco, P. A.,.** 2008 *Brain-Computer Interfaces: An International Assessment of Research and Development Trends,* Springer.

14. **Jones, K.S., Middendorf, M., McMillan, G.R., Calhoun, G. & Warm, J.** 2003 *Comparing mouse and steady-state visual evoked response-based control*, Interact. Computers, Vol. 15, pp. 603-621.

15. **Mason, S.G., Bohringer, R., Borisoff, J.F., & Birch, G.E.** 2004 *Real-time control of a video game with a direct brain-computer interface*, J. Clin. Neurophysiol., Vol. 21, pp. 404-408.

16. **Pfurtscheller, G., Flotzinger, D., & Kalcher, J.** 1993 *Brain-computer interface: a new communication device for handicapped persons.*, J. Microcomput. Appl., Vol. 16, pp. 293-299.

17. **Birbaumer, N., Elbert, A.G., Canavan, A.G. & Rockstroh, B.** 1990 *Slow potentials of the cerebral cortex and behavior.*, Physiol. Rev., Vol. 70, pp. 1-40.

18. **Kubler, A., Kotchoubey, B., Kaiser, J., Wolpaw, J. R., Birbaumer, N.** 2001 *Brain-computer communication: unlock the locked-in*, Psychol Bull, Vol. 127, pp. 358-375.

19. **Donchin, E., Spencer, K.M. & Wijesinghe, R.** 2000 *The mental prosthesis: assessing the speed of a P300-based brain-computer interface*, IEEE Trans. Rehab. Eng., Vol. 8, pp. 174-179.

20. **Sellers, E. W., Krusienski, D. J., McFarland, D. J., Vaughan, T. M., Wolpaw, J. R.** 2006 *A P300 event-related potential brain–computer interface (BCI): The effects of matrix size and inter stimulus interval on performance.*, Biological Psychology, Vol. 73, pp. 242-252.

21. **Krusienski, D.J., Sellers, E.W., McFarland, D.J., Vaughan, T.M. & Wolpaw, J.R.** 2006 *Toward enhanced P300 speller performance*, J. Neuroscience Methods, Vol. 3, pp. 299-305.

22. **Serby, H., Yom-Tov, E., & Inbar, G.F.** 2005 *An improved P300-based brain-computer interface*, IEEE Trans. Neural Syst. Rehab. Eng., Vol. 13, pp. 89-98.

23. **Vaughan, T.M., McFarland, D.J., Schalk, G., Sarnacki, W.A., Krusienski, D.J., Sellers, E.W. & Wolpaw, J.R.** 2006 *The Wadsworth BCI research and development program: at home with BCI*, IEEE Trans. Neural Syst. Rehab. Eng., Vol. 14, pp. 229-233.

24. **Schalk, G., McFarland, D.J., Hinterberger, T., Birbaumer, N., & Wolpaw, J.R.** 2004 *BCI2000: A General-Purpose Brain-Computer Interface (BCI) System*, IEEE Trans. on Biomedical Eng., Vol. 51, pp. 1034-1043.

25. **Glover, A.A., Onofrj, M.C., Ghilardi, M.F., Bodis-Wollner, I.** 1986 *P300-like potentials in the normal monkey using classical conditioning and the auditory 'oddball' paradigm*, Electroenceph clin Neurophysiol, Vol. 65, pp. 231-235.

26. **Klobassa, D.S., Vaughan, T.M., Brunner, P., Schwartz, N.E., Wolpaw, J.R., Neuper, C., Sellers, E.W.** 2009 *Toward a high-throughput auditory P300-based brain-computer interface*, Clin. Neurophysiol., Vol. 120, pp. 1252-1261.

27. **Bayliss, J.D. & Ballard, D.H.** 2000 *A virtual reality tested for brain-computer interface research*, IEEE Trans. Rehabil. Eng., Vol. 8, pp. 188-190.

28. **Kozelka, J.W.,& Pedley, T.A.** 1990 *Beta and mu rhythms*, J. Clin. Neurophysiol., Vol. 7, pp. 191-207.

29. **Neidermeyer, E.** 1999 The normal EEG of the waking adult. [ed.] E. & Lopes da Silva, F.H. Neidermeyer. *Electroencephalography: basic principles, clinical applications and related fields.* 4th ed. pp. 149-173.

30. **Pfurtscheller, G.** 1989 *Functional topography during sensorimotor activation studied with event-related desynchronization mapping*, J. Clin. Neurophysiol., Vol. 6, pp. 75-84.

31. **Pfurtscheller, G.** 1999 EEG event-related desynchronization (ERD) and event-related synchronization (ERS). [ed.] E., Lopes da Silva, F.H. Niedermeyer. *Electroencephalography: basic principles, clinical applications and related fields.* 4th ed. Williams and Wilkins pp. 958-967.

32. **Pfurtscheller, G., Neuper, C.** 1997 *Motor imagery activates primary sensorimotor area in man*, Neurosci. Lett., Vol. 239, pp. 65-68.

33. **Mason, S.G. & Birch, G.E.** 2000 *A brain-controlled switch for asynchronous control applications.*, IEEE Trans. Biomed. Eng., Vol. 47, pp. 1297-1307.

34. **Blankertz, B., Dornhege, G., Schafer, C., Krepki, R., Kohlmorgen, J., Muller, R.K., Kunzmann, V., Losch, F., & Curio. G.** 2003 *Boosting bit rates and error detection for the classification of fast-paced motor commands based on single-trial EEG analysis*, IEEE Trans. Neural Syst. Rehab. Eng., Vol. 11, pp. 100-104.

35. **Blankertz, B., G. Dornhege, M. Krauledat, K-R. Muller, V. Kunzmann, F. Losch, and G. Curio.** 2006 *The Berlin brain-computer interface: EEG-based communication without subject training*, IEEE Trans. Neural Syst. Rehab Eng., Vol. 14, pp. 147-152.

36. **Birbaumer, N., Kubler, A., Ghanayim, N., Hinterberger, T., Perelmouter, J., Kaiser, J., Iversen, I., Kotchoubey, B., Neumann, N., Flor, H.** 2000 *The thought translation device (TTD) for completely paralyzed patients*, IEEE Trans. Rehabil Eng., Vol. 8, pp. 190-192.

37. **Kubler, A.** 2000 *Brain-computer communication - development of a brain-computer interface for locked-in patients on the basis of the psychophysiological self-regulation training of slow cortical potentials.* Tu¨bingen: Schwa¨bische Verlagsgesellschaft.

38. **Perelmouter, J., Birbaumer, N.** 2000 *A binary spelling interface with random errors*, IEEE Trans. Rehabil Eng., Vol. 8, pp. 227-232.

39. **Wolpaw, J. R., & McFarland, D. J.** 2004 *Control of a two-dimensional movement signal by a noninvasive brain-computer interface in humans.* Proceedings of the National Academy of Sciences of the United States of America. Vol. 101, pp. 17849-17854.

40. **McFarland, D. J.,W. A. Sarnacki, and J. R.Wolpaw.** 2003 *Brain-computer interface (BCI) operation: optimizing information transfer rates*, Biological Psychology, Vol. 63, pp. 237-251.

41. **McFarland, D. J.,W. A. Sarnacki, T.M. Vaughan, and J. R.Wolpaw.** 2005 *Brain-computer interface (BCI) operation:signal and noise during early training sessions*, Clinical Neurophysiology, Vol. 116, pp. 56-62.

42. **Pregenzer, M., G. Pfurtscheller, and D. Flotzinger.** 1996 *Automated feature selection with a distinction sensitive learning vector quantizer*, Neurocomputing, Vol. 11, pp. 19-29.

43. **N. Birbaumer, T. Hinterberger, I. Iversen, B. Kotchoubey, A. Kubler, J. Perelmouter, E. Taub, and H. Flor.** 1999 *A spelling device for the paralysed*, Nature, Vol. 398, pp. 297-298.

44. **Scherer R, Müller GR, Neuper C, Graimann B, Pfurtscheller G.** 2004 *An asynchronously controlled EEG-based virtual keyboard: improvement of the spelling rate.*, IEEE Trans. Biomed. Eng., Vol. 51, pp. 979-984.

45. **X. Gao, D. Xu, M. Cheng, S. Gao.** 2003 *A BCI based environmental controller for the motion-disabled*, IEEE Transactions on Neural Systems and Rehabilitation Engineering., Vol. 11, pp. 137-140.

46. **Bayliss, J. D.** 2003 *Use of the evoked P3 component for control in a virtual apartment*, IEEE Trans on Neural Sys. and Rehabil. Eng., Vol. 11, pp. 113-116.

47. **Rebsamen, B., et al.** 2006 *A Brain-Controlled Wheelchair Based on P300 and Path Guidance.* Pisa, International Conference on Biomedical Robotics and Biomechatronics, BioRob. The First IEEE/RAS-EMBS. pp. 1101-1106.

48. **J. Millan, F. Renkens, J. Mourino, W. Gerstner.** 2004 *Noninvasive brain-actuated control of a mobile robot by human EEG*, IEEE Trans. on Biomedical Eng., Vol. 51, pp. 1026-1033.

49. **Taylor, D., Tillery, S., Schwartz, A.** 2002 *Direct cortical control of 3D neuroprosthetic devices*, Science, Vol. 296, pp. 1829-1832.

50. **Pfurtscheller, G., Müller-Putz, G. R., Pfurtscheller, J., & Rupp, R.** 2005 *EEG-based asynchronous BCI controls functional electrical stimulation in a tetraplegic patient*, EURASIP Journal on Applied Signal Processing, Vol. 19, pp. 3152-3155.

51. **Garcia, G. N.** 2004 Direct Brain-Computer Communication through Scalp Recorded EEG Signals. PhD Thesis. École Polytechnique Fédérale de Lausanne, Switzerland.

52. **E. C. Lalor, S. P. Kelly, C. Finucane, R. Burke, R. Smith, R. B. Reilly, and G. McDarby.** 2005 *Steady-State VEP-Based Brain-Computer Interface Control in an Immersive 3D Gaming Environment.*, EURASIP Journal on Applied Signal Processing, Vol. 2005, pp. 3156-3164.

6. Experimental Design with Single Shape

6.1 Introduction

Visual information is distributed to several brain structures in the form of action potentials by the axons of retinal neurons which are bundled into optic nerves. Different brain structures perform different functions. As an example, visual information is processed in occipital and parietal lobe of the brain. In the visual cortex, it appears that parallel paths may process different visual attributes. For example, the distinction in the retina between neurons that do and do not convey certain stimuli can be found mapped in the visual cortex. In general, each one of the more than two dozen visual cortical areas may be specialized for the analysis of different types of retinal output. Visual *phototransduction* is a process by which light is converted into action potential in the rod cells, cone cells and photosensitive ganglion cells of the retina of the eye. This continuous process of signal generation result in a change in the action potential firing frequency of the ganglion cells whose receptive field centers receive input from long, middle and short wave sensitive cones (briefly: red, green and blue). In general, color sensation derives from the spectrum of light interacting with the spectral sensitivities of the light receptors. These signals are carried to the human brain, that forms color sensation by the comparison of the readout of three cone types, e.g. upon equal activation of all types of cones (red, green and blue), white color sensation derives. Vision actually involves numerous different properties of objects i.e. color, form, movement and different cells of visual system are responsible for concurrent processing of these properties.

In this chapter we shall discuss about our experiment and the results obtained. Up till this chapter we have prepared the grounds for necessary background required to understand the basic principles and underlying theory involved in developing brain-computer interfaces. It was necessary for the onwards implementation of our results based on our hypothesis. To the best of our knowledge, we did not find any brain-computer interface system that relies only on color information because all the BCI systems we have studied during this course are based on EEG signals produced either by motor execution or its imagination, visual or auditory stimulation in terms of instructions given to the subjects in order to perform the required tasks. Our main focus and goal in the experiment is on the offline analysis and classification of color information into red, green and blue classes using Support Vector Machine (SVM), obtained from EEG signals produced by the uniform primary colors stimulation in order to be utilized for future BCI applications. In this context we have used only three colors, Red, Green and Blue for our experiment in order to avoid expected complications and to achieve more precise results. We believe that the results we obtained and presented here would serve as necessary means to develop future BCI applications.

Since several applications for Brain-Computer Interaction (BCI) like P300 Speller application or mu rhythm cursor movement have been developed but regarding colors different types of other studies are done, for example, a similar work was done in (1) in which authors have used only RGB colored sheets of paper to examine the arousal-calming effects, using each EEG band power and the total band power (beta+alpha+theta) and the alpha attenuation test as standard indices of arousal and to analyze the human brain activities in perception and attention referred to EEG alpha band response but not particularly related to BCI application's point of view. The ultimate task of any BCI system is the classification of EEG signals which reflects the growing interest of researchers in EEG-based BCI. For any successful BCI application, it is necessary to implement online classification in order to see real time execution which is a challenging task for signal processing and machine learning experts. However, an earlier offline analysis of EEG signals helps us in improving our classification accuracies. Once the brain signal is classified, it is fed to the outer world application to perform the desired operation. In this study, we have presented the results for offline spectral analysis and classification (using three different kernels, linear, polynomial and RBF) of EEG signals recorded from the scalp, produced by primary colours stimuli, red, green and blue, presented at random.

To explore the dynamics of brain in response to presentation of primary colors, i.e. red, green and blue, we performed an experiment in which subjects were exposed to random occurring of RGB colors and instructed to imagine the same color that was exposed most recently while keeping the eyes closed, in a Virtual Reality set to provide an immersive experience on a large screen keeping the luminance of colors constant. Frequency bands under investigation are delta (0.1 – 4 Hz), theta (4 – 8 Hz), alpha (8 – 12 Hz) and beta (12 – 30 Hz). The purpose of the experiment is to verify, if either the observation of different real colours or their corresponding imagination of colours can be detected in the selected EEG frequency combination, and to select best frequency combination to maximize differences through colour signals in order to find a Way-In to further establish our argument and to provide a baseline to be compared with more complex visual stimuli to evaluate the effects of colours to navigate in an immersive VR environment. For example, we can develop a virtual reality (VR) application in which first and preliminary version will exhibit the traffic light signals. A moving vehicle is expected to stop when turning ON the Red light, upon recognition of red colour through EEG signals. Similarly, upon recognition of the green light, a stopped vehicle is expected to start moving. We suggest that this method would be faster and provide more effective communication channel than those based on motor imagery described in (2) because colors deliver fastest information and help greatly in making decision immediately. As a simple example, in real life traffic signal light colors let us decide in a fraction of second either to keep going or slowdown or stop even while driving at the farther distance. Moreover, on several other public places different colors are used for recognition of terminals for services quickly and easy to understand, react immediately and greatly affects human emotional status. This way we may use colours as controllable parameter in VR environments. Another application of such colour recognition system could

be for colour blind and/or blind people (3). These applications are quite novel in their fields and needs extensive collaborative research work in different domains. We shall extend this study to further investigate the dynamics of brain activities to provide feedback for BCI systems to navigate into virtual environments to control motion, referring to consider the effects of color stimuli in VR environment. The results obtained and presented here are not used yet for online BCI system.

6.2 Experimental Design and Methods

Concerning the experimental settings, seven subjects have under gone the experiment, age ranging from 20 to 36 years. All subjects were free of neurological and psychiatric disorders and have normal colour vision. Experiment was performed in a dark room in front of a large curved screen (see figure 6.1) on which the colour was presented as a square with size of 10 degree angle on a much wider gray background. The subjects were seated on a comfortable chair. Distance between the subjects and the screen was 3.5 meters and 1.5 meters high from the ground. The luminosity of each colour was kept constant at about 4.5 cd/m^2 and measured using the device Minolta SPOTMETER F. Screw-able gold EEG electrodes were used on the subject's scalp at P3, P4, O1 and O2 sites and referenced to right ear lobe and grounded at site AFz as shown in figure 6.2.

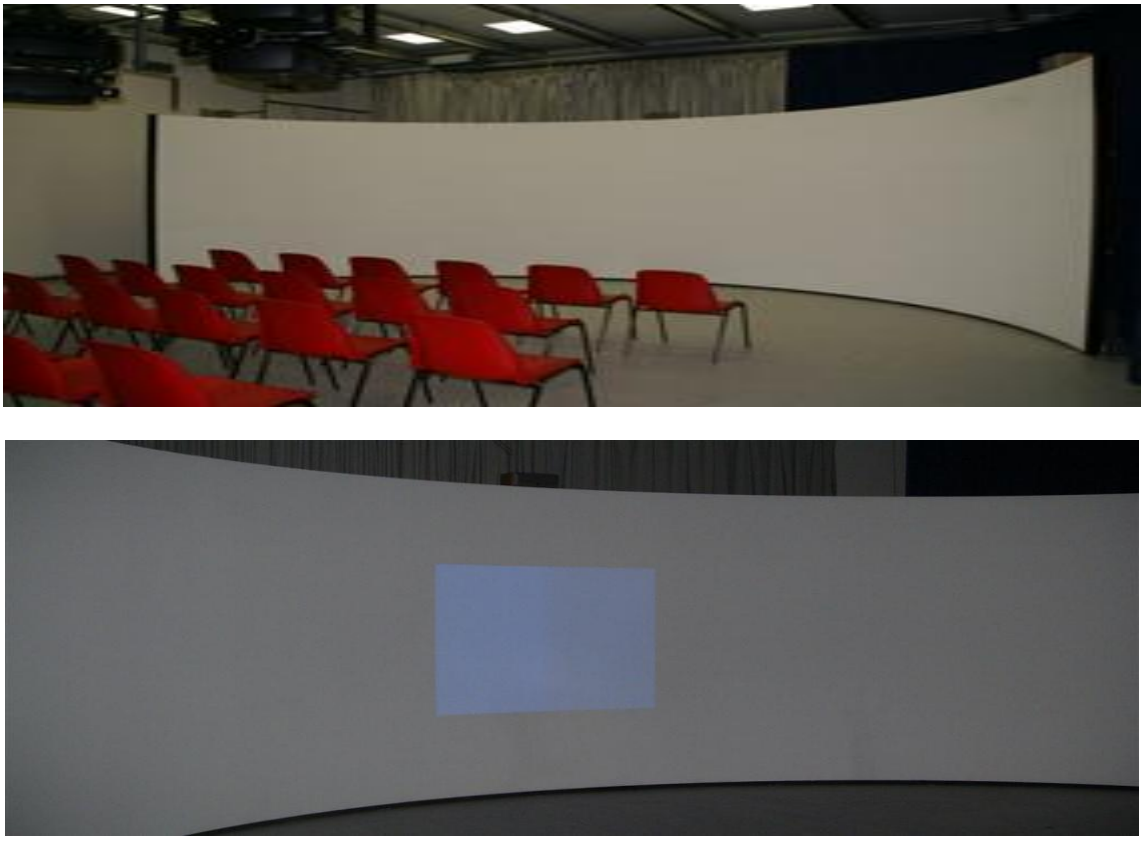

Figure 6.1 Experimental environment: Virtual Theater with large curved screen along with presented stimuli.

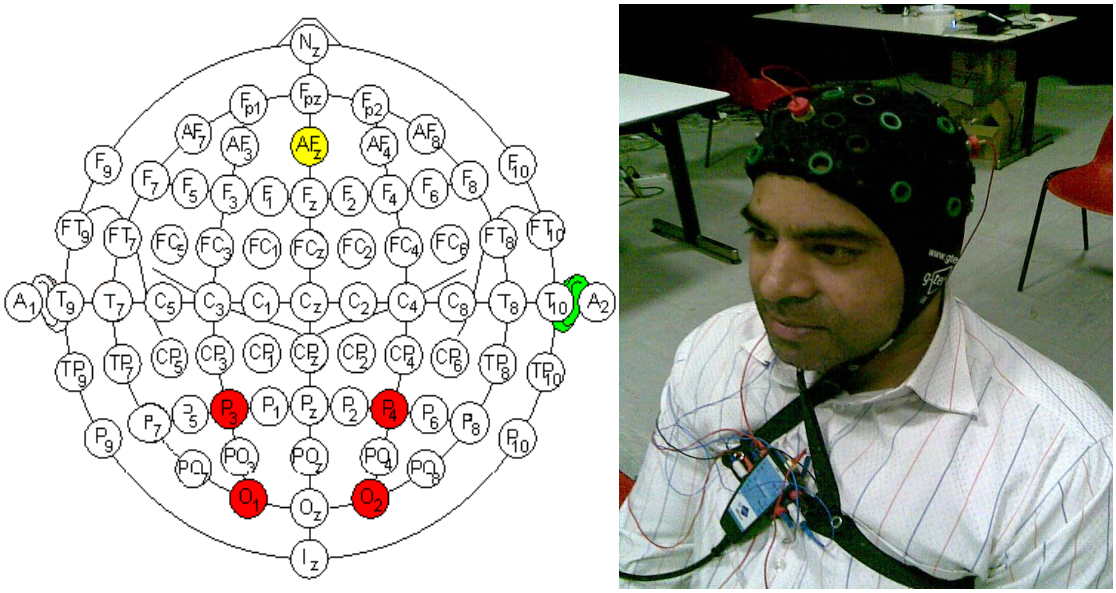

Figure 6.2 International 10-20 electrode placement layout and subject with mounted cap.

Experiment protocol is shown in figure 6.3 that depicts the duration of one sequence. In this protocol, each colour was presented for three seconds, twice in one sequence and the subject was instructed to imagine also the same colour for three seconds in the same sequence twice to analyze the spectrum of color imagination, in order to see any differences between real color and imagined color. There are eight events in one sequence. Only one colour is presented in one sequence. After all the events are occurred in a sequence then the next sequence is started and another colour is presented. When all the 3 colors are presented at random, the subjects were given a rest for 9 seconds after every 3 sequences while keeping eyes closed. Uniform gray background colour was displayed before and after every real colour to reduce and balance the possible after-effects of the RGB stimuli (1). All impedances were kept below 5kΩ. EEG signals were recorded using BCI2000 (4) with g.tec's (http://www.gtec.at) g.MOBIlab+ portable device sampled at 256 Hz, processed and analyzed offline using EEGLAB (5) that runs with MATLAB. Signals were band pass filtered from 0.1 Hz to 30 Hz. Each colour was presented 60 times randomly, resulting in 60 trials of each colour from each subject. Each trial contains 768 data points after the onset of stimulus. Once, all the EEG signals were recorded they were brought into EEGLAB for offline processing and analysis. EEGLAB has a vast compatibility to import EEG signals into MATLAB's workspace which are recorded with different devices using BCI2000. Epochs were extracted from continuous data for each colour and their corresponding imagination individually. Each epoch is extracted in way that it lasts for three seconds i.e. one second before the event occurred and two seconds afterwards. To reduce the effects of abnormal values, those trials for which EEG signals crossed ± 60 µV were rejected and some segments were also dropped by visual inspection that did not cross ± 60 µV but were unreliable in further computations. During recording of EEG signals, some other artifacts like EOG/EMG signals interfere with EEGs which produces unwanted neuronal activities due to volume conduction in the brain which may be dropped by the visual inspection. However, if

distributions of potential values are further away from a Gaussian distribution compared to the other scalp channels then data statistics may be used to drop empirically bad channels. For the moment, we do not need to drop any such bad channel because the methods are available for separating eye or muscle artifacts from neuronal activities.

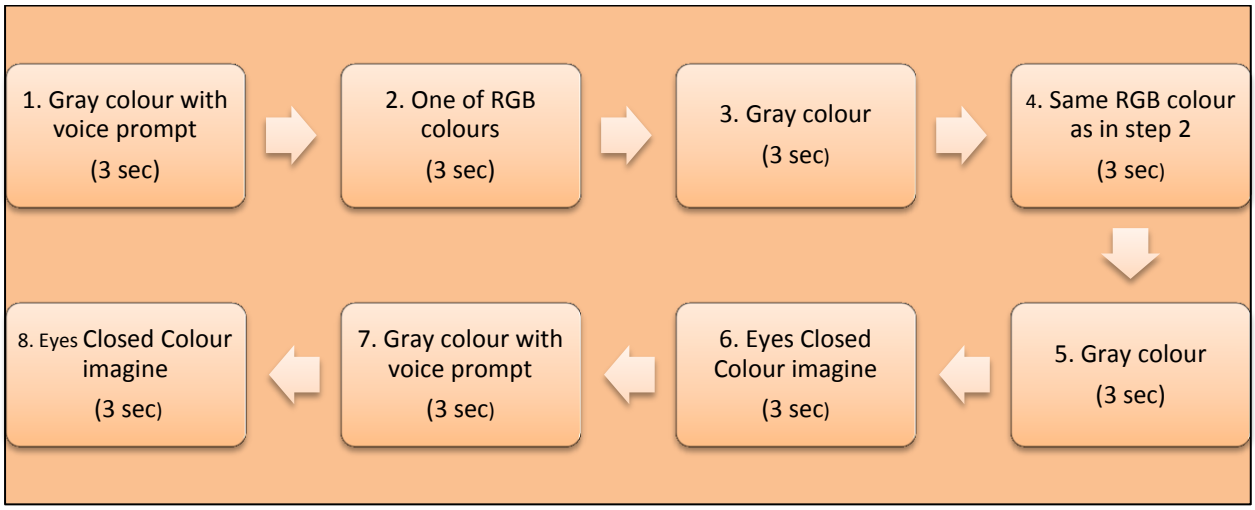

Figure 6.3 Experiment protocol

We have used a method based on blind source separation by independent component analysis decomposition (ICA) to remove such artifacts, because it has the capability to preserve contribution of ERP from different scalp locations even when there is no single trial without these artifacts. It uses spatial filters derived by ICA, which does not necessarily require us to record separate channels for these artifact sources (6). In figure 6.4 (a), we can see two different EEG signals before and after application of ICA decomposition because the EEG signals were decomposed into four independent components derived from EEG signals recorded from four different channels.

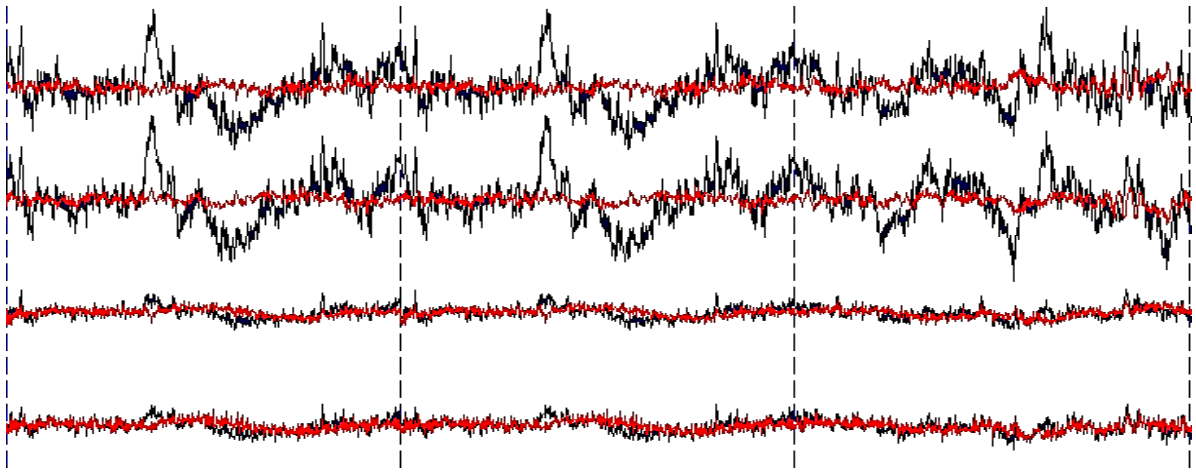

Figure 6.4 (a) Raw EEG signals (in black) and Artifact free EEG signals (in red)

After the application of ICA, EEG signal trials were subjected to create a STUDY structure within the EEGLAB for multiple subjects to compute and analyze the ERP waveforms, power

spectrum, event-related spectral perturbation and inter-trial coherence for the real color exposure as well as for the imagination of colors. So here we present these results.

6.3. Results and Discussion

6.3.1 ERP Waveforms

Across varying scalp locations, averaged ERPs are evoked by sudden onsets of visual stimuli that contain a prominent negative peak (N1) around 150 to 200 ms and a positive peak (P3) around 300ms, which are quite visible in figure 6.4.

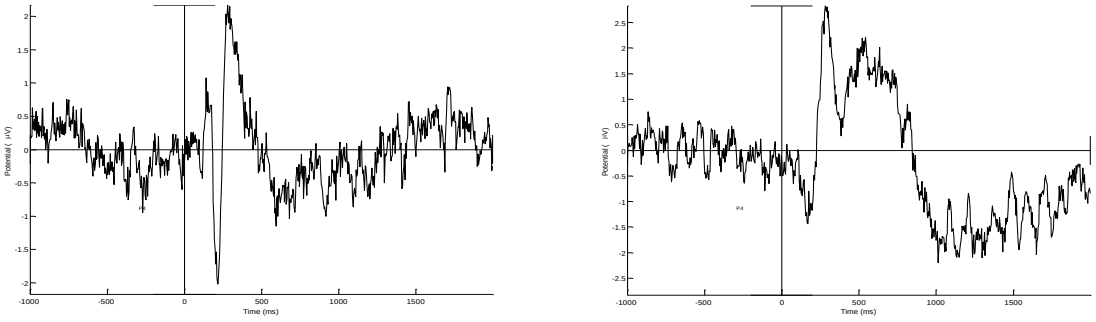

(a)

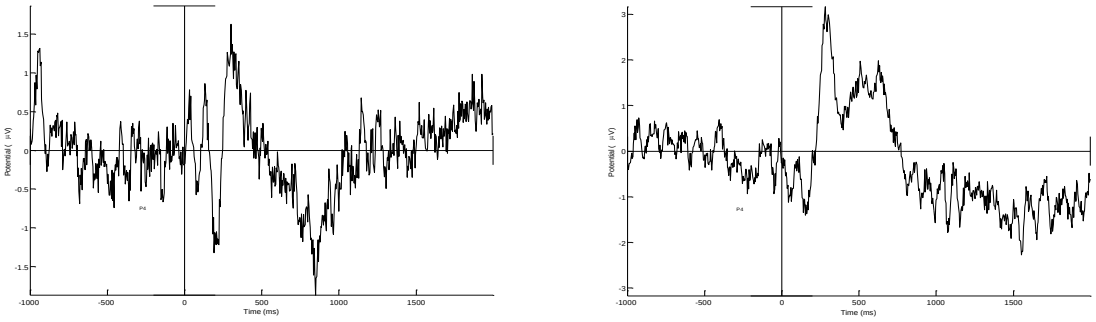

(b)

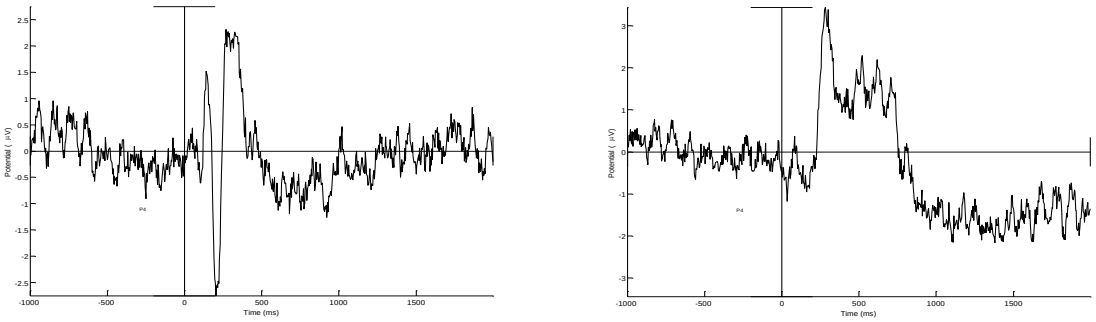

(c)

Figure 6.4 Averaged ERP waveforms for each color exposure on left and corresponding imagination on right. Red is shown in (a), Green in (b) and Blue in (c).

In figure 6.4, X-axis represents time in milliseconds (ms) and Y-axis represents potential values in microvolts (µV). Latencies and amplitudes of these peaks may vary among different scalp locations and different subjects. In (7), Makeig and his colleagues reported that many ERP features are mainly generated by partial stimulus induced phase resetting of multiple EEG processes. In order to compare event-related EEG dynamics for a subject in two or more conditions from the same experiment, we created datasets containing epochs for each condition i.e. red, green and blue for color exposure and as well as for color imagination among all subjects. Figure 5 shows the grand mean ERP waveforms generated by the exposure of red, green and blue colors in each subject at scalp electrode P4 in the right parietal region. Average event-related potentials (ERPs) are shown among 7 subjects; each trial contains samples from -1s before to 2s after the time locking event of the onset of color stimulus. Although no significant response is visible in ERPs of red, green and blue color, however, positive peaks around 300 ms are almost equivalent in red and blue and relatively higher than in green. A significant negative peak centered at 800 ms is visible in green color but not in its imagination. Usually data averaging collapses the dynamic information in the data so it might not be effective in the analysis. In color imagination waveforms, a positive peak centered around 500 ms is visible unlike real color exposure. This peak drops down zero around 800 ms and remains negative until the end of epoch extracted whereas it becomes positive in the real exposure around 1000 ms in all the colors. These variations in the waveforms reflect how the event-related synchronization and desynchronization occurs in response to visual stimulus. Please note that, the potential level remains almost same in the baseline segment with no high variability among the real color exposure and in their corresponding imaginations. The peaks and valleys in these ERP waveforms could serve as possible features for the classifier but may not provide satisfactory results because Makeig in (8) reported that according to several studies, event-related potentials (ERPs) are not capable of capturing maximum brain's response to events due to their instability and not being fully independent of EEG. This reason lacks our interest in analyzing ERP waveforms in more depth.

6.3.2 Spectral Plots

Figure 6.5 shows the frequency versus power ($10*\log_{10}(\mu V^2/Hz)$) spectrum plots for the seven subjects in blue traces across three different conditions each for red, green and blue, along with their average spectrum in black traces. Spectrum is shown for channel P4 from the right parietal region. In figure 6.5 (a) significant activity is found in alpha frequency (8 - 12 Hz) band and higher theta frequency (6 – 8 Hz) band with lower power than alpha band, in all the subjects for each color. Spectrum shows some insignificant activities in the beta frequency (13 – 30 Hz) band with slight variations in power increases and/or decreases in all the subjects however power in the beta band was found below level zero. Imagination of colors show similar frequency spectrum with higher power values in the alpha band, as figure 6.5 (b) shows that the average power in black trace is close to 4, where as in real colors average power is close to zero. A sudden decrease in power is seen in delta band (0.1

– 4 Hz). Upon having more close observation in all cases, one subject is found that has highest power value in the higher beta band (25 – 30 Hz) and lowest power value in alpha band than other subjects. However, its power spectrum oscillations are relatively same in alpha and beta bands.

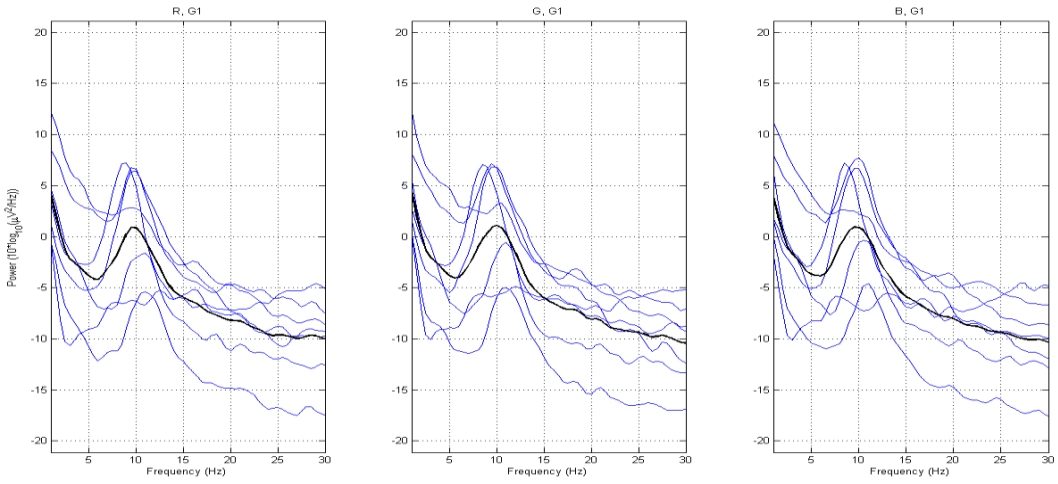

(a)

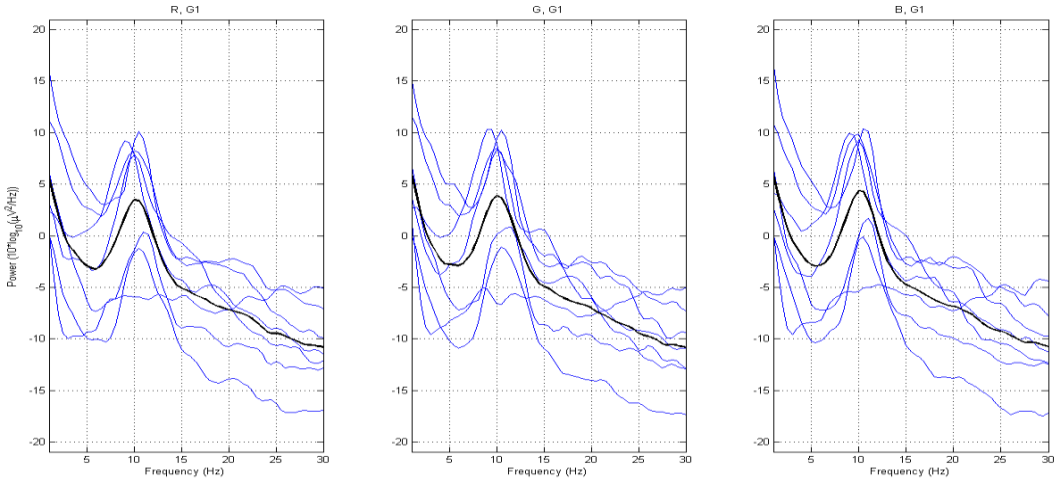

(b)

Figure 6.5 Power spectrum of each real color exposure in figure (a) and its corresponding imagination in figure (b). Red's response is on left, Green's in the middle and Blue's in right. X-axis represents Frequency (Hz); Y-axis represents Power.

Highest power spectrum value in real colors exposure is found to be 7 in alpha band where as in imagination of colors it is 10. Spectrum was computed using FFT algorithm. Since there is no time information in these plots so it would not serve us to make analyses on event-related response. That's why we do not prefer to use these features for the classifier

because overall there is not much discrimination between the colors and also their imagination.

6.3.3 Event-related Spectral Perturbation

This is something where we are most interested in the results. Event-related Spectral Perturbation (ERSP) is a measure to study the event-related brain dynamics. It reflects the information about variation in power at different frequencies at a certain time point. Calculating an ERSP requires computing the power spectrum over a sliding latency window then averaging across data trials. Narrow band event-related desynchronization and synchronization is generalized by the ERSP measures. As we have discussed earlier that event-related potential (ERPs) are not capable of capturing maximum brain's response so due to this limitation of ERPs we have used event-related spectral perturbation (ERSP) (9) (10) values in terms of time-frequency measurements as features for the classifier and the classification results dramatically improved as compared to when ERP waveforms were used as features for the classifier. ERSP is computed by calculating baseline spectra from the EEG immediately preceding each event. Overlapping data windows are created by splitting the epoch to create the moving average of the amplitude spectra. Normalization is performed on individual response epochs for each spectral transforms by dividing by their respective mean baseline spectra. An ERSP is produced by taking average of normalized response for many trials. For n trials, if $F_k(f,t)$ is the spectral estimate of trial k at frequency f and time t, then ERSP is computed using following formula,

$$ERSP(f,t) = \frac{1}{n}\sum_{k=1}^{n}\left|F_k(f,t)\right|^2$$

Here $F_k(f,t)$ is computed using sinusoidal wavelet transform in which the number of cycles is increased slowly with frequency and provides better frequency resolution at higher frequencies than a conventional wavelet approach that uses constant cycle length.

Figure 6.6 represents averaged event-related spectral perturbation (ERSP) plots among all the subjects from electrode position P4, distributed in time-frequency frame. The color at each image pixel indicates power (in dB) at a given frequency and latency relative to the time locking event. As we can see in figure 6.6 (a), response for red color exposure, ERSP is more concentrated (yellow color) around 300 ms in delta (1 – 4 Hz) and theta (4 – 8 Hz) frequency bands than green and blue which means there is an increase in power in this time span and frequency bands. Green color has lowest positive activity in delta and theta bands around 300 ms. In alpha frequency band (8 – 12 Hz) and lower beta frequency band (13 – 18 Hz), responses for all the colors are relatively the same, centered around 600 ms, starting from 400 ms until 1000 ms that shows significant decrease in power with lowest value in red. In higher beta band, evidences of slight increase in power are found around 1500ms. Figure 6.6 (b) shows ERSP responses for all the color imaginations in which a similar pattern of distribution of power is seen. In delta and theta band, from 200 ms to 500 ms, increase in

power is higher than in real color exposure whereas decrease in upper theta band, alpha band and lower beta band from 300 to 800 ms is relatively less than found in real color exposure. However, more significant increase in power is found from 9 Hz to 18 Hz starting from 800 ms until the end of epoch extracted.

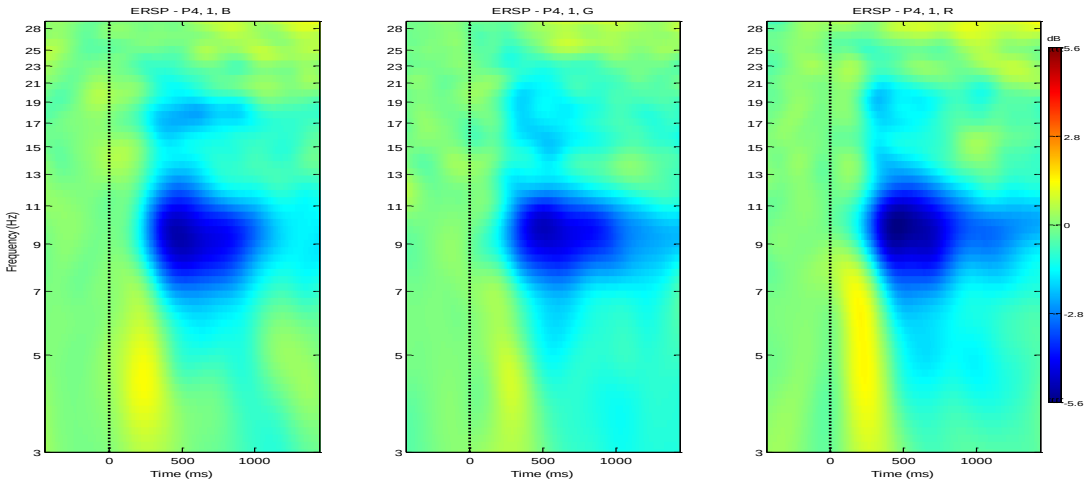

(a)

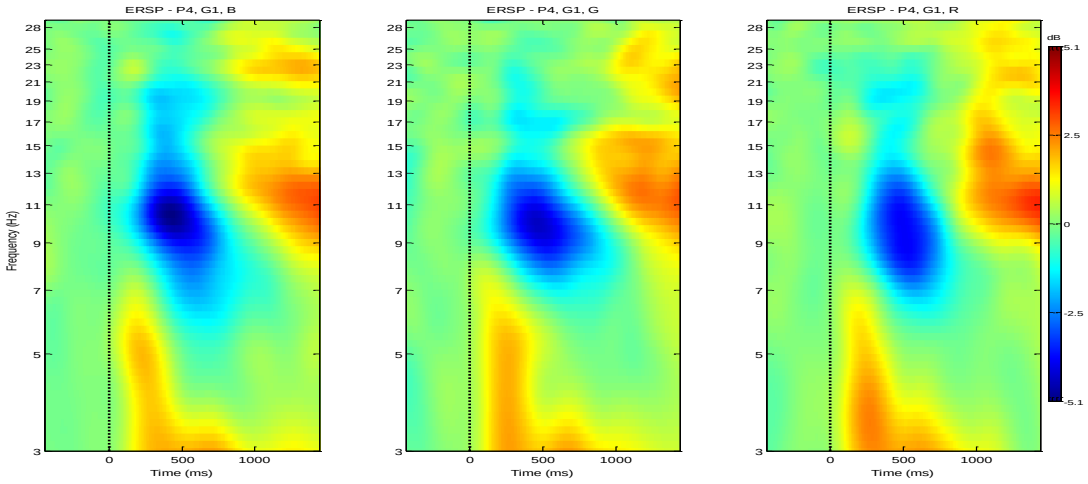

(b)

Figure 6.6 Averaged ERSP plots of each real color exposure in (a) and corresponding imagination in (b). Red's response is on right, Green's in the middle and Blue's is on the left. X-axis represents time (ms) and Y-axis represents frequency (Hz).

Now we will also present ERSP plots for each individual subjects from the same electrode P4 in order to better analyze the responses and also because we have used these features in our classifier and sooner we will present the results of our classifier.

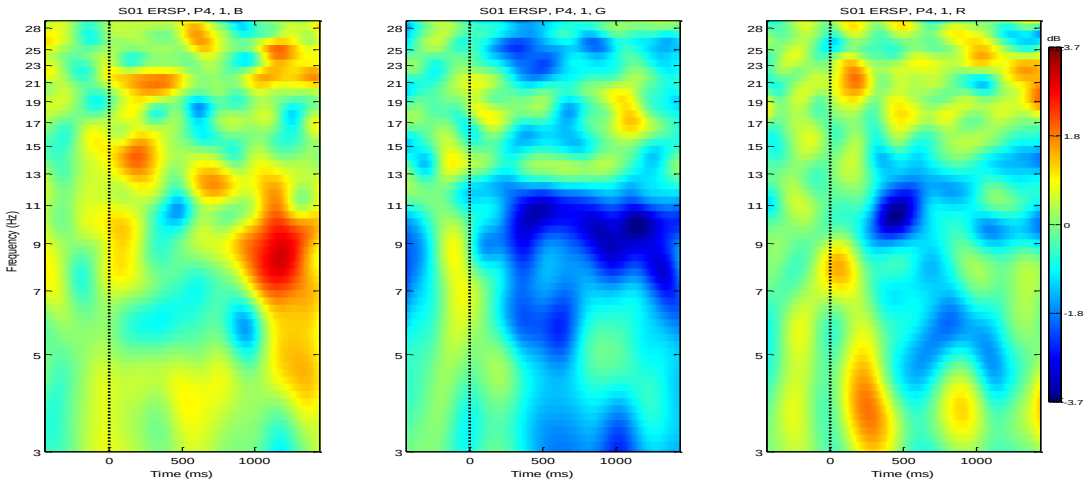

(a)

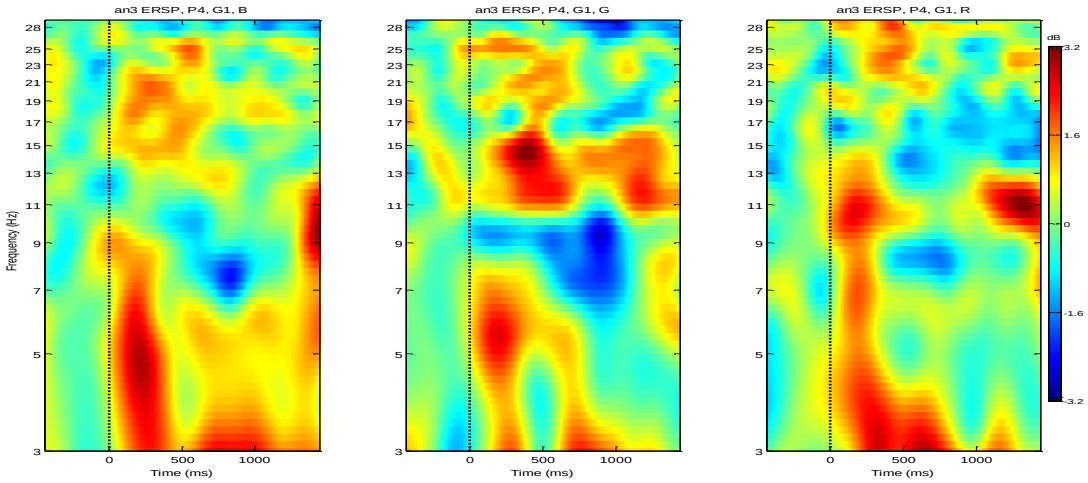

(b)

Figure 6.7 Subject '01': ERSP plots of each real color exposure in (a) and corresponding imaginations in (b). Red's response is on right, Green's in the middle and Blue's is on the left. X-axis represents time (ms) and Y-axis represents frequency (Hz).

Figure 6.7 shows the variation in power distribution for subject 1 in time-frequency domain. Among the real color exposure, red color has higher power i.e. event related synchronization, than green and blue in delta band at around 300ms. In Green color's exposure EEG activity is greatly desynchronized in alpha band and relatively less desynchronized in delta and theta bands starting from 400 ms until 1000ms, however this desynchronization in alpha band lasts until 1500 ms. In green color exposure, an increase in power is seen in lower beta band after one second of onset of stimulus where as in beta band red and blue colors exposure have slight variations in power increase at variable latencies. Among the imagination of colors, red color has increase in power in delta, theta and alpha band starting after 100 ms of onset of stimulus and lasts until 800 ms in delta band and lasts until 400 ms in theta and alpha band. Green color's imagination has increase in power in theta band and lower beta band whereas alpha band has decrease in power

around 400 ms until 800 ms in all the color's imagination. It is also clear that blue color's imagination is increased in power within delta and theta bands around 100 to 400 ms. Overall, event-related synchronization and desynchronization is scattered in all frequency bands among variable latencies both in real color exposure and their corresponding imaginations.

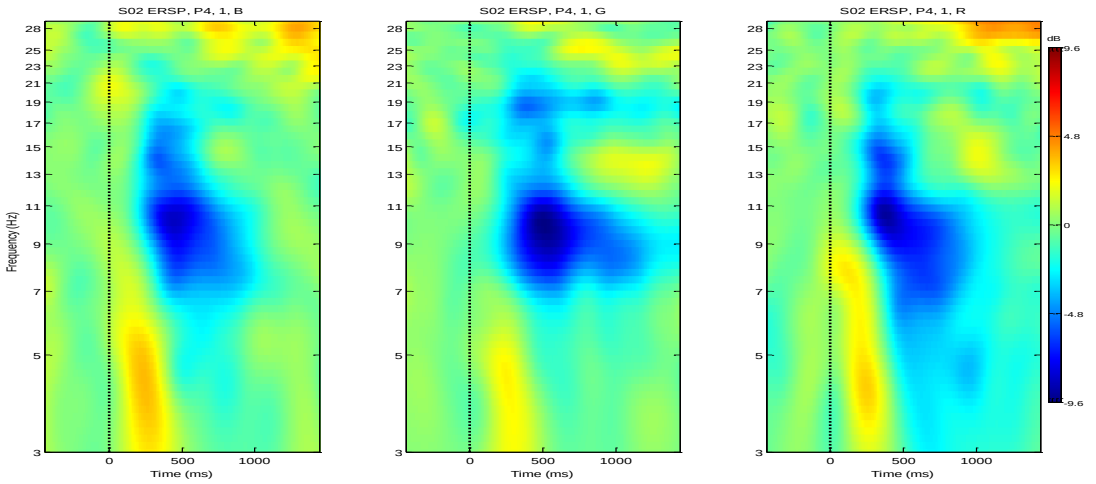

(a)

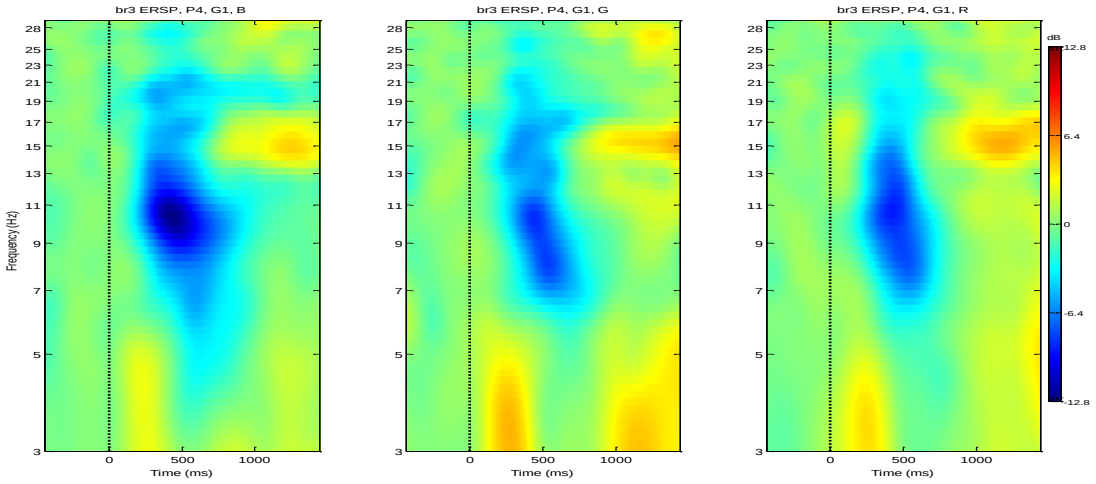

(b)

Figure 6.8 Subject '02': ERSP plots of each real color exposure in (a) and corresponding imaginations in (b). Red's response is on right, Green's in the middle and Blue's is on the left. X-axis represents time (ms) and Y-axis represents frequency (Hz).

Figure 6.8 illustrates the even-related synchronization and desynchronization for subject 2, both in real color exposure and their corresponding imaginations. We can see that subject 2's response is nicely distributed and do not have scattered variations like in subject 1's response. An increase in power is seen in delta and theta bands around a fixed latency of 100 to 400 ms, not only in all the real colors exposure but also in the imagination of colors, i.e. subject 2's colors exposure response for distribution of power in time frequency domain

is well synchronized with the distribution of power in their corresponding imaginations. This increase in power is highest in blue and lowest in green, among the real colors exposure and highest in green with lowest in blue among the imaginations of colors. Moreover, a decrease in power is visible in all cases within higher theta band, alpha band and lower beta bands during 300 ms onwards until 800 ms to 1000 ms. In addition, a slight increase in power is seen in beta band after one second of onset of stimulus among the imaginations.

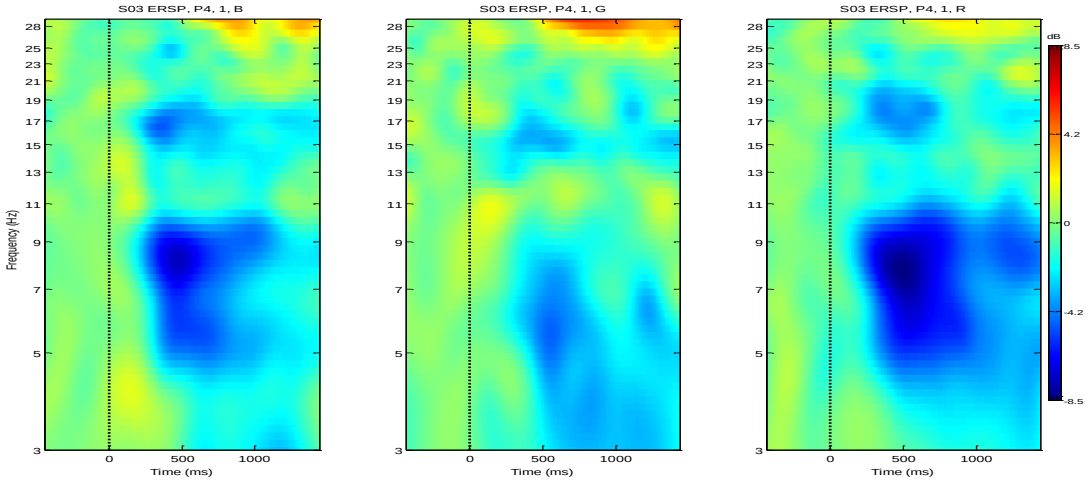

(a)

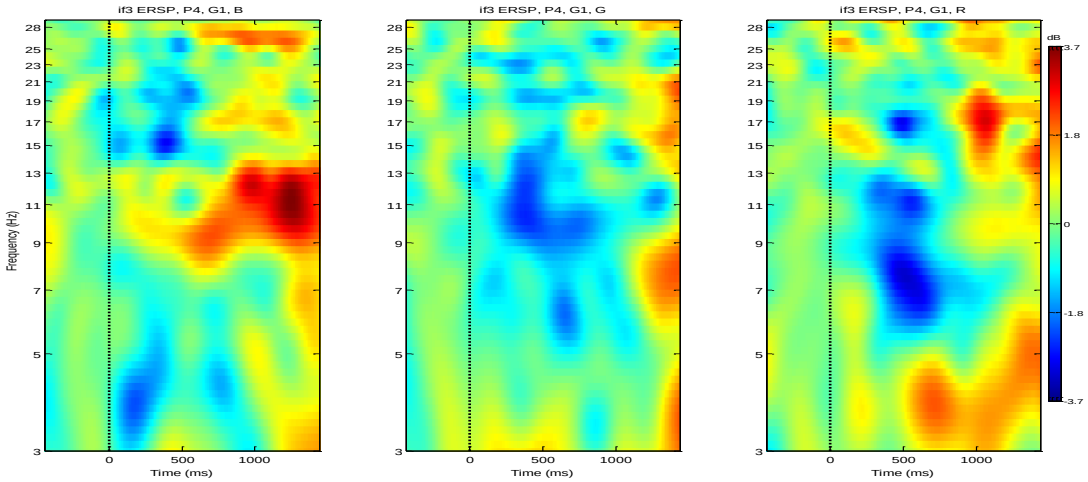

(b)

Figure 6.9 Subject '03': ERSP plots of each real color exposure in (a) and corresponding imaginations in (b). Red's response is on right, Green's in the middle and Blue's is on the left. X-axis represents time (ms) and Y-axis represents frequency (Hz).

Figure 6.9 shows the ERSP response for subject 3. Increase in power in delta and theta bands is very low whereas decrease in power is significant in red and blue colors exposure but not in green starting from 200 ms after the onset of stimulus and desynchronization lasts until 700 ms in blue exposure and until 1000 ms in red exposure. Among imagination of

colors, an increase in power is seen in alpha band during 1000 to 1500 ms in blue colors whereas this increase is not significant in green and red.

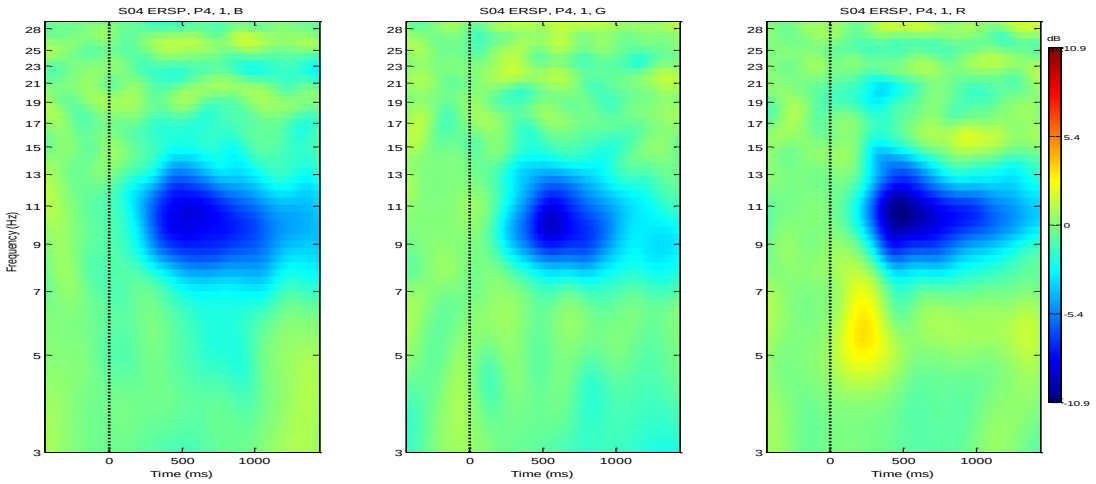

(a)

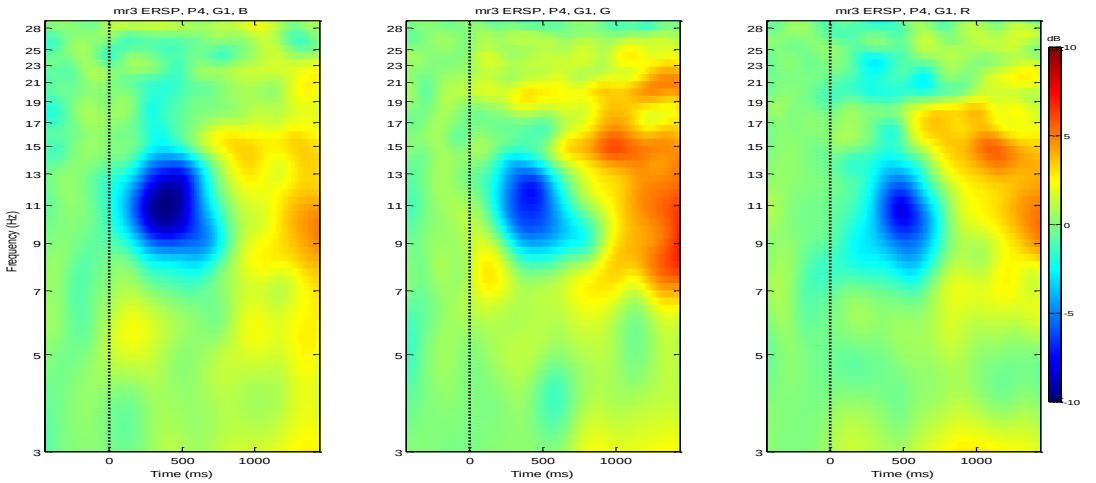

(b)

Figure 6.10 Subject '04': ERSP plots of each real color exposure in (a) and corresponding imaginations in (b). Red's response is on right, Green's in the middle and Blue's is on the left. X-axis represents time (ms) and Y-axis represents frequency (Hz).

Figure 6.10 reflects ERSP plots for subject 4. Event-related desynchronization is significant in alpha band starting from 300 ms until 800 to 1200 ms among the color exposure along with a slight increase in power in theta band during100 to 400 ms only in red color exposure. This event-related desynchronization is also seen in imagination of all colors for lesser time spans in alpha band with highest increase in power in green color imagination in upper theta band, alpha band and lower beta band during 800 ms until 1500 ms.

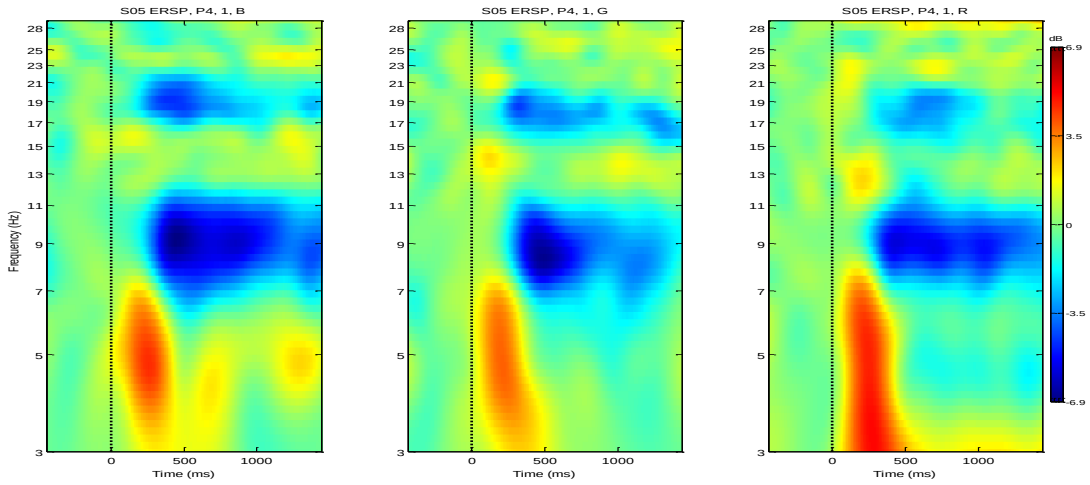

(a)

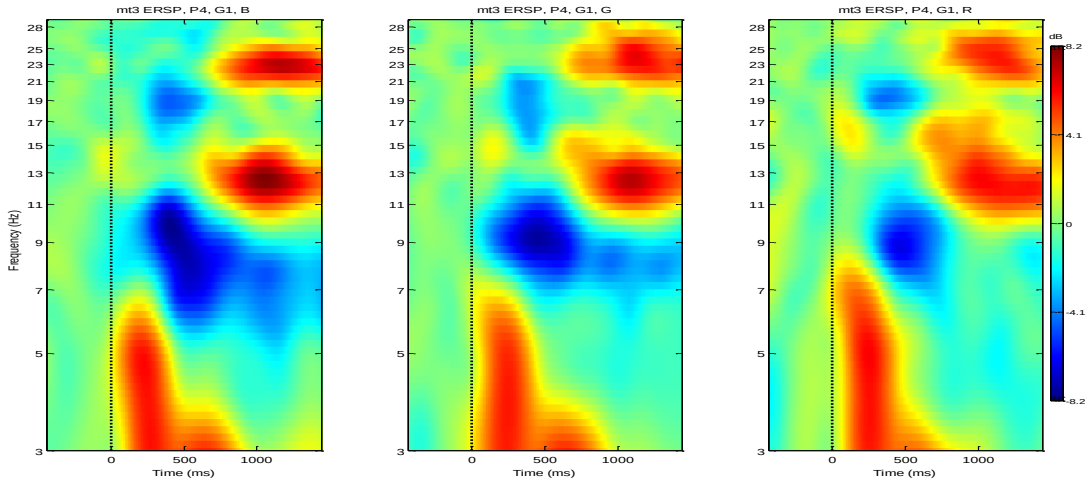

(b)

Figure 6.11 Subject '05': ERSP plots of each real color exposure in (a) and corresponding imaginations in (b). Red's response is on right, Green's in the middle and Blue's is on the left. X-axis represents time (ms) and Y-axis represents frequency (Hz).

Figure 6.11 show the ERSP plots for subject 5. Variation in power distribution for real colors exposure is nicely synchronized with variation in power distribution for colors imagination which means that subject was trained enough to start imagine the exposed color well in a given time at synchronized latency measures. Red exposure has the greatest increase in delta and theta bands during 100 to 500 ms. Among the imaginations of colors, event-related synchronization is visible in delta and theta bands whereas event-related desynchronization is also seen in alpha band during 300 ms to 100 ms similar to real color exposure. An important observation is that in the lower beta and higher beta bands increase in power is significant after the one second of onset of stimulus. This increase is higher in blue and lower in red among imaginations. Please note that the distribution of power is not scattered in subject 5, both for real color exposure and their corresponding imaginations,

like the distribution of power is scattered in subject 1's and subject 3's imagination of colors in figures 6.7 (b) and 6.9 (b) respectively. Similar behavior about the distribution of power is also seen in subject 2 and 4 like it is seen in subject 5. However the intensity of distribution of power was greater in subject 5 than in subject 2 and 4.

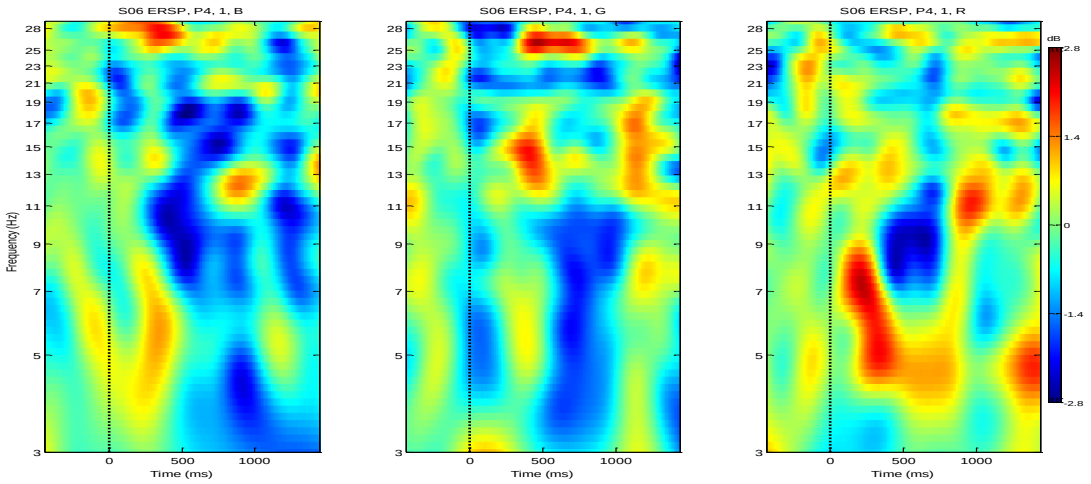

(a)

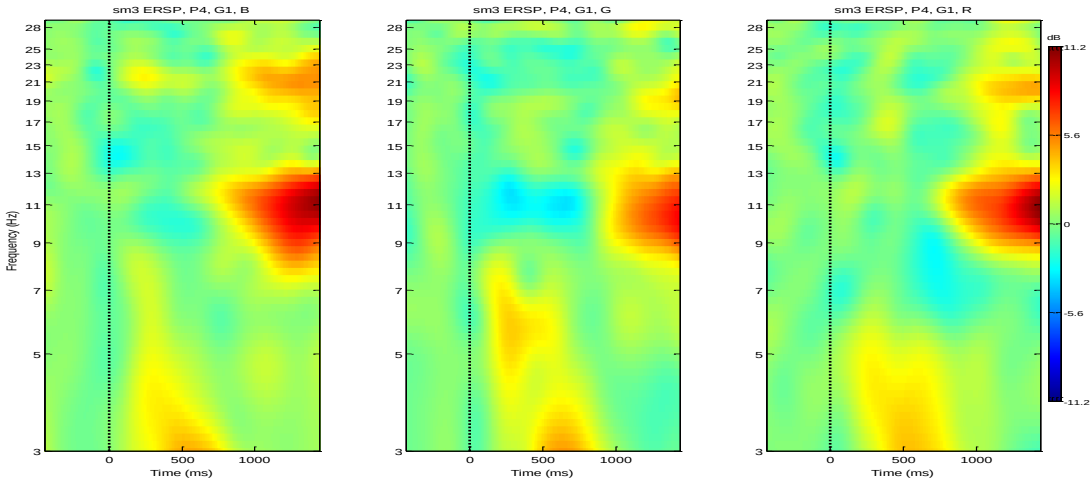

(b)

Figure 6.12 Subject '06': ERSP plots of each real color exposure in (a) and corresponding imaginations in (b). Red's response is on right, Green's in the middle and Blue's is on the left. X-axis represents time (ms) and Y-axis represents frequency (Hz).

Figure 6.12 illustrates the distribution of power in time-frequency domain for subject 6 and we can see that event-related synchronization and desynchronization is highly scattered in all frequency bands during the whole time span of epoch among all the real colors exposure. Whereas such desynchronization and synchronization of powers are nicely distributed and symmetric among all the colors imaginations i.e. an increase in power is seen in delta band during 200 ms to 800 ms along with an increase in power in alpha band starting after the one second of onset of stimulus among all the colors imaginations. Another observation in

this case is that a slight decrease in power is seen within alpha band during 200 ms to 800 ms on average as this decrease in power is very common in all other cases of real color exposure and also in imaginations of colors but in this subject decrease is lower than other subjects.

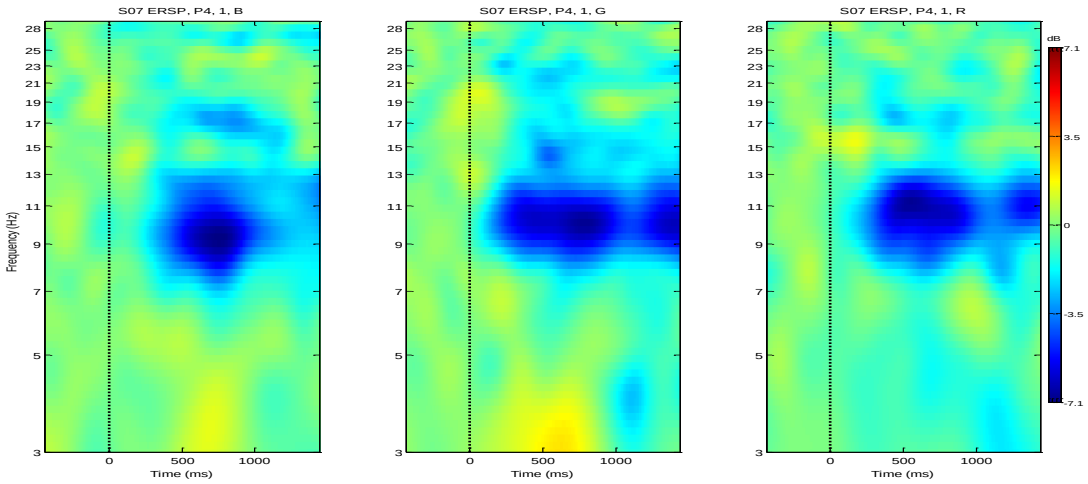

(a)

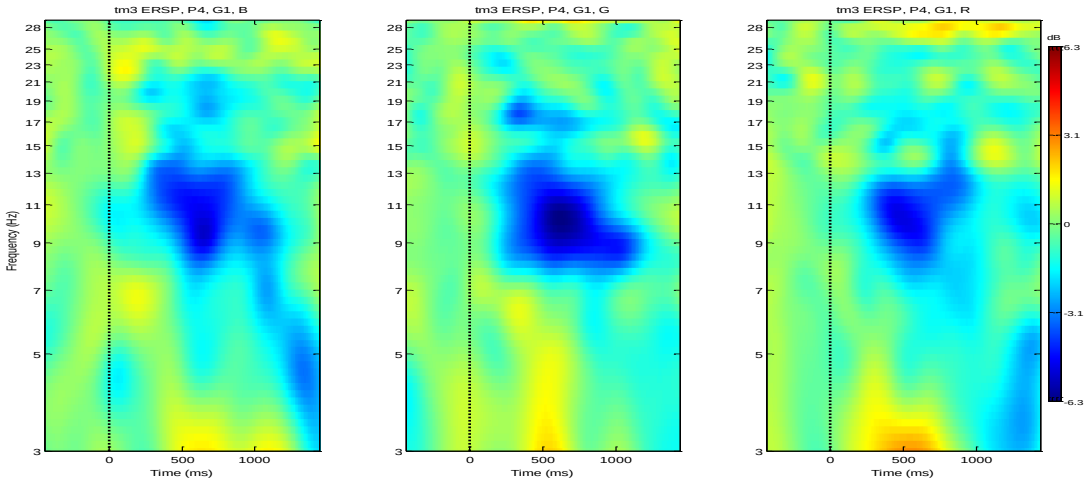

(b)

Figure 6.13 Subject '07': ERSP plots of each real color exposure in (a) and corresponding imaginations in (b). Red's response is on right, Green's in the middle and Blue's is on the left. X-axis represents time (ms) and Y-axis represents frequency (Hz).

Figure 6.13 reflects the ERSP plots for subject 7 and we can see in this case, that an activity corresponding to event-related desynchronization is quite significant as compare to an activity corresponding to event-related synchronization and similar behavior is also visible in in imaginations of colors. Please note one of the observation that among all the subjects whenever there is non-scattered distribution of power is seen in imaginations of colors then the corresponding real color exposures also have the non-scattered distribution of power in a symmetric manner, whereas in the case of subject 6, figure 6.12, the distribution of power

is seen non-scattered among the colors imagination but seen highly scattered in real colors exposure. However, if the distribution of power is seen as non-scattered in real colors exposure then the distribution of power may or may not be scattered among colors imaginations.

6.3.4 Inter-Trial Coherence

Inter-Trial Coherence (ITC) is a frequency domain measure of the partial or exact synchronization of activity at a particular latency and frequency to a set of experimental events to which EEG data trials are time locked. The measure was introduced by Tallon-Baudry et al. (11) and termed a 'phase locking factor.' The term 'inter-trial coherence' refers to its interpretation between recorded EEG activity and an event-phase indicator function (e.g. a Dirac or cosine function centered on the time locking event). ITC is defined by the following formula,

$$ITC(f,t) = \frac{1}{n}\sum_{k=1}^{n}\frac{F_k(f,t)}{\left|F_k(f,t)\right|}$$

Here $\left|\ \right|$ represents the complex norm.

ITC values lies between zero and 1. If the ITC value is zero then it shows that there is no synchronization between the EEG data and time locking events whereas the value of 1 reflects the perfect synchronization. The spectral estimates are returned as complex vectors in 2-D phase space. The norm and phase angle of each vector are represented by the magnitude and phase of the spectral estimate. To compute (ITC), the lengths of each of the trial activity are normalized to 1 and then complex average is computed. ITC significance levels are assessed using surrogate data by randomly shuffling the single-trial spectral estimates from different latency windows during the baseline period.

Figure 6.14, shows inter-trial coherence (ITC) that measures the degree of phase consistency or phase synchronization. It should be kept in mind while assessing the ITC data that frequency bands under considerations are delta (0.1 – 4 Hz), theta (4 – 8 Hz), alpha (8 – 12 Hz) and beta (13 – 30 Hz). Figure 6.14 (a) reflects significant ITC in delta (0.1 – 4 Hz), theta (4 – 8 Hz), relatively less in alpha (8 – 12 Hz) and lower beta (13 – 22 Hz) bands starting from 100 ms of the onset of stimuli and lasts until 400 ms with highest concentration in red than in green and blue. Also, green has higher concentration than blue which force the blue color to be lowest synchronized than red and green. To some extent, a synchronized activity is found in upper beta (22 – 30 Hz) band in red color which is relatively darker than green. A similar pattern is exhibited in figure 6.14 (b) for imagination of colors. We can see during the same time period there are significant ITC values in delta, theta and partially in alpha band where as in beta band occurrence of synchronization between EEG data and time locking events is very rare. Partial spreads of synchronization are seen at variable times and frequencies mostly in imaginations and highly synchronized signal is found in blue in delta

band (0.1 – 4 Hz) around 200 to 400 ms in imaginations of colors. Overall synchronized activity was found in red color exposure.

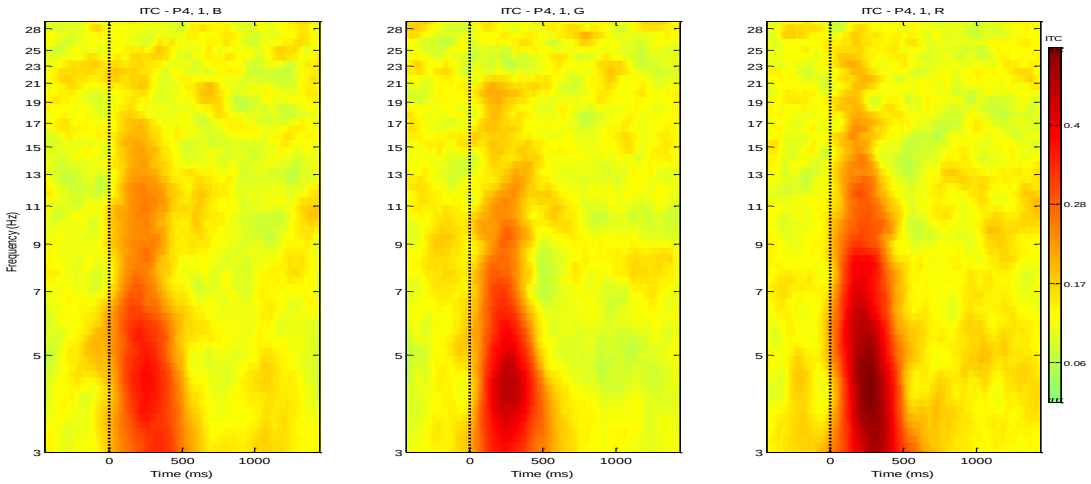

(a)

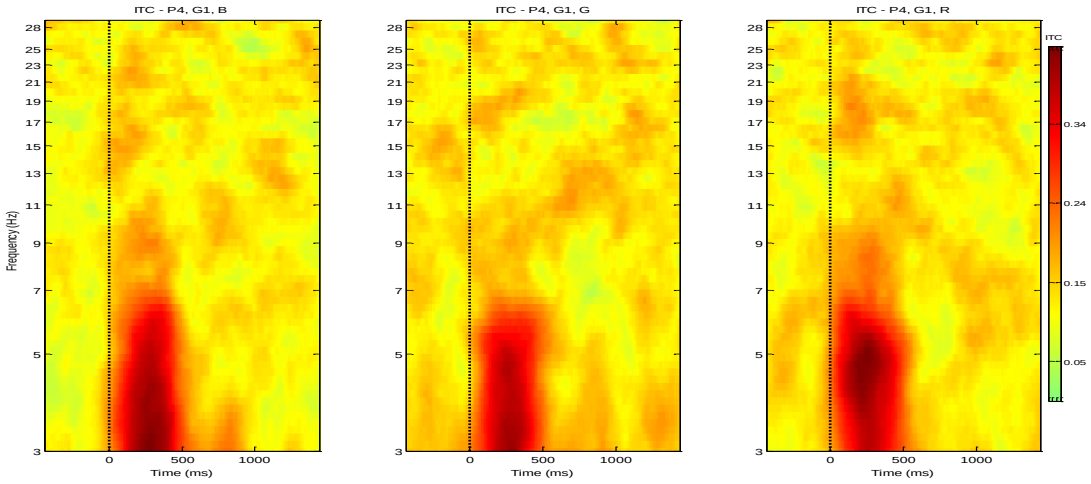

(b)

Figure 6.14 Averaged ITC plots of each real color exposure in (a) and its corresponding imagination in (b). Red's response is on left, Green's in the middle and Blue's is on the right. X-axis represents time (ms) and Y-axis represents frequency (Hz).

Let us now analyze the individual activity of each subject and see how well synchronized the EEG data is with the time locking events.

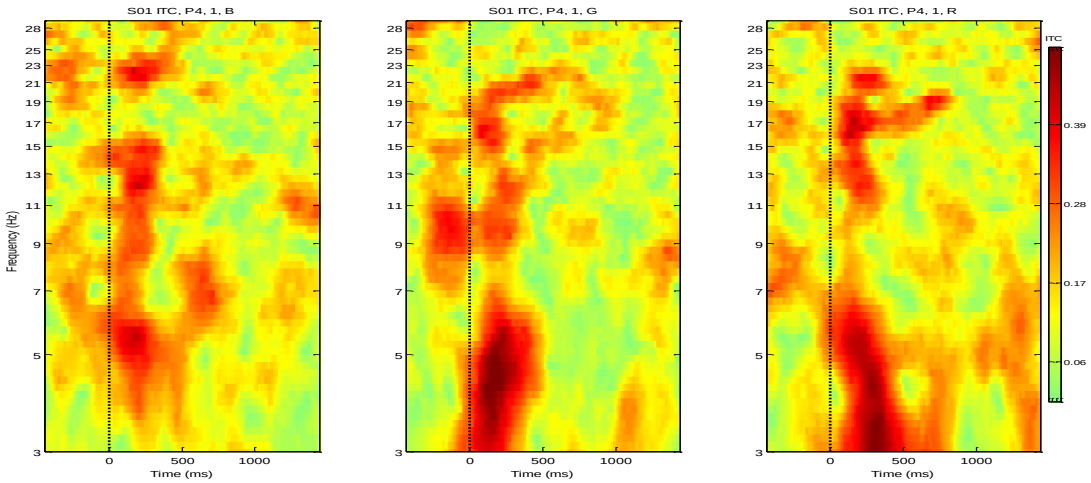

(a)

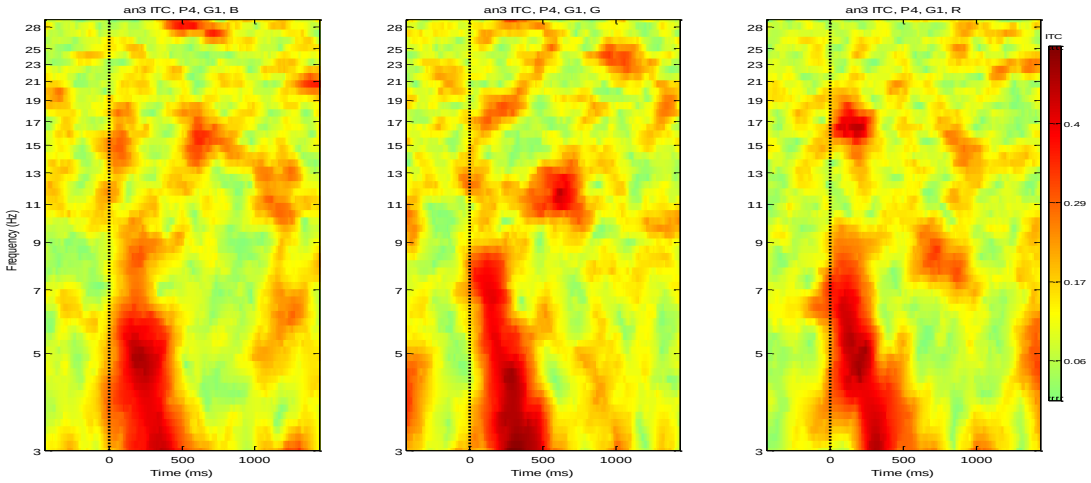

(b)

Figure 6.15 Subject '01' ITC plots of each real color exposure in (a) and its corresponding imagination in (b). Red's response is on right, Green's in the middle and Blue's is on the left. X-axis represents time (ms) and Y-axis represents frequency (Hz).

Figure 6.15 shows the ITC values for Subject 01 where EEG data is the better synchronized with time locking events in delta band among red and green colors exposure whereas blue has relatively less synchronized data in all frequency bands throughout its latency times. However the synchronization is scattered in the beta frequency bands in all the color imaginations of subject 1.

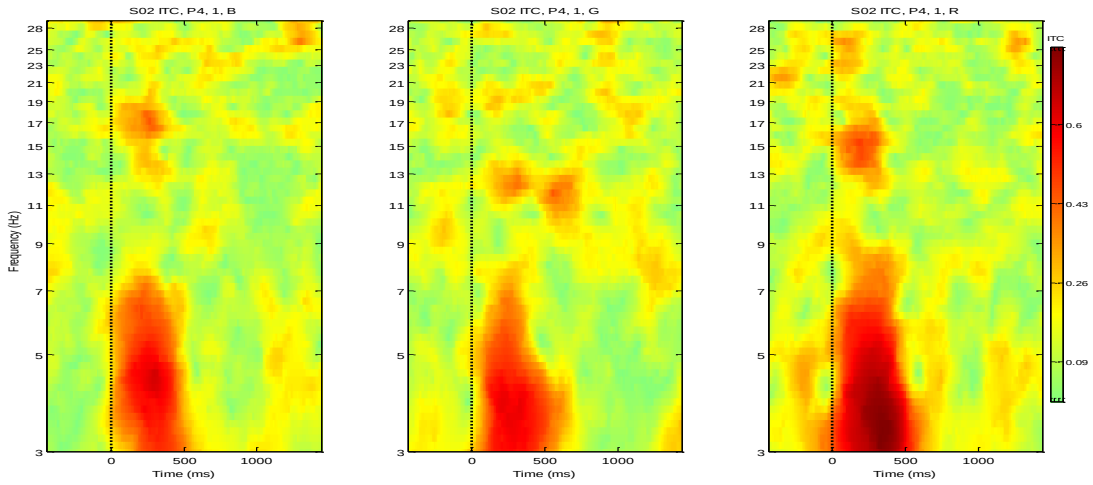

(a)

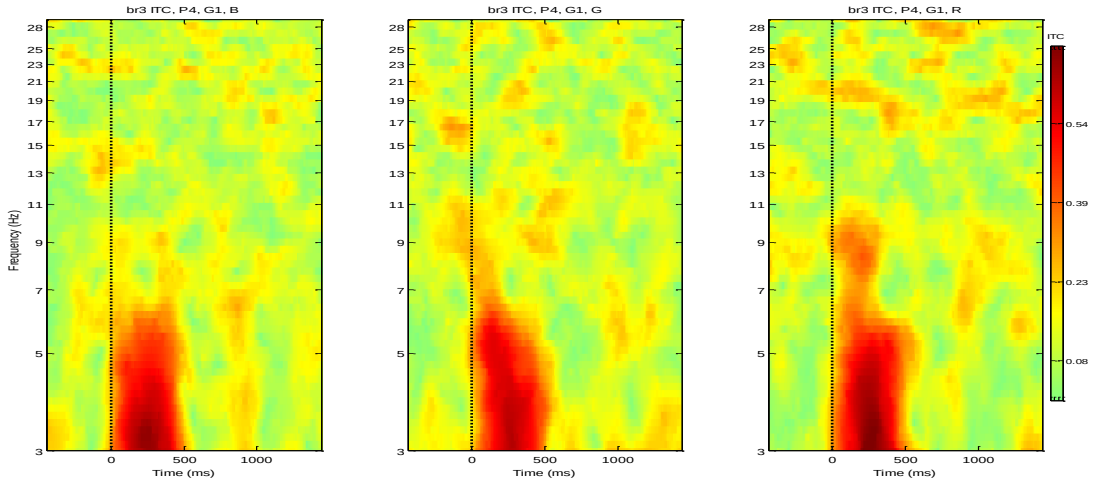

(b)

Figure 6.16 Subject '02' ITC plots of each real color exposure in (a) and its corresponding imagination in (b). Red's response is on right, Green's in the middle and Blue's is on the left. X-axis represents time (ms) and Y-axis represents frequency (Hz).

Figure 6.16 shows the ITC response of subject 02. We can see that subject 2's EEG data is very nicely synchronized both in real colors exposure and their corresponding imaginations only in delta and theta bands. Among the real colors exposure red has the highest synchronized data and green has the lowest synchronized data whereas among the imaginations of colors, red and blue have probably the same synchronization in delta bands. One thing is common in both subject 01 and 02 that higher the frequency band, the lesser the synchronization is, and it is expected to be common also in other subjects. Another thing is that, subject 1 is able to imagine the color well in almost all the trials i.e. starts imagination in given time well before it ends.

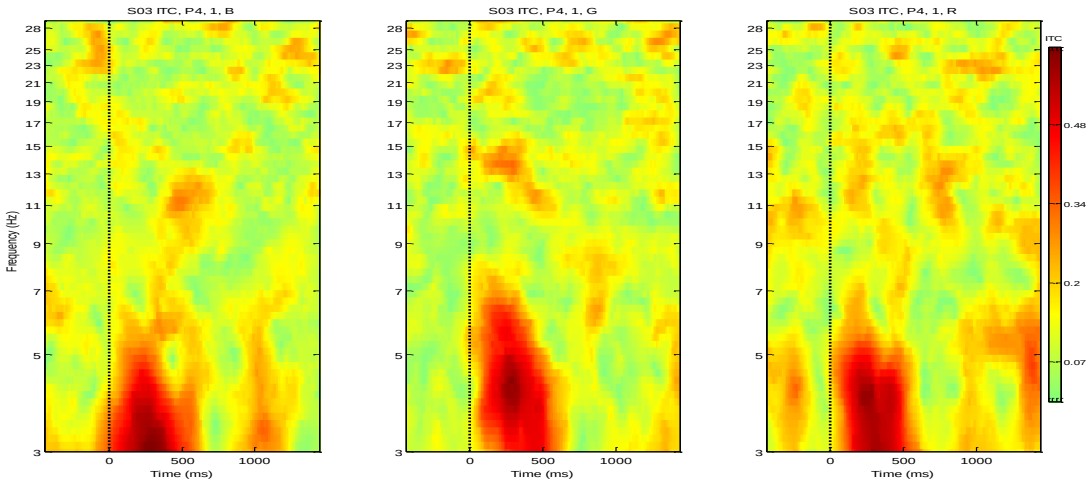

(a)

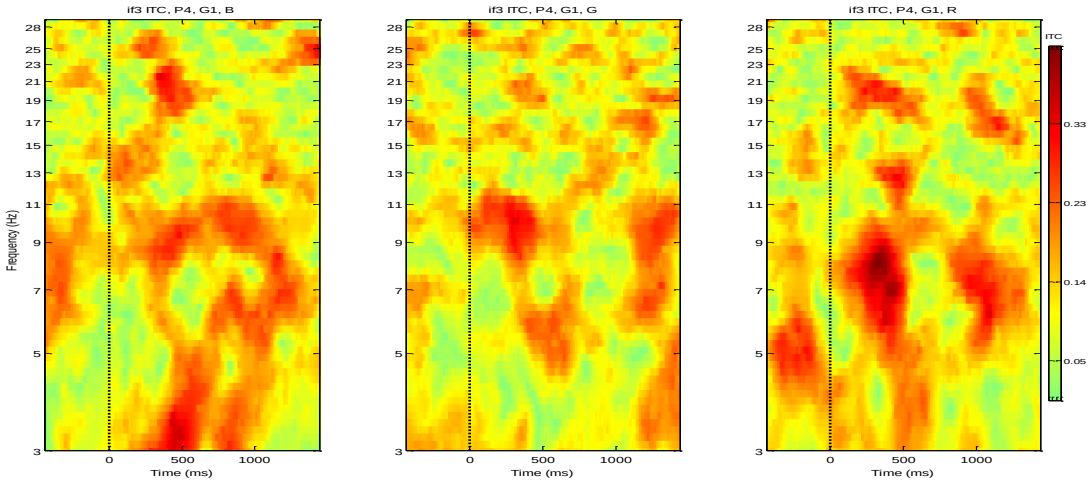

(b)

Figure 6.17 Subject '03' ITC plots of each real color exposure in (a) and its corresponding imagination in (b). Red's response is on right, Green's in the middle and Blue's is on the left. X-axis represents time (ms) and Y-axis represents frequency (Hz).

Figure 6.17 reflects the synchronization of subject 3's EEG activities. We can see that among all the real color exposures, once again the delta band is better synchronized than other frequency bands whereas in imaginations of colors the synchronization of EEG data with time locking events is highly scattered and relatively less than real exposures in all the frequency bands and at all latencies measures which means that the subjects 3's response to real color exposures is well but not able to imagine the colors well in a given time of 3 seconds and starts imaging at variable latencies in all the trials.

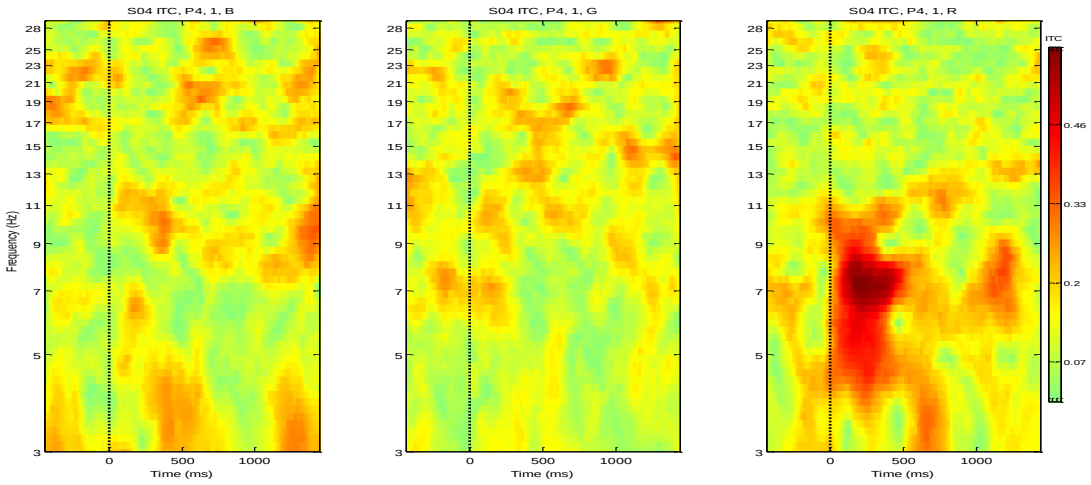

(a)

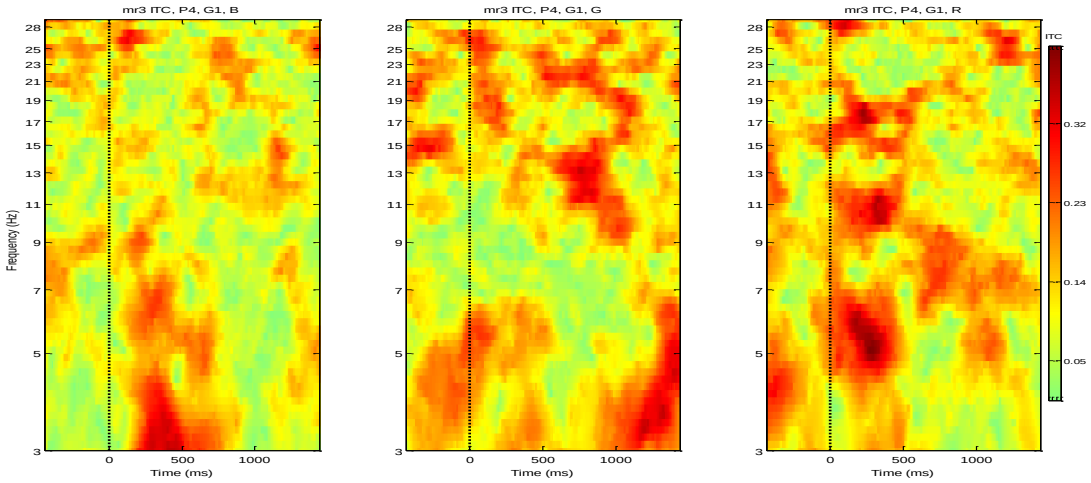

(b)

Figure 6.18 Subject '04' ITC plots of each real color exposure in (a) and its corresponding imagination in (b). Red's response is on right, Green's in the middle and Blue's is on the left. X-axis represents time (ms) and Y-axis represents frequency (Hz).

Figure 6.18 shows the ITC values of subject 4, according to which red has the highest synchronization activity in theta (4 – 8 Hz) frequency band among the real colors exposure whereas EEG activities for green and blue color's response is less synchronized not only in theta but also in delta band. However, green and blue colors response is relatively better synchronized than red in beta band at variable latencies. Among the imaginations of subject 4, synchronization of EEG data with the time locking event is almost similar to subject 3 which means that subject 3 and 4 both were not good in imaginations of colors. Moreover, subject 3 and 4 have the EEG activity synchronized to some extent in the baseline latency.

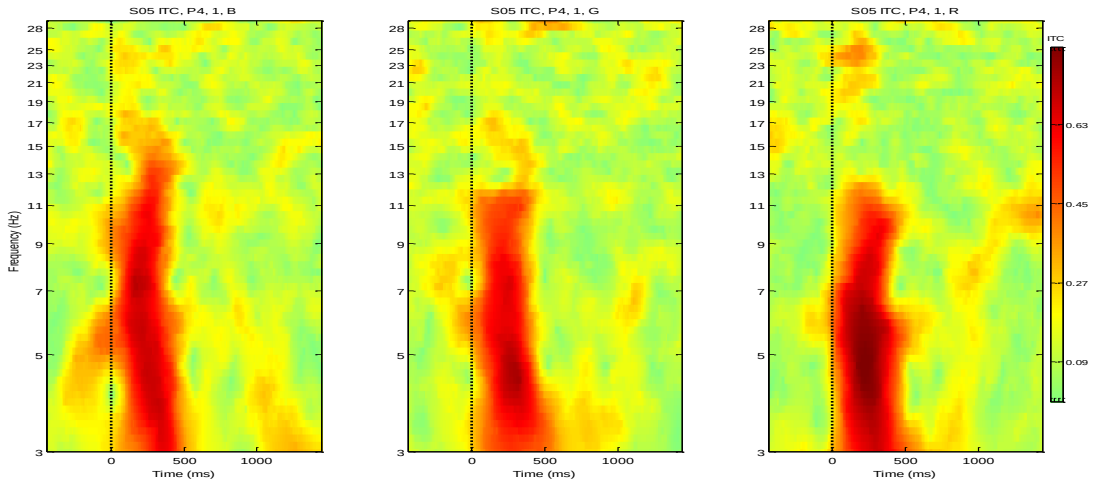

(a)

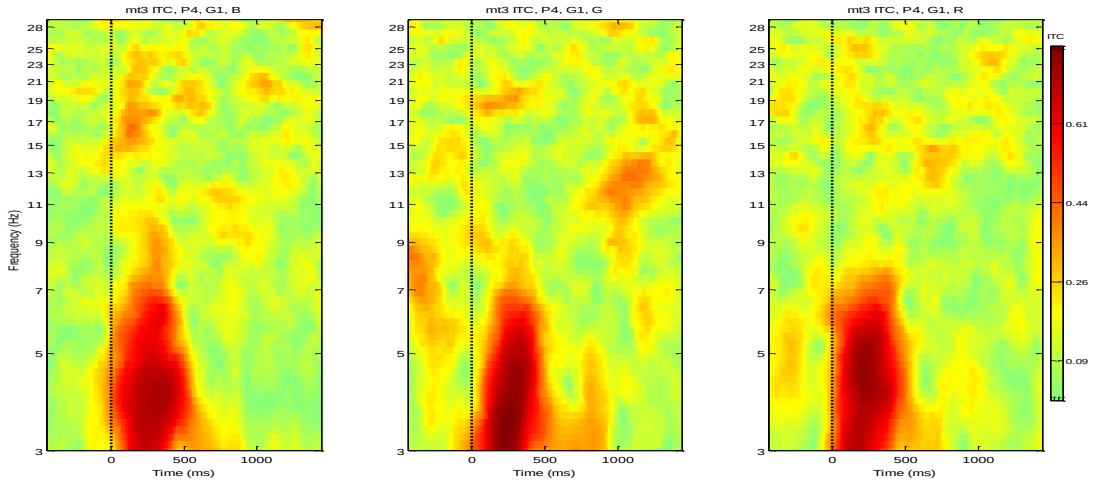

(b)

Figure 6.19 Subject '05' ITC plots of each real color exposure in (a) and its corresponding imagination in (b). Red's response is on right, Green's in the middle and Blue's is on the left. X-axis represents time (ms) and Y-axis represents frequency (Hz).

Figure 6.19 illustrates the synchronization of its EEG activities with the experimental events very nicely in three frequency bands i.e. delta, theta and alpha but not in beta band among the real colors exposure with highest synchronization in red whereas among the imagination of colors EEG data is only synchronized in delta and theta band but not in alpha band with highest ITC value in green and lowest in blue keeping the red in the middle which means that subject 5's imagination of colors is better than the subjects 1, 3 and 4 but more or less same as subject 2's imaginations of colors. One more thing is visible in figure 6.19 that all the EEG activities are synchronized in same latencies from the onset of stimulus until 500 ms, not only color exposure but also for imagination of colors.

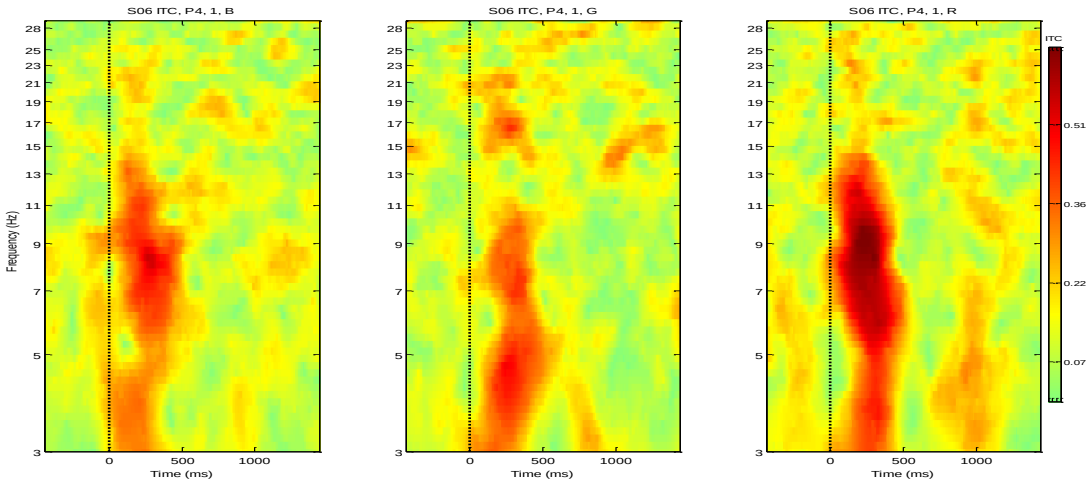

(a)

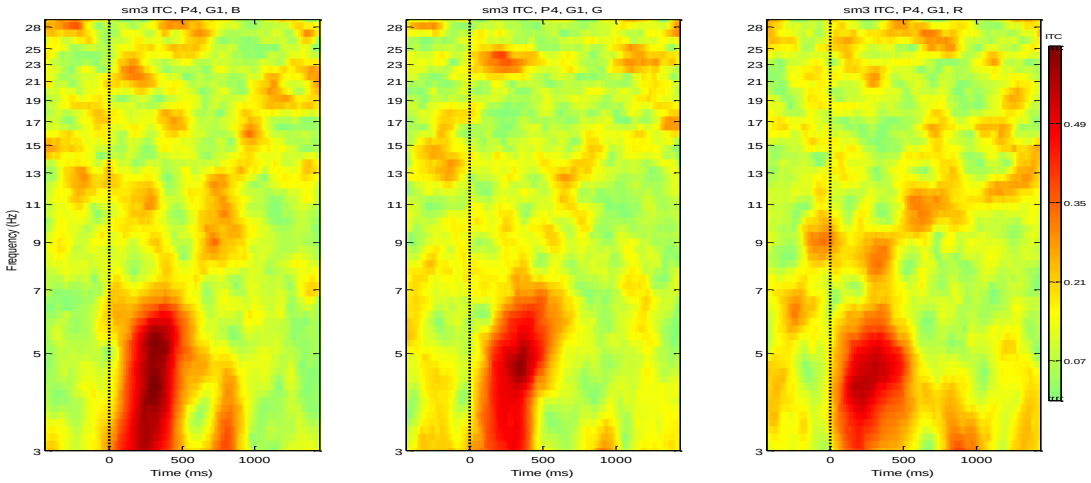

(b)

Figure 6.20 Subject '06' ITC plots of each real color exposure in (a) and its corresponding imagination in (b). Red's response is on right, Green's in the middle and Blue's is on the left. X-axis represents time (ms) and Y-axis represents frequency (Hz).

Figure 6.20 shows the ITC data for subject 6. Among the real colors exposure, red has higher synchronized activity than both the green and blue in alpha band but having relatively less synchronized activity in its delta and theta bands in comparison with its own alpha band at around 200 to 400 ms of time. Whereas among the imagination, all the colors are synchronized in delta and lower theta bands with blue color has the highest synchronization activity within 100 to 400 ms of latencies having very less synchronized activity in alpha and beta bands. Moreover, the subject 6 is good at imagination of colors but not better than subject 5.

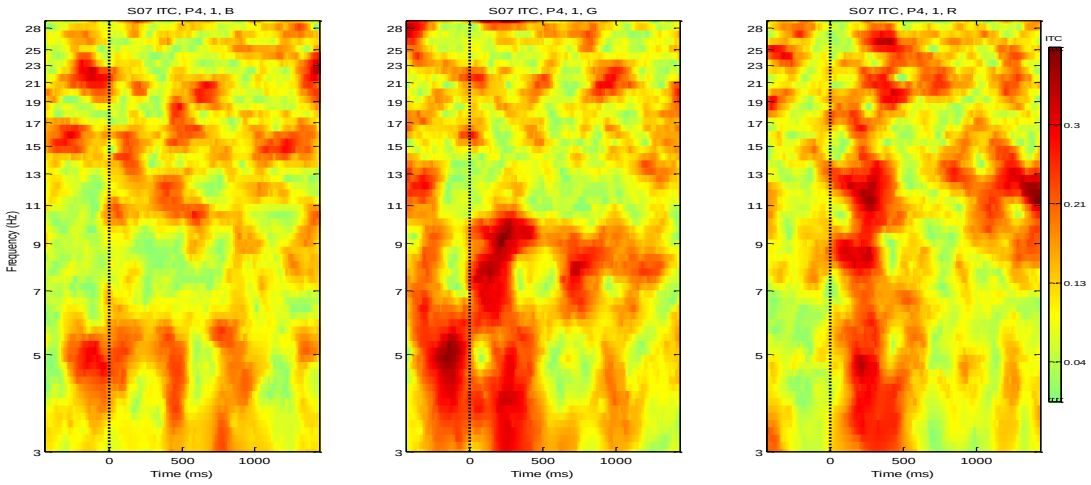

(a)

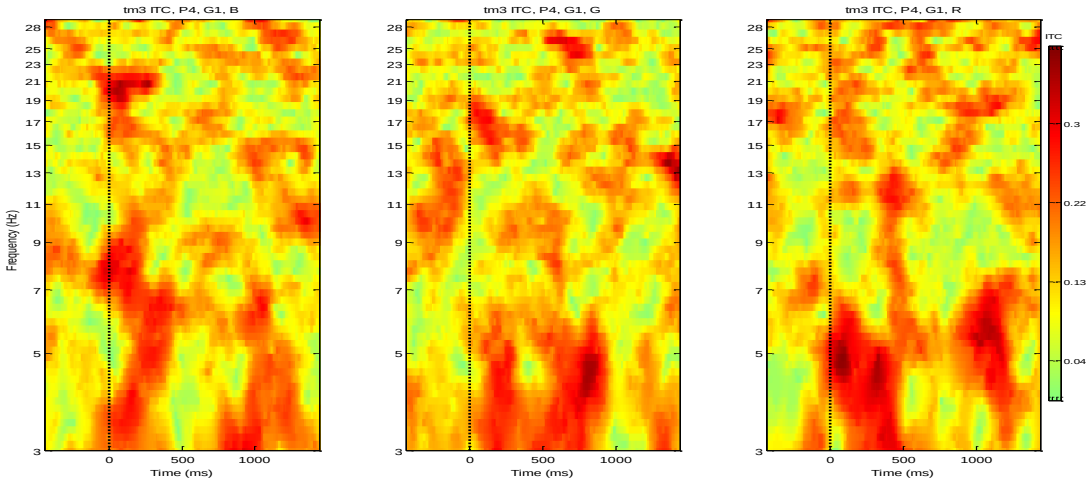

(b)

Figure 6.21 Subject '07' ITC plots of each real color exposure in (a) and its corresponding imagination in (b). Red's response is on right, Green's in the middle and Blue's is on the left. X-axis represents time (ms) and Y-axis represents frequency (Hz).

Figure 6.21 illustrates the synchronization activity of subject 7 which is quite visible that all the activities are scattered with respect to frequency bands and variable latencies, not only in real color exposure but also in imagination of colors. In this case, EEG activities are synchronized in all the frequency bands.

One thing is very clear from the ITC responses that not all the subject are able to imagine the colors in a given time of 3 seconds that caused them to produce non synchronized EEG activity. Subjects 2, 5 and 6 all are better than subjects 1, 3, 4 and 7 both in real color exposure and imaginations. So the inter-trial coherence varies greatly depending on the subjects mental condition i.e. if he is relaxed or confused or tensed due to environmental setup during the experiment and also if the subject is seated in a comfortable positions. All these conditions may greatly affect the subject's perception to colors.

6.3.5 ERP Image Plots

In order to better understand electrophysiological data analysis we used ERP image plots that are 2-D transforms of epoched data expressed as rectangular colored image, where every horizontal line represents activity occurring in a single experimental trial; data epochs are first sorted along some relevant dimension, for example, latency or phase-sorted trials at stimulus onset. ERP image provide more effective analysis than one dimensional ERP waveforms. Please note that like earlier plots, here also the data is considered from electrode position P4.

Figure 6.22 represents ERP image plot for red color exposure in (a) and its imagination in (b). In Figure 6.22 (a), first row shows head plot, top left containing a red dot indicates the position of the electrode in the montage i.e. in this case P4 and on the top right, frequency spectrum is shown up to beta band where a significant peak is found in the alpha band (already shown in figure 6.5). In the second row, ERP image is presented with respect to phase-sorted trials. It is produced by stimulus induced phase resetting of ongoing EEG activity. The sigmoidal shape of the phase-sorted post stimulus alpha wave fronts (red and blue) indicate the uneven distribution of post stimulus alpha phase (7) that starts around 150 ms before stimulus onset. An ERP alpha phase time series is shown in the third row. We can see a negative peak N1 around 250 ms in ERP waveform that is sum of more negative than positive single-trial values, evidently visible in ERP image at the same latency in the second row. Event-related spectral power (ERSP) waveform in time domain is reflected in the fourth row that shows a significant power decrease in alpha band after 200 ms of the onset of stimulus which is compatible with the average ERSP plots for red color in figure 6.6 (a) right most plot i.e. blue concentrated area in the alpha band (8 – 12 Hz) along with upper theta (6 – 8 Hz) and lower beta (13 – 22 Hz) bands. The number 10.78 dB (visible by zooming the image) in the baseline (i.e. left side of vertical bar) indicates the absolute baseline power level. Fifth row represents inter-trial coherence (ITC), having significant increase in ITC in alpha band with highest value at a single frequency of 9.75 Hz which is selected as analysis frequency in the alpha band together with (p=0.05) ITC significance level, centered from 100 to 400 ms which is also evident in figure 6.14 (a). As we can see, phase synchronization gets stronger than our specified p=0.05 significance cutoff at about 250 ms in figure 6.14 (a) and 6.14 (b). A significant difference of increase in power is found in all ERSP waveforms of all the color imaginations unlike real color exposure in the last one second of epoched data which could be due to delay in starting imagination of colors. Figures 6.23 and 6.24, show ERP image plots for green and blue colors respectively. In figure 6.23 (a) and 6.24 (a), negative peak occurs at 250 ms and a positive peak occurs at 400 ms visible in ERP alpha waveforms. ERSP waveforms show more decrease in power starting from 200 ms while exposure of real colors than imagination of colors in both figures 6.23 and 6.24.

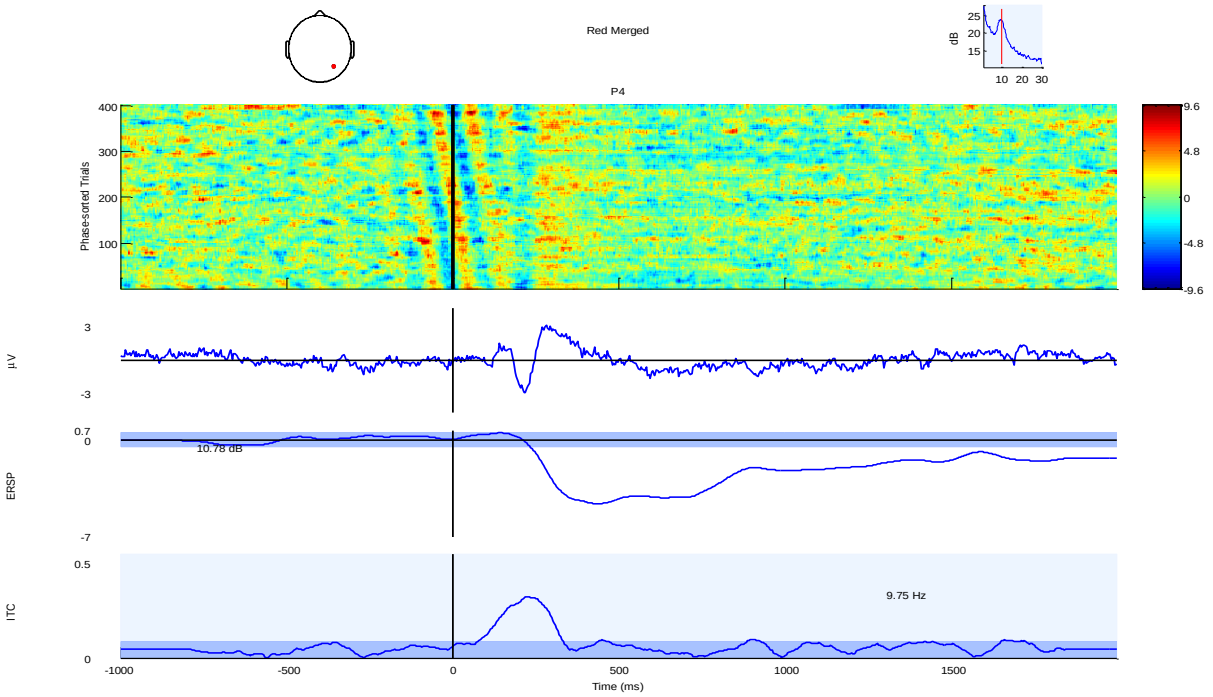

(a)

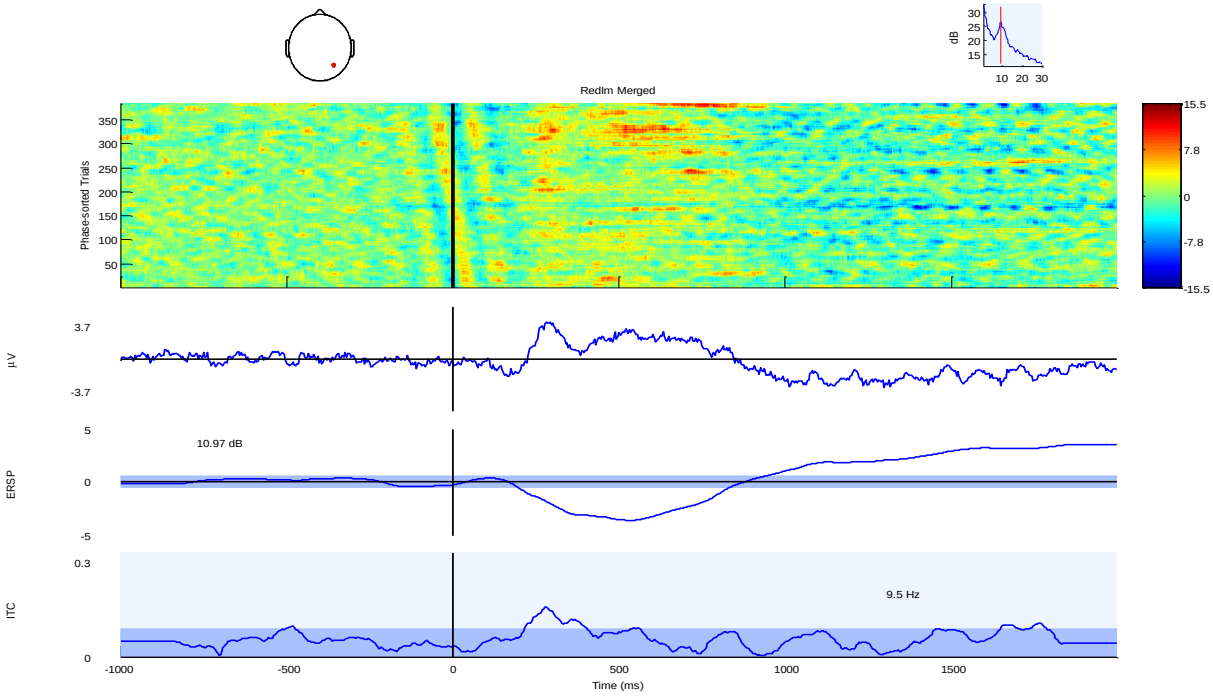

(b)

Figure 6.22 ERP Image plots of **Red** color in (a) and its corresponding imagination in (b). First row – Head plot and Frequency Spectrum. Second row – ERP image. Third row – ERP waveform. Fourth row – ERSP in waveform. Fifth row – ITC waveform.

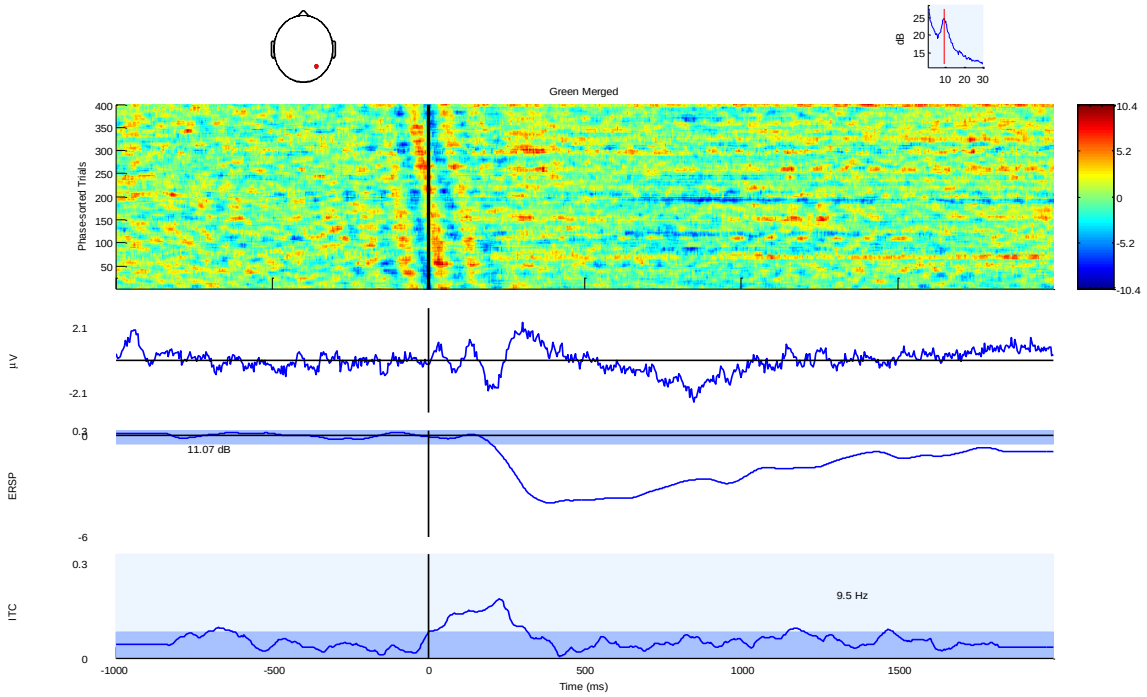

(a)

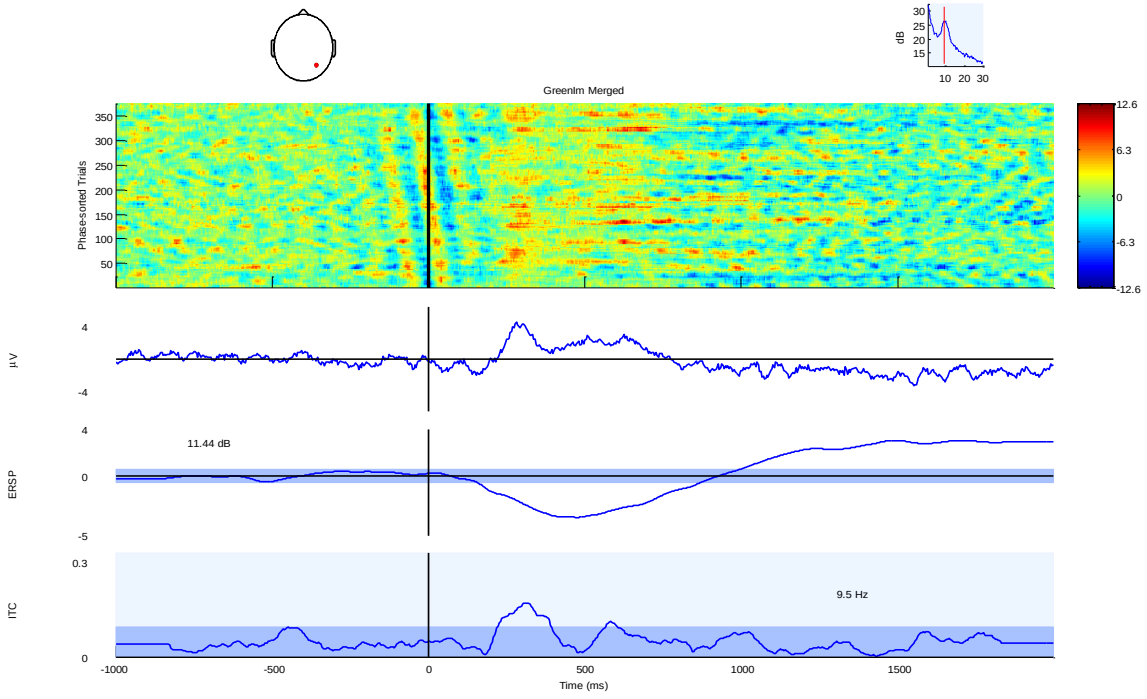

(b)

Figure 6.23 ERP Image plots of **Green** color in (a) and its corresponding imagination in (b). First row – Head plot and Frequency Spectrum. Second row – ERP image. Third row – ERP waveform. Fourth row – ERSP in waveform. Fifth row – ITC waveform.

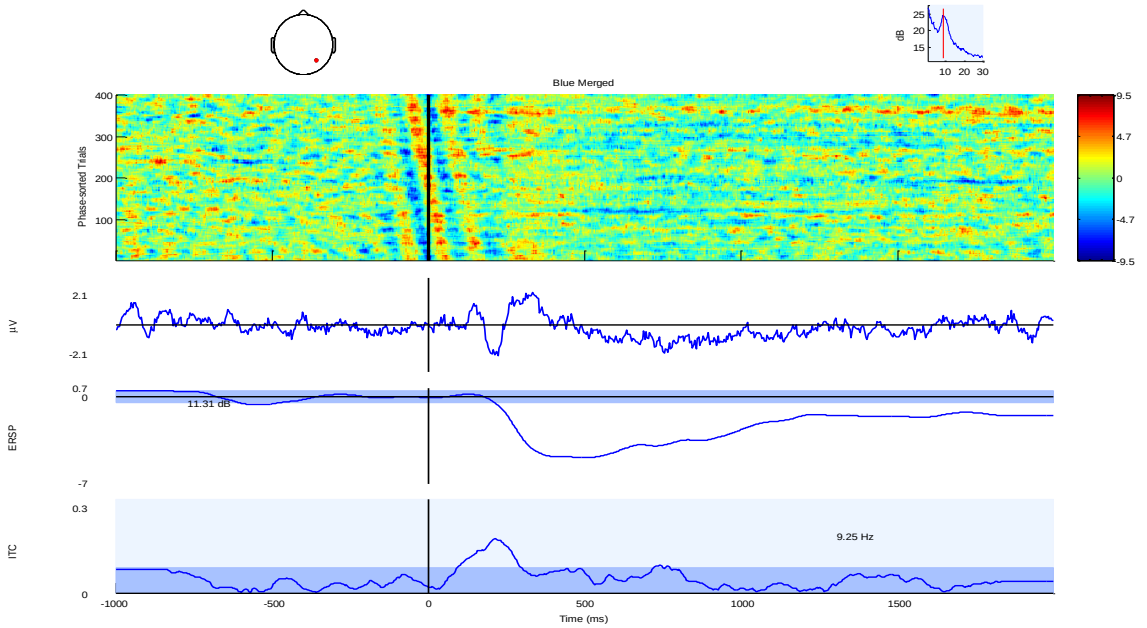

(a)

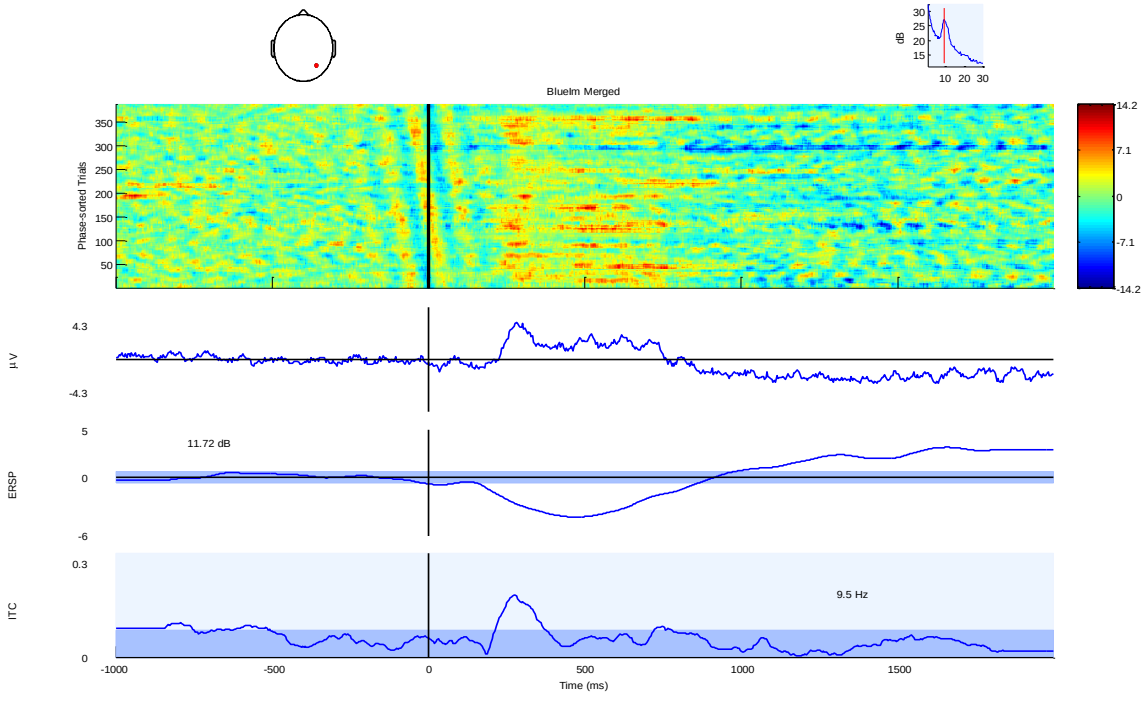

(b)

Figure 6.24 ERP Image plots of **Blue** color in (a) and its corresponding imagination in (b). First row – Head plot and Frequency Spectrum. Second row – ERP image. Third row – ERP waveform. Fourth row – ERSP in waveform. Fifth row – ITC waveform.

Frequencies selected for ITC analysis among alpha oscillations in red exposure is 9.75 Hz, 9.5 Hz in green and 9.25 Hz in blue exposure where as a unique frequency of 9.5 Hz for all color imaginations. Phase synchronization gets stronger than our specified p=0.05 significance at

about 200 ms to 300 ms in both green and blue color exposure and their corresponding imaginations like red colors. During real color exposure, phase synchronization remains within our specified significance except in real blue exposure, slightly around 500 ms as depicted in figure 6.24 (a).

6.4 Classification using SVM with ERSP as Features for Real Exposure of Colors

In this section we will not discuss the theoretical parts of classification using support vector machines because we have already discussed SVM in detail in chapter 4. In this section we will describe the results for classification of EEG signals produced by real colors exposure only whereas the classification results for the imagination of colors are presented in the next section. As you know that we have EEG signals belonging to three classes in our experiment to be classified as Red, Green and Blue and as you also know that ERSP data that was computed using EEGLAB (5) Toolbox. We have ERSP datasets for each colour i.e. red, green and blue, for each subject. To acquire these datasets, ERSP was calculated for each trial in terms of time-frequency framework, for each colour among all the subjects. An average ERSP was taken across the trials for each colour as shown in figure 6.25 which represents the ERSP response for electrode position O2 across all the subjects for the real colours exposed to the subjects. It is clearly visible in all the colours that distribution of power in a specific frequency band at a certain time point is quite discriminative and remains discriminative for individual subjects for each colour. After the onset of stimuli, the highest increase in power is seen in red and lowest in blue during an interval from 100 to 400ms within delta and theta band. However, the lowest decrease in power is seen in blue and highest in green during an interval from 250 to 1000ms within the alpha frequency band. These features were fed into SVM classifier.

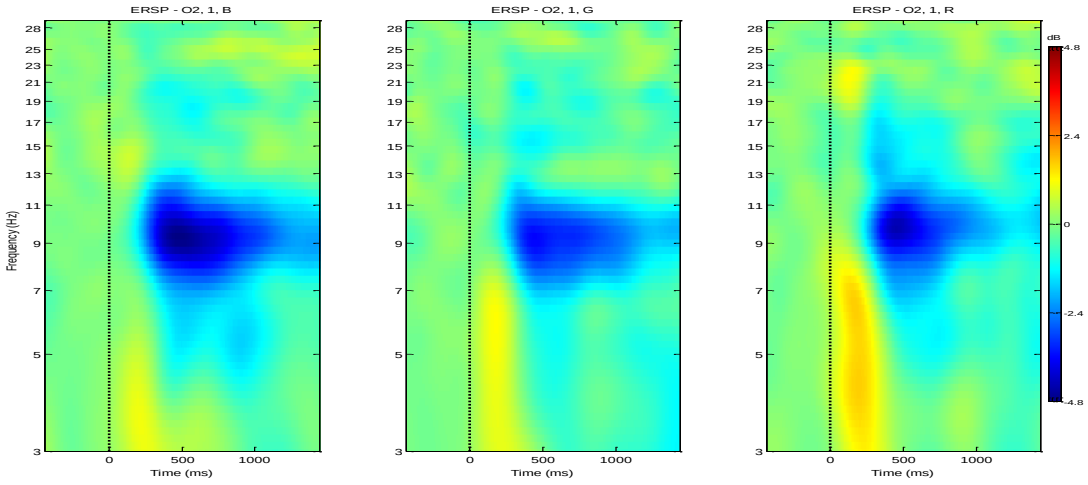

Figure 6.25 Averaged ERSP shown for electrode position O2. Right (Red), Middle (Green) and Left (Blue).

To classify EEG signals into red, green and blue classes, LIBSVM (12) Toolbox was used which requires a specific format of data as follows in general,

<Label Class1> <index1> : <feature1> <index2> : <feature2> <index3> : <feature3> …

<Label Class2> <index1> : <feature1> <index2> : <feature2> <index3> : <feature3> …

<Label Class3> <index1> : <feature1> <index2> : <feature2> <index3> : <feature3> …

⋮ ⋮ ⋮ ⋮

Each row represents an instance or observation and each column represents the feature after the label column. Data was labeled before feeding to the classifier i.e. red labeled as 1, green labeled as 2 and blue labeled as 3. Numerically, ERSP data is present in two dimensional dataset of 100*200 values which indicate that there are 100 frequency points along rows and 200 time points along columns. For instance, to convert the data of subject 1 for channel P3, all the subject 1's colours i.e. red, green and blue are taken into account and each time point along its frequency points is chosen randomly within a single colour and placed according to above format into the target dataset which will be used for training and testing of classifier. Once a time point is chosen from red class then a time point is chosen from green and finally from blue. This sequence continues until all the time points are chosen randomly within a single colour. Since there are 100 frequency points indicating 100 feature values in the target dataset against each label. Having three classes in hand, there would be 600 instances for data coming from channel P3, in the target dataset as each class contains 200 instances of time points i.e. each time point becomes an instance along the row in the target dataset with the corresponding label. After conversion, target dataset is divided into two subsets, one for training of classifier and the other is used for testing the classifier. As we have used four channels, two from parietal lobe and two from occipital lobe i.e. P3, P4, O1 and O2, the data was fed into the classifier not only as an individual channel but also in combination of different channels i.e. P3, P4, O1, O2, P3P4 (parietal region), O1O2(occipital region), P4O2(right occi-parietal), P3O1(left occi-parietal) and P3P4O1O2 (All). We have used C-SVC with linear kernel, polynomial kernel and RBF kernel where $\gamma = 0.1$ and degree of polynomial kernel is 3 along with default parameters. Tables 1, 2 and 3 present classification accuracies for linear, polynomial and RBF kernels respectively, for all the groups of data within all the subjects.

Table 1 presents the classification accuracies with an average accuracy of 84% for seven subjects among different groups of data which were used with linear kernel, **for real exposure of colors. (ERSP features)**

	S1	S2	S3	S4	S5	S6	S7
P3	90.74	83.7	85.19	85.93	84.82	84.82	81.85
P4	81.11	83.7	84.44	84.07	87.78	84.07	84.82
O1	81.11	86.3	81.85	84.82	88.15	82.96	87.78
O2	82.22	84.07	82.22	87.04	84.44	87.04	84.44
P3P4	83.7	85.93	83.89	87.41	88.15	84.63	84.44
O1O2	85	84.26	83.89	84.63	83.15	85.56	82.59
P4O2	85	82.78	83.89	84.26	85.93	85.93	82.59
P3O1	85	85.37	85.74	84.63	84.82	86.67	82.59
All	84.63	84.17	85	84.17	84.85	83.98	80.83

Table 2 presents classification accuracies with an average accuracy of 89% for seven subjects among different groups of data which were used with polynomial kernel of degree 3, **for real exposure of colors. (ERSP features)**

	S1	S2	S3	S4	S5	S6	S7
P3	90	85.93	84.07	88.52	85.56	93.7	90.37
P4	83.7	86.67	86.3	89.63	91.11	89.63	91.85
O1	85.56	87.41	86.67	90.37	87.78	91.11	92.22
O2	83.7	86.67	89.25	87.04	86.3	87.78	88.15
P3P4	88.7	87.22	92.96	91.85	96.3	93.15	89.82
O1O2	85.74	82.59	81.48	88.33	90.56	87.41	89.07
P4O2	90.19	87.96	87.41	88.7	86.48	82.96	87.96
P3O1	87.41	84.63	84.26	92.22	90.56	92.96	87.78
All	92.59	90.74	88.89	91.57	95.56	89.17	87.41

Table 3 presents the classification accuracies with an average accuracy of 98% for seven subjects among different groups of data which were used with RBF kernel, **for real exposure of colors. (ERSP features)**

	S1	S2	S3	S4	S5	S6	S7
P3	99.63	96.3	99.26	96.67	97.04	97.41	99.63
P4	96.3	95.56	97.78	100	97.78	97.04	98.89
O1	94.82	96.3	95.93	99.63	97.04	96.67	98.15
O2	95.56	97.04	99.26	100	93.7	92.22	98.15
P3P4	97.78	94.63	99.63	99.82	100	99.44	97.78
O1O2	97.41	95	99.96	99.44	97.59	90.37	97.04
P4O2	98.33	93.7	99.3	99.3	96.85	95.93	97.59
P3O1	98.52	97.04	98.7	98.33	97.41	98.7	98.89
All	99.26	95.37	98.8	99.72	98.43	96.11	97.87

Classification accuracies for the data from all the channels (P3P4O1O2) with in all the subjects is shown in figure 7 for the three kernels used. Linear kernel has come up with lowest accuracy and RBF with highest accuracy in all the subjects. Similar results for the rest of the groups of data were also seen with an ascending order from lower to higher accuracy for linear, polynomial and RBF kernels in all the subjects. However, in some cases linear kernel has proven to be slightly better than polynomial in occipital region. Results regarding linear, polynomial and RBF kernels performances are shown in figures 6.26, 6.27 and 6.28 for data groups ‘All’, ‘parietal’ and ‘occipital’ channels respectively. However, the results for individual channels and right and left occi-parietal channels are similar. Tools used in this study are BCI2000 (4), EEGLAB (5) and LIBSVM (12) (13).

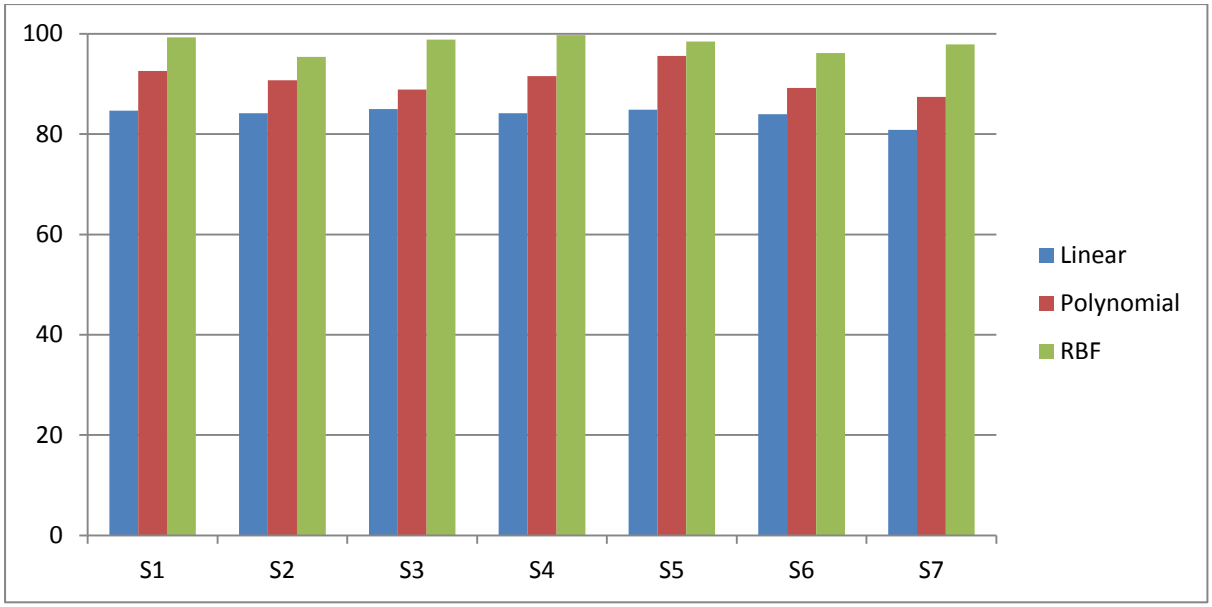

Figure 6.26 Classification accuracies in comparison among linear, polynomial and RBF kernels for data from all channels (P3P4O1O2). X-axis shows the number of subjects and Y-axis show the classification accuracy in (%).

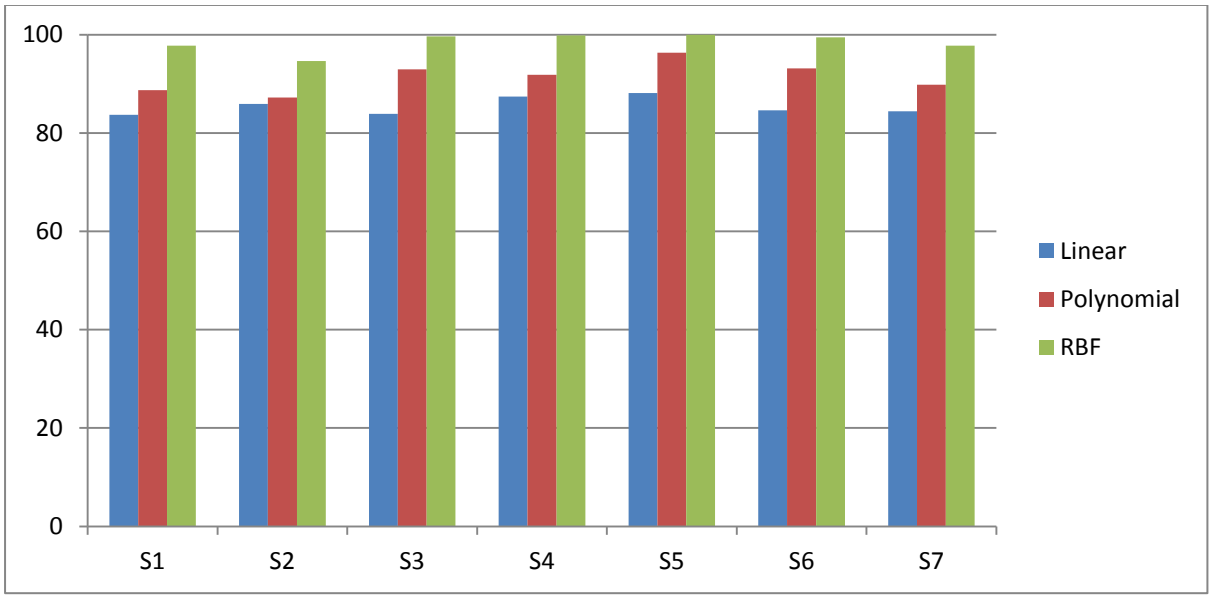

Figure 6.27 Classification accuracies in comparison among linear, polynomial and RBF kernels for data from parietal channels (P3P4). X-axis shows the number of subjects and Y-axis show the classification accuracy in (%).

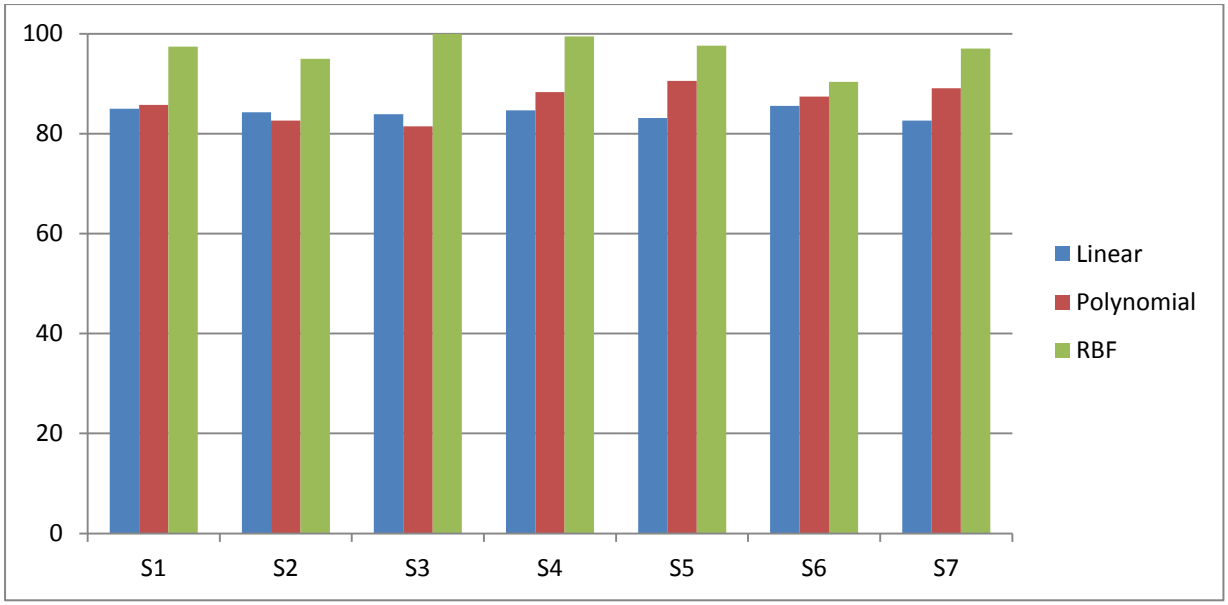

Figure 6.28 Classification accuracies in comparison among linear, polynomial and RBF kernels for data from occipital channels (O1O2). X-axis shows the number of subjects and Y-axis shows the classification accuracy in (%).

6.5 Classification using SVM with ERSP as Features for Imagination of Colors

Since our experimental protocol has two parts, one is exposure of real colors and the other is imagination of colors so in this section we have presented the classification results for imagination of colors. We have found several studies like described in (2), that discuss BCI application based on imagination of hands movement and foot movement. Literature show that EEG signals produced by imagination of limbs movement can be successfully classified with high accuracy and utilized with BCI applications. The study on imagination of colors is not found in literature in context with BCI applications. We have classified the color signals with a very good accuracy but did not use the classified signal with BCI applications; however we have plans in future to implement the classified signals. Tables 4, 5 and 6 present classification results for linear, polynomial and RBF kernels respectively, for all the groups of data within all the subjects. As we can see from tables 4, 5 and 6 that classification accuracies on average for imagination of colors are 64%, 70% and 76% respectively which are quite below as compare to exposure of real colors. It is clear that classification accuracy for imagination of colors is not as good as it was in real exposure of colors. However, results produced with linear kernel are lowest likewise classification results with linear kernel in case of real color exposure and highest with RBF kernel. Focusing on the classification results with linear kernel, the highest accuracy is seen in subject 1 at electrode position P3 with 70.51% whereas the lowest is seen in subject 7 at 'All' channels with 60.6%. Polynomial kernel produced highest accuracy in subject 5 at electrode positions P3P4 with 77.61% and lowest is seen in subject 3 at electrode positions O1O2 with 62.79% whereas RBF kernel produced highest accuracy in subject 4 at electrode positions P4 and O2 with 78.44% and lowest accuracy was produced in subject 6 at electrode position O1O2 with 68.81%.

Table 4 presents the classification accuracies with an average accuracy of 64% for seven subjects among different groups of data which were used with linear kernel, **for imagination of colors. (ERSP features)**

	S1	S2	S3	S4	S5	S6	S7
P3	70.51	63.47	64.96	65.7	64.59	64.59	61.62
P4	60.88	63.47	64.21	63.84	67.55	63.84	64.59
O1	60.88	66.07	61.62	64.59	67.92	62.73	67.55
O2	61.99	63.84	61.99	66.81	64.21	66.81	64.21
P3P4	63.47	65.7	63.66	67.18	67.92	64.4	64.21
O1O2	64.77	64.03	63.66	64.4	62.92	65.33	62.36
P4O2	64.77	62.55	63.66	64.03	65.7	65.7	62.36
P3O1	64.77	65.14	65.51	64.4	64.59	66.44	62.36
All	64.4	63.94	64.77	63.94	64.62	63.75	60.6

Table 5 presents classification accuracies with an average accuracy of 70% for seven subjects among different groups of data which were used with polynomial kernel of degree 3, **for imagination of colors. (ERSP features)**

	S1	S2	S3	S4	S5	S6	S7
P3	71.31	67.24	65.38	69.83	66.87	75.01	71.68
P4	65.01	67.98	67.61	70.94	72.42	70.94	73.16
O1	66.87	68.72	67.98	71.68	69.09	72.42	73.53
O2	65.01	67.98	70.56	68.35	67.61	69.09	69.46
P3P4	70.01	68.53	74.27	73.16	77.61	74.46	71.13
O1O2	67.05	63.9	62.79	69.64	71.87	68.72	70.38
P4O2	71.5	69.27	68.72	70.01	67.79	64.27	69.27
P3O1	68.72	65.94	65.57	73.53	71.87	74.27	69.09
All	73.9	72.05	70.2	72.88	76.87	70.48	68.72

Table 6 presents the classification accuracies with an average accuracy of 76% for seven subjects among different groups of data which were used with RBF kernel, **for imagination of colors. (ERSP features)**

	S1	S2	S3	S4	S5	S6	S7
P3	78.07	74.74	77.7	75.11	75.48	75.85	78.07
P4	74.74	74	76.22	78.44	76.22	75.48	77.33
O1	73.26	74.74	74.37	78.07	75.48	75.11	76.59
O2	74	75.48	77.7	78.44	72.14	70.66	76.59
P3P4	76.22	73.07	78.07	78.26	78.44	77.88	76.22
O1O2	75.85	73.44	78.4	77.88	76.03	68.81	75.48
P4O2	76.77	72.14	77.74	77.74	75.29	74.37	76.03
P3O1	76.96	75.48	77.14	76.77	75.85	77.14	77.33
All	77.7	73.81	77.24	78.16	76.87	74.55	76.31

Tables 4, 5 and 6 are summarized in figure 6.29 in order to see the performance of all the three kernels within all the groups of data among all the 7 subjects through visual inspection. As we can see that none of kernels have produced more than 80% of accuracy at all electrode locations in any subject. This accuracy may be increased by better training of the subjects to imagine the colors and also by changing the different experimental conditions during recording of EEG data and/or by better removing artifacts from EEG data. The more the cleaner data is, the more the better and reliable results may be achieved. However, keeping in mind all the classification results for real color exposure and their corresponding imaginations, it is observed that RBF kernel always produced most of the times best results so we suggest to always use RBF kernel in such kind of studies. Please note that the complexity and online performance still needs to be addressed.

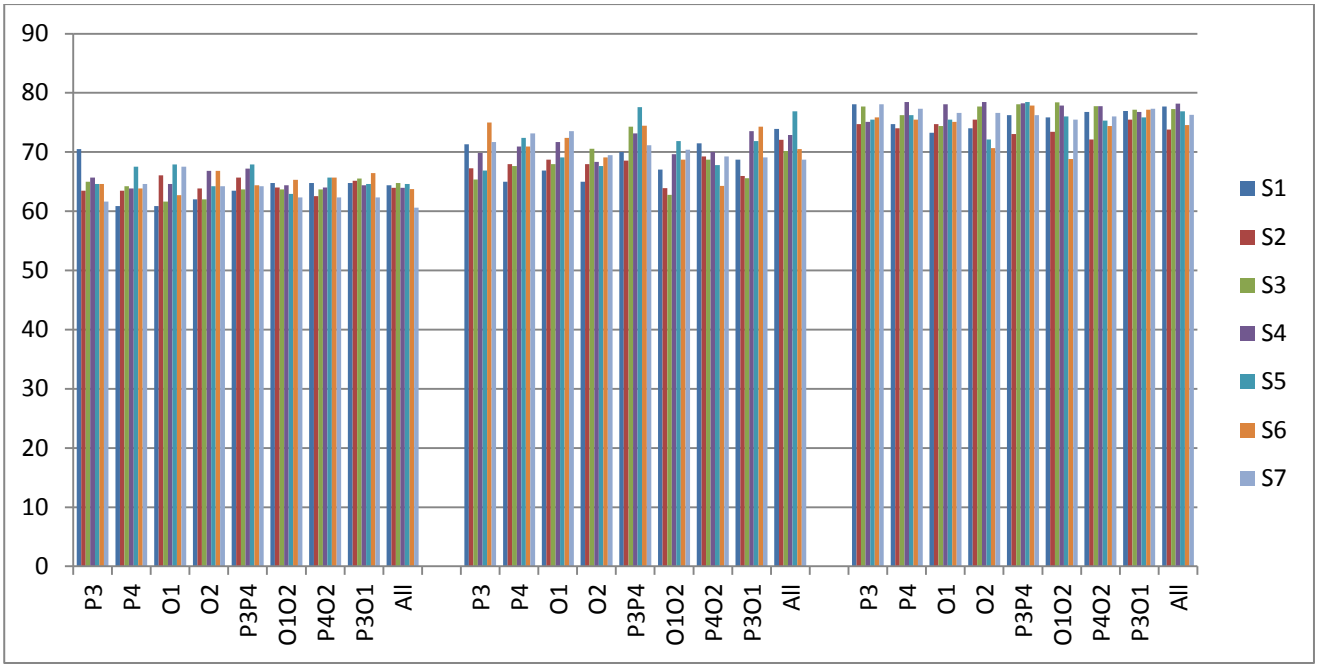

Figure 6.29 Classification accuracies altogether in linear (on left), polynomial (in center) and RBF (on right) kernels for data from all the groups of channels. X-axis shows the groups of channels of data and Y-axis shows the classification accuracy in (%) and each group of vertical bars shows the number of 7 subjects for imagination of colors. **(ERSP features, imagination)**

6.6 Classification using SVM with Extreme Energy Ratio and Difference Criterions

In this section, we have presented the classification results for real exposure of colors using Extreme Energy Ratio (14) and Extreme Energy Difference (15) features as suggested by Prof. Shiliang Sun in order to see if colors information in EEG is classifiable using features other than ERSP. We have seen that EEG signals can be successfully classified with EER and EED features and accuracy obtained with EED is better than EER. For this purpose we have used ERP signals as shown in figure 6.4 instead of using ERSP which is already a transformed form of ERPs into time-frequency domain. It is commonly known that EEG signals are the neuronal brain activities generated from different underlying sources beneath the cortex. For complimentary reasons, we first present here theoretical aspects of EER and EED for a single source and then for multiple sources. For complete details, please see (14) and (15).

6.6.1 Extreme Energy Ratio Criterion

Extreme Energy Ratio Criterion for Single Source

This method of feature extraction is based on EEG covariances of two different classes of brain activity and suppose the two different classes are A and B e.g. imagery of right hand movement and foot movement and having some EEG samples must belong to one of these two classes. Assume that there are N number of electrodes and T be the number of total points in the EEG trial of recording period then a raw matrix X^{raw} of order $N \times T$ can

represent an EEG sample. In this matrix, single observation is a vector that consists of $N-$ dimensional Euclidean space and thus an EEG sample makes a distribution of T such vectors. Usually, a normalization process is performed before any other processing in order to eliminate the energy difference caused by the varying recording time. So the normalization process is defined as follows

$$X \triangleq X^{raw} / \left\| X^{raw} \right\|_F \tag{1}$$

Where $\left\| X^{raw} \right\|_F = \sqrt{\sum_{i=1}^{N} \sum_{j=1}^{T} \left| X_{ij}^{raw} \right|^2}$ is the Frobenius norm.

The covariance of an EEG sample is computed as in the equation (2),

$$C \triangleq XX^T \tag{2}$$

To compute the covariances of the two classes A and B, usually an average is taken for the covariances of all the samples belonging to that particular class so the covariances for classes A and B are represented as C_A and C_B. If $\phi_{(N\times 1)}$ denotes the spatial filter for the EEG sample X then the spatially filtered signal is defined as $\phi^T X$ and the signal energy is defined as $\phi^T XX^T \phi = \phi^T C \phi$. So the discriminative criterion of EER for binary classification task is defined as follows in equation (3), indicating the energy ratio after spatial filtering for two classes A and B, also known as generalized Rayleigh quotient.

$$R(\phi) \triangleq \frac{\phi^T C_A \phi}{\phi^T C_B \phi} \tag{3}$$

To compute the extreme energy ratio we need to find the filter, say ϕ^* which maximizes or minimizes the ratio so there exist two optimal spatial filters $\phi_{\max}^*$ and $\phi_{\min}^*$ to be sought which satisfy,

$$\begin{cases} \phi_{\max}^* = \arg\max_{\phi} R(\phi) = \arg\max_{\phi} \dfrac{\phi^T C_A \phi}{\phi^T C_B \phi} \\ \phi_{\min}^* = \arg\min_{\phi} R(\phi) = \arg\min_{\phi} \dfrac{\phi^T C_A \phi}{\phi^T C_B \phi} \end{cases} \tag{4}$$

Maximum and minimum Rayleigh quotients are represented as follows in equation (5)

$$\begin{cases} R_{\max}(\phi) = \lambda_{\max} \quad if \quad C_A \phi = \lambda_{\max} C_B \phi \\ R_{\min}(\phi) = \lambda_{\min} \quad if \quad C_A \phi = \lambda_{\min} C_B \phi \end{cases} \tag{5}$$

Where $\lambda_{\min} = \lambda_1 \le \lambda_2 \le \cdots \le \lambda_{N-1} \le \lambda_N = \lambda_{\max}$ are the eigenvalues of matrix $C_B^{-1} C_A$, that is, the generalized eigenvalues of the matrix pair (C_A, C_B). The corresponding eigenvectors represent the optimal filters as defined in equation (4), so finally for a new EEG sample, its energy feature will be a vector consisting of two entries which are the energy values of the sample respectively filtered by $\phi^*_{\max}$ and $\phi^*_{\min}$. Until now we have discussed EER criterion for a single source and now we shall present the criterion for multiple sources.

Extreme Energy Ratio Criterion for Multiple Sources

In case of one dimensional signal, the variance actually reflects the energy value where EER criterion searches for a direction so that the variance of the EEG signal projected to this direction is maximized or minimized. However, in case of multidimensional signals, it is important to understand the following lemma (16) which indicates that the determinant is closely related to the concept of energy.

Lemma: For any matrix $U_{n\times n}$, denote its eigenvalues as $\gamma_i \ (i = 1, \cdots, n)$. The determinant of U is equal to the product of its all eigenvalues, that is

$$|U| = \prod_{i=1}^{n} \gamma_i \tag{6}$$

This lemma manifests that the determinant of covariance matrix represents the product of signal energy from all the principal directions.

Now suppose having m sources, EER will seek totally $2m$ sources, half of which maximizes the objective criterion and the other half minimizes the objective criterion. So a spatial filter bank $\Phi \triangleq \phi_1, \phi_2, \cdots \phi_m$ will be constituted for m spatial filters to extract m sources. Therefore the discriminative criterion can be rewritten as follows in equation (7)

$$R(\Phi) \triangleq \frac{\left|\Phi^T C_A \Phi\right|}{\left|\Phi^T C_B \Phi\right|} \tag{7}$$

Where $R(\Phi)$ shows the energy ratio after spatial filtering for two classes A and B. This process continues to find filter bank Φ^* which maximizes or minimizes the ratio as follows in equation (8).

$$\begin{cases} \Phi^*_{\max} = \arg\max\limits_{\Phi} R(\Phi) = \arg\max\limits_{\Phi} \dfrac{\Phi^T C_A \Phi}{\Phi^T C_B \Phi} \\ \Phi^*_{\min} = \arg\min\limits_{\Phi} R(\Phi) = \arg\min\limits_{\Phi} \dfrac{\Phi^T C_A \Phi}{\Phi^T C_B \Phi} \end{cases} \tag{8}$$

Here, $\Phi^*_{\max}$ consists of m generalized eigenvectors of the matrix pair (C_A, C_B) which correspond to the m maximal eigenvalues while $\Phi^*_{\min}$ consists of other m generalized eigenvectors whose corresponding eigenvalues are minimal. Therefore, an energy feature for a new EEG sample will be a vector consisting of $2m$ entries which are the energy values of the sample respectively filtered by $2m$ spatial filters coming from two filter banks $\Phi^*_{\max}$ and $\Phi^*_{\min}$. Until now we have discussed the theoretical aspects of EER criterion and now we present here the classification results for exposure of real colors. We have three classes Red (X_R), Green (X_G) and Blue (X_B). Unlike the ERSP features, here we have considered the binary classification problem having three groups of classification (Blue, Green), (Red, Green) and (Red, Blue). Moreover, EER features are applied on ERP data which is available in a matrix, 'X' of order $4 \times 768 = N \times T$ which means there are 4 electrodes and 768 time points as we already know that our ERP starts at -1 sec and ends at 2 sec, where zero second is time point of event occurrence and data was recorded at 256 Hz. Therefore, each trial was 768 data points long. We used Matlab for this job, and the data was placed in a three dimensional matrix. We already know about the two dimensions as we described earlier but the third dimension contains the number of trials so we have computed separate features for all the trials of both the classes. Taking into account the pair (Blue, Green) first of all computing covariances (C_B, C_G) of each trial belonging to both the classes. These covariances are also stored into three dimensional matrixes i.e. one for C_B and one for C_G and then computed $C_G^{-1}C_B$ which was again stored into three dimensional matrix, likewise third dimension for number of trials. The resultant of $C_G^{-1}C_B$ was used to find the eigenvalues and eigenvectors. These eigenvectors are considered to be the spatial filters and applied over the Green (X_G) and Blue (X_B) data. So we have now spatially filtered data for both the classes so the features for the matrixes X_B and X_G are simply the variances of these spatially filtered data in order to produce a four dimensional feature vector for a single matrix. Similarly the procedures are done with other two groups of classification. We have used only linear kernel SVM with EER features and achieved average accuracy of 79%, 78% and 80% for the classification groups (Blue, Green), (Red, Green) and (Red, Blue) respectivley, presented in tables 7, 8 and 9. Figure 6.30 summarized all the results for EER on a single plane for all the three groups of binary classification at all the electrode positions among all the subjects. The ERP data was taken from the same experiment as with ERSP features. It is clear that the accuracy achieved with EER features is good with an overall average of 78% but there appears to be quite varying accuracy as compare to the previous accuracy results for real exposure of colors and imaginations of colors with ERSP features. Therefore ERSP features seem to be more consistent in producing accuracy with less deviation among all the subjects at all the groups of data channels.

Table 7 shows classification results with an average accuracy of 79% for seven subjects among different groups of electrodes data used with linear kernel for the classification group (Blue, Green**), for real exposure of colors (EER features)**

	S1	S2	S3	S4	S5	S6	S7
P3	92.593	77.778	79.31	98.214	95	64.286	85.185
P4	83.333	77.778	72.414	96.429	91.667	66.071	90.741
O1	83.333	75.926	77.586	69.643	86.667	66.071	90.741
O2	83.333	79.63	77.586	55.357	86.667	66.071	96.296
P3P4	88.889	75.926	74.138	71.429	81.667	67.857	88.889
O1O2	81.481	83.333	79.31	78.571	86.667	76.786	87.037
P4O2	61.111	77.778	75.862	83.929	95	64.286	88.889
P3O1	87.037	75.926	81.034	87.5	95	66.071	83.333
All	75.926	59.259	70.69	71.429	73.333	58.929	64.815

Table 8 shows classification results with an average accuracy of 78% for seven subjects among different groups of electrodes data used with linear kernel for the classification group (Red, Green), **for real exposure of colors (EER features)**

	S1	S2	S3	S4	S5	S6	S7
P3	88.889	76.923	82.759	91.071	90	70.69	83.333
P4	88.889	75	87.931	89.286	90	72.414	85.185
O1	90.741	78.846	56.897	62.5	85	65.517	88.889
O2	83.333	78.846	56.897	58.929	86.667	58.621	96.296
P3P4	83.333	73.077	72.414	73.214	81.667	62.069	85.185
O1O2	81.481	76.923	79.31	69.643	80	65.517	92.593
P4O2	75.926	73.077	81.034	91.071	86.667	74.138	83.333
P3O1	87.037	76.923	81.034	83.929	100	65.517	85.185
All	59.259	63.462	75.862	57.143	68.333	55.172	61.111

Table 9 shows classification results with an average accuracy of 80% for seven subjects among different groups of electrodes data used with linear kernel for the classification group (Red, Blue), **for real exposure of colors (EER features)**

	S1	S2	S3	S4	S5	S6	S7
P3	89.286	73.077	91.379	87.5	88.333	69.643	82.759
P4	85.714	76.923	89.655	87.5	83.333	71.429	86.207
O1	91.071	86.538	94.828	66.071	80	73.214	87.931
O2	87.5	75	94.828	66.071	80	58.929	93.103
P3P4	83.929	76.923	70.69	82.143	75	67.857	91.379
O1O2	83.929	80.769	98.276	73.214	76.667	67.857	89.655
P4O2	73.214	78.846	91.379	91.071	81.667	71.429	82.759
P3O1	91.071	80.769	93.103	91.071	85	75	82.759
All	71.429	67.308	70.69	73.214	65	55.357	70.69

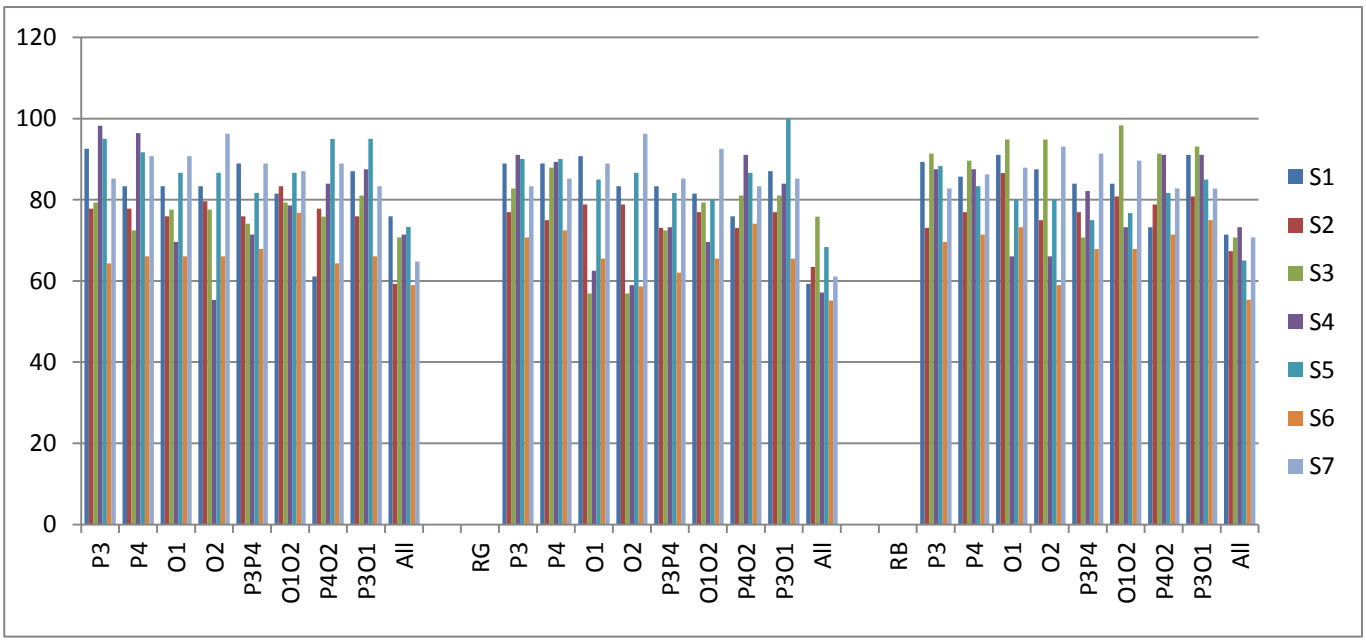

Figure 6.30 Classification accuracies altogether for the group (Blue, Green) on left, for the group (Red, Green) in center and for the group (Red, Blue) on right. for data from all the groups of electrodes. X-axis shows the groups of electrodes and Y-axis shows the classification accuracy in (%) and each group of vertical bars shows the number of 7 subjects for real exposure of colors. **(EER features, real exposure of colors)**

Table 10 shows classification results with an average accuracy of 72% for seven subjects among different groups of electrodes data used with linear kernel for the classification group (Blue, Green), **for imagination of colors, (EER features)**

	S1	S2	S3	S4	S5	S6	S7
P3	85.223	70.408	71.94	90.844	87.63	56.916	77.815
P4	75.963	70.408	65.044	89.059	84.297	58.701	83.371
O1	75.963	68.556	70.216	62.273	79.297	58.701	83.371
O2	75.963	72.26	70.216	47.987	79.297	58.701	88.926
P3P4	81.519	68.556	66.768	64.059	74.297	60.487	81.519
O1O2	74.111	75.963	71.94	71.201	79.297	69.416	79.667
P4O2	53.741	70.408	68.492	76.559	87.63	56.916	81.519
P3O1	79.667	68.556	73.664	80.13	87.63	58.701	75.963
All	68.556	51.889	63.32	64.059	65.963	51.559	57.445

Table 11 shows classification results with an average accuracy of 70% for seven subjects among different groups of electrodes data used with linear kernel for the classification group (Red, Green), **for imagination of colors, (EER features)**

	S1	S2	S3	S4	S5	S6	S7
P3	81.849	69.883	75.719	84.031	82.96	63.65	76.293
P4	81.849	67.96	80.891	82.246	82.96	65.374	78.145
O1	83.701	71.806	49.857	55.46	77.96	58.477	81.849
O2	76.293	71.806	49.857	51.889	79.627	51.581	89.256
P3P4	76.293	66.037	65.374	66.174	74.627	55.029	78.145
O1O2	74.441	69.883	72.27	62.603	72.96	58.477	85.553
P4O2	68.886	66.037	73.994	84.031	79.627	67.098	76.293
P3O1	79.997	69.883	73.994	76.889	92.96	58.477	78.145
All	52.219	56.422	68.822	50.103	61.293	48.132	54.071

Table 12 shows classification results with an average accuracy of 73% for seven subjects among different groups of electrodes data used with linear kernel for the classification group (Red, Blue), **for imagination of colors. (EER features)**

	S1	S2	S3	S4	S5	S6	S7
P3	81.726	65.517	83.819	79.94	80.773	62.083	75.199
P4	78.154	69.363	82.095	79.94	75.773	63.869	78.647
O1	83.511	78.978	87.268	58.511	72.44	65.654	80.371
O2	79.94	67.44	87.268	58.511	72.44	51.369	85.543
P3P4	76.369	69.363	63.13	74.583	67.44	60.297	83.819
O1O2	76.369	73.209	90.716	65.654	69.107	60.297	82.095
P4O2	65.654	71.286	83.819	83.511	74.107	63.869	75.199
P3O1	83.511	73.209	85.543	83.511	77.44	67.44	75.199
All	63.869	59.748	63.13	65.654	57.44	47.797	63.13

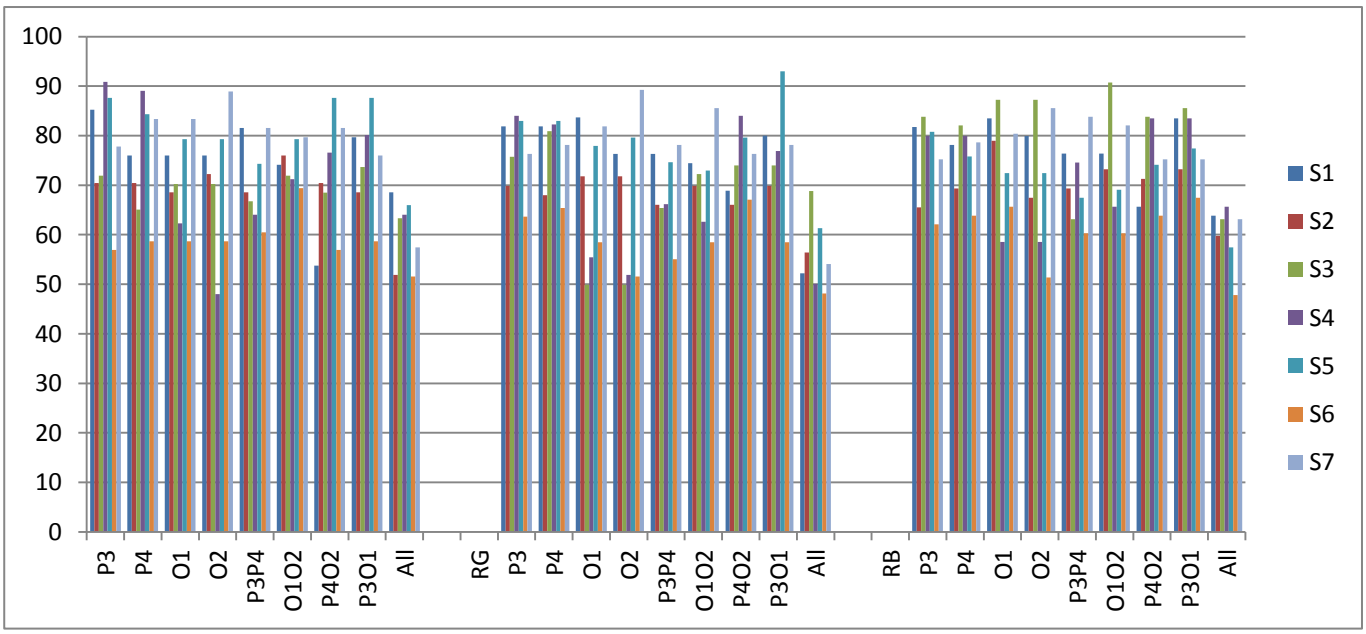

Figure 6.31 Classification accuracies altogether for the group (Blue, Green) on left, for the group (Red, Green) in center and for the group (Red, Blue) on right for data from all the groups of electrodes. X-axis shows the groups of electrodes and Y-axis shows the classification accuracy in (%) and each group of vertical bars shows the number of 7 subjects for imagination of colors. **(EER features, imagination of colors)**

For imagination of colors, we have again used only linear kernel SVM with EER features and achieved average accuracy of 72%, 70% and 73% for the classification groups (Blue, Green), (Red, Green) and (Red, Blue) respectivley, presented in tables 10, 11 and 12. Figure 6.31 summarized all the results for EER on a single plane for all the three groups of binary classification at all the electrode positions among all the subjects. The ERP data was taken from the same experiment as with ERSP features. It is clear that the accuracy achieved with EER features is good with an overall average of 72% but again there appears to be quite varying accuracy as compare to the previous accuracy results for real exposure of colors and imaginations of colors with ERSP features. Therefore ERSP features again seem to be more consistent in producing accuracy with less deviation among all the subjects at all the groups of data channels.

6.6.2 Extreme Energy Difference Criterion

In this criterion definitions for normalization of EEG sample, covariance, spatially filtered signal and signal energy will remain same as described in the previous section. The discriminative criterion EED, with feature extraction for binary classification, is defined as follows in equation (9) *for a single source*,

$$D(\phi) \triangleq \phi^T C_A \phi - \phi^T C_B \phi, \; s.t. \; \phi^T \phi = 1 \tag{9}$$

Where $D(\phi)$ indicates the energy disparity after spatial filtering for two classes A and B. To optimize $D(\phi)$, the method of Lagrange multipliers is used in conjunction with the constraint $\phi^T \phi = 1$, so the Lagrange function is defined as

$$L(\phi, \lambda) = D(\phi) - \lambda(\phi^T \phi - 1) \tag{10}$$

Where λ is a Lagrange multiplier. This optimization problem is transformed into following equations (11) and (12) by taking derivatives of equation (10) with respect to its inputs,

$$\frac{\partial L(\phi, \lambda)}{\partial \phi} = 2(C_A - C_B)\phi - 2\lambda\phi = 0 \tag{11}$$

$$\frac{\partial L(\phi, \lambda)}{\partial \lambda} = -(\phi^T \phi - 1) = 0 \tag{12}$$

From equation (11), we get

$$(C_A - C_B)\phi = \lambda\phi \tag{13}$$

Using equation (13), the EED criterion can be rewritten as

$$D(\phi) = \lambda \phi^T \phi = \lambda \tag{14}$$

Now to optimize $D(\phi)$, two spatial filters $\phi^*_{\max}$ and $\phi^*_{\min}$ are required in order to have the following conclusions,

$$D(\phi^*_{\max}) = \lambda_{\max} \quad (15)$$

$$D(\phi^*_{\min}) = \lambda_{\min} \quad (16)$$

where $\lambda_{\min} = \lambda_1 \leq \lambda_2 \leq \cdots \leq \lambda_{N-1} \leq \lambda_N = \lambda_{\max}$ are eigenvalues of matrix $C_A - C_B$ according to equation (13) and $\phi^*_{\max}$ and $\phi^*_{\min}$ are the corresponding eigenvectors or spatial filters. So the energy feature for a new EEG sample will be a vector consisting of two entries which are respectively the energy values of the sample spatially filtered by $\phi^*_{\max}$ and $\phi^*_{\min}$. For EED criterions of multiple sources please refer to (15). Until now we have presented theoretical aspects of EED and now we present here its classification results for real exposure of colors along with their corresponding imaginations of colors. In EED features the procedure remains almost same, the only difference for computing EED features is to compute the difference of covariance matrices as $C_G - C_B$ and then continue to construct the feature matrix the same way we have done with EER. The tool used for this job in addition to LIBSVM was MatLab's Bioinformatics Toolbox which provides 'smvtrain' and 'svmclassify' functions to facilitate the computations. The classification results for real exposure of colors are presented in tables 13, 14 and 15 for all the three groups of classification (Blue, Green), (Red, Green) and (Red, Blue) respectively with in average accuracy of 82%, 83% and 84% which I believe is more than a good accuracy. Moreover, the results for imagination of colors are presented in tables 16, 17 and 18, also figure 6.33 summarized all the results on a single plane.

EED in comparison with EER has proved to be relatively better features in case of real exposure of colors, e.g. taking into account figures 6.32 and 6.30 and having visual inspection and counting it is clearly visible that majority of subjects having accuracy above 80% are seen in EED features while considering all the three groups of classification and all the groups of data channels. Another observation is seen in EER that none of the subjects have achieved 80% of accuracy among 'All' group of data channels whereas in EED several subjects achieved 80% of accuracy. Moreover, the average accuracies for (EER, EED) pair are found as (79%, 82%) for (Blue, Green) group, (78%, 83%) for (Red, Green) group and (80%, 84%) for (Red, Blue) classification group, respectively which proved EED to be relatively better than EER. A similar performance of EED is also visible in case of imagination of colors where EED has again appeared to be better than EER however, the overall average accuracies in imagination of colors appear to be less accurate as compare to real exposure of colors, likewise it appeared in ERSP features.

Table 13 shows classification results with an average accuracy of 82% for seven subjects among different groups of electrodes data used with linear kernel for the classification group (Blue, Green**), for real exposure of colors (EED features)**

	S1	S2	S3	S4	S5	S6	S7
P3	94.444	77.778	79.31	94.643	95	55.357	87.037
P4	90.741	79.63	77.586	94.643	95	66.071	90.741
O1	83.333	79.63	46.552	66.071	86.667	64.286	88.889
O2	75.926	75.926	72.414	66.071	88.333	60.714	96.296
P3P4	92.593	75.926	72.414	92.857	93.333	67.857	94.444
O1O2	83.333	81.481	81.034	96.429	88.333	60.714	94.444
P4O2	81.481	75.926	74.138	91.071	93.333	69.643	92.593
P3O1	90.741	81.481	89.655	92.857	95	64.286	79.63
All	87.037	83.333	72.414	82.143	93.333	58.929	88.889

Table 14 shows classification results with an average accuracy of 83% for seven subjects among different groups of electrodes data used with linear kernel for the classification group (Red, Green), **for real exposure of colors (EED features)**

	S1	S2	S3	S4	S5	S6	S7
P3	92.593	80.769	84.483	85.714	90	65.517	87.037
P4	87.037	82.692	77.586	92.857	90	68.966	85.185
O1	83.333	80.769	68.966	64.286	81.667	65.517	92.593
O2	77.778	71.154	70.69	67.857	85	55.172	92.593
P3P4	90.741	80.769	84.483	89.286	90	70.69	90.741
O1O2	81.481	78.846	98.276	92.857	88.333	68.966	96.296
P4O2	81.481	78.846	84.483	92.857	93.333	75.862	90.741
P3O1	87.037	80.769	89.655	89.286	93.333	70.69	83.333
All	96.296	75	82.759	83.929	91.667	68.966	87.037

Table 15 shows classification results with an average accuracy of 84% for seven subjects among different groups of electrodes data used with linear kernel for the classification group (Red, Blue), **for real exposure of colors (EED features)**

	S1	S2	S3	S4	S5	S6	S7
P3	94.643	75	86.207	87.5	86.667	64.286	86.207
P4	89.286	80.769	86.207	87.5	90	75	86.207
O1	85.714	82.692	93.103	69.643	85	73.214	86.207
O2	87.5	78.846	96.552	58.929	78.333	64.286	93.103
P3P4	92.857	76.923	86.207	92.857	86.667	73.214	84.483
O1O2	92.857	86.538	100	80.357	85	71.429	96.552
P4O2	87.5	80.769	87.931	87.5	86.667	67.857	84.483
P3O1	92.857	75	98.276	91.071	86.667	73.214	84.483
All	92.857	78.846	91.379	73.214	86.667	69.643	86.207

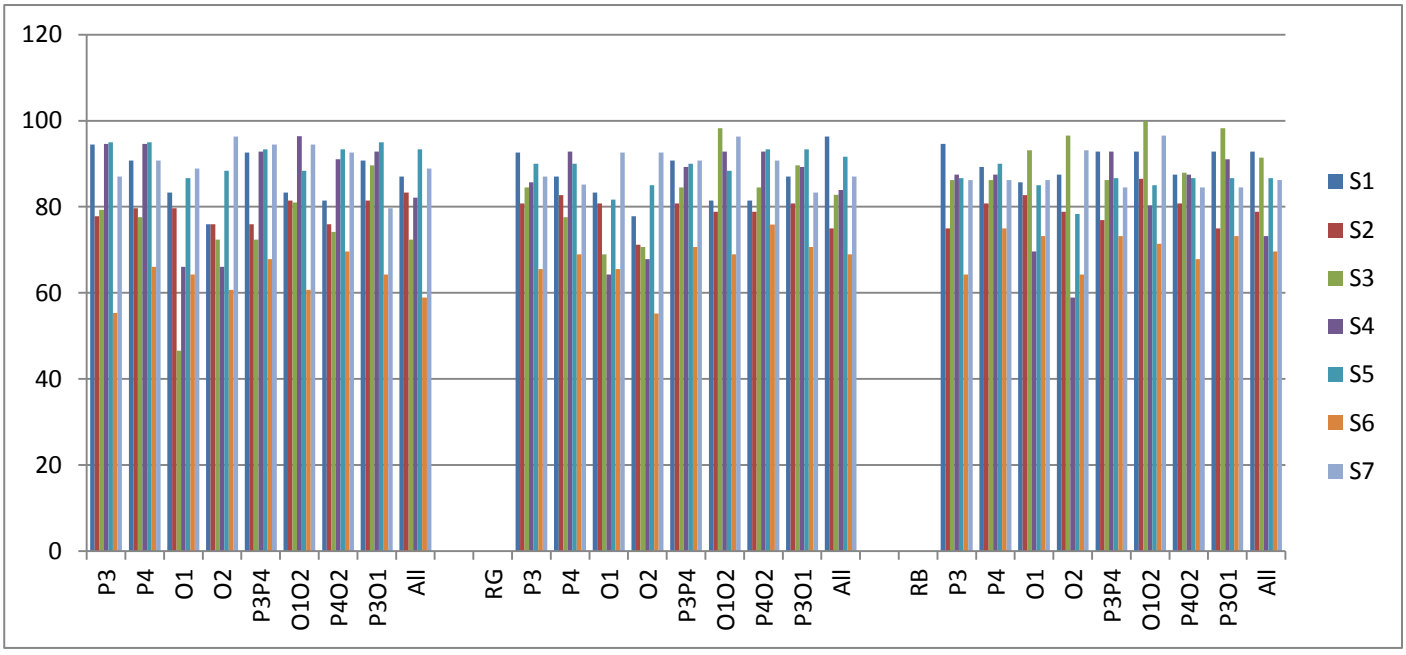

Figure 6.32 Classification accuracies altogether for the group (Blue, Green) on left, for the group (Red, Green) in center and for the group (Red, Blue) on right. for data from all the groups of electrodes. X-axis shows the groups of electrodes and Y-axis shows the classification accuracy in (%) and each group of vertical bars shows the number of 7 subjects for real exposure of colors. **(EED features, real exposure of colors)**

Table 16 shows classification results with an average accuracy of 73% for seven subjects among different groups of electrodes data used with linear kernel for the classification group (Blue, Green), **for imagination of colors, (EED features)**

	S1	S2	S3	S4	S5	S6	S7
P3	85.954	69.288	70.82	86.153	86.51	46.867	78.547
P4	82.251	71.14	69.096	86.153	86.51	57.581	82.251
O1	74.843	71.14	38.062	57.581	78.177	55.796	80.399
O2	67.436	67.436	63.924	57.581	79.843	52.224	87.806
P3P4	84.103	67.436	63.924	84.367	84.843	59.367	85.954
O1O2	74.843	72.991	72.544	87.939	79.843	52.224	85.954
P4O2	72.991	67.436	65.648	82.581	84.843	61.153	84.103
P3O1	82.251	72.991	81.165	84.367	86.51	55.796	71.14
All	78.547	74.843	63.924	73.653	84.843	50.439	80.399

Table 17 shows classification results with an average accuracy of 75% for seven subjects among different groups of electrodes data used with linear kernel for the classification group (Red, Green), **for imagination of colors, (EED features)**

	S1	S2	S3	S4	S5	S6	S7
P3	84.833	73.009	76.723	77.954	82.24	57.757	79.277
P4	79.277	74.932	69.826	85.097	82.24	61.206	77.425
O1	75.573	73.009	61.206	56.526	73.907	57.757	84.833
O2	70.018	63.394	62.93	60.097	77.24	47.412	84.833
P3P4	82.981	73.009	76.723	81.526	82.24	62.93	82.981
O1O2	73.721	71.086	90.516	85.097	80.573	61.206	88.536
P4O2	73.721	71.086	76.723	85.097	85.573	68.102	82.981
P3O1	79.277	73.009	81.895	81.526	85.573	62.93	75.573
All	88.536	67.24	74.999	76.169	83.907	61.206	79.277

Table 18 shows classification results with an average accuracy of 72% for seven subjects among different groups of electrodes data used with linear kernel for the classification group (Red, Blue), **for imagination of colors. (EED features)**

	S1	S2	S3	S4	S5	S6	S7
P3	82.973	63.33	74.537	75.83	74.997	52.616	74.537
P4	77.616	69.099	74.537	75.83	78.33	63.33	74.537
O1	74.044	71.022	81.433	57.973	73.33	61.544	74.537
O2	75.83	67.176	84.882	47.259	66.663	52.616	81.433
P3P4	81.187	65.253	74.537	81.187	74.997	61.544	72.813
O1O2	81.187	74.868	88.33	68.687	73.33	59.759	84.882
P4O2	75.83	69.099	76.261	75.83	74.997	56.187	72.813
P3O1	81.187	63.33	86.606	79.401	74.997	61.544	72.813
All	81.187	67.176	79.709	61.544	74.997	57.973	74.537

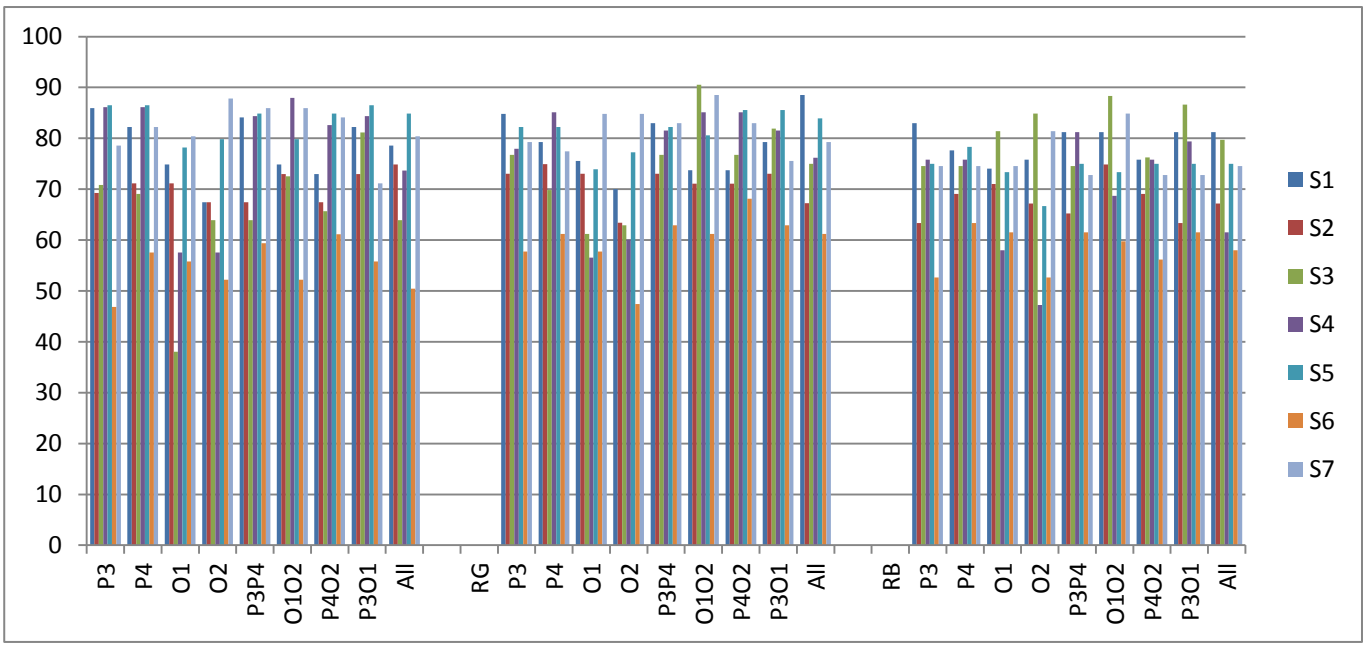

Figure 6.33 Classification accuracies altogether for the group (Blue, Green) on left, for the group (Red, Green) in center and for the group (Red, Blue) on right for data from all the groups of electrodes. X-axis shows the groups of electrodes and Y-axis shows the classification accuracy in (%) and each group of vertical bars shows the number of 7 subjects for imagination of colors. **(EED features, imagination of colors)**

Table 19, 20 and 21 present the averaged classification results of ERSP, EER and EED features for real exposure of colors and imaginations.

Table 19 classification results of ERSP

ERSP features	**Linear**	**Polynomial**	**RBF**
Real exposure	84	89	98
Imagination	64	70	76

Table 20 classification results of EER with only linear kernel

EER features	**BG**	**RG**	**RB**
Real exposure	79	78	80
Imagination	72	70	73

Table 21 classification results of EED with only linear kernel

EED features	**BG**	**RG**	**RB**
Real exposure	82	83	84
Imagination	73	75	72

Bibliography

1. **A. Yoto, T. Katsuura, K. Iwanaga, and Y. Shimomura,** 2007. *Effects of Object color stimuli on human brain activities in perception and attention referred to EEG alpha band response.* Physiological Anthropology, Vol. 26, pp. 373-379.

2. **Leeb, R., Keinrath, C., Friedman, D., Guger, C., Scherer, R., Neuper, C., Garau, M., Antley, A., Steed, A., Slater, M.** 2006 *Walking by thinking: The brainwaves are crucial, not the muscles!*, Presence, Vol. 15, pp. 500-514.

3. **Dobelle, W. H.** 2000 *Artificial vision for the blind by connecting a television Camera to the visual cortex.*, Journal of ASAIO, Vol. 46, pp. 3-9.

4. **Schalk, G., McFarland, D.J., Hinterberger, T., Birbaumer, N., & Wolpaw, J.R.** 2004 *BCI2000: A General-Purpose Brain-Computer Interface (BCI) System.*, IEEE Trans. on Biomedical Eng., Vol. 51, pp. 1034-1043.

5. **Delorme, A. and Makeig, S.** 2004 *EEGLAB: an open source toolbox for analysis of single-trial EEG dynamics including independent component analysis.*, J. of Neuroscience Methods, Vol. 134, pp. 9-21.

6. **J. Townsend, E. Courchesne, and T.J. Sejnowski,.** 2000 *Removal of eye activity artifacts from visual event-related potentials in normal and clinical subjects.* **,** , Clinical Neurophysiology, Vol. 111, pp. 1745-1758.

7. **S. Makeig, M. Westerfield, T.P. Jung, S. Enghoff, J. Townsend, E. Courchesne, and T.J. Sejnowski,.** 2002 *Dynamic Brain Sources of Visual Evoked Responses.* New York, N.Y. , ScienceMag, Vol. 295, pp. 690-694.

8. **Makeig, S.** 1993 *Auditory event-related dynamics of the EEG spectrum and effects of exposure to tones.*, Electroencephalography and Clinical Neurophysiology, Vol. 86, pp. 283-293.

9. **Makeig, S., Debener, S., Onton, J., and Delorme, A.** 2004 *Mining event-related brain dynamics.*, Trends in Cognitive Sciences., Vol. 8, pp. 204-210.

10. **Huang, R., Jung, T., and Makeig, S. 2005** *Analyzing event-related brain dynamics in continuous compensatory tracking tasks.* Shanghai, IEEE-EMBS 27th Annual Int. Conf. on Engineering in Medicine and Biology. pp. 5750-5753.

11. **Tallon-Baudry, C., Bertrand, O., Delpuech, C., Pernier, J.** 1996 *Stimulus specificity of phase-loacked and non-phase locked 40 Hz visual responses in human*, Journal of Neuroscience, Vol. 16, pp. 4240-9.

12. **Chang, C., and Lin, C.** 2010 *LIBSVM: a library for support vector machines.* National Taiwan University, Taiwan.

13. **Hsu, C., Chang, C., and Lin, C.** 2003 *A practical guide to support vector classification.* National Taiwan University. Taiwan.

14. **Shiliang, S.** 2008 *The Extreme nergy Ratio Criterion for EEG Feature Extraction.* SpringerLink, Lecture Notes in Computer Science, Vol. 5164, pp. 919-928.

15. **Shiliang, S.** 2010 *Extreme energy difference for feature extraction of EEG signals.* Elsevier, Expert Systems with Applications, Vol. 37, pp. 4350-4357.

16. **Searle, S. R.** 1982 *Matrix Algebra Useful for Statistics.* New York : John Wiley & Sons.

7. Experimental Design with Multiple Shapes

7.1 Introduction

In our earlier experiment the colors were exposed in a single shape i.e. square and in this chapter we have discussed about another experiment performed with multiple shapes i.e. Square, Circle and Triangle. The colors presented were again the Red, Green and Blue so we have the same colors but with different shapes. In this new experiment we have made the changes as follows. 1) Imagination part is removed and all the concentration is devoted to the real exposure of colors. 2) We have again used the four electrodes but this time electrode were placed on TP7 and TP8 instead of using P3 and P4, however the electrodes at the occipital region remained same like earlier experiment i.e. O1 and O2. 3) We have reduced the stimulus time from three seconds to one second after the onset of stimulus because of three reasons. Firstly, Most of the meaningful information lies in the first second after the onset of stimulus that could give us most relevant features for classification. Secondly, to reduce the computational time i.e. lesser the number of features, lesser will be the time. Thirdly, to reduce the experimental time in order to keep the subjects feeling comfortable during the experiment. 4) The experiment was performed on 5 subjects. Rest of all the parameters, experimental setup and environment remained same as already discussed in section 6.2 in the previous chapter.

In the previous experiment we had only three conditions to analyze and classify our data i.e. (Red Square, Green Square and Blue Square) but in this experiment we have nine different conditions to analyze and classify our data i.e.

(Red Square, Green Square and Blue Square)

(Red Circle, Green Circle and Blue Circle)

(Red Square, Green Square and Blue Square)

This means we have RGB colors within each shape and different shapes within each color. Therefore, we have the following study regarding all the nine conditions. 1) ERP waveforms. 2) ERSP information 3) Classification of RGB colors within each shape i.e. within Square we have three different classes of RGB colors, similarly, for circle and triangle which creates three classification problem and each problem will have three classes. 4) Classification of RGB colors after combining data of similar colors from all different shapes i.e. Red square, Red circle and Red triangle's data will be combined together to produce data of Red class. Similarly, the data will be produced for Green and Blue classes, so finally we will have three classes. 5)

Classification of different shapes after combining data of RGB colors within a shape in order to produce data of three different classes i.e. Square, Circle and Triangle. 6) Classification of all the nine different conditions at once.

7.2 Experimental Protocol

In this section, we shall discuss our experimental protocol following which the colors were exposed to the subjects. After the subject is prepared with all the electrodes montage and gets ready, the experiment runs in the following sequence of events as shown in figure 7.1. This is a part of a sequence that is repeated several times in order to produce sufficient number of trials to have sufficient data for analysis and classification. Almost 72 trials are acquired for each color of all the shapes i.e. 72 trials for all the 9 conditions each. Almost 5 to 10% of trials are dropped due to rejected artifacts.

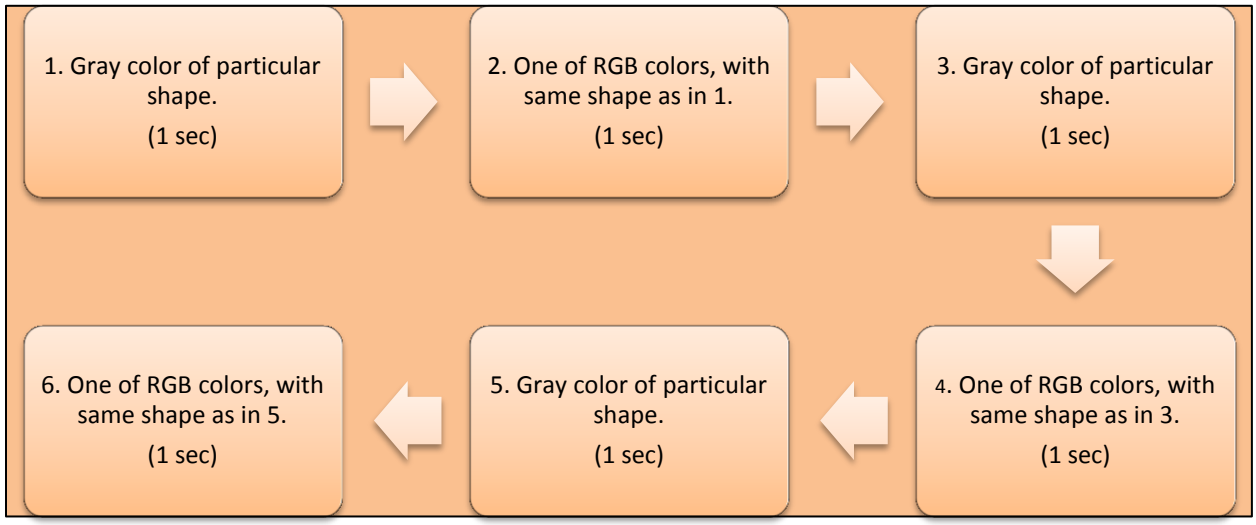

Figure 7.1 Experiment protocol for multiple shapes

In the figure 7.1, we can see six events of interest, three of which are the gray exposures and three are RGB colors. The experiment starts with eyes closing instruction and then the subject is prompted by voice to open the eyes after 7 seconds and then event 1 is occurred e.g. Gray square is exposed and then in event 2 any of RGB color is exposed in a square shape. Similarly, in event 3 again the gray color is exposed followed by one of RGB colors in event 4, keeping the shape same from event 3 to event 4. Events 5 and 6 occur in the same way. The shapes in event 1, 3 and 5 are adopted randomly and also the colors in events 2, 4 and 6 are exposed randomly. Subjects are also given rest for few seconds randomly after several repetitions of above sequence so the all the trials of particular conditions are not recorded continuously but with short breaks for the subjects to keep feeling comfortable and to adjust their positions while they are seated. After all the trials are recorded, epochs were extracted from continuous data for each colour and shape resulting 9 different epochs for each of the 9 different conditions. Each epoch is extracted in a way that it lasts for 1.5 seconds i.e. 0.5 second before the event occurred and one second afterwards.

7.3 Analysis of ERP and ERSP Results

7.3.1 ERP Waveforms

In this section we have presented ERP waveforms of RGB colors for all the conditions in figures 7.2, 7.3 and 7.4 for circle, square and triangle respectively. Like ERPs of previous experiment X-axis represents time in milliseconds (ms) and Y-axis represents potential values in microvolts (μV). Latencies and amplitudes of these peaks may vary among different scalp locations and different subjects. Here the ERPs are presented for all the electrode positions. These ERP waveforms start at -500 ms and ends at 1000 ms, we can clearly see the P300 component centered at 400 ms starting from 300 ms to 600 ms having higher amplitudes in blue colors as compare to red and green colors in all the shapes, however considering only the blue colors, blue circle has the higher amplitude as compare to blue square and triangle. Moreover a negative component is also visible around 200 ms which has deeper amplitude in all shapes of red color and square and triangle of green color as compare to circle in green color and all the shapes in blue color. All the ERP waveforms are quite varying depending on the color and shape among all the subjects. Change of stimulus occurs at zero second from gray (also known as baseline) to RGB colors and it is seen that starting potential of baseline at -500 ms remains mostly in between 1 to 2 microvolts and ending potential at 1000 ms remains mostly in between -1 to 0 microvolts. Highest potential of 5.8 microvolts is seen in blue circle at a latency of 406 ms and lowest potential of 3.4 microvolts is seen in Green Square at a latency of 375 ms. Usually data averaging collapses the dynamic information in the data so it might not be effective in the analysis.

In ERPs of circle among all the colors, since P300 wave drops down zero a bit earlier than 600 ms and then it remains negative until the end of waveform. This behavior is also seen in green triangle along with red circle and square however, couple of times positive peaks are seen in green circle and square after 800 ms along with red triangle at about 700 ms. Focusing our attention in between 0 to 200 ms after the onset of stimulus, fluctuation in potential is seen in all the conditions however, another small positive prominent peak is seen in red color of all shapes at latency of almost 150 ms also known as P100 wave which is not prominent in blue and green colors of all shapes. These variations in the waveforms reflect how the event-related synchronization and desynchronization occurs in response to visual stimulus. Please note that, the potential in the baseline fluctuates in between -1 and 1 microvolt in almost all the conditions after the epoch is started. The peaks and valleys in these ERP waveforms could serve as possible features for the classifier but may not provide satisfactory results because Makeig in (8) reported that according to several studies, event-related potentials (ERPs) are not capable of capturing maximum brain's response to events due to their instability and not being fully independent of EEG. This reason lacks our interest in analyzing ERP waveforms in more depth.

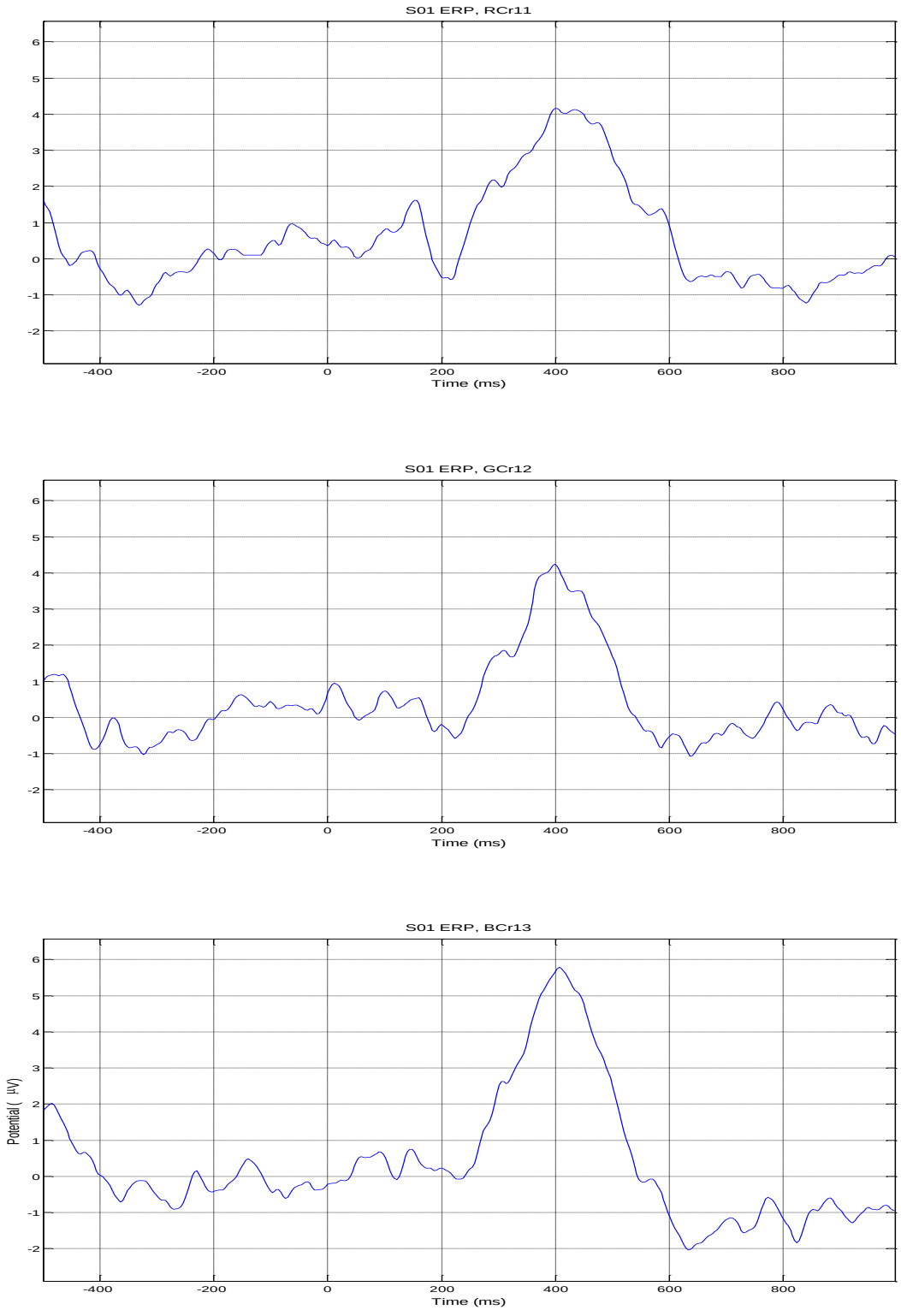

Figure 7.2 ERP waveforms: **Red** Circle (Top), **Green** Circle (Middle) and **Blue** Circle (Bottom). All channels averaged ERP over all the trials.

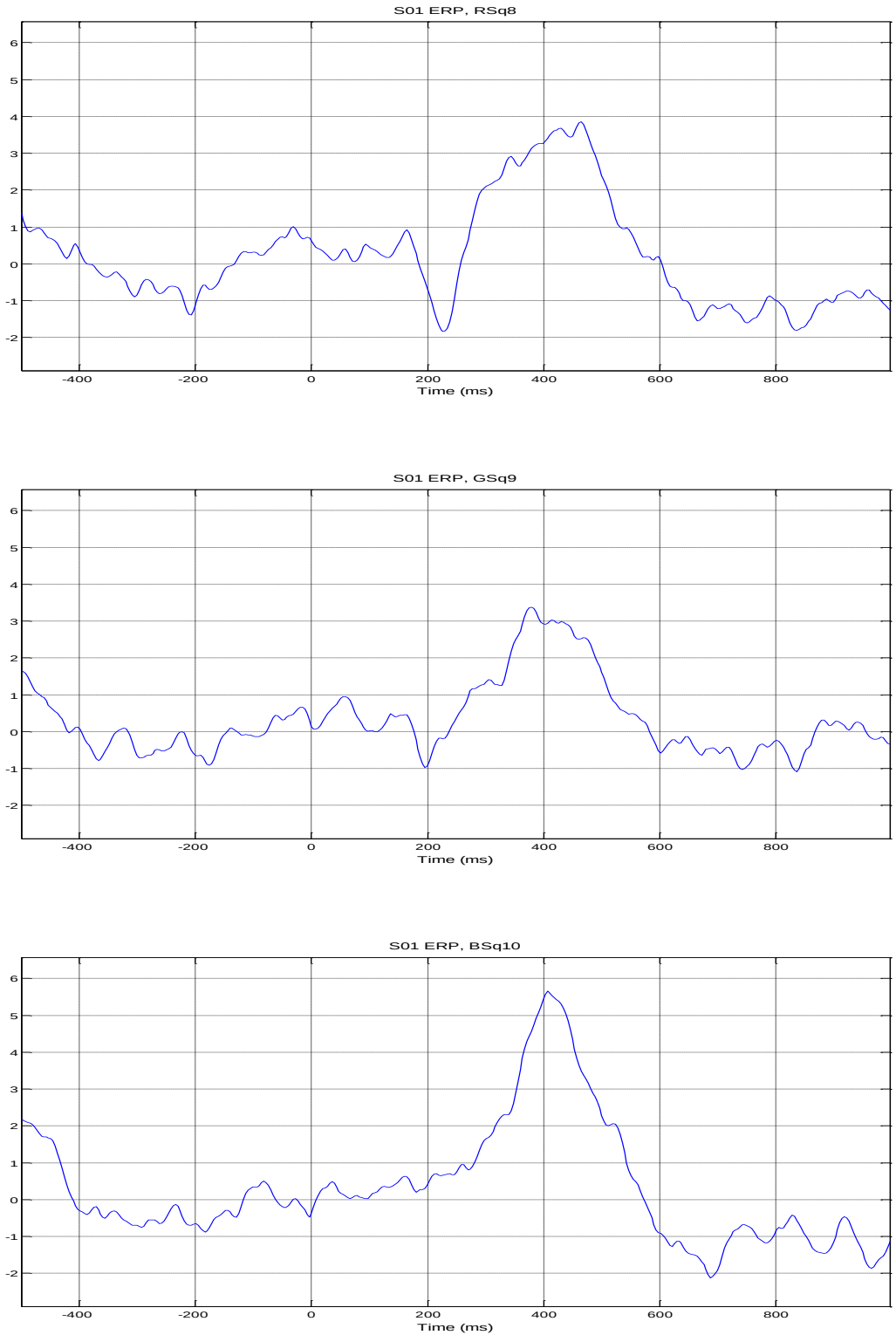

Figure 7.3 ERP waveforms: **Red** Square (Top), **Green** Square (Middle) and **Blue** Square (Bottom). All channels averaged ERP over all the trials.

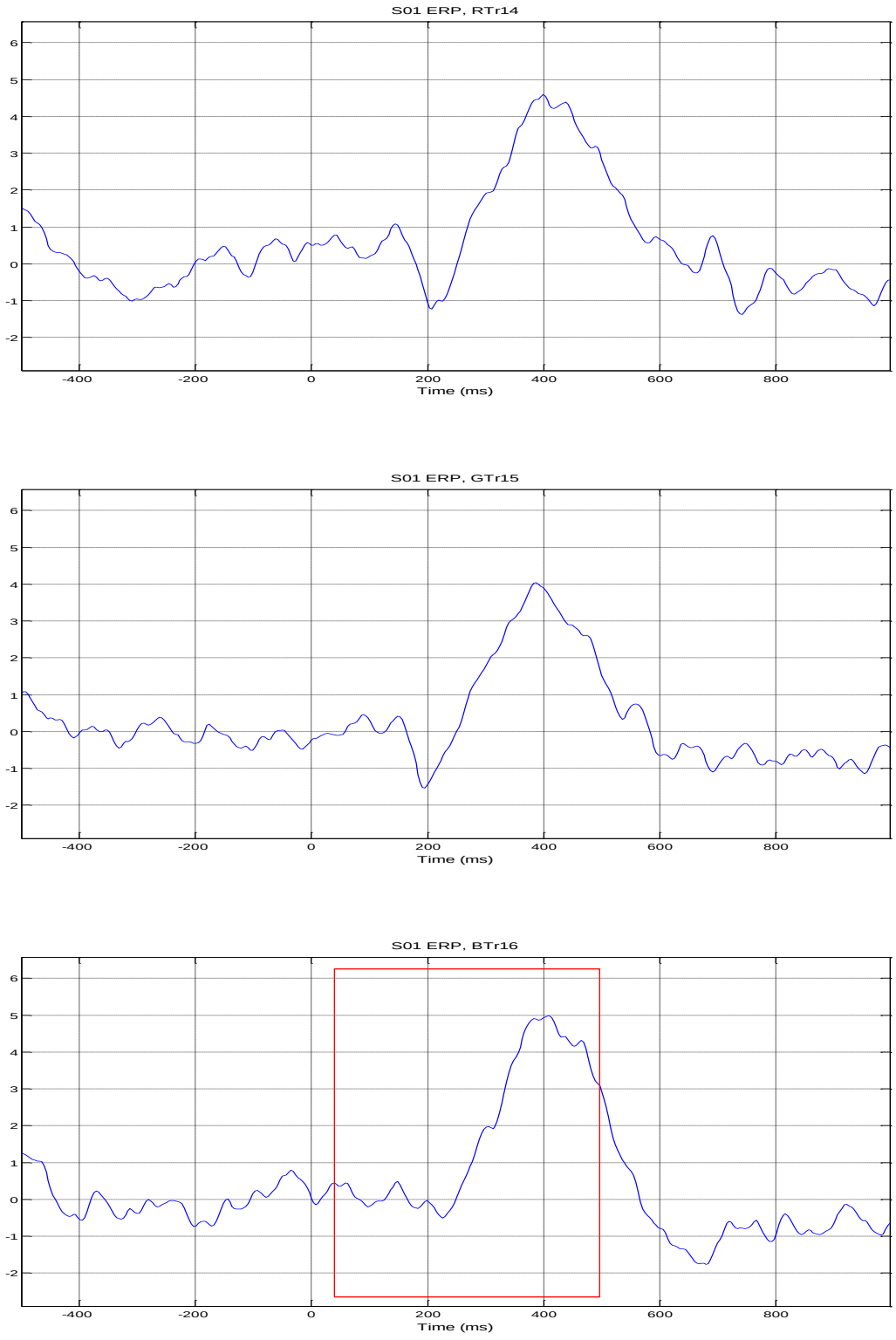

Figure 7.4 ERP waveforms: **Red** Triangle (Top), **Green** Triangle (Middle) and **Blue** Triangle (Bottom). All channels averaged ERP over all the trials.

7.3.2 Event-Related Spectral Perturbation

In this section, we have presented ERSP plots in which we are most interested because we have used ERSP features with SVM for classification likewise we used it in our earlier experiment in chapter 6. Figures 7.5, 7.6 and 7.7 reflect the ERSP plots of RGB colors for circle, square and triangle respectively. ERSP plots give us the distribution of power (dB) in time-frequency frame which means it defines the patterns of event related synchronization and de-synchronization. As we can see in figure 7.4 (ERP wave bottom plot), a window starting from 50 ms to 450 ms includes the most influential part of ERP waveforms in all the colors of all the shapes, therefore we decided to reduce the timing to compute ERSP in order to save the computational time and also because SVM classifier needs these features for classification so feeding the classifier with less number of features again reduced the computational time while keeping the classification accuracy at very good rate which we will discuss in the next section. This will also help us in online classification because in the previous experiment we had computed ERSP features for -500 to 1500 ms which were obviously very large number of features so can't be sued for online classification, however the classification was very good in the earlier experiment. Whereas the frequency axis kept the same range of frequency bands i.e. from 1 Hz to 30Hz Please also note that online classification is not a part of this thesis, which would be done later.

An ERSP is produced by taking average of normalized response for many trials. For n trials, if $F_k(f,t)$ is the spectral estimate of trial k at frequency f and time t, then ERSP is computed using following formula,

$$ERSP(f,t) = \frac{1}{n}\sum_{k=1}^{n}\left|F_k(f,t)\right|^2$$

Here $F_k(f,t)$ is computed using sinusoidal wavelet transform in which the number of cycles is increased slowly with frequency and provides better frequency resolution at higher frequencies than a conventional wavelet approach that uses constant cycle length.

Let us now examine the ERSP plots in order to analyze the distribution of power in the specified time and frequency range. First of all examine the ERSP responses of RGB colors for circle given in figure 7.5. Red circle shows a slight decrease in power or de-synchronization in the beginning of epoch until almost 200 ms in the delta band (1 – 4 Hz) and in green circle this desynchronization is more visible in the same frequency band as in red circle whereas blue circle has the greater desynchronization from 50 to 200 ms of interval and also includes theta band (4 – 8 Hz) along with delta band as compare to red and green circle. An event-related synchronization is seen in the alpha band (8 – 12 Hz) within the same time span. This synchronization is most significant in red circle, then in green circle and the lowest in blue circle. On the other hand, focusing our attention on opposite side of ERSP responses i.e. from

300 to 450 ms, blue circle reflects an event-related synchronized activity not only in delta band but also in alpha band however red and green circles show an event-related desynchronized activity in alpha band with greater decrease in red circle than in green circle. This desynchronization appears to be insignificant in delta and theta bands of red and green circle. Moreover, a slight synchronization is seen in beta band of red circle and delta band of green circle within 300 to 450 ms. Please note that the time from 200 to 300 ms is a transition time in all the frequency bands i.e. either transitioning from synchronization to desynchronization or vice versa. Secondly, we examine the ERSP responses of RGB colors for square given in figure 7.6. In these ERSP responses, a similar activity is seen as in figure 7.5, related to desynchronization within 50 to 200 ms in the delta band. In squares, this decrease in power is greater in red square as compare to green and blue squares and lower in green square as compare to red and blue squares which keeps the blue square activity in the middle of red and green's activity of desynchronization. Similarly within the same time range of 50 to 200 ms, a significant event-related synchronization is seen in alpha band and relatively slighter synchronization in beta band (13 – 30 Hz). This synchronization is also seen in alpha band in green and blue squares. On the other hand, within 300 to 450 ms an increase in power is seen in delta band of red and blue squares and relatively lesser increase in power is seen not only in delta but also in theta band of green square. Again a slight decrease in power is seen in alpha and theta bands of all the colors in squares with in the time range of 300 to 450 ms. Likewise in circle, again the time range from 200 to 300 ms works as transition time. Thirdly, taking into account the ERSP responses of RGB colors of triangle as shown in figure 7.7 we can clearly see activities of synchronization in alpha band of red and green triangles and also in beta band of blue triangle within 50 to 200 ms of time along with synchronization in delta bands of red, green and blue triangles within time range of 300 to 450 ms. Moreover, a significant decrease in power is seen in delta and theta bands of all the colors of triangle within 50 to 200 ms along with alpha band of all the colors of triangle within 300 to 450 ms. Again the time range from 200 to 300 ms is transition range.

ERSP responses are again found to be differentiated responses as we found them in the previous experiment, not only within a shape but also across the different shapes. Therefore, it could be very effective for classification tasks because the spread of power increase and decrease is highly differentiated which makes them distinctive features to let them successfully work with SVM classifier. Figures, from 7.5 to 7.7 represent the averaged ERSP responses for channel TP7 and discussed earlier. Since it would be very lengthier to present and discuss in detail, the ERSP responses of all the four channels, therefore we restrict ourselves to only present the ERSP responses of another channel and leave the detailed discussion on discretion of reader because it would be similar to interpret these responses the same way we have done earlier. So now we present the ERSP responses for channel O2 in figures 7.8, 7.9 and 7.10.

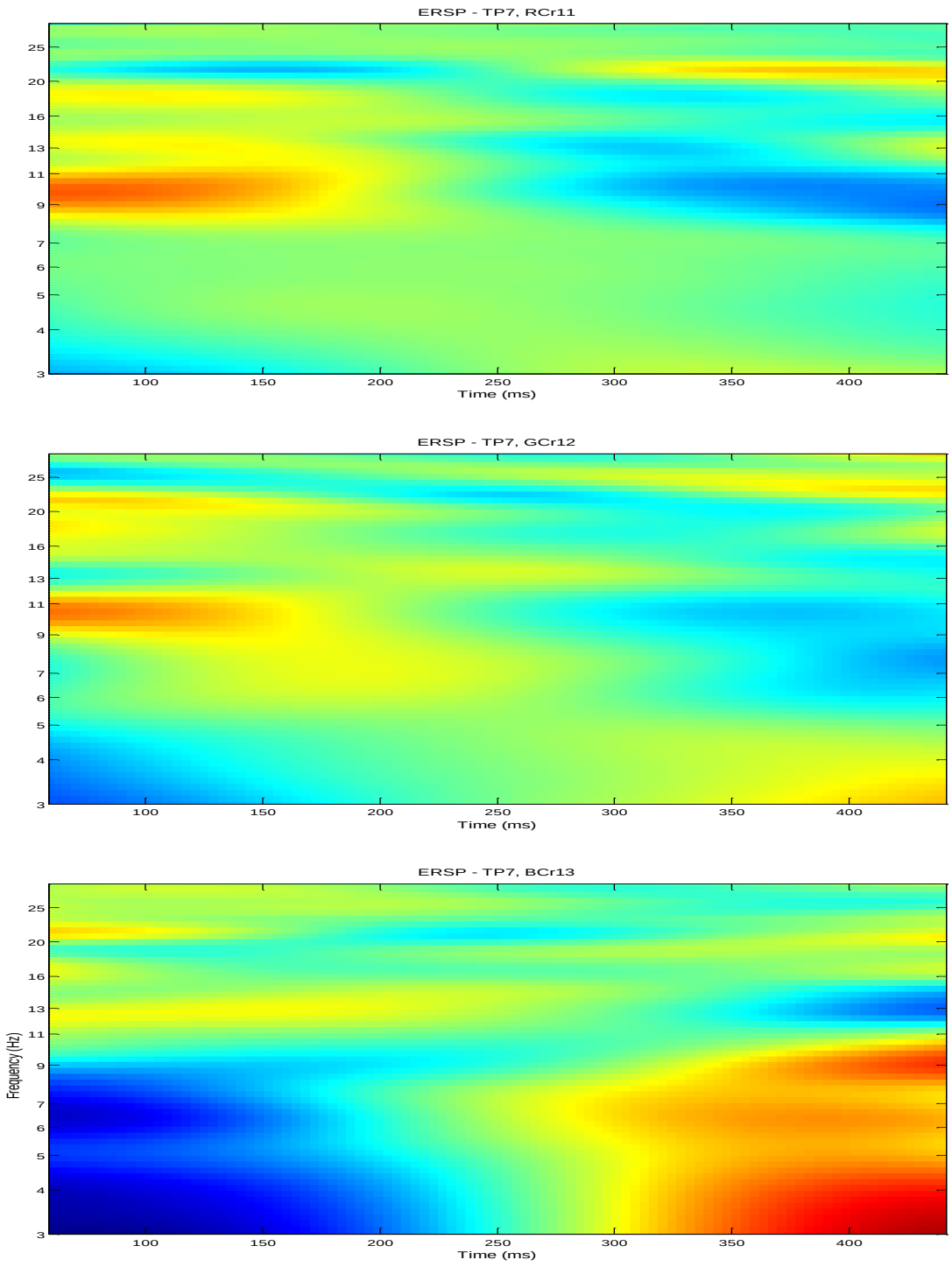

Figure 7.5 ERSP: **Red** Circle (Top), **Green** Circle (Middle) and **Blue** Circle (Bottom). Channel TP7, averaged over all trials and all subjects. X-axis represents time (ms) and Y-axis represents frequency (Hz).

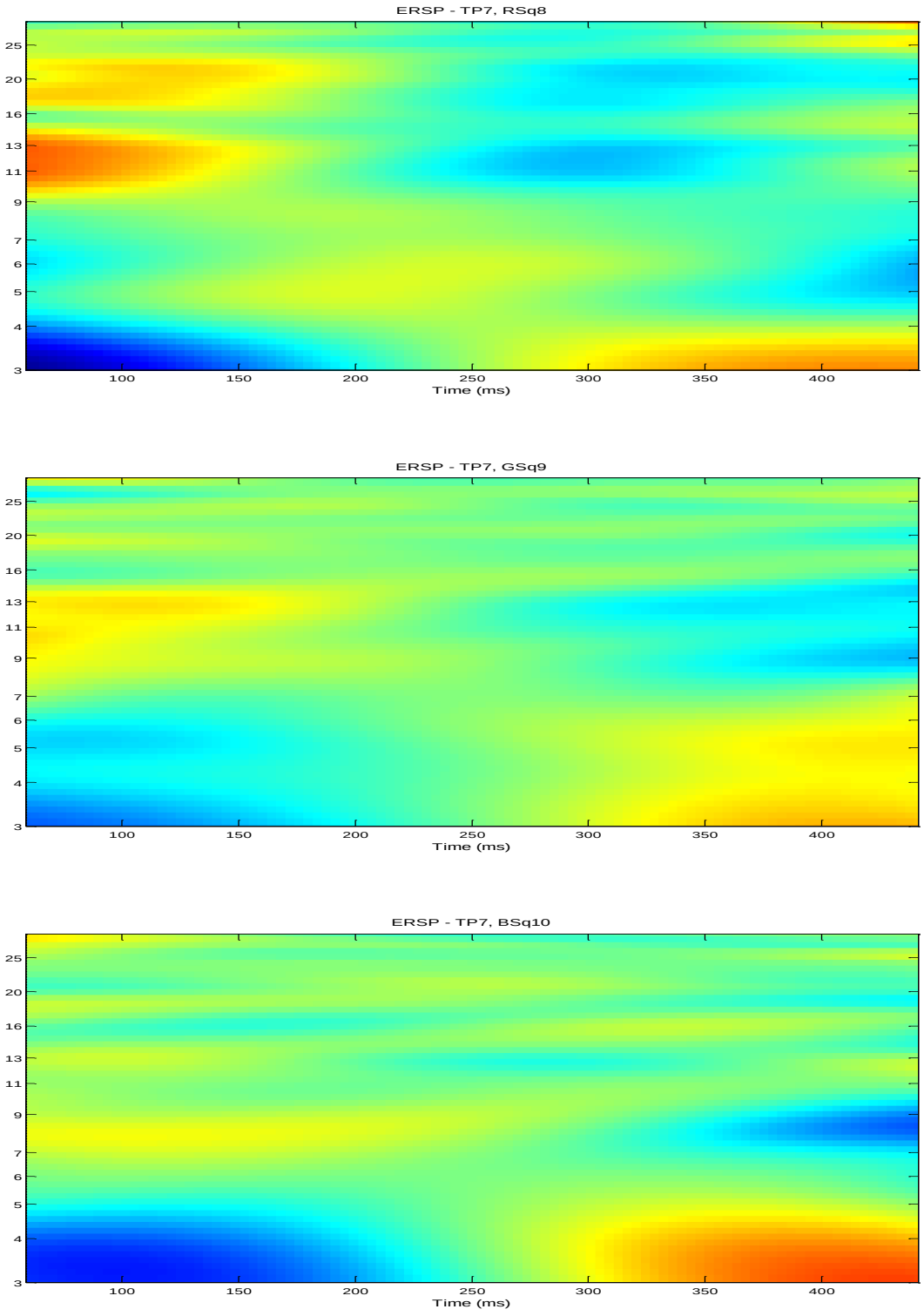

Figure 7.6 ERSP: **Red** Square (Top), **Green** Square (Middle) and **Blue** Square (Bottom). Channel TP7, averaged over all trials and all subjects. X-axis represents time (ms) and Y-axis represents frequency (Hz).

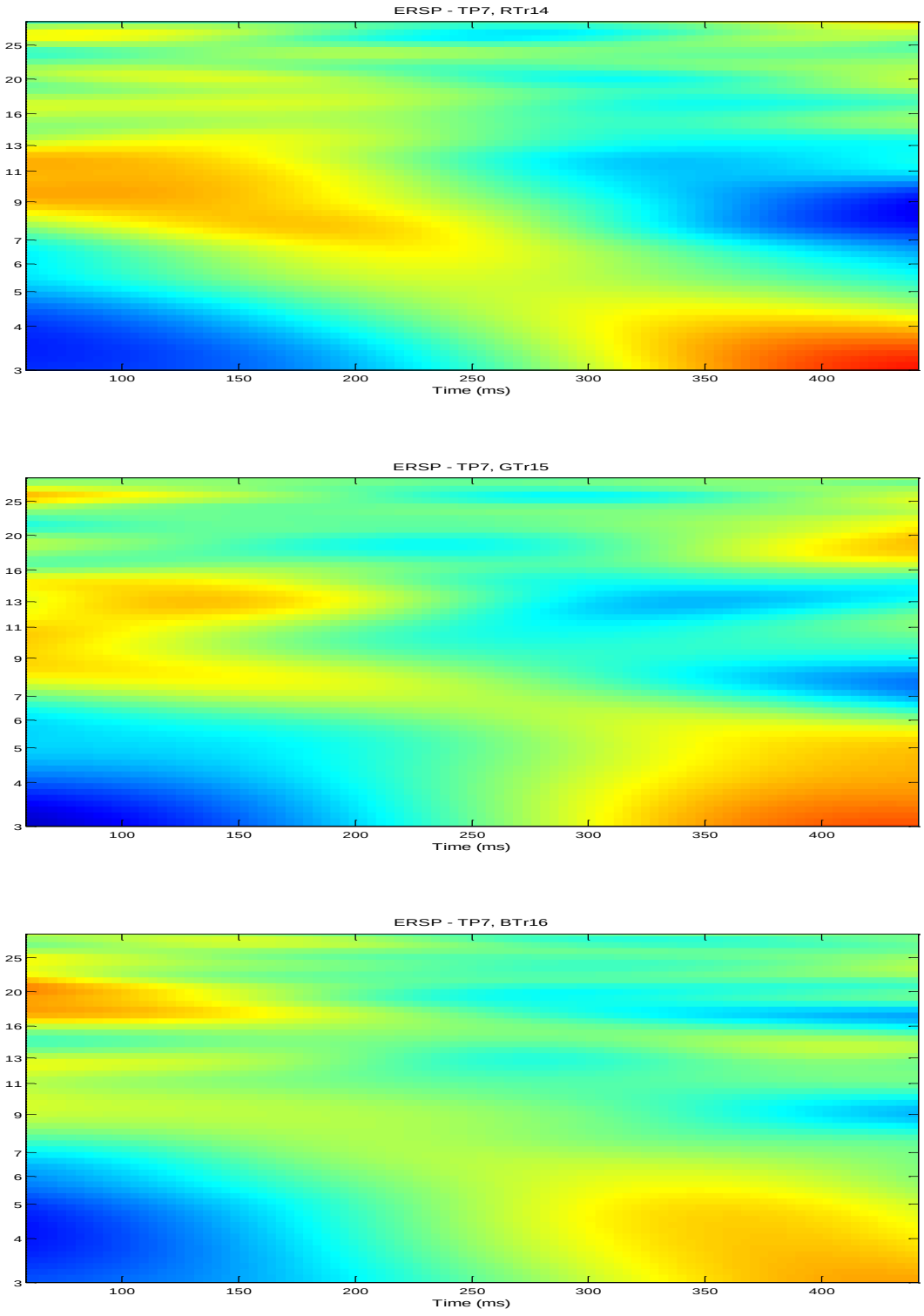

Figure 7.7 ERSP: **Red** Triangle (Top), **Green** Triangle (Middle) and **Blue** Triangle (Bottom). Channel TP7, averaged over all trials and all subjects. X-axis represents time (ms) and Y-axis represents frequency (Hz).

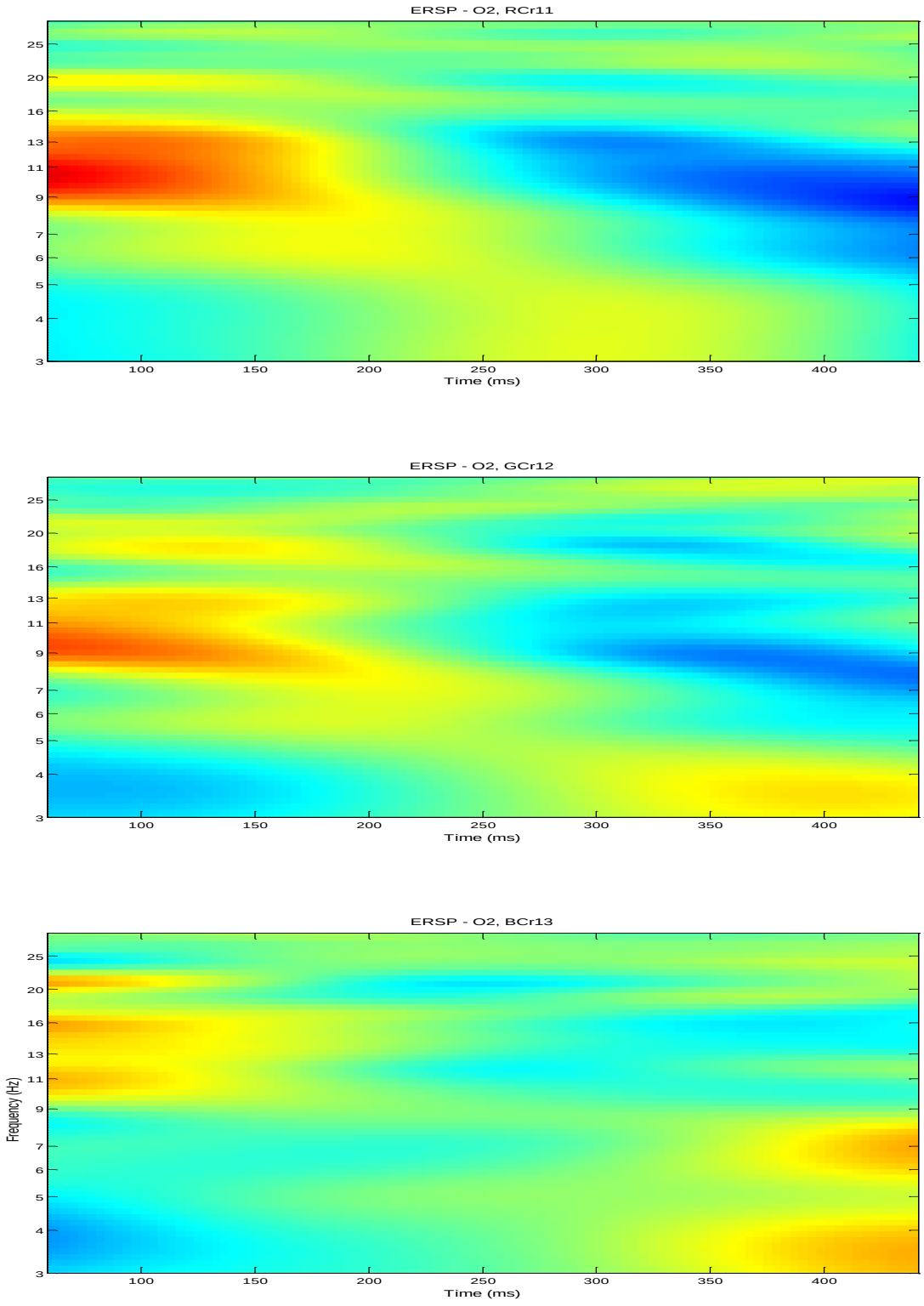

Figure 7.8 ERSP: **Red** Circle (Top), **Green** Circle (Middle) and **Blue** Circle (Bottom). Channel O2, averaged over all trials and all subjects. X-axis represents time (ms) and Y-axis represents frequency (Hz).

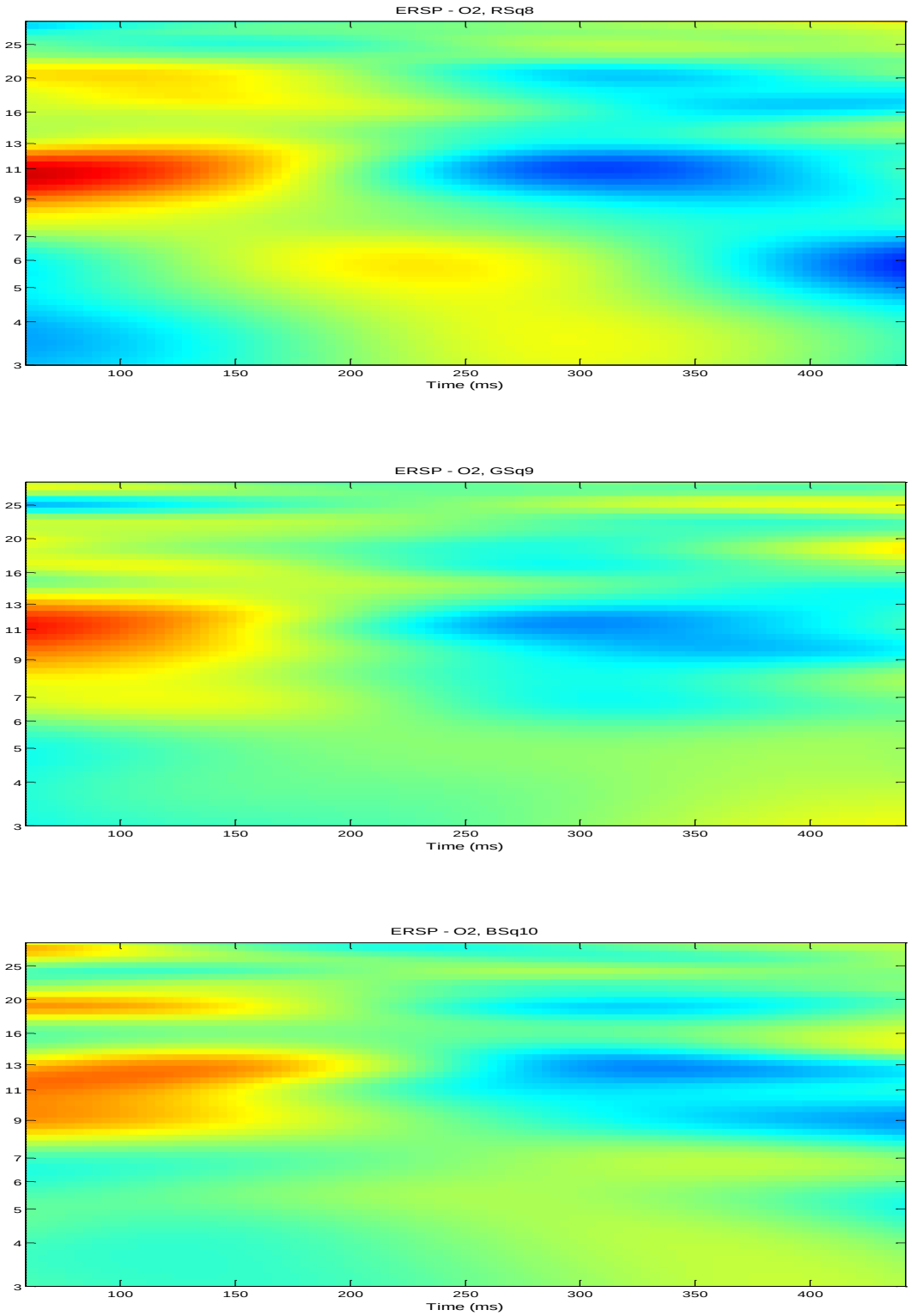

Figure 7.9 ERSP: **Red** Square (Top), **Green** Square (Middle) and **Blue** Square (Bottom). Channel O2, averaged over all trials and all subjects. X-axis represents time (ms) and Y-axis represents frequency (Hz).

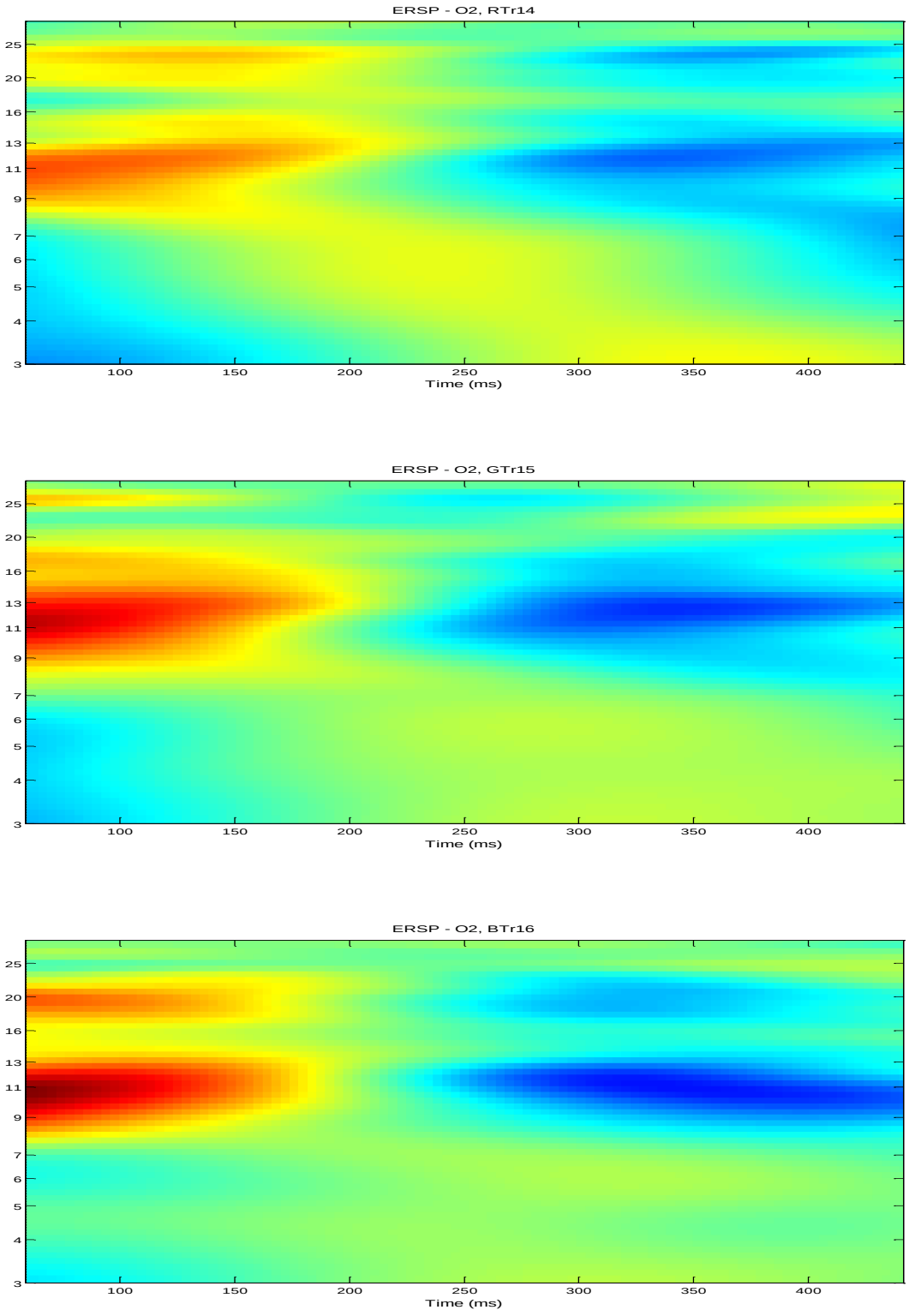

Figure 7.10 ERSP: **Red** Triangle (Top), **Green** Triangle (Middle) and **Blue** Triangle (Bottom). Channel O2, averaged over all trials and all subjects. X-axis represents time (ms) and Y-axis represents frequency (Hz).

7.4 Classification Results using SVM with ERSP features

We have created different groups of classification problems from the data we have recorded from the following nine different conditions as follows:

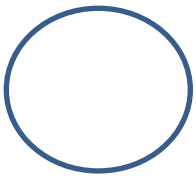

Red Circle (RCr)

Green Circle (GCr)

Blue Circle (BCr)

Red Square (RSq)

Green Square (GSq)

Blue Square (BSq)

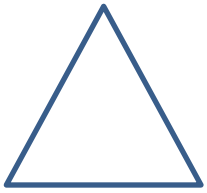

Red Triangle (RTr)

Green Triangle (GTr)

Blue Triangle (BTr)

Group 1: Classification of colors within shapes

Group 2: Classification of colors across shapes

Group 3: Classification of shapes

Group 4: Classification of all conditions simultaneously

7.4.1 Classification of RGB colors within shapes: Group 1

In this group we have classified RGB colors within shapes by treating each condition a separate class so we have three classification problems, one for circle, one for square and one for triangle. Each problem is a three class problem, for example, within Circle we have data for three different classes of RGB colors i.e. RCr, GCr and BCr, similarly for Square (RSq, GSq and BSq) and Triangle (RTr, GTr, BTr). All the three problems work similar to earlier classification problem whose results are presented in tables 1, 2 and 3 in chapter 6, specially the classification of square because the shape of object in each classification problem do not change. However, it is seen that the accuracy for the three classification problems is reduced due to the involvement of multiple shapes at the time of exposure of colors. Here we again

used three kernels i.e. linear, polynomial and RBF kernel. In all the three classification problems linear and RBF kernels worked very well but the performance with polynomial kernel is dramatically reduced. The average accuracy with linear kernel for Circle, Square and Triangle is 88%, 84%, 84% and with RBF kernel is 94%, 89%, 94% respectively whereas the average accuracy with polynomial kernel is 52%, 47% and 49% respectively. The results for all the three classification problems are given in tables from 7.1 to 7.9. We can see that the highest accuracy is always achieved with RBF kernel and lowest with polynomial kernel.

Table 7.1 presents the classification accuracies with an average accuracy of 88% for five subjects among different groups of data which were used with linear kernel. **(Circle)**

	S1	S2	S3	S4	S5
TP7	100	100	100	100	100
TP8	100	100	100	96.2406	100
O1	94.73684	97.74436	100	90.22556	96.2406
O2	92.4812	93.23308	90.97744	96.2406	93.98496
TP7TP8	92.13483	95.50562	97.37828	94.38202	93.63296
O1O2	77.90262	76.40449	74.90637	79.40075	79.77528
TP8O2	83.89513	83.89513	88.01498	89.13858	92.8839
TP7O1	77.15356	74.1573	77.52809	71.91011	71.91011
All	75.46816	69.28839	63.67041	71.91011	71.34831

Figures 7.11, 7.12 and 7.13 show the classification results with linear (left), polynomial (middle) and RBF (right) for the three classification problems of Circle, Square and Triangle respectively. An important observation is seen in these figures that regardless of whatever the accuracy is, the consistency is found to be good in all the classification problems as there is only a minor varying accuracy or less deviation in all groups of data channels across all the subjects.

Table 7.2 presents classification accuracies with an average accuracy of 52% for five subjects among different groups of data which were used with polynomial kernel of degree 3, **(Circle)**

	S1	S2	S3	S4	S5
TP7	60.15038	58.64662	54.13534	58.64662	67.66917
TP8	57.14286	63.90977	53.38346	56.39098	52.63158
O1	43.60902	42.10526	43.60902	46.61654	49.62406
O2	42.85714	48.87218	48.87218	49.62406	45.86466
TP7TP8	53.55805	56.17978	54.68165	56.55431	59.92509
O1O2	46.81648	46.06742	48.68914	46.06742	50.18727
TP8O2	55.80524	56.55431	58.05243	55.05618	55.80524
TP7O1	50.5618	53.18352	50.5618	51.31086	49.06367
All	50.93633	51.68539	52.80899	48.50187	57.6779

Table 7.3 presents the classification accuracies with an average accuracy of 94% for five subjects among different groups of data which were used with RBF kernel. **(Circle)**

	S1	S2	S3	S4	S5
TP7	93.98496	93.98496	93.23308	98.49624	100
TP8	100	100	100	97.74436	100
O1	95.48872	84.96241	82.70677	90.97744	90.97744
O2	91.72932	100	100	100	100
TP7TP8	96.62921	96.25468	95.13109	91.38577	97.75281
O1O2	95.50562	94.00749	92.8839	89.88764	95.13109
TP8O2	91.7603	88.38951	89.88764	86.89139	86.51685
TP7O1	95.88015	97.00375	97.37828	97.37828	96.25468
All	85.20599	90.82397	91.7603	87.64045	86.89139

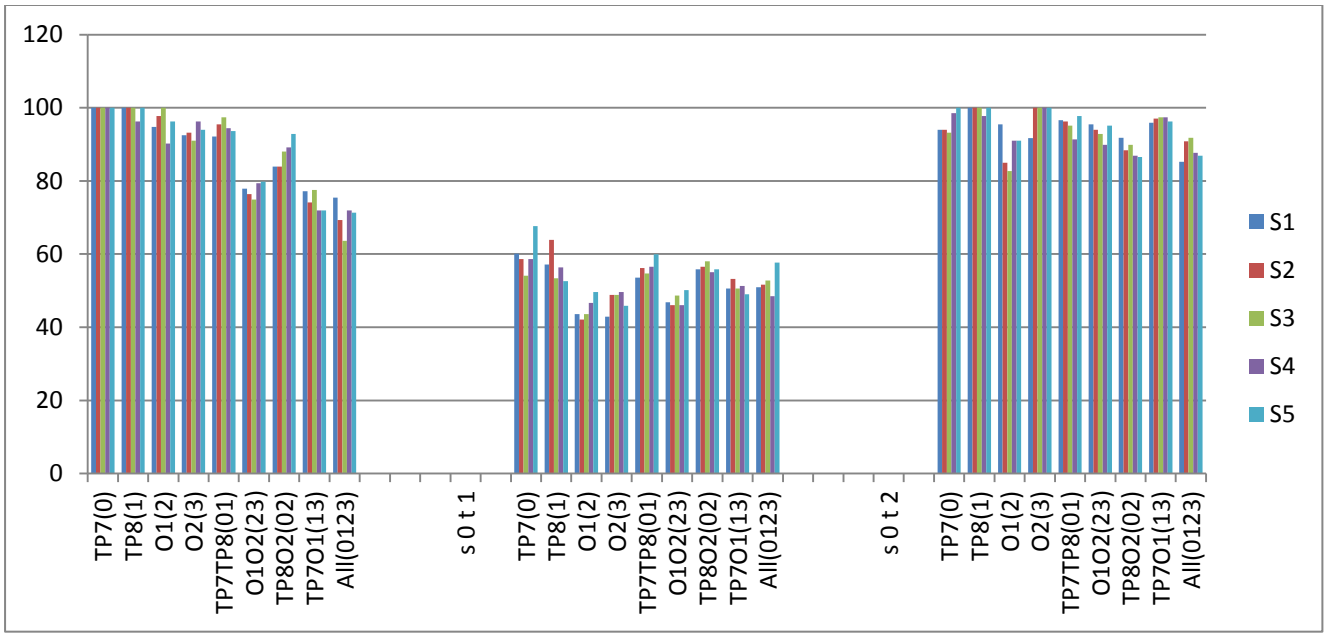

Figure 7.11 Classification accuracies are summarized on a single plane in linear (on left), polynomial (in center) and RBF (on right) kernels for data from all the groups of channels. X-axis shows the groups of channels of data and Y-axis shows the classification accuracy in (%) and each group of vertical bars shows the number of five subjects. **(Circle)**

Table 7.4 presents the classification accuracies with an average accuracy of 84% for five subjects among different groups of data which were used with linear kernel. **(Square)**

	S1	S2	S3	S4	S5
TP7	100	100	100	100	100
TP8	93.23308	100	100	100	87.96992
O1	69.17293	60.90226	60.90226	75.18797	71.42857
O2	82.70677	95.48872	90.97744	87.21805	80.45113
TP7TP8	91.38577	91.7603	89.51311	95.50562	87.26592
O1O2	82.77154	70.03745	68.53933	74.90637	72.65918
TP8O2	77.90262	85.39326	84.64419	81.27341	78.65169
TP7O1	76.77903	90.6367	85.01873	83.89513	85.76779
All	78.83895	74.34457	73.59551	71.91011	73.22097

Table 7.5 presents the classification accuracies with an average accuracy of 47% for five subjects among different groups of data which were used with polynomial kernel of degree 3. **(Square)**

	S1	S2	S3	S4	S5
TP7	52.63158	55.6391	59.3985	57.14286	53.38346
TP8	47.36842	46.61654	48.1203	51.12782	46.61654
O1	45.86466	39.84962	40.6015	40.6015	38.34586
O2	41.35338	36.84211	42.10526	38.34586	35.33835
TP7TP8	53.93258	53.93258	54.68165	57.30337	57.6779
O1O2	43.07116	46.81648	46.81648	56.17978	52.43446
TP8O2	44.94382	49.06367	47.56554	53.18352	48.68914
TP7O1	43.07116	40.82397	42.69663	42.69663	41.57303
All	46.81648	46.25468	46.44195	46.44195	46.81648

Table 7.6 presents the classification accuracies with an average accuracy of 89% for five subjects among different groups of data which were used with RBF kernel. **(Square)**

	S1	S2	S3	S4	S5
TP7	95.48872	91.72932	82.70677	93.23308	89.47368
TP8	92.4812	96.2406	95.48872	96.2406	87.96992
O1	97.74436	88.7218	87.21805	90.22556	93.23308
O2	86.46617	91.72932	90.97744	95.48872	88.7218
TP7TP8	89.13858	93.63296	86.14232	88.38951	84.64419
O1O2	85.01873	87.64045	90.6367	86.14232	85.39326
TP8O2	88.38951	89.13858	87.64045	90.6367	83.5206
TP7O1	87.26592	86.89139	87.64045	88.01498	88.76404
All	84.83146	86.32959	85.20599	85.58052	85.39326

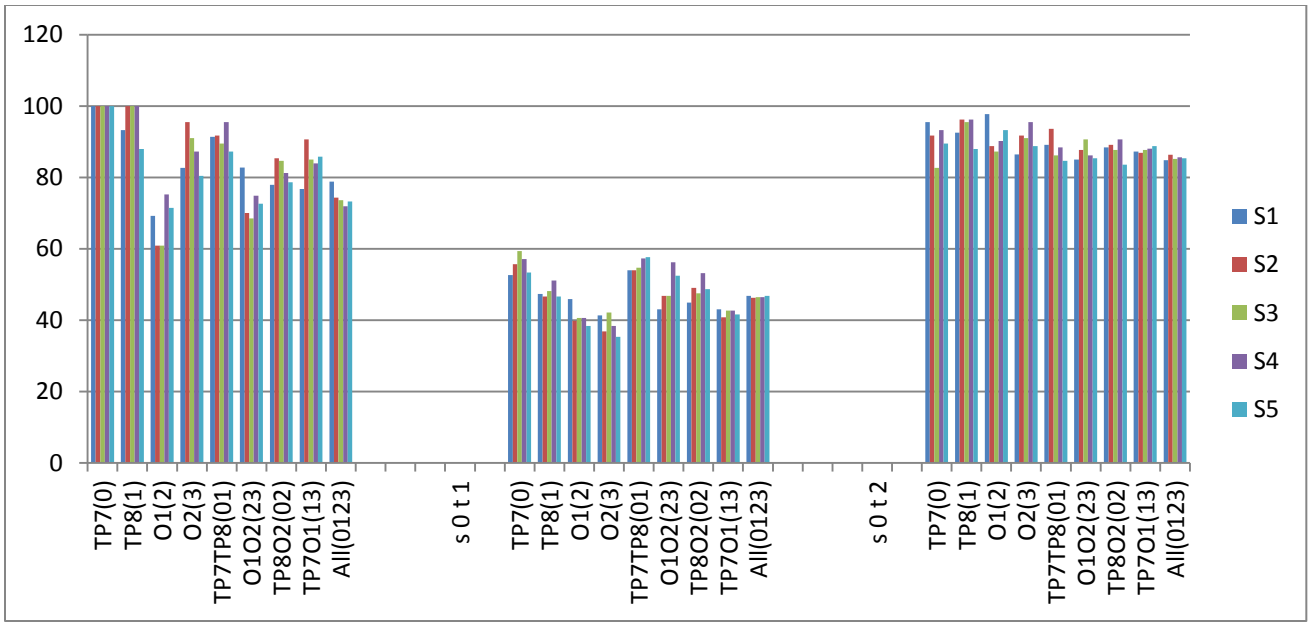

Figure 7.12 Classification accuracies are summarized on a single plane in linear (on left), polynomial (in center) and RBF (on right) kernels for data from all the groups of channels. X-axis shows the groups of channels of data and Y-axis shows the classification accuracy in (%) and each group of vertical bars shows the number of five subjects. **(Square)**

Table 7.7 presents the classification accuracies with an average accuracy of 84% for five subjects among different groups of data which were used with linear kernel. **(Triangle)**

	S1	S2	S3	S4	S5
TP7	84.21053	84.96241	79.69925	74.43609	84.96241
TP8	81.95489	84.21053	71.42857	93.23308	80.45113
O1	93.98496	100	100	100	100
O2	90.97744	90.22556	98.49624	85.71429	94.73684
TP7TP8	83.89513	81.64794	79.40075	80.14981	81.64794
O1O2	93.63296	86.89139	85.39326	86.51685	84.26966
TP8O2	83.89513	89.13858	78.65169	88.76404	87.64045
TP7O1	82.77154	73.78277	83.14607	86.89139	75.2809
All	67.41573	68.16479	62.92135	70.03745	67.79026

Table 7.8 presents classification accuracies with an average accuracy of 49% for five subjects among different groups of data which were used with polynomial kernel of degree 3. **(Triangle)**

	S1	S2	S3	S4	S5
TP7	57.14286	60.90226	49.62406	66.16541	55.6391
TP8	47.36842	45.86466	43.60902	45.86466	46.61654
O1	52.63158	48.87218	48.1203	51.8797	48.87218
O2	38.34586	50.37594	49.62406	46.61654	45.11278
TP7TP8	54.30712	54.30712	48.68914	52.05993	55.80524
O1O2	46.81648	47.19101	48.31461	44.94382	46.06742
TP8O2	54.30712	51.68539	59.92509	52.43446	50.93633
TP7O1	43.07116	45.69288	41.57303	43.82022	45.31835
All	51.49813	49.4382	48.12734	52.05993	49.4382

Table 7.9 presents the classification accuracies with an average accuracy of 94% for five subjects among different groups of data which were used with RBF kernel. **(Triangle)**

	S1	S2	S3	S4	S5
TP7	93.98496	93.23308	93.98496	92.4812	94.73684
TP8	96.99248	94.73684	84.21053	96.99248	96.2406
O1	93.23308	93.23308	90.97744	93.98496	93.23308
O2	97.74436	93.98496	88.7218	98.49624	92.4812
TP7TP8	92.13483	99.25094	93.25843	94.75655	88.76404
O1O2	96.25468	97.00375	97.00375	99.25094	96.62921
TP8O2	96.62921	96.25468	97.00375	96.62921	94.00749
TP7O1	93.63296	94.75655	95.50562	94.00749	94.38202
All	91.38577	92.8839	92.8839	93.07116	92.13483

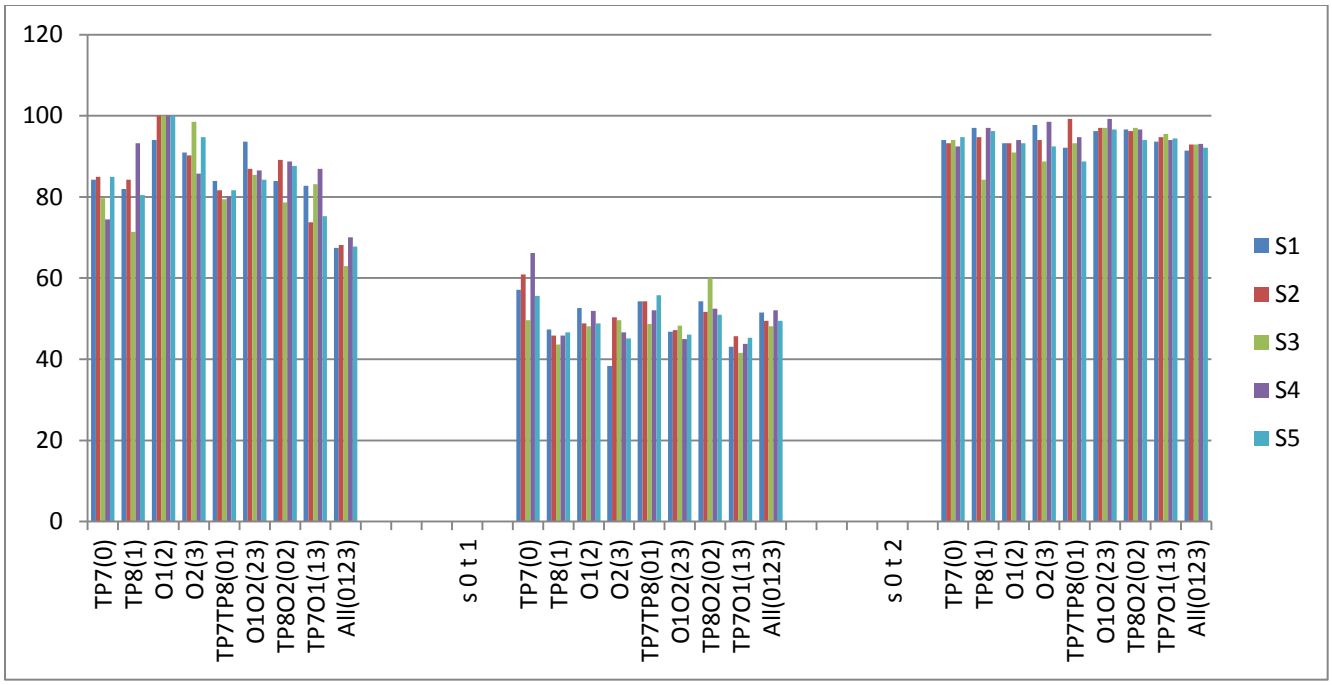

Figure 7.13 Classification accuracies are summarized on a single plane in linear (on left), polynomial (in center) and RBF (on right) kernels for data from all the groups of channels. X-axis shows the groups of channels of data and Y-axis shows the classification accuracy in (%) and each group of vertical bars shows the number of five subjects. **(Triangle)**

7.4.2 Classification of RGB colors across shapes: Group 2

In this group of classification, the data is being used after combining the data of similar colors from different shapes in order to produce a combined class for a particular color. For example, Red square, Red circle and Red triangle's data will be combined together to produce data of Red class. Similarly, the data will be produced for Green and Blue classes, so finally we will have three classes of RGB colors. Now the classification problem has become same as it was in group1 in section 7.4.1 with one of the difference that RGB classes data from different shapes. This formation of classes is shown on the next page 'Formation of Classes: Group 2'. The classification results for this problem are shown in table 7.11, 7.12 and 7.13 for linear, polynomial and RBF kernels respectively. It is seen that the average accuracy with linear kernel is dropped down to 71% in comparison with the performance of linear kernel for all the three classification problems in group 1 where the average accuracy was found to be 88, 84 and 84% respectively. The polynomial kernel has shown again the bad performance whereas RBF kernel appeared to be very consistent in showing very good accuracy. Keeping in view these results, we can assume that the classification of data belonging to different shapes of exposures may or may not affect the classification accuracy. Figure 7.14 show all the results of group 2 in a summarized form on a single plane.

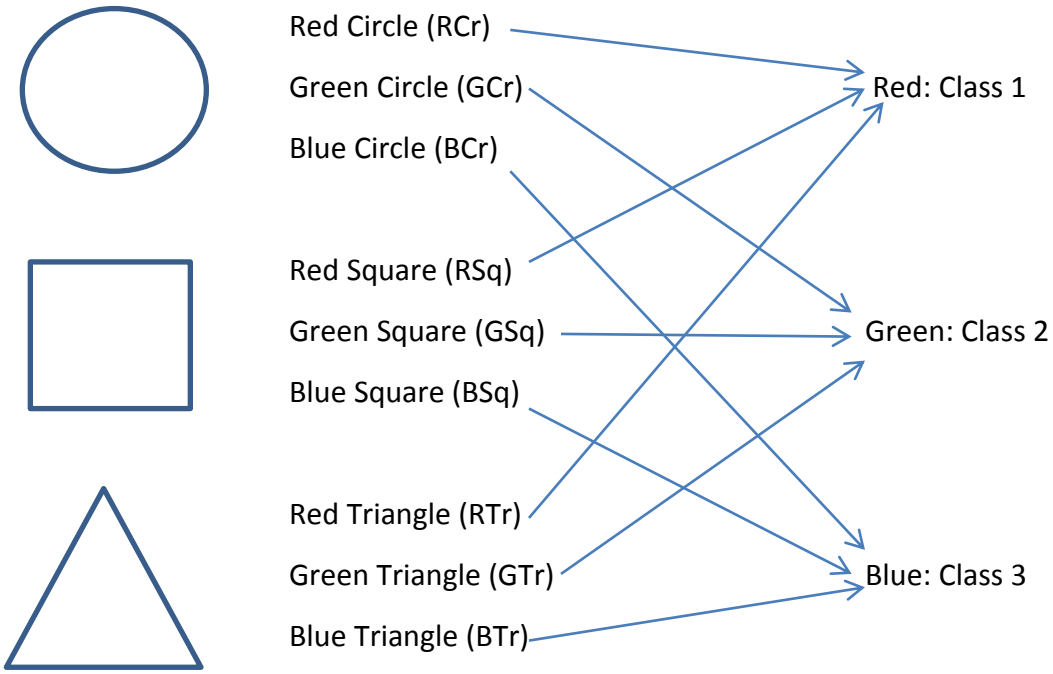

Formation of Classes: Group 2

Table 7.10 presents the classification accuracies with an average accuracy of 71% for five subjects among different groups of data which were used with linear kernel.

	S1	S2	S3	S4	S5
TP7	91.75	86.75	90.75	91.5	86.75
TP8	79	86.75	75.75	82.5	78.25
O1	78.25	78.5	78.5	73.75	75.25
O2	72.25	78	70	71	70.25
TP7TP8	69.41323	70.41199	72.28464	72.03496	70.91136
O1O2	60.42447	60.799	62.67166	62.67166	59.17603
TP8O2	66.41698	67.79026	73.2834	71.53558	69.53808
TP7O1	65.41823	71.16105	64.54432	64.16979	69.0387
All	54.95945	50.03119	49.53213	49.84404	49.84404

Table 7.11 presents the classification accuracies with an average accuracy of 50% for five subjects among different groups of data which were used with polynomial kernel of degree 3.

	S1	S2	S3	S4	S5
TP7	66	58.25	59.5	58.75	58.25
TP8	48	53.25	48.25	47.5	51.75
O1	45.5	50	48.25	43.75	46.75
O2	44.5	45	44.5	43.75	47.5
TP7TP8	54.93134	53.55805	53.55805	54.68165	56.804
O1O2	47.4407	46.19226	45.19351	45.19351	45.19351
TP8O2	58.05243	51.68539	51.68539	49.06367	52.68414
TP7O1	48.68914	46.81648	42.44694	42.94632	51.93508
All	49.65689	48.22208	49.71928	51.96507	49.40736

Table 7.12 presents the classification accuracies with an average accuracy of 94% for five subjects among different groups of data which were used with RBF kernel.

	S1	S2	S3	S4	S5
TP7	100	100	100	100	100
TP8	96.75	96	95.5	98.25	94.25
O1	87.25	92.75	87.25	86.25	94.25
O2	93.25	94.5	93.75	96	98.25
TP7TP8	97.25343	94.38202	95.00624	96.8789	95.50562
O1O2	91.7603	94.38202	92.25968	93.88265	93.25843
TP8O2	92.25968	88.88889	91.51061	90.6367	87.89014
TP7O1	96.62921	92.13483	93.63296	92.25968	96.00499
All	89.20774	88.77105	87.1491	90.14348	89.02059

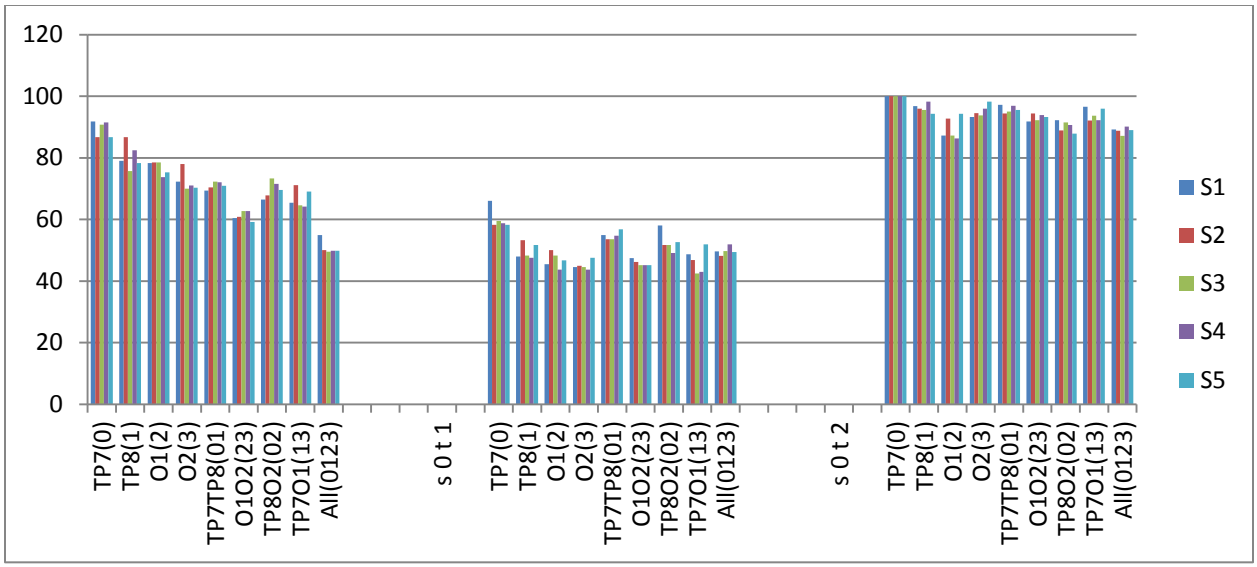

Figure 7.14 Classification accuracies are summarized on a single plane in linear (on left), polynomial (in center) and RBF (on right) kernels for data from all the groups of channels. X-axis shows the groups of channels of data and Y-axis shows the classification accuracy in (%) and each group of vertical bars shows the number of five subjects.

7.4.3 Classification of shapes: Group 3

As we have seen in the previous group 2 that the accuracy may be affected due to change of shape therefore, we have introduced another group to perform classification in a different context in order to see if the shapes are classifiable or not having data that belongs to different classes of colors so we did not classify colors but shapes. For example, we have three data sets each belonging to circle, square and triangle, in total nine data sets so by combining data of Red circle, Green circle and Blue circle will create one class of circle shape. Similarly, two other classes will be formed for Square and Triangle. Thus in this problem we will have three classes of Circle, Square and Triangle but each class will have the data of all the three colors. We can see the formation of these classes on the next page 'Formation of Classes: Group 3'. The classification results for this group are shown in tables 7.13, 7.14 and 7.15 for linear, polynomial and RBF kernels with an average accuracy of 60%, 48% and 92% respectively. We can see that the performance of linear classifier is more reduced to 60% in comparison with earlier group 2's linear classifier's performance and polynomial kernel with an average accuracy of 48% is still not able to classify shapes at good rate whereas the RBF kernel again worked very well with an average accuracy of 92% like always. If we analyze the performance of linear kernel from beginning in this experiment, it would be clear that its performance is continuously decreasing; however the performances of polynomial and RBF kernels are quite consistent around 50% and 92% respectively, regardless of the fact that the polynomial worked bad and RBF worked very well. Figure 7.15 summarized all the results in group 3.

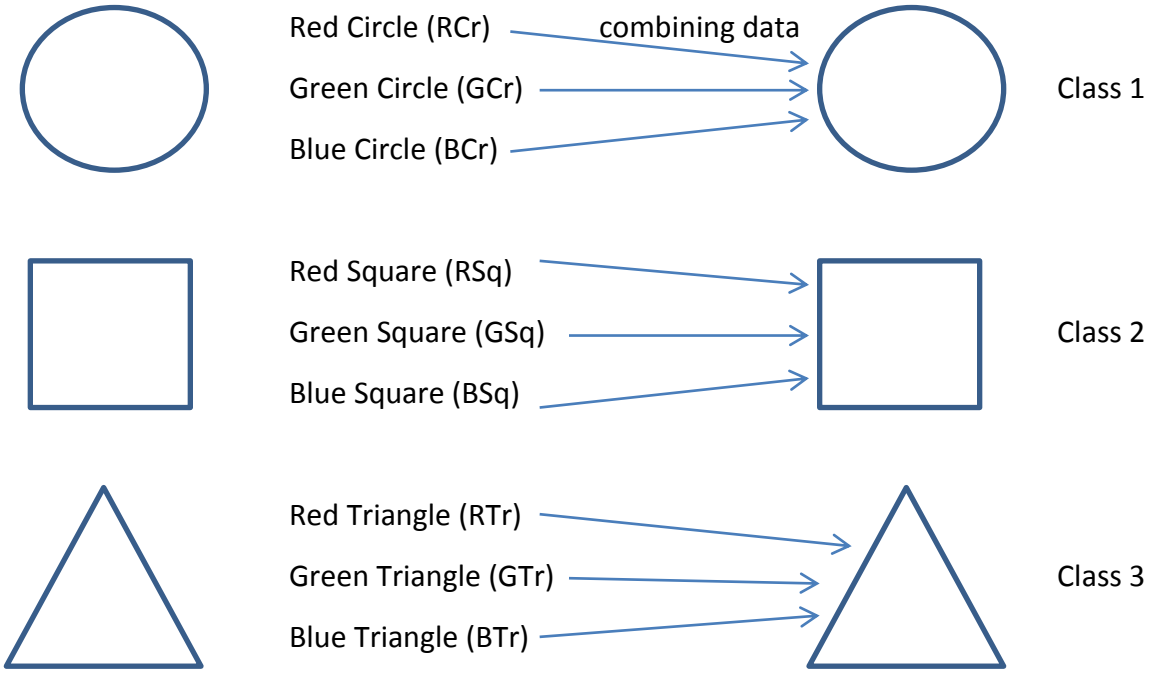

Formation of Classes: Group 3

Table 7.13 presents the classification accuracies with an average accuracy of 60% for five subjects among different groups of data which were used with linear kernel.

	S1	S2	S3	S4	S5
TP7	82.5	87.25	81.25	87	84
TP8	73.25	73	74	70.5	72.25
O1	66	62.5	57.25	56.5	59.5
O2	65.75	62.25	66.5	63	61.25
TP7TP8	53.30836	51.68539	54.18227	49.68789	58.55181
O1O2	46.81648	53.30836	55.05618	53.6829	48.18976
TP8O2	56.67915	55.55556	54.43196	54.5568	52.18477
TP7O1	54.18227	54.93134	53.6829	52.80899	49.93758
All	46.47536	48.34685	47.72302	49.2826	51.15409

Table 7.14 presents the classification accuracies with an average accuracy of 48% for five subjects among different groups of data which were used with polynomial kernel of degree 3.

	S1	S2	S3	S4	S5
TP7	54.25	55	51.75	47.25	57
TP8	47.5	49.75	50	48.5	49.25
O1	48.25	45.25	44.75	48	46.75
O2	43	43.5	43	45.75	42.5
TP7TP8	51.18602	50.18727	51.93508	51.43571	51.18602
O1O2	44.19476	44.56929	44.19476	43.196	44.81898
TP8O2	51.43571	49.31336	46.94132	49.68789	52.5593
TP7O1	42.94632	45.81773	46.56679	45.56804	46.69164
All	53.27511	54.08609	52.90081	52.40175	52.52651

Table 7.15 presents the classification accuracies with an average accuracy of 92% for five subjects among different groups of data which were used with RBF kernel.

	S1	S2	S3	S4	S5
TP7	98.25	98.75	98.25	98.5	100
TP8	93.5	94.75	95.5	89	93.5
O1	89.25	90.75	89.25	92	87.25
O2	90.25	93	94.5	93.75	87.5
TP7TP8	92.38452	92.75905	94.50687	90.26217	94.8814
O1O2	87.89014	89.51311	85.64295	87.76529	87.64045
TP8O2	93.38327	94.00749	95.38077	95.13109	94.38202
TP7O1	84.64419	89.01373	89.63795	90.26217	91.13608
All	87.58578	89.89395	87.71054	88.20961	90.58016

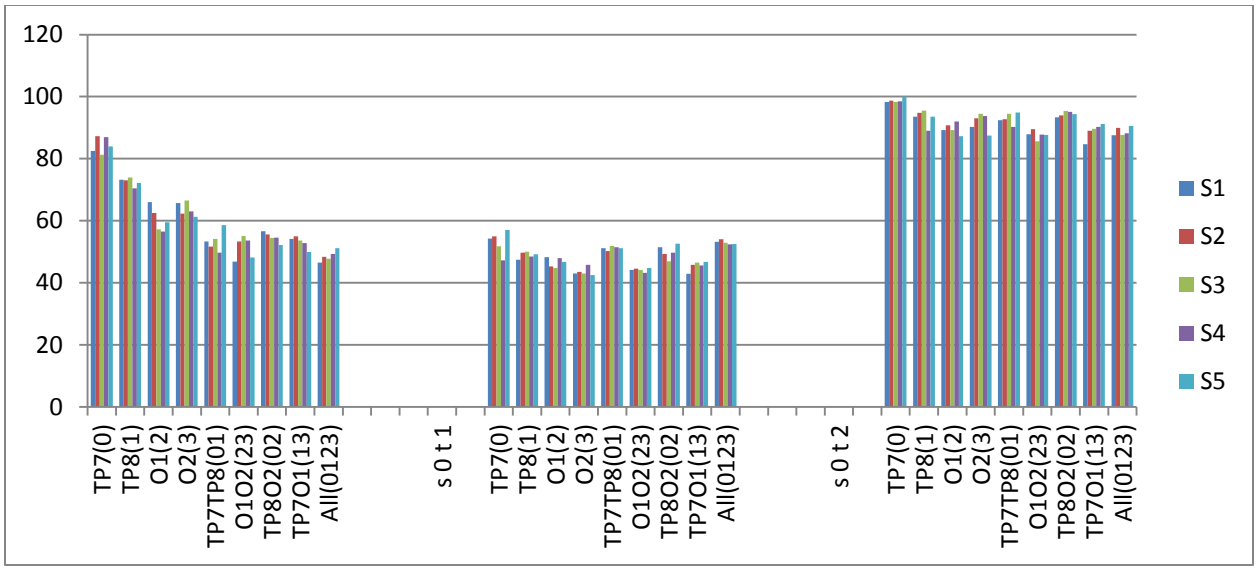

Figure 7.15 Classification accuracies are summarized on a single plane in linear (on left), polynomial (in center) and RBF (on right) kernels for data from all the groups of channels. X-axis shows the groups of channels of data and Y-axis shows the classification accuracy in (%) and each group of vertical bars shows the number of five subjects.

7.4.4 Classification of all conditions simultaneously. Group 4

In all the previous groups, all the classification problems consists of three classes but here we have considered 9 different classes, treating each condition, a separate class. The results for this group of classification are shown in tables 7.16, 7.17 and 7.18. Having such a complex data for the SVM classifier, average accuracy with linear kernel reduces to 57%, polynomial kernel has dramatically reduced to 29% and RBF kernel as usual worked very well with an accuracy of 94%. It is seen that throughout these classification problems the performance of the linear kernel kept reducing as the complexity of the problem increases. However, regardless of the complexity of classification problem, the performance of RBF kernel surprisingly remained always same with minor variations in accuracy rate. Therefore, we suggest to work to use always RBF kernel with SVM for such kind of color classification or shape classifications problems. Figure 7.16 summarized all the results of group 4.

Table 7.19 summarizes all the classification results in all the groups.

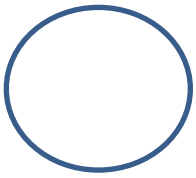

Red Circle (RCr) : Class 1

Green Circle (GCr) : Class 2

Blue Circle (BCr) : Class 3

Red Square (RSq) : Class 4

Green Square (GSq) : Class 5

Blue Square (BSq) : Class 6

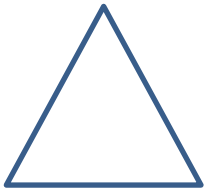

Red Triangle (RTr) : Class 7

Green Triangle (GTr) : Class 8

Blue Triangle (BTr) : Class 9

Table 7.16 presents the classification accuracies with an average accuracy of 57% for five subjects among different groups of data which were used with linear kernel.

	S1	S2	S3	S4	S5
TP7	60.25	63.5	63.75	66.5	55.25
TP8	68	73.25	72	72	65.25
O1	60.25	56	67	54.75	59.5
O2	62.75	59	55	55.75	57.25
TP7TP8	46.94132	45.4432	46.44195	51.68539	48.31461
O1O2	46.06742	45.94257	52.68414	50.18727	42.3221
TP8O2	48.93883	45.31835	50.43695	40.94881	46.3171
TP7O1	51.81024	50.5618	58.17728	56.55431	51.56055
All	67.81036	66.00125	66.00125	69.80661	68.99563

Table 7.17 presents the classification accuracies with an average accuracy of 29% for five subjects among different groups of data which were used with polynomial kernel of degree 3.

	S1	S2	S3	S4	S5
TP7	42	39.75	41	37.5	39.25
TP8	33.5	31.75	30	31	28.75
O1	21.75	22.25	21.75	22.75	22.5
O2	19.75	18.5	20	19.75	21.25
TP7TP8	36.45443	36.20474	36.45443	34.20724	34.9563
O1O2	27.8402	28.83895	27.34082	26.34207	25.71785
TP8O2	30.9613	31.46067	30.71161	33.70787	34.70662
TP7O1	24.96879	24.21973	23.84519	24.09488	25.71785
All	29.13288	29.94386	28.19713	30.63007	29.63194

Table 7.18 presents the classification accuracies with an average accuracy of 94% for five subjects among different groups of data which were used with RBF kernel.

	S1	S2	S3	S4	S5
TP7	100	100	100	100	100
TP8	95.25	94	91.25	94.25	88
O1	92.5	85.5	94.75	88	94
O2	91	92.75	95.75	92.25	92.25
TP7TP8	92.50936	95.88015	95.38077	95.63046	95.00624
O1O2	92.38452	89.26342	87.89014	91.7603	89.38826
TP8O2	95.38077	96.37953	97.75281	95.63046	97.62797
TP7O1	94.00749	92.38452	92.50936	91.26092	92.8839
All	92.82595	90.70493	92.13974	93.32502	91.95259

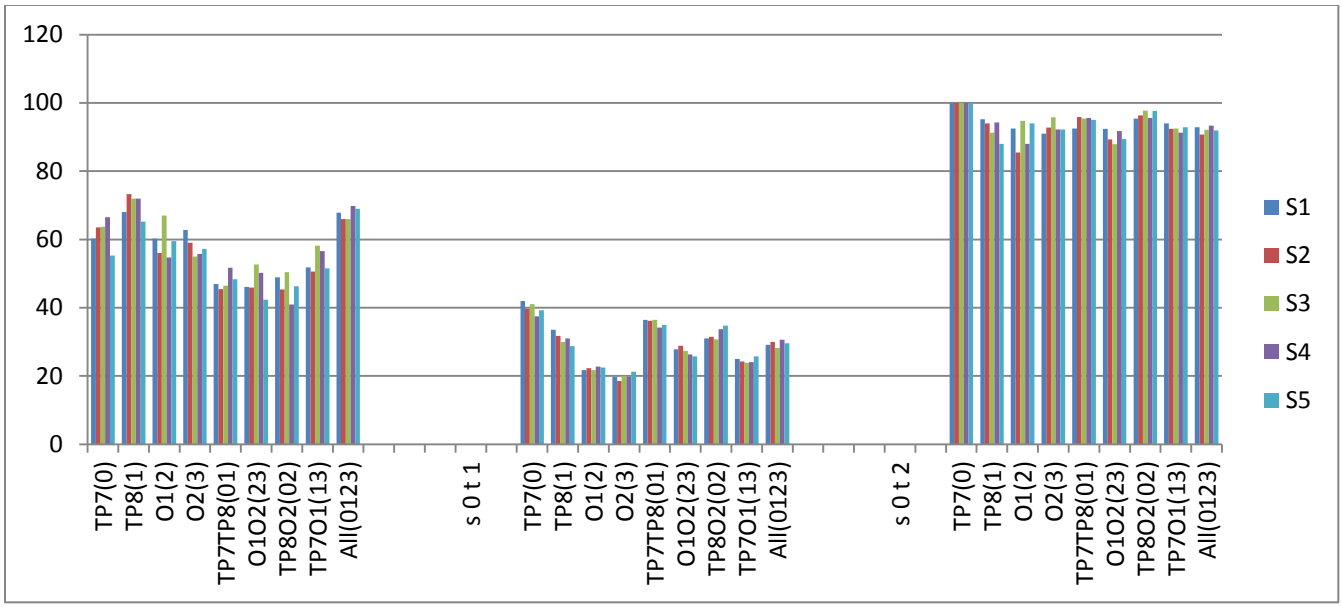

Figure 7.16 Classification accuracies are summarized on a single plane in linear (on left), polynomial (in center) and RBF (on right) kernels for data from all the groups of channels. X-axis shows the groups of channels of data and Y-axis shows the classification accuracy in (%) and each group of vertical bars shows the number of five subjects.

Table 7.19 Classification results (%) of all groups

ERSP features were used		Linear	Polynomial	RBF
Group 1	Circle	88	52	94
	Square	84	47	89
	Triangle	84	49	94
Group 2		71	50	94
Group 3		60	48	92
Group 4		57	29	94

8. Summary and Conclusion

In this study, we have performed an experiment of presenting primary color stimuli to have visual evoked potential from the occipital and parietal lobe of the brain and subjects were instructed to imagine the same color by keeping their eyes closed, that was presented in a sequence. We have discussed ERP waveforms, frequency spectrum, ERSP, ITC and ERP image features generated as a result of exposure of real primary colors and their imaginations. Responses of real color and the corresponding imagination are shown together for each color. Slight differences have been noticed in all types of responses for each color which are visually seen and inspected among intra-class (color exposure) and interclass (corresponding imaginations). To visualize the presented data, we have used STUDY[1] structure to process multiple data sets from multiple subjects across multiple conditions. For more information, see http://sccn.ucsd.edu/wiki/EEGLAB. Taking into account, grand mean ERP, real exposure of green color, which is perceived as lighter than others (red and blue), has a difference of significant negative peak centered at 800ms and is only visible in exposure of green color but neither in imagination of green color nor in the real exposure of red and blue colors. However, it is interesting to see in the imagination of all the colors, a wider positive peak centered at 500 ms starting around 300 ms until 700 ms that remains negative after it drops down zero in the last one second of the epoched extracted where as in the real color exposure it remains positive. Considering the frequency spectrum, a significant activity is found in the alpha band (8 – 12 Hz), not only in real color exposure but also in imagination of colors. In imagination of colors, maximum and average power in the alpha band was found larger than the power in real color exposures.

To interpret more accurately the differences among the exposure of primary colors, event related spectral power (ERSP) results in terms of time-frequency frame are presented, that have shown the variation in distribution of power in the delta, theta, alpha and beta bands. Taking into account averaged ERSP, red exposure has shown higher power increase starting from 200 ms to 400 ms in delta and theta band than green and blue exposures whereas green exposure has the lowest increase in power within the same time period and frequency band. Blue color is only influential in delta and lower theta (4 – 6 Hz) bands and green color is slightly influential in upper delta (2 – 4 Hz) and lower theta (4 – 6 Hz) bands. Looking at ERSP of color imagination we came across that red imagination exhibited higher ERSP increase than green and blue, during same time period from 200 ms to 400 ms in delta and theta band whereas the lowest ERSP was seen in blue imagination. A significant decrease was seen in alpha band centered around 500 ms among exposure of all colors as well as their corresponding imagination. Here we see that red has the largest decrease in ERSP and green shows the lowest decrease in exposure of colors whereas during imagination of colors red was found to have

lowest decrease and blue with largest decrease in ERSP. Interestingly, a significant increase in ERSP is seen in imagination of colors, more precisely with in the alpha band and partially with in the beta band, starting after one second of onset of instruction to the subject "Eyes Closed, Color Imagination". This instruction was displayed on black background with gray font. Delay of one second in this increase is expected due to adjustment time in imagination because most of the subjects took some time to start imagination. Red imagination has shown the largest increase and green exhibited lowest increase. To analyze phase synchronization we further presented inter-trial coherence (ITC) for primary color exposure and also for their imaginations. While exposure of colors we noticed that phase is highly synchronized in red color within delta and beta bands, relatively less synchronized in alpha band and partially synchronized in beta band, for around 200 ms in length, starting from 200 ms until 400 ms whereas green color is relatively less synchronized than red and blue has the lowest synchronization than red and green. However, imagination of colors reveals that phase synchronization is higher in red and blue within delta and theta band and relatively lower in green, whereas almost equally synchronized within alpha band among all the color imaginations. ERP image plots shown in figure 6.22, 6.23 and 6.24 reflects ERSP and ITC in waveforms and supports the evidences which we have visualized in figures 6.6 and 6.14 respectively.

Moreover, we have used ERSP data as features and C-SVM as classifier with three different kernels i.e. linear kernel, polynomial kernel and RBF kernel for the classification of EEG signals recorded as event-related potentials in response to RGB uniform colour stimuli. To interpret more accurately the differences among the exposure of primary colours, average event related spectral perturbation (ERSP) results in terms of time-frequency frame are presented in figure 6.25 that have shown significant power variations in the delta, theta and alpha bands. Red exposure has shown highest power increase starting from 100 ms to 400 ms in delta and theta bands than green and blue exposures, however the blue exposure has the lowest increase in power within the same time period and frequency bands. Moreover, a discriminative decrease in power among all the colours is seen in alpha band within 1000ms after the onset of stimulus. We have seen that these differences against the visual conditions in terms of single uniform colours are successfully classified using support vector machines. We have found very good accuracy results, on average 84%, 89% and 98% for linear, polynomial and RBF kernels respectively, with in all the groups of data among all the subjects. Highest accuracy was found in RBF kernel with nowhere less than other kernels in any group of data in any subject. As a next step, we have performed the classification on EEG signals belonging to imagination of colors. It is seen that the imagination of colors can also be classified like the imagination of movement of body limbs which are mostly found in the BCI literatures. The accuracy results for imagination of colors were found to be 64%, 70% and 76% with linear, polynomial and RBF kernels respectively. Although the results for imagination of colors are not as good as for the real exposure of colors but again we have seen that RBF kernel produced best results and linear

kernel's performance appeared to be less than the others. Please note that we have used ERSP features with SVM for both the classification problems of real exposure and imagination of colors.

As an alternative we have used extreme energy ratio (EER) and extreme energy difference (EED) criterions to extract energy features for the classification of EEG signals acquired by the exposure of RGB colors and for the classification EEG signals acquired by the imagination of RGB colors. We have applied EER and EED criterions on ERP waveforms with only linear SVM (No polynomial and RBF kernels were used) to solve the binary classification problems because we created three groups of binary classification as follows: (Blue, Green), (Red, Green) and (Red, Blue). So first of all we applied EER criteria on both the real exposure of colors and imagination of colors and achieved 79%, 78% and 80% of accuracy for BG, RG and RB classification problems, respectively, on real exposure of colors, however the accuracy seen as 72%, 70% and 73% for BG, RG and RB problems, respectively, on imagination of colors. Secondly we applied EED on both the real exposure and imagination of colors and achieved 82%, 83% and 84% of accuracy for BG, RG and RB problems respectively, whereas the accuracy seen in imagination of colors is 73%, 75% and 72% respectively. It shows that EED is better than EER for the classification of real exposure of colors and slightly better for imagination of colors.

Apart from the experiment, to expose colors in single shape we performed another experiment to expose colors that involves multiple shapes i.e. Circle, Square and Triangle. In this experiment part of imagination of colors was removed and all the concentration was focused on the classification of real exposure of colors. In this experiment we divided the data into four different groups as follows: Group1 - Classification of colors within shapes, Group2 – Classification of colors across shapes, Group3 – Classification of shapes and Group4 – Classification of all the nine conditions simultaneously. The SVM classifier was used with ERSP features along with linear, polynomial and RBF kernels. Group2 to group4 consists of one classification problem whereas group1 consists of three classification problems, one for each circle, square and triangle. In group1, the classification accuracies for circle, square and triangle are found to be (88%, 52%, 94%), (84%, 47%, 89%) and (84%, 49%, 94%) respectively as triplet (linear, polynomial, RBF). In group 2, 3 and 4 classification accuracies achieved are (71%, 50%, 94%), (60%, 48%, 92%) and (57%, 29%, 94%) respectively as triplet of (linear, polynomial, RBF) kernels. It is seen that linear classifier's performance kept on decreasing with the increase in complexity of classification problems starting from group1 to group4 and polynomial kernel's performance is found to be consistent around 50% regardless of how good the performance is, whereas polynomial kernel's performance also found to be very consistent in all the groups around 92%. From all these statistics, we can assume that the classification of real exposure of colors and their corresponding imaginations is possible using SVM classifier and best results are supported with RBF kernels.

We also propose to do comparative study in future on different classifiers in conjunction with dimensionality reduction to select the most suitable data features in order to eliminate redundant information for the sake of online classification. We suggest that ERSP and ITC variations may be utilized computationally in conjunction with statistical analysis for further useful feature extraction and efficient classification of different EEG signals, produced in response to the exposure of red, green and blue colors. Although visual inspection could be useful for offline analysis, we still need to use more efficient and robust algorithms to analyze the presented differences online for future Brain-Computer Interface applications.

This is first step towards contribution to provide a base for BCI applications based on uniform color stimuli with single and multiple shapes. We also suggest that color information and shape information along with imagination of colors is identifiable from EEG signals. As a possible future work we are further designing more new experiments under more variable conditions to refine the results presented in chapter 6 and 7 for real time implementation. We have partially investigated this study from Neuro-scientific point of view while being skeptical. We believe that this study could further be used for simulating a scenario of traffic light signals in virtual environment for possible BCI applications along with analysis of depth perception or this study could further be extended to identify any possibility of analyzing the EEG signals and developing BCI applications for color blind and/or blind people. However such an application is quite novel in its field of BCI, therefore requires extensive collaborative research work in different domains including neuroscientists and engineers.

Any feedbacks, suggestions or ideas are warmly welcome and would greatly be appreciated to improve the work.

Saim Rasheed

saim.rasheed@unimi.it